MINISTRY OF EDUCATION AND TRAINING

HO CHI MINH CITY UNIVERSITY OF TECHNOLOGY AND EDUCATION

NGUYEN NGOC DUONG

VIBRATION, BUCKLING AND STATIC ANALYSIS OF LAMINATED COMPOSITE BEAMS WITH VARIOUS CROSS-SECTIONS

Ph.D THESIS

MAJOR: ENGINEERING MECHANICS

HCMC, December 2019

BỘ GIÁO DỤC VÀ ĐÀO TẠO
TRƯỜNG ĐẠI HỌC SƯ PHẠM KỸ THUẬT
THÀNH PHỐ HỒ CHÍ MINH

Số: 2369/QĐ-ĐHSPKT

CỘNG HÒA XÃ HỘI CHỦ NGHĨA VIỆT NAM
Độc lập – Tự do – Hạnh phúc

Tp. Hồ Chí Minh, ngày 05 tháng 10 năm 2015

QUYẾT ĐỊNH

V.v giao đề tài luận án và người hướng dẫn nghiên cứu sinh khóa 2015-2018

HIỆU TRƯỞNG TRƯỜNG ĐẠI HỌC SƯ PHẠM KỸ THUẬT TP. HỒ CHÍ MINH

Căn cứ Quyết định số 118/2000/QĐ-TTg ngày 10 tháng 10 năm 2000 của Thủ tướng Chính phủ về việc thay đổi tổ chức của Đại học Quốc gia TP. Hồ Chí Minh, tách Trường Đại học Sư phạm Kỹ thuật TP. Hồ Chí Minh trực thuộc Bộ Giáo dục và Đào tạo

Căn cứ Quyết định số 70/2014/QĐ-TTg ngày 10/12/2014 của Thủ tướng Chính phủ về ban hành Điều lệ trường Đại học

Căn cứ Thông tư số 10/2009/TT-BGDĐT ngày 07/5/2009 của Bộ Giáo dục và Đào tạo về việc Ban hành Qui chế đào tạo trình độ tiến sĩ;

Căn cứ Thông tư số 05/2012/TT-BGDĐT ngày 15/02/2012 của Bộ Giáo dục và Đào tạo về việc sửa đổi, bổ sung một số điều của Quy chế đào tạo trình độ tiến sĩ ban hành kèm theo Thông tư số 10/2009/TT-BGDĐT ngày 07/5/2009 của Bộ trưởng Bộ Giáo dục và Đào tạo;

Xét nhu cầu công tác và khả năng cán bộ;

Xét đề nghị của Trưởng phòng Đào tạo,

QUYẾT ĐỊNH:

Điều 1. Giao đề tài luận án tiến sĩ và người hướng dẫn cho:

Nghiên cứu sinh : ***Nguyễn Ngọc Dương***

Ngành : ***Cơ kỹ thuật*** Khoá: ***2015 – 2018***

Tên luận án : ***Phát triển mô hình phân tích dầm composite và ứng dụng phân tích một số kết cấu thành mỏng***

Người HD thứ nhất (HD chính): ***PGS.TS Nguyễn Trung Kiên***

Người HD thứ hai : ***TS. Võ Phương Thức***

Thời gian thực hiện : ***05/10/2015 đến 05/10/2018***

Điều 2. Giao cho Phòng Đào tạo quản lý, thực hiện theo đúng Qui chế đào tạo trình độ tiến sĩ của Bộ Giáo dục & Đào tạo đã ban hành.

Điều 3. Trưởng các đơn vị, phòng Đào tạo, các Khoa quản ngành tiến sĩ và các Ông (Bà) có tên tại Điều 1 chịu trách nhiệm thi hành quyết định này.

Quyết định có hiệu lực kể từ ngày ký./.

SAO Y BẢN CHÍNH
Ngày 30 tháng 12 năm 2019

Nơi nhận :
- BGH (để biết);
- Như điều 2, 3;
- Lưu: VT, SĐH.

TL. HIỆU TRƯỞNG
KT. TRƯỞNG PHÒNG TCHC
PHÓ TRƯỞNG PHÒNG

ThS. Lê Phan Nhật Hằng

HIỆU TRƯỞNG
PHÓ HIỆU TRƯỞNG

PGS.TS. Lê Hiếu Giang

BỘ GIÁO DỤC VÀ ĐÀO TẠO
TRƯỜNG ĐẠI HỌC SƯ PHẠM KỸ THUẬT
THÀNH PHỐ HỒ CHÍ MINH

Số: 943 /QĐ-ĐHSPKT

CỘNG HÒA XÃ HỘI CHỦ NGHĨA VIỆT NAM
Độc lập – Tự do – Hạnh phúc

Tp. Hồ Chí Minh, ngày 30 tháng 5 năm 2017

QUYẾT ĐỊNH

Về việc đổi tên luận án và người hướng dẫn nghiên cứu sinh khóa 2015
HIỆU TRƯỞNG TRƯỜNG ĐẠI HỌC SƯ PHẠM KỸ THUẬT TP. HỒ CHÍ MINH

Căn cứ Quyết định số 118/2000/QĐ-TTg ngày 10 tháng 10 năm 2000 của Thủ tướng Chính phủ về việc thay đổi tổ chức của Đại học Quốc gia TP. Hồ Chí Minh, tách Trường Đại học Sư phạm Kỹ thuật TP. Hồ Chí Minh trực thuộc Bộ Giáo dục và Đào tạo;

Căn cứ Quyết định số 70/2014/QĐ-TTg ngày 10/12/2014 của Thủ tướng Chính phủ về ban hành Điều lệ trường Đại học;

Căn cứ Thông tư số 10/2009/TT-BGDĐT ngày 07/5/2009 của Bộ Giáo dục và Đào tạo về việc Ban hành Qui chế đào tạo trình độ tiến sĩ;

Căn cứ Thông tư số 05/2012/TT-BGDĐT ngày 15/02/2012 của Bộ Giáo dục và Đào tạo về việc sửa đổi, bổ sung một số điều của Quy chế đào tạo trình độ tiến sĩ ban hành kèm theo Thông tư số 10/2009/TT-BGDĐT ngày 07/5/2009 của Bộ trưởng Bộ Giáo dục và Đào tạo;

Xét nhu cầu công tác và khả năng cán bộ;

Xét đề nghị của Trưởng phòng Đào tạo,

QUYẾT ĐỊNH

Điều 1: Đổi tên đề tài luận án tiến sĩ cho:

Nghiên cứu sinh : ***Nguyễn Ngọc Dương***

Ngành : Cơ kỹ thuật Khoá: ***2015 – 2018***

Tên luận án mới : ***Nghiên cứu ứng xử tĩnh, ổn định và dao động dầm composite với tiết diện khác nhau***

Người HD thứ nhất (HD chính): ***PGS.TS Nguyễn Trung Kiên***

Người HD thứ hai : ***TS. Võ Phương Thức***

Thời gian thực hiện : ***05/10/2015 đến 05/10/2018***

Điều 2: Giao cho Phòng Đào tạo quản lý, thực hiện theo đúng Qui chế đào tạo trình độ tiến sĩ của Bộ Giáo dục & Đào tạo đã ban hành.

Điều 3: Trưởng các đơn vị: phòng Đào tạo, khoa quản ngành, phòng KHTC và các Ông (Bà) có tên ở Điều 1 chịu trách nhiệm thi hành quyết định này.

Quyết định có hiệu lực kể từ ngày ký./.

Nơi nhận:
- BGH (để chỉ đạo);
- Như điều 3;
- Lưu: VT, SĐH (3b).

KT. HIỆU TRƯỞNG
PHÓ HIỆU TRƯỞNG

ĐẠI HỌC SƯ PHẠM KỸ THUẬT TP. HỒ CHÍ MINH

PGS. TS Lê Hiếu Giang

Declaration

I declare that this thesis is all my own work based on instruction of Associate Professor Dr. Trung-Kien Nguyen and Dr. Thuc P. Vo.

The work contained in this thesis has not been submitted for any other award.

Name: Ngoc-Duong Nguyen

Signature:

Acknowledgement

Firstly, I wish to express my deep gratitude to my advisor, Associate Professor Dr. Trung-Kien Nguyen, for his warm guidance, suggestions and support during my study. He has influenced my career by coaching me the work ethics and responsibilities, along with research skills, which are required of a good researcher. The completion of this work would not have been possible without his detailed advice, constructive criticism and constant encouragement and patience.

I am also extremely grateful to Dr. Thuc P. Vo at Northumbria University who generously spent a great deal of time providing me with alternative viewpoints to my ideas through many helpful discussions. His invaluable knowledge, experience and moral support proved to be of inestimable value to the revision and completion of this thesis.

In addtion, I am grateful to Dr. Huu-Tai Thai for his comments in my publications, and Mr. Thien-Nhan Nguyen for sharing his Matlab code.

My special thanks are extended to my colleagues at Department of Structural Engineering in Falcuty of Civil Engineering, HCMC University Technology and Education, who have offered me intellectual stimulation, friendship and provided a warm and inspiring environment.

Finally, I wish to express my deep appreciation to my family and wife for their continued encouragement and support during my study. Without their presence, this work would have never been possible.

Ngoc-Duong Nguyen

Abstract

Composite materials are widely used in many engineering fields owing to their high stiffness-to-weight, strength-to-weight ratios, low thermal expansion, enhanced fatigue life and good corrosive resistance. Among them, laminated composite beams are popular in application and attract a huge attention from reseacher to study the their structural behaviours. Many theories are proposed for the bending, buckling and vibration analysis. They can be divided into classical beam theory (CBT), first-order beam theory (FOBT), higher-order beam theory (HOBT) and quasi-three dimension (quasi-3D) beam theory. It should be noted that classical continuum mechanics theories are just suitable for macro beams. For analysing microbeams, researchers proposed many non-classical theories. Among them, the modified couple stress theory (MCST) is the most popular and commonly applied owing to its simplicity in formulation and programming. In order to accurately predict behaviours of beams, a large number of methods are developed. Numerical approaches are used increasingly, however, analytical methods are also used by researchers owing to their accuracy and efficiency. Among analytical approaches, Ritz method is the most general one, which accounts for various boundary conditions, however, it has seldom been used to analyse the bending, buckling and free vibration behaviours of beams. This is also the main motivation of this study.

This dissertation focuses on propsing new approximation functions to analyse laminated composite beams with various cross-sections and boundary conditions. The displacement field is based on the FOBT, HOBT and quasi-3D theories. Size-dependent effect for microbeams is investigated using the MCST. Poisson's effect is considered by integrating in the constitutive equations. The governing equations of motion are derived from Lagrange's equations. Numerical results for beam with various boundary conditions are presented and compared with existing ones available in the literature. The effects of fiber angle, length-to-height ratio, material anisotropy, shear and normal strains on the displacements, stresses, natural frequencies, mode shape and buckling loads of the composite beams are investigated. Some of numerical

results are presented at the first time and can be used as the benchmark results for numerical methods. Besides, a study on efficacy of approximation functions for analysis of laminated composite beams with simply-supported boundary conditions is carried out.

List of Publications

ISI papers with peer-reviews:

1. **N.-D. Nguyen**, T.-K. Nguyen, T.P. Vo, T.-N. Nguyen, and S. Lee, Vibration and buckling behaviours of thin-walled composite and functionally graded sandwich I-beams, Composites Part B: Engineering. 166 (2019) 414-427.

2. **N.-D. Nguyen**, T.-K. Nguyen, T.P. Vo, and H.-T. Thai, Ritz-based analytical solutions for bending, buckling and vibration behavior of laminated composite beams, International Journal of Structural Stability and Dynamics. 18(11) (2018) 1850130.

3. **N.-D. Nguyen**, T.-K. Nguyen, H.-T. Thai, and T.P. Vo, A Ritz type solution with exponential trial functions for laminated composite beams based on the modified couple stress theory, Composite Structures. 191 (2018) 154-167.

4. **N.-D. Nguyen**, T.-K. Nguyen, T.-N. Nguyen, and H.-T. Thai, New Ritz-solution shape functions for analysis of thermo-mechanical buckling and vibration of laminated composite beams, Composite Structures. 184 (2018) 452-460.

5. T.-K. Nguyen, **N.-D. Nguyen**, T.P. Vo, and H.-T. Thai, Trigonometric-series solution for analysis of laminated composite beams, Composite Structures. 160 (2017) 142-151.

Domestic papers with peer-reviews:

6. T.-K. Nguyen and **N.-D. Nguyen**, Effects of transverse normal strain on bending of laminated composite beams, Vietnam Journal of Mechanics. 40(3) (2018) 217-232.

7. X.-H. Dang, **N.-D. Nguyen**, T.-K. Nguyen, Dynamic analysis of composite beams resting on winkler foundation, Vietnam Journal of Construction (8-2017) 123-129.

8. **N.-D. Nguyen**, T.-K. Nguyen, T.-N. Nguyen, Ritz solution for buckling analysis of thin-walled composite channel beams based on a classical beam theory, Journal of Science and Technology in Civil Engineering (STCE)-NUCE. 13(3) (2019) 34-44.

Conference papers:

9. **N.-D. Nguyen**, T.-K. Nguyen, T.-N. Nguyen, and T.P. Vo, Bending Analysis of Laminated Composite Beams Using Hybrid Shape Functions, International Conference on Advances in Computational Mechanics. (2017), (503-517).

10. **N.-D. Nguyen**, T.-K. Nguyen, Free vibration analysis of laminated composite beams based on higher – order shear deformation theory. Proceeding of National Confrence-Composite Material and Structure (2016) 157-164.

11. **N.-D. Nguyen**, T.-K. Nguyen, and T.P. Vo, Hybrid-shape-functions for free vibration analysis of thin-walled laminated composite I-beams with different boundary conditions, Proceeding of National Mechanical Confrence (2017) 424-433

Table of content

List of Figures

List of Tables

Nomenclature

b, h, L: Width, height and length of rectangular beam

b_1, b_2, b_3: Top flange width, bottom flange width and web of I-section or channel section

h_1, h_2, h_3: Thichness of top flange, bottom flange and web of I-section or channel section

u_0: Axial displacement

w_0: Transverse (vertical) displacement

u_1: Rotation of a transverse normal about the y axis

w_1, w_2: Additional higher-order terms

$f(z)$: Shear variation function

u, v, w: Displacement components in x, y and z directions

$\overline{u}$, $\overline{v}$, $\overline{w}$: Mid-surface displacement components in x, y and z directions of thin-walled beam

t: Time

E or $E(n)$: Young's modulus

E_1, E_2, E_3: Young's modulus in the fibre and transverse directions

G_{12}, G_{13}, G_{23}: Shear moduli

ν, ν_{12}, ν_{13}, ν_{23}: Poisson's coefficient

p: Material parameter

α_1, α_2: Thickness ratio of ceramic material of the top and bottom flange

α_1^*, α_2^*: Thermal coefficients in local coordinate

α_x, α_y, α_{xy}: Thermal coefficients in global coordinate

β: Thickness ratio of ceramic material of the web

ρ: Mass density

ρ_c and ρ_m: Mass density of ceramic and metal

V_c: Volume fraction of ceramic material

C_{ij}: Material stiffness coefficients in local coordinate

$\bar{C}_{ij}$: Transformed material stiffness coefficients in global coordinate

$\bar{\bar{C}}_{ij}$ or $\bar{\bar{C}}^*_{ij}$: Reduced material stiffness coefficients in global coordinate

ε_{ij} or γ_{ij}: Strain

σ_{ij}: Stress

Q_{ij}: Plan stress-reduced stiffness coefficients in local coordinate

$\bar{Q}_{ij}$: Plan stress-reduced stiffness coefficients in global coordinate

Π_E: Strain energy

Π_W: Work done

Π_K: Kinetic energy

Π: Total energy

ψ_j, φ_j, ξ_j: Approximation functions

$\mathbf{K}$: Stiffness matrix

$\mathbf{M}$: Mass matrix

$\mathbf{F}$: Load Vecter

θ_x, θ_y, θ_z: Rotation about the x-, y-, z-axes

χ_{xy}, χ_{zy}: Curvature fields

m_{xy}, m_{zy}: Stress-curvature

$\xi_{kb}\left(\xi_b\right)$, ξ_{km1}, ξ_{km2}: The MLSPs in x-, y- and z-directions

U, V, W: Displacement of shear center (P) in the $x-$, $y-$, $z-$direction

ϕ: Rotation angle about pole axis

θ_s: Angle of orientation between (n,s,x) and (x,y,z) coordinate systems

ψ_y, ψ_z, ψ_ϖ: Rotations of the cross-section with respect to y, z, ϖ

ϖ:	Wapping function
I_y, I_z:	Second moment of inertia with respect $y-$, $z-$ axis
I_P:	Polar moment of inertia of the cross-section about the centroid
k_s:	Shear correction factor
ω:	Natural frequency
N_{cr}:	Critical buckling load
N_0, N_x^{0m}:	Axial mechanical load
N_x^{0t}:	Axial thermal load
q:	Uniformly distributed load
"-":	The results are not available

Abbreviations

BCs:	Boundary condition(s)
C-F:	Clamped-free
C-S:	Clamped-simply supported
C-H:	Clamped-hinged
C-C:	Clamped-clamped
CUF:	Carrera's unified formulation
CBT:	Classical beam theory
DQM:	Differential quadrature method
ESLT:	Equivalent single layer theory
FOBT:	First-order beam theory
FEM:	Finite element method
FIG:	Figure
HOBT:	Higher-order beam theory
H-H:	Hinged-hinged
LWT:	Layer-wise theory
MAT:	Material
MCST:	Modified Couple Stress Theory
MLSP:	Material Length Scale Parameter
MGLCB:	Micro general laminated composite beam
Quasi-3D:	Quasi-three dimension beam theory
S-S:	Simply-supported
ZZT:	Zig-zag theory

Chapter 1. INTRODUCTION

1.1. Composite material

1.1.1. Fiber and matrix

A composite material, which is combined of two or more materials, leads to improve properties such as stiffness, strength, weight reduction, corrosion resistance, thermal properties... than those of the individual components used alone. It is made from a reinforcement as fiber and a base as matrix, and is divided into commonly three different types [1]:

(1) Fibrous materials: fibers of one material and matrix of another one (Fig. 1.1a).

(2) Particulate composites: macro size particles of one material and matrix of another one (Fig. 1.1b).

(3) Laminate composites: made of several layers of different materials, including of the first two types.

Fiber and particle, which are harder, stronger and stiffer than matrix, provide the strength and stiffness. Matrix can be classified by strength and stiffness such as polymer (low), metal (intermediate) or ceramic (high but brittle). The matrix maintains the fibers in the right angle, spacing and protects them from abrasion and the environment.

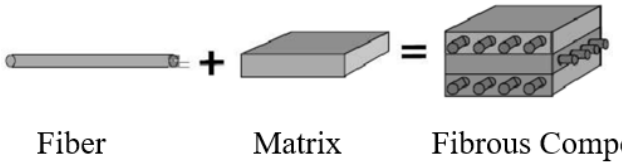

a. Fiber Composite

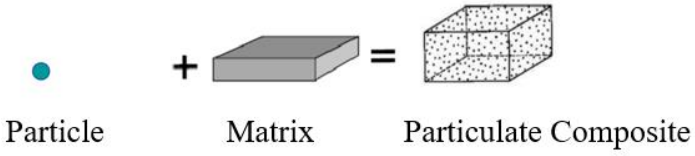

b. Particulate Composite

Figure 1.1. Composite material classification [1]

1.1.2. Lamina and laminate

A fiber-reinforced lamina consists of many fiber embedded in a matrix material. The fiber can be continuous or discontinuous, woven, unidirectional, bidirectional or randomly distributed. (Fig.1.2)

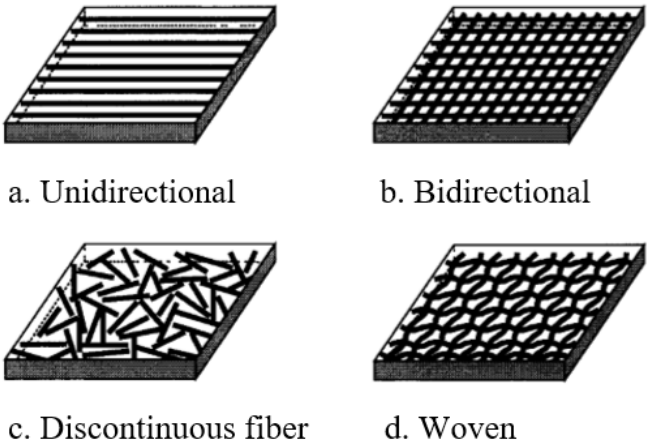

Figure 1.2. Various types of fiber-reinforced composite lamina [1]

A laminate is a collection of lamina with various orientations which are stacked to achieve the desired stiffness and thickness. The layers are usually bonded together with the same matrix material as that in a lamina. The stiffness and strength of the laminate can be tailored to meet requirements by selecting the lamination scheme and material properties of individual lamina.

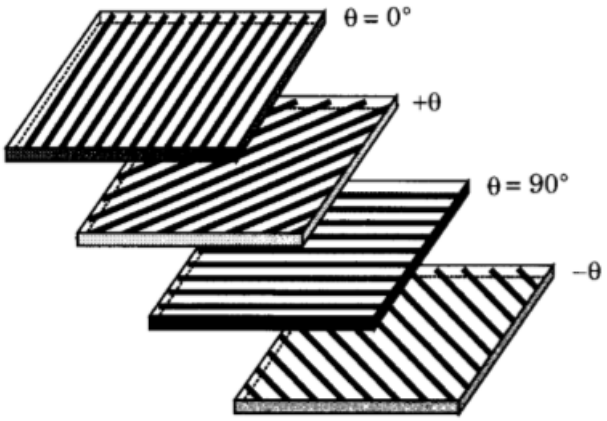

Figure 1.3. A laminate made up of laminae with different fiber orientations [1]

1.1.3. Applications

In recent years, composite materials are widely used in many fields of civil, aeronautical and mechanical engineering. The most well-known advantages of these materials are high stiffness-to-weight and strength-to-weight ratios, low thermal expansion, enhanced fatigue life and good corrosive resistance.

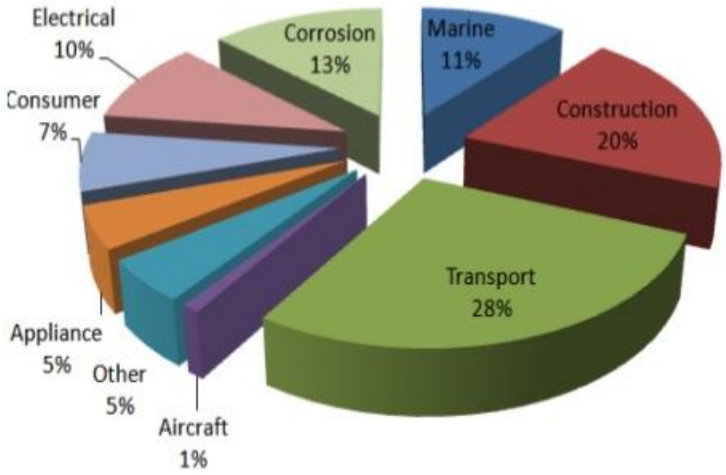

Figure 1.4. Composite material applied in engineering field [1]

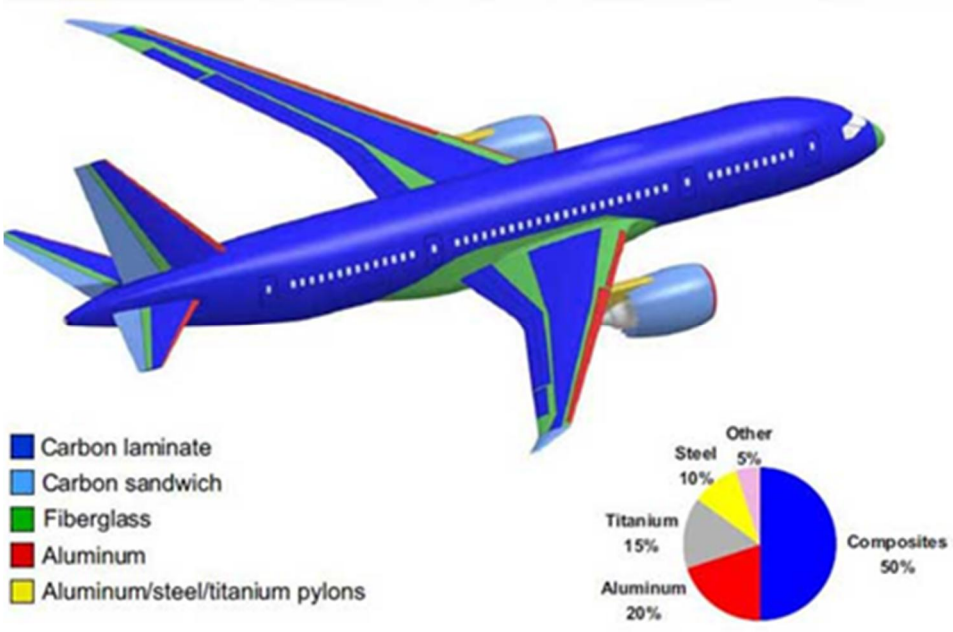

Figure 1.5. Material used in Boeing 787 [2]

1.2. Review

[1] https://www.slideshare.net/NAACO/vat-lieu-composite-frp-trong-xay-dung
[2] https://www.1001crash.com/index-page-composite-lg-2.html

In this section, a general literature review on composite beams will be performed. Next, objectives of thesis are presented. Finally, theoretical formulation and constitutive laws of laminated composite beams are established.

1.2.1. Literature review

In order to use composite materials in practice, the available literatures indicate that a large number of studies have been conducted to analyse their structural responses. Beam theories, constitutive laws and methods are proposed in order to predict vibration, buckling and bending behaviours of beams. In this section, a bief review study for laminated composite beams is presented. More review details for specific topic are available in the beginning of each chapter.

For composite beam models, a literature review on the composite beam theories can be seen in the previous works of Ghugal and Shimpi [2]. Based on equivalent single layer theories, beam theories can be divided into main categories: classical beam theory, first order beam theory, higher-order beam theory and quasi-3D beam theory. The classical beam theory neglects transverse shear strain effects, and therefore it is only suitable for thin beams. The first order shear deformation theory accounts for the transverse shear strain effect, however it requires a shear correction factor to correct inadequate distributions of the transverse shear stresses through its thickness. In order to overcome this problem, the higher-order beam theory is proposed by using distribution functions of transverse shear stresses. However, this theory ignores transverse normal strain effect, and therefore quasi-3D beam theory is presented. It can be seen that the accuracy of beam responses depends on the choices of appropriate theories, and quasi-3D beam theory is the most general one. The review work of Ghugal and Shimpi [2] also indicates that Poisson's effect on behaviours of laminated composite beams is not paid much attention. Moreover, when the behaviours of structures are considered at a small scale, the experimental studies showed that the size effect is significant to be accounted, that led to the development of Eringen's nonlocal elasticity theory [3] and strain gradient theory [4-6]. Based on this approach, many studies are investigated and applied for analysis of

composite microbeam [7-13]. The available literature indicate that studies mainly focus on cross-ply microbeams. Therefore, the study of micro general laminated composite beams with arbitrary lay-ups is necessary.

Furthermore, composite materials are applied for thin-walled structures with different sections, many studies are developed based on the thin-walled structures theory. Vlasov [14] proposed a thin-walled structure theory for isotropic materials. Bauld and Tzeng [15] expanded Vlasov's theory for buckling analysis of laminated composite thin-walled rods in which the authors analysed linear and nonlinear responses of laminated composite beams with open sections. Song and Librescu [16] investigated dynamic responses of laminated composite beams with arbitrary sections. Lee and Kim [17, 18] presented a general model to predict vibration and buckling responses of laminated composite thin-walled beams with I-sections by classical beam theory. It is clear that shear deformation effects on behaviours of thin-walled composite beams is still limited.

For computational methods, many computational methods have been developed in order to predict accurately responses of composite structures, namely, analytical, numerical and semi-numerical. The nature of these methods has been either exact or approximate. For numerical method, finite element method (FEM) is the most widely used numerical method for the free vibration, buckling and bending analysis of composite beams [19-28]. In addition, finite difference method [29, 30], Chebyshev collocation technique [31], dynamic stiffness matrix method [32] are also used to predict behaviours of beams. In recent year, isogeometric analysis [33, 34] attracted an interest of many researchers. This thesis will focus more details on analytical solutions. Among them, Navier procedure can be seen as the simplest one. Although this method is only suitable for simply supported boundary condition, it has widespread used by many authors owing to its simplicity [35, 36]. Other analytical approaches have been investigated for analysis of composite beams, including differential quadrature method (DQM) [37, 38], Galerkin method [39-41] or differential transform method [42, 43]. The Ritz method, which mainly uses in this

thesis, is the most general one which accounts for various boundary conditions. It is a variational approach in which the shape functions are chosen to approximate the unknown displacement fields. The displacement functions should be complete in the function space, and inappropriate choices of the unknown functions may cause numerical instabilities and slow convergence rates. The available literatures indicated that polynomial and orthogonal polynomial functions are used commonly for laminated composite beams. The polynomial functions usually do not satisfy the boundary conditions. Therefore, the penalty method or langrage multiplier method is used to compose the boundary conditions [44, 45]. This leads to an increase in the dimension of the stiffness and mass matrices and thus causes computational costs. The orthogonal polynomial functions overcome this drawback by satisfying the specific boundary conditions [46-48]. However, these functions have seldom been used to analyse bending behaviour of laminated composite beams. Therefore, it can be seen that there is a need for further studies about Ritz method for beam problems.

In Vietnam, the behaviour analysis of composite structures have attracted a number of researches. Nguyen-Xuan et al. [49-52], Nguyen et al. [53-55] analyse behaviours of composite plate. These studies focus on the development of advanced numerical methods such as the FEM, mesh-less method, isogeometry method and optimization theory of structures. Nguyen et al. [56-59] developed analytical methods for analysis of composite plates and shells with various geometric shapes and loading conditions. Tran et al. [60, 61] carried out some experimental studies on composite structures. Hoang et al. [62, 63] studied responses of functionally graded plates and shells under thermo-mechanical loads. Nguyen et al. [64, 65] investigated behaviors of functionally graded beams by the FEM under some different geometric and loading conditions. It is interesting that researchers in Vietnam have not paid much attention to laminated composite beam problems, especially composite thin-walled beams yet.

1.2.2. Objectives of the thesis

The literature review on the behaviours of composite beams shows that Ritz method is efficient to analyse the behaviours of composite beams with various

boundary conditions, however, the number of researches used this method is still limited. Therefore, developing the simple, effective and accurate approximation functions to solve structural behaviours of composite beams with various cross-sections is one of the primary motivations of this study. In addition, the available literature indicate that effects of Poisson ratio, normal strain, size dependent on behaviours of composite beams are not well-investigated. The main contents of this thesis include:

- Analyse free vibration, buckling and static of laminated composite beams using HOBT.
- Analyse free vibration, buckling and static of laminated composite beams using quasi-3D theory.
- Analyse free vibration, buckling and static of general micro laminated composite beams using modified couple stress theory.
- Analyse free vibration, buckling and static of thin-walled laminated composite beams using FOBT.
- Appraise and select approximation functions for analysis of laminated composite beams.

1.2.3. Beam theory

A large number of beam theories are developed to analyse the laminated composite beams. They can be divided into following categories: layer-wise theories (LWT) [66, 67], equivalent single layer theories (ESLT) [20, 35, 36, 68, 69], zig-zag theories (ZZT) [70-72], Carrera's Unified Formulation (CUF) [73, 74]… in which the ESLT are widely used owing to their simplicity in formulation as well as programming. To describe beam theories, the following coordinate system (Fig. 1.6) is introduced. The x-, y- and z-axis are taken along the length, width and height of the beam, respectively.

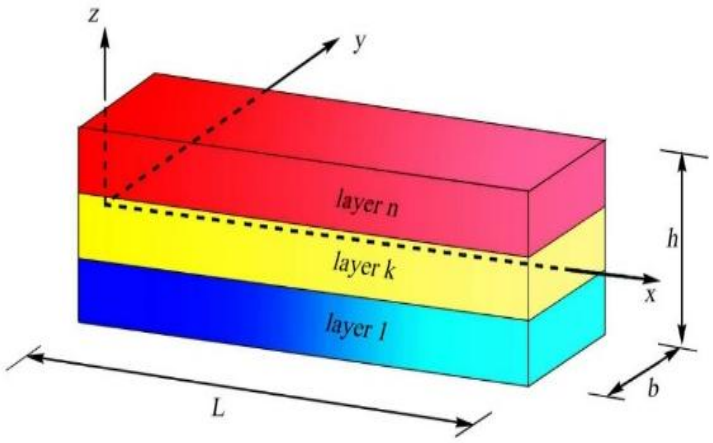

Figure 1.6. Geometry and coordinate of a rectangular laminated composite beam.

For a general beam theory, the axial and transverse displacements are presented as products of two sets of seperated unknown functions, namely the *z*-variation and *x*-variation.

$$u(x,z,t) = u_0(x,t) + zu_1(x,t) + z^2u_2(x,t) + z^3u_3(x,t) + \ldots \tag{1.1}$$

$$w(x,z,t) = w_0(x,t) + zw_1(x,t) + z^2w_2(x,t) + \ldots \tag{1.2}$$

The most simple and commonly used beam theory is the Euler-Bernoulli or classical beam theory (CBT) [75], which is based on the displacement field:

$$u(x,z,t) = u_0(x,t) - z\frac{\partial w_0(x,t)}{\partial x} \tag{1.3}$$

$$w(x,z,t) = w_0(x,t) \tag{1.4}$$

where u_0 and w_0 are the axial and vertical displacements at mid-plane of the beam, respectively. The CBT is widely used for thin beams because it ignored shear deformation effect. In order to consider this effect, Timoshenko's beam theory or the first order beam theory (FOBT) [76-78] is presented:

$$u(x,z,t) = u_0(x,t) + zu_1(x,t) \tag{1.5}$$

$$w(x,z,t) = w_0(x,t) \tag{1.6}$$

where u_1 denotes rotation of a transverse normal about the *y*-axis. FOBT requires a shear correction factor, which depends not only on the material and geometric parameters, but also on the boundary conditions and loading. In general, the determination of shear correction factor is a challenging task. For this reason, higher-

order beam theories (HOBT) have been developed. Many researcher ([69, 79-82]) proposed a third-order beam theory, which based on the displacement field:

$$u(x,z,t) = u_0(x,t) + zu_1(x,t) + z^2u_2(x,t) + z^3u_3(x,t) \tag{1.7}$$

$$w(x,z,t) = w_0(x,t) \tag{1.8}$$

By imposing traction-free boundary condition on the top and bottom face of the beam, Eqs. (1.7) and (1.8) lead to:

$$u(x,z,t) = u_0(x,t) + \left(z - \frac{4z^3}{3h^2}\right)u_1(x,t) - \frac{4z^3}{3h^2}\frac{\partial w_0}{\partial x} \tag{1.9}$$

$$w(x,z,t) = w_0(x,t) \tag{1.10}$$

The displacement field in Eqs. (1.9) and (1.10) is known as Reddy's third-order beam theory [81] . Besides, many researchers published refined high-order theories, which represent the higher-order variation of axial displacement by using $f(z)$:

$$u(x,z,t) = u_0(x,t) - z\frac{\partial w_0}{\partial x} + f(z)u_1(x,t) \tag{1.11}$$

$$w(x,z,t) = w_0(x,t) \tag{1.12}$$

It should be noted that $f(z)$ have to meets the traction-free boundary condition of beams. Some of shear functions are presented in Table 1.1.

It can be observed that the HOBT neglected transverse normal strain. To take into account this strain, quasi-3D theories [36, 83-85] have been developed based on the higher-order variations of both axial and transverse displacement:

$$u(x,z,t) = u_0(x,t) + zu_1(x,t) + z^2u_2(x,t) + z^3u_3(x,t) \tag{1.13}$$

$$w(x,z,t) = w_0(x,t) + zw_1(x,t) + z^2w_2(x,t) \tag{1.14}$$

where $w_1(x,t)$ and $w_2(x,t)$ are additional higher-order terms.

By using traction-free boundary condition on the top and bottom face of the beam, Eqs. (1.13) and (1.14) lead to:

$$u(x,z,t) = u_0(x,t) + zu_1(x,t) - \frac{1}{2}z^2\frac{\partial w_1}{\partial x} + z^3\left[-\frac{4}{3h^2}\left(\frac{\partial w_0}{\partial x} + u_1(x,t)\right) - \frac{1}{3}\frac{\partial w_2}{\partial x}\right] \tag{1.15}$$

$$w(x,z,t) = w_0(x,t) + zw_1(x,t) + z^2w_2(x,t) \tag{1.16}$$

In recent year, researchers [35, 86, 87] also proposed various quasi-3D theories which used $f(z)$ in displacement field:

$$u(x,z,t) = u_0(x,t) - z\frac{\partial w_0}{\partial x} + f(z)u_1(x,t) \tag{1.17}$$

$$w(x,z,t) = w_0(x,t) + f_{,z}(z)w_1(x,t) \tag{1.18}$$

Table 1.1. Shear variation functions $f(z)$

Model	$f(z)$
Kaczkowski [88], Panc [89], Reissner [90]	$\frac{5z}{4} - \frac{5z^3}{3h^2}$
Levinson [91], Murthy [92] , Reddy [81]	$z - \frac{4z^3}{3h^2}$
Nguyen et al. [93]	$\frac{7z}{8} - \frac{2z^3}{h^2} + \frac{2z^5}{h^4}$
Arya et al. [94]	$\sin\left(\frac{\pi z}{h}\right)$
Soldatos [95]	$h\sinh\left(\frac{z}{h}\right) - z\cosh\left(\frac{1}{2}\right)$
Karama et al. [96]	$ze^{-2\left(\frac{z}{h}\right)^2}$
Thai et al. [97]	$\sinh^{-1}\left[\sin\left(\frac{\pi z}{h}\right)\right]$
Nguyen et al. [98]	$\cot^{-1}\left(\frac{h}{z}\right) - \frac{16z^3}{15h^3}$
Nguyen et al. [99]	$z + \frac{8rz^3}{3h^2\sqrt{r^2+4}} - \sinh^{-1}\left(\frac{rz}{h}\right),\ r = 1$

1.2.4. Constitutive relation

The stress-strain relations for laminated composite beams are derived from the general three-dimensional state of stress and strain for an orthotropic ply. The

constitutive relations for the k^{th}-ply of a laminated orthotropic ply in local coordinate are defined as:

$$\begin{Bmatrix} \sigma_1 \\ \sigma_2 \\ \sigma_3 \\ \sigma_{23} \\ \sigma_{13} \\ \sigma_{12} \end{Bmatrix}^{(k)} = \begin{pmatrix} C_{11} & C_{12} & C_{13} & 0 & 0 & 0 \\ C_{12} & C_{22} & C_{23} & 0 & 0 & 0 \\ C_{13} & C_{23} & C_{33} & 0 & 0 & 0 \\ 0 & 0 & 0 & C_{44} & 0 & 0 \\ 0 & 0 & 0 & 0 & C_{55} & 0 \\ 0 & 0 & 0 & 0 & 0 & C_{66} \end{pmatrix}^{(k)} \begin{Bmatrix} \varepsilon_1 \\ \varepsilon_2 \\ \varepsilon_3 \\ \gamma_{23} \\ \gamma_{13} \\ \gamma_{12} \end{Bmatrix} \tag{1.19}$$

where C_{ij} are material stiffness coefficients. If the transverse stress is neglected $(\sigma_3 = 0)$ [1], the stress-strain relations are remained:

$$\begin{Bmatrix} \sigma_1 \\ \sigma_2 \\ \sigma_{23} \\ \sigma_{13} \\ \sigma_{12} \end{Bmatrix}^{(k)} = \begin{pmatrix} Q_{11} & Q_{12} & 0 & 0 & 0 \\ Q_{12} & Q_{22} & 0 & 0 & 0 \\ 0 & 0 & Q_{44} & 0 & 0 \\ 0 & 0 & 0 & Q_{55} & 0 \\ 0 & 0 & 0 & 0 & Q_{66} \end{pmatrix}^{(k)} \begin{Bmatrix} \varepsilon_1 \\ \varepsilon_2 \\ \gamma_{23} \\ \gamma_{13} \\ \gamma_{12} \end{Bmatrix} \tag{1.20}$$

where $Q_{ij}^{(k)}$ are the plane stress-reduced stiffness coefficients, see Appendix A. Using transformation equations, the constitutive equations for the k^{th}-ply in the global coordinate system (x,y,z) are given by:

$$\begin{Bmatrix} \sigma_x \\ \sigma_y \\ \sigma_{yz} \\ \sigma_{xz} \\ \sigma_{xy} \end{Bmatrix}^{(k)} = \begin{pmatrix} \bar{Q}_{11} & \bar{Q}_{12} & 0 & 0 & \bar{Q}_{16} \\ \bar{Q}_{12} & \bar{Q}_{22} & 0 & 0 & \bar{Q}_{26} \\ 0 & 0 & \bar{Q}_{44} & \bar{Q}_{45} & 0 \\ 0 & 0 & \bar{Q}_{45} & \bar{Q}_{55} & 0 \\ \bar{Q}_{16} & \bar{Q}_{26} & 0 & 0 & \bar{Q}_{66} \end{pmatrix}^{(k)} \begin{Bmatrix} \varepsilon_x \\ \varepsilon_y \\ \gamma_{yz} \\ \gamma_{xz} \\ \gamma_{xy} \end{Bmatrix} \tag{1.21}$$

where $\bar{Q}_{ij}^{(k)}$ are indicated in Appendix A. The one-dimensional stress states of laminated composite beams are contained by assuming plane strain in x-z plane $(\varepsilon_y = \gamma_{yz} = \gamma_{xy} = 0)$ [69, 100, 101]

$$\begin{Bmatrix} \sigma_x \\ \sigma_{xz} \end{Bmatrix}^{(k)} = \begin{pmatrix} \bar{Q}_{11} & 0 \\ 0 & \bar{Q}_{55} \end{pmatrix}^{(k)} \begin{Bmatrix} \varepsilon_x \\ \gamma_{xz} \end{Bmatrix} \tag{1.22}$$

Neglecting the strain out of *x-z* plane is equivalent to ignoring of the Poisson's effect ([85]). Therefore, this constitutive relations would be well-known as neglecting the Poisson's effect.

Another assumption is used by researchers to obtain the stress-strain relations for laminated composite beams as followings. Using transformation equations for Eq. (1.19), the elastic strain and stress relations of k^{th}-ply in global coordinate are given by:

$$\begin{Bmatrix} \sigma_x \\ \sigma_y \\ \sigma_z \\ \sigma_{yz} \\ \sigma_{xz} \\ \sigma_{xy} \end{Bmatrix}^{(k)} = \begin{pmatrix} \overline{C}_{11} & \overline{C}_{12} & \overline{C}_{13} & 0 & 0 & \overline{C}_{16} \\ \overline{C}_{12} & \overline{C}_{22} & \overline{C}_{23} & 0 & 0 & \overline{C}_{26} \\ \overline{C}_{13} & \overline{C}_{23} & \overline{C}_{33} & 0 & 0 & \overline{C}_{36} \\ 0 & 0 & 0 & \overline{C}_{44} & \overline{C}_{45} & 0 \\ 0 & 0 & 0 & \overline{C}_{45} & \overline{C}_{55} & 0 \\ \overline{C}_{16} & \overline{C}_{26} & \overline{C}_{36} & 0 & 0 & \overline{C}_{66} \end{pmatrix}^{(k)} \begin{Bmatrix} \varepsilon_x \\ \varepsilon_y \\ \varepsilon_z \\ \gamma_{yz} \\ \gamma_{xz} \\ \gamma_{xy} \end{Bmatrix} \tag{1.23}$$

where the $\overline{C}_{ij}$ are transformed elastic coefficients, see Appendix A for more detail. Moreover, a plane stress constitutive relation ([83-85, 102]) in *x-z* plane can be assumed for laminated beams. By setting $\sigma_y = \sigma_{xy} = \sigma_{yz} = 0$, Eq. (1.23) is reduced to:

$$\begin{Bmatrix} \sigma_x \\ \sigma_z \\ \sigma_{xz} \end{Bmatrix}^{(k)} = \begin{pmatrix} \overline{\overline{C}}_{11} & \overline{\overline{C}}_{13} & 0 \\ \overline{\overline{C}}_{13} & \overline{\overline{C}}_{33} & 0 \\ 0 & 0 & \overline{\overline{C}}_{55} \end{pmatrix}^{(k)} \begin{Bmatrix} \varepsilon_x \\ \varepsilon_z \\ \gamma_{xz} \end{Bmatrix} \tag{1.24}$$

where $\overline{\overline{C}}_{11}$, $\overline{\overline{C}}_{13}$, $\overline{\overline{C}}_{33}$, $\overline{\overline{C}}_{55}$ are reduced stiffness constants of k^{th}-layer in global coordinates.

If the transverse normal stress is omitted ($\sigma_z = 0$), the one-dimensional stress states of laminated composite beams are contained:

$$\begin{Bmatrix} \sigma_x \\ \sigma_{xz} \end{Bmatrix}^{(k)} = \begin{pmatrix} \overline{\overline{C}}^{*}_{11} & 0 \\ 0 & \overline{\overline{C}}^{*}_{55} \end{pmatrix}^{(k)} \begin{Bmatrix} \varepsilon_x \\ \gamma_{xz} \end{Bmatrix} \tag{1.25}$$

where $\overline{\overline{C}}^{*}_{11}$ and $\overline{\overline{C}}^{*}_{55}$ are indicated in Appendix A

It can be stated that in Eqs. (1.24) and (1.25), the Poisson's effect is incorporated in the constitutive equation.

1.3. Organization

There are eight chapters in this thesis as followings:

- Chapter One describes the purpose, scope and organization as well as the review study on laminated composite beams.
- Based on the HOBT, Chapter Two deals with the buckling, bending and free vibration behaviours of laminated composite beam. In this Chapter, new trigonometric functions are proposed for beams under various boundary conditions.
- The theoretical formulation in Chapter Two is extended in Chapter Three. Effect of mechanical and thermal load on buckling and free vibration behaviours of composite beams are considered. New hybrid functions based on a combination of admissible and exponential functions for various boundary conditions are proposed.
- Chapter Four focuses on the effects of normal strain and Poisson's ratio on buckling, bending and free vibration behaviours of beams. Both HOBT and quasi-3D theories are used to investigate effects of normal strain and Poisson's ratio, which is integrated in constitutive equations.
- The modified couple stress theory is employed in Chapter Five for micro-laminated composite beams using HOBT and the exponential functions are proposed to solve problem. Poisson's effect on buckling, bending and free vibration behaviours of general micro-laminated composite beams is investigated.
- Chapter Six analyses thin-walled laminated composite and functionally graded thin-walled beams based on FOBT. Numerical results about frequency, critical buckling load and displacement of channel and I-beams are presented.

- Study on new approximation functions is carried in Chapter Seven. Convergence, computational cost and numerical stability are investigated to verify efficiency of proposed functions.
- In the last Chapter, the main conclusions and recommendations for future research are presented.

Chapter 2. ANALYSIS OF LAMINATED COMPOSITE BEAMS BASED ON A HIGH-ORDER BEAM THEORY [3]

2.1. Introduction

In order to predict accurately structural responses of composite laminated beams, various beam theories with different approaches have been developed. A general review and assessment of these theories for composite beams can be found in [2, 103-105]. It should be noted that HOBT has been increasingly applied in predicting responses of composite beams.

For numerical methods, finite element method has been widely used to analyse composite beams [20-27, 106-108]. For analytical approach, Navier solution is the simplest one, which is only applicable for simply supported boundary conditions (BCs) [35, 36, 83, 109]. In order to deal with arbitrary boundary conditions, many researchers developed different methods. Ritz-type method is commonly used [44, 47, 48, 100]. Khdeir and Reddy [101, 110] developed state-space approach to derive exact solutions for the natural frequencies and critical buckling loads of cross-ply composite beams. Chen et al. [84] also proposed an analytical solution based on state-space differential quadrature for vibration of composite beams. By using the dynamic stiffness matrix method, Jun et al. [32, 111] calculated the natural frequencies of composite beams based on third-order beam theory. A literature review shows that although Ritz procedure is efficient to deal with static, buckling and vibration problems of composite beams with various boundary conditions, the research on this interesting topic is still limited.

The objectives of this Chapter is to develop a new trigonometric-series solution for analysis of composite beams. It is based on a higher-order beam theory which accounts for a higher-order variation of the axial displacement. By using Lagrange equations, the governing equations of motion are derived. Ritz-type analytical solution with new trigonometric series is developed for beams under various boundary conditions. The convergence and verification studies are carried out to

[3] A slightly different version of this chapter has been published in Composite Structures in 2017

demonstrate the accuracy of the proposed solution. Numerical results are presented to investigate the effects of length-to-height ratio, fibre angle and material anisotropy on the deflections, stresses, natural frequencies and critical buckling loads of composite beams.

2.2. Beam model based on the HOBT

A laminated composite beam with rectangular section (bxh) and length L as shown in Fig. 2.1 is considered. It is made of n plies of orthotropic materials in different fibre angles with respect to the x-axis.

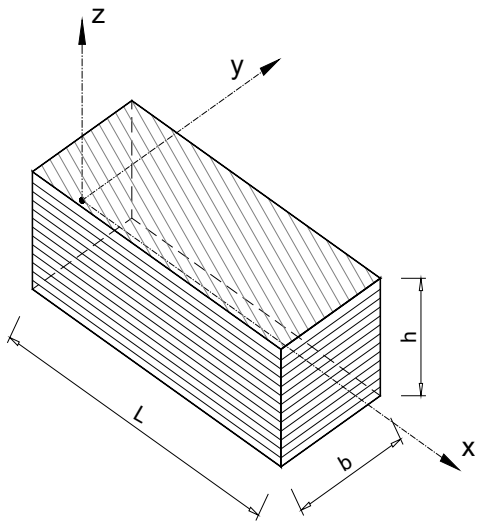

Figure 2.1. Geometry and coordinate of a laminated composite beam.

2.2.1. Kinetic, strain and stress relations

In this Chapter, the displacement field of composite beams is based on the HOBT [89, 90] as:

$$u(x,z,t) = u_0(x,t) - z\frac{\partial w_0(x,t)}{\partial x} + \left(\frac{5z}{4} - \frac{5z^3}{3h^2}\right)u_1(x,t) = u_0(x,t) - zw_{0,x} + f(z)u_1(x,t) \tag{2.1}$$

$$w(x,z,t) = w_0(x,t) \tag{2.2}$$

where the comma indicates the partial differentiation with respect to the corresponding subscript coordinate; $u_0(x,t)$ and $w_0(x,t)$ are the axial and vertical displacements at mid-plane of the beam, respectively; $u_1(x,t)$ is the rotation of a transverse normal about the y-axis; $f(z)$ represents the higher-order variation of axial displacement. The non-zero strain of beams is obtained as:

$$\varepsilon_x = \frac{\partial u}{\partial x} = \varepsilon_x^0 + z\kappa_x^b + f\kappa_x^s \tag{2.3}$$

$$\gamma_{xz} = \frac{\partial u}{\partial z} + \frac{\partial w}{\partial x} = gu_1 \tag{2.4}$$

where

$$\kappa_x^b = -w_{0,xx}, \kappa_x^s = u_{1,x}, g = f_{,z} \tag{2.5}$$

The elastic strain and stress relations of k^{th}-layer in global coordinates is given by:

$$\begin{Bmatrix} \sigma_x \\ \sigma_{xz} \end{Bmatrix}^{(k)} = \begin{pmatrix} \overline{Q}_{11} & 0 \\ 0 & \overline{Q}_{55} \end{pmatrix}^{(k)} \begin{Bmatrix} \varepsilon_x \\ \gamma_{xz} \end{Bmatrix} \tag{2.6}$$

where the $\overline{Q}_{ij}^{(k)}$ are showed in Appendix A.

2.2.2. Variational formulation

The strain energy Π_E of beam is given by:

$$\Pi_E = \frac{1}{2}\int_V \left(\sigma_x\varepsilon_x + \sigma_{xz}\gamma_{xz}\right)dV$$

$$= \frac{1}{2}\int_0^L \left[A(u_{0,x})^2 - 2Bu_{0,x}w_{0,xx} + D(w_{0,xx})^2 + 2B^s u_{0,x}u_{1,x} - 2D^s w_{0,xx}u_{1,x} + H^s(u_{1,x})^2 + A^s(u_1)^2 \right]dx \tag{2.7}$$

where the stiffness coefficients of the beam are determined as follows:

$$\left(A, B, D, B^s, D^s, H^s\right) = \sum_{k=1}^{n}\int_{z_k}^{z_{k+1}} \overline{Q}_{11}^{(k)}\left(1, z, z^2, f, zf, f^2\right)bdz \tag{2.8}$$

$$A^s = \sum_{k=1}^{n}\int_{z_k}^{z_{k+1}} \overline{Q}_{55}^{(k)} g^2 bdz \tag{2.9}$$

The work done Π_W by the compression load N_0 and transverse load q is given by:

$$\Pi_W = \int_0^L qw_0 bdx - \frac{1}{2}\int_0^L N_0(w_{0,x})^2 bdx \tag{2.10}$$

The kinetic energy Π_K of beam is expressed as:

$$\Pi_K = \frac{1}{2}\int_V \rho(z)\left(\dot{u}^2 + \dot{w}^2\right)dV$$

$$= \frac{1}{2}\int_0^L \left[I_0 \dot{u}_0^2 - 2I_1 \dot{u}_0 \dot{w}_{0,x} + I_2 \left(\dot{w}_{0,x} \right)^2 + 2J_1 \dot{u}_1 \dot{u}_0 - 2J_2 \dot{u}_1 \dot{w}_{0,x} + K_2 \dot{u}_1^2 + I_0 \dot{w}_0^2 \right] dx \qquad (2.11)$$

where dot-superscript denotes the differentiation with respect to the time t; ρ is the mass density of each layer, and I_0, I_1, I_2, J_1, J_2, K_2 are the inertia coefficients determined by:

$$\left(I_0, I_1, I_2, J_1, J_2, K_2 \right) = \sum_{k=1}^{n} \int_{z_k}^{z_{k+1}} \rho^{(k)} \left(1, z, z^2, f, zf, f^2 \right) b dz \qquad (2.12)$$

The total energy Π of beam is obtained as:

$$\Pi = \Pi_E + \Pi_W - \Pi_K$$

$$\Pi = \frac{1}{2}\int_0^L \left[A(u_{0,x})^2 - 2Bu_{0,x}w_{0,xx} + D(w_{0,xx})^2 + 2B^s u_{0,x}u_{1,x} - 2D^s w_{0,xx}u_{1,x} + H^s (u_{1,x})^2 + A^s (u_1)^2 \right] dx$$

$$+ \int_0^L q w_0 b dx - \frac{1}{2}\int_0^L N_0 (w_{0,x})^2 b dx$$

$$- \frac{1}{2}\int_0^L \left[I_0 \dot{u}_0^2 - 2I_1 \dot{u}_0 \dot{w}_{0,x} + I_2 \left(\dot{w}_{0,x} \right)^2 + 2J_1 \dot{u}_1 \dot{u}_0 - 2J_2 \dot{u}_1 \dot{w}_{0,x} + K_2 \dot{u}_1^2 + I_0 \dot{w}_0^2 \right] dx \qquad (2.13)$$

In this Chapter, Ritz solution is used to approximate the displacement field as:

$$u_0(x,t) = \sum_{j=1}^{m} \psi_j(x) u_{0j} e^{i\omega t} \qquad (2.14)$$

$$w_0(x,t) = \sum_{j=1}^{m} \varphi_j(x) w_{0j} e^{i\omega t} \qquad (2.15)$$

$$u_1(x,t) = \sum_{j=1}^{m} \xi_j(x) u_{1j} e^{i\omega t} \qquad (2.16)$$

where ω is the frequency, $i^2 = -1$ the imaginary unit; u_{0j}, w_{0j}, u_{1j} are values to be determined; $\psi_j(x)$, $\varphi_j(x)$, and $\xi_j(x)$ are approximation functions which proposed simply-supported (S-S), clamped-free (C-F) and clamped-clamped (C-C) (see Table 2.1). It is clear that the proposed approximation functions satisfy various boundary conditions given in Table 2.2. It is noted that the inappropriate approximation functions may cause slow convergence rates and numerical instabilities [48, 100]. In

addition, for approximation functions which do not satisfy boundary conditions, Lagrangian multipliers method can be used to impose boundary conditions [98, 112].

Table 2.1. Approximation functions of the beams.

BC	$\psi_j(x)$	$\varphi_j(x)$	$\xi_j(x)$
S-S	$\cos\left(\frac{j\pi x}{L}\right)$	$\sin\left(\frac{j\pi x}{L}\right)$	$\cos\left(\frac{j\pi x}{L}\right)$
C-F	$\sin\left(\frac{(2j-1)\pi x}{2L}\right)$	$1-\cos\left(\frac{(2j-1)\pi x}{2L}\right)$	$\sin\left(\frac{(2j-1)\pi x}{2L}\right)$
C-C	$\sin\left(\frac{2j\pi x}{L}\right)$	$\sin^2\left(\frac{j\pi x}{L}\right)$	$\sin\left(\frac{2j\pi x}{L}\right)$

Table 2.2. Kinematic BCs of the beams.

BC	Position	Value
S-S	x=0	$w_0 = 0$
	x=L	$w_0 = 0$
C-F	x=0	$u_0 = 0, w_0 = 0, w_{0,x} = 0, u_1 = 0$
	x=L	
C-C	x=0	$u_0 = 0, w_0 = 0, w_{0,x} = 0, u_1 = 0$
	x=L	$u_0 = 0, w_0 = 0, w_{0,x} = 0, u_1 = 0$

The governing equations of motion can be obtained by substituting Eqs. (2.14, 2.15 and 2.16) into Eq. (2.13) and using Lagrange's equations:

$$\frac{\partial \Pi}{\partial p_j} - \frac{d}{dt}\frac{\partial \Pi}{\partial \dot{p}_j} = 0 \tag{2.17}$$

with p_j representing the values of (u_{0j}, w_{0j}, u_{1j}), the bending, buckling and vibration responses of beams can be obtained from the following equations:

$$\left(\begin{bmatrix} \mathbf{K}^{11} & \mathbf{K}^{12} & \mathbf{K}^{13} \\ {}^T\mathbf{K}^{12} & \mathbf{K}^{22} & \mathbf{K}^{23} \\ {}^T\mathbf{K}^{13} & {}^T\mathbf{K}^{23} & \mathbf{K}^{33} \end{bmatrix} - \omega^2 \begin{bmatrix} \mathbf{M}^{11} & \mathbf{M}^{12} & \mathbf{M}^{13} \\ {}^T\mathbf{K}^{12} & \mathbf{M}^{22} & \mathbf{M}^{23} \\ {}^T\mathbf{K}^{13} & {}^T\mathbf{M}^{23} & \mathbf{M}^{33} \end{bmatrix}\right) \begin{Bmatrix} \mathbf{u_0} \\ \mathbf{w_0} \\ \mathbf{u_1} \end{Bmatrix} = \begin{Bmatrix} \mathbf{0} \\ \mathbf{F} \\ \mathbf{0} \end{Bmatrix} \tag{2.18}$$

where the components of stiffness matrix **K**, mass matrix **M** and vector **F** are given by:

$$K_{ij}^{11} = A\int_0^L \psi_{i,x}\psi_{j,x}dx,\ K_{ij}^{12} = -B\int_0^L \psi_{i,x}\varphi_{j,xx}dx,\ K_{ij}^{13} = B^s\int_0^L \psi_{i,x}\xi_{j,x}dx$$

$$K_{ij}^{22} = D\int_0^L \varphi_{i,xx}\varphi_{j,xx}dx - N_0\int_0^L \varphi_{i,x}\varphi_{j,x}dx,\ K_{ij}^{23} = -D^s\int_0^L \varphi_{i,xx}\xi_{j,x}dx,$$

$$K_{ij}^{33} = -H^s\int_0^L \xi_{i,x}\xi_{j,x}dx + A^s\int_0^L \xi_i\xi_j dx,\ M_{ij}^{11} = I_0\int_0^L \psi_i\psi_j dx,\ M_{ij}^{12} = -I_1\int_0^L \psi_i\varphi_{j,x}dx$$

$$M_{ij}^{13} = -J_1\int_0^L \psi_i\xi_j dx, M_{ij}^{22} = I_0\int_0^L \varphi_i\varphi_j dx + I_2\int_0^L \varphi_{i,x}\varphi_{j,x}dx,\ M_{ij}^{23} = -J_2\int_0^L \varphi_{i,x}\xi_j dx,$$

$$M_{ij}^{33} = K_2\int_0^L \xi_i\xi_j dx,\quad F_i = \int_0^L q\varphi_i dx \tag{2.19}$$

The deflection, stresses, critical buckling loads and natural frequencies of composite beams can be determined by solving Eq. (2.18).

2.3. Numerical examples

In this section, convergence and verification studies are carried out to demonstrate the accuracy of the proposed solution and to investigate the responses of composite beams with various boundary conditions for bending, vibration and buckling problems. For static analysis, the beam is subjected to a uniformly distributed load with density q. Laminates are supposed to have equal thicknesses and made of the same orthotropic materials (MAT) whose properties are followed:

- Material I.2 $E_1 / E_2 = \text{open}$, $G_{12} = G_{13} = 0.6E_2$, $G_{23} = 0.5E_2$, $\upsilon_{12} = 0.25$ (2.20)
- Material II.2 $E_1 / E_2 = \text{open}$, $G_{12} = G_{13} = 0.5E_2$, $G_{23} = 0.2E_2$, $\upsilon_{12} = 0.25$ (2.21)
- Material III.2 $E_1 = 144.9\,\text{GPa}$, $E_2 = 9.65\,\text{GPa}$, $G_{12} = G_{13} = 4.14\,\text{GPa}$, $G_{23} = 3.45\,\text{GPa}$ $\upsilon_{12} = 0.3$, $\rho = 1389\,kg/m^3$ (2.22)

For convenience, the following normalized terms are used:

$$\bar{w} = \frac{100w_0E_2bh^3}{qL^4},\ \sigma_{xx} = \frac{bh^2}{qL^2}\sigma_{xx}\left(\frac{L}{2},\frac{h}{2}\right),\ \sigma_{xz} = \frac{bh}{qL}\sigma_{xz}\left(0,0\right) \tag{2.23}$$

$$\bar{\omega} = \frac{\omega L^2}{h}\sqrt{\frac{\rho}{E_2}} \text{ for Material I.2 and II.2, } \bar{\omega} = \frac{\omega L^2}{h}\sqrt{\frac{\rho}{E_1}} \text{ for Material III.2} \tag{2.24}$$

$$\bar{N}_{cr} = N_{cr}\frac{L^2}{E_2 bh^3} \text{ for Material I.2 and II.2, } \bar{N}_{cr} = N_{cr}\frac{L^2}{E_1 bh^3} \text{ for Material III.2} \quad (2.25)$$

In order to evaluate the convergence and reliability of the proposed solution, ($0^0/90^0/0^0$) composite beams (L/h = 5) with MAT I.2 and $E_1 / E_2 = 40$ are considered. The mid-span displacements, fundamental natural frequencies and critical buckling loads with respect to the series number m for different boundary conditions are given in Table 2.3. It is observed that the responses converge quickly for three boundary conditions: m = 2 for buckling, m = 12 for vibration, and m = 14 for deflection. Thus, these numbers of series terms will be used for buckling, vibration and static analysis, respectively throughout the numerical examples. In comparison, the present trigonometric solution appears convergence more quickly than the polynomial series solution [98] especially for buckling analysis.

Table 2.3. Convergence studies for the non-dimensional fundamental frequencies, critical buckling loads and mid-span displacements of ($0^0/90^0/0^0$) composite beams (MAT I.2, $L / h = 5$, $E_1/E_2 = 40$).

BC	m							
	2	4	6	8	10	12	14	16
a. Fundamental frequency								
S-S	9.2084	9.2084	9.2084	9.2084	9.2084	9.2084	9.2084	9.2084
C-F	4.3499	4.2691	4.2473	4.2394	4.2359	4.2342	4.2332	4.2327
C-C	11.8716	11.6673	11.6269	11.6143	11.6093	11.6069	11.6056	11.6048
b. Critical buckling load								
S-S	8.6132	8.6132	8.6132	8.6132	8.6132	8.6132	8.6132	8.6132
C-F	4.7080	4.7080	4.7080	4.7080	4.7080	4.7080	4.7080	4.7080
C-C	11.6518	11.6518	11.6518	11.6518	11.6518	11.6518	11.6518	11.6518
c. Deflection								
S-S	1.4978	1.4632	1.4685	1.4671	1.4676	1.4674	1.4675	1.4674
C-F	3.6160	4.0311	4.1035	4.1380	4.1499	4.1571	4.1604	4.1626
C-C	0.8696	0.9183	0.9274	0.9301	0.9311	0.9316	0.9319	0.9320

2.3.1. Static analysis

As the first example, $(0^0/90^0/0^0)$ and $(0^0/90^0)$ composite beams with MAT II.2 and $E_1 / E_2 = 25$ are considered. Their mid-span displacements for various boundary conditions with 4 ratios of length-to-height, L/h = 5; 10; 20; 50 are given in Tables 2.4 and 2.5, and then being compared to earlier studies. It is observed that the present solutions are in excellent agreement with those calculated by various higher-order beam theories [20, 22, 24, 36, 69]. The axial and transverse shear stresses of these beams with L/h = 5; 10 are presented in Table 2.6 and compared to solutions obtained by Vo and Thai [22], and Zenkour [36]. Good agreements with the previous models are also found.

Table 2.4. Normalized mid-span displacements of $(0^0/90^0/0^0)$ composite beam under a uniformly distributed load (MAT II.2, E_1/E_2 = 25).

BC	Theory	L/h			
		5	10	20	50
S-S	Present	2.412	1.096	0.759	0.665
	Murthy et al. [24]	2.398	1.090	-	0.661
	Khdeir and Reddy [69]	2.412	1.096	-	0.665
	Vo and Thai (HOBT) [22]	2.414	1.098	0.761	0.666
	Zenkour [36]	2.414	1.098	-	0.666
	Mantari and Canales [20]	-	1.097	-	-
C-F	Present	6.813	3.447	2.520	2.250
	Murthy et al. [24]	6.836	3.466	-	2.262
	Khdeir and Reddy [69]	6.824	3.455	-	2.251
	Vo and Thai (HOBT) [22]	6.830	3.461	2.530	2.257
	Mantari and Canales [20]	-	3.459	-	-
C-C	Present	1.536	0.531	0.236	0.147
	Khdeir and Reddy [69]	1.537	0.532	-	0.147
	Mantari and Canales [20]	-	0.532	-	-

Table 2.5. Normalized mid-span displacements of ($0^0/90^0$) composite beam under a uniformly distributed load (MAT II.2, $E_1/E_2 = 25$).

BC	Theory	L/h			
		5	10	20	50
S-S	Present	4.777	3.688	3.413	3.336
	Murthy et al. [24]	4.750	3.668	-	3.318
	Khdeir and Reddy [69]	4.777	3.688	-	3.336
	Vo and Thai (HOBT) [22]	4.785	3.696	3.421	3.344
	Zenkour [36]	4.788	3.697	-	3.344
	Mantari and Canales [20]	-	3.731	-	-
C-F	Present	15.260	12.330	11.556	11.335
	Murthy et al. [24]	15.334	12.398	-	11.392
	Khdeir and Reddy [69]	15.279	12.343	-	11.337
	Vo and Thai (HOBT) [22]	15.305	12.369	11.588	11.363
	Mantari and Canales [20]	-	12.475	-	-
C-C	Present	1.920	1.004	0.752	0.679
	Khdeir and Reddy [69]	1.922	1.005	-	0.679
	Mantari and Canales [20]	-	1.010	-	-

Table 2.6. Normalized stresses of ($0^0/90^0/0^0$) and ($0^0/90^0$) composite beams with simply-supported boundary conditions (MAT II.2, $E_1/E_2 = 25$).

Lay-up	Theory	$\bar{\sigma}_{xx}$		$\bar{\sigma}_{xz}$	
		L/h=5	10	L/h=5	10
$0^0/90^0/0^0$	Present	1.0696	0.8516	0.4050	0.4289
	Zenkour [36]	1.0669	0.8500	0.4057	0.4311
	Vo and Thai (HOBT) [22]	1.0670	0.8503	0.4057	0.4311
$0^0/90^0$	Present	0.2362	0.2343	0.9174	0.9483
	Zenkour [36]	0.2362	0.2343	0.9211	0.9572
	Vo and Thai (HOBT) [22]	0.2361	0.2342	0.9187	0.9484

The variation of the axial and shear stress through the beam depth is displayed in Fig. 2.2 in which a parabolic distribution and traction-free boundary conditions of shear stress is observed.

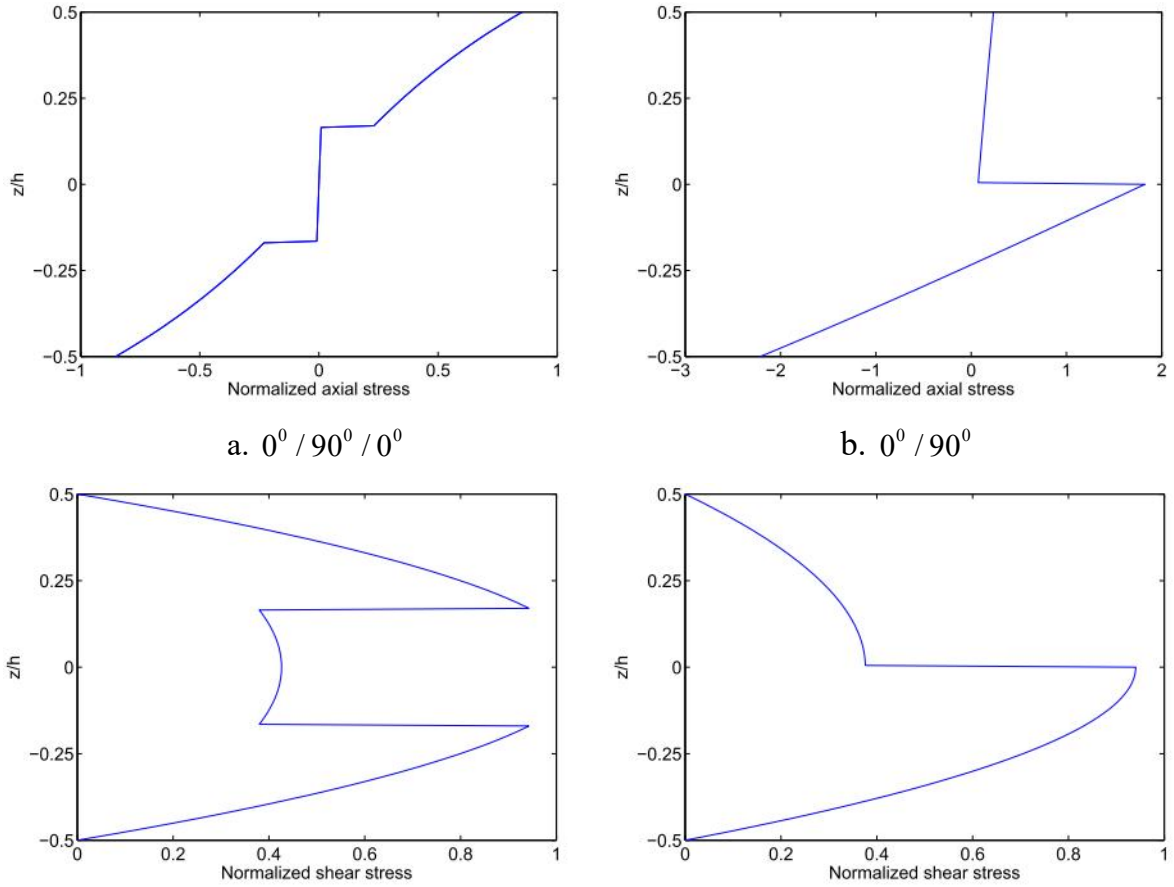

a. $0^0 / 90^0 / 0^0$ b. $0^0 / 90^0$

c. $0^0 / 90^0 / 0^0$ d. $0^0 / 90^0$

Figure 2.2. Distribution of the normalized stresses ($\bar{\sigma}_{xx}$, $\bar{\sigma}_{xz}$) through the beam depth of ($0^0/90^0/0^0$) and ($0^0/90^0$) composite beams with simply-supported boundary conditions (MAT II.2, $E_1/E_2 = 25$).

Next, the effect of fiber angle change on the mid-span displacements of $(\theta/-\theta)_S$ composite beams ($L/h = 10$) with MAT II.2 and $E_1 / E_2 = 25$ is plotted in Fig. 2.3. It can be seen that the mid-span transverse displacement increases with the fibre angle, the lower curve corresponds to the C-F beams while the highest curve is C-C ones.

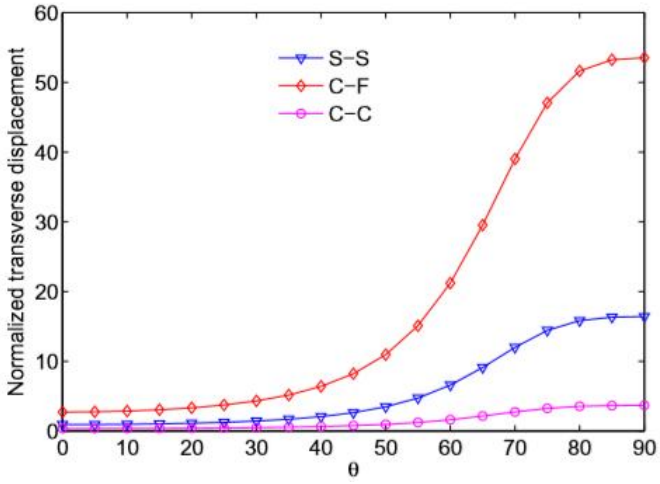

Figure 2.3. Effects of the fibre angle change on the normalized transverse displacement of $(\theta/-\theta)_s$ composite beams ($L/h=10$, MAT II.2, $E_1/E_2=25$).

2.3.2. Vibration and buckling analysis

Table 2.7. Normalized critical buckling loads of ($0^0/90^0/0^0$) and ($0^0/90^0$) composite beams (MAT I.2, $E_1/E_2=40$).

BC	Lay-ups	Theory	*L*/*h*			
			5	10	20	50
S-S	($0^0/90^0/0^0$)	Present	8.613	18.832	27.086	30.906
		Mantari and Canales [44]	8.585	18.796	-	-
		Khdeir and Reddy [110]	8.613	18.832	-	-
	($0^0/90^0$)	Present	3.907	4.942	5.297	5.406
		Aydogdu [48]	3.906	-	-	-
		Mantari and Canales [44]	3.856	4.887	-	-
C-F	($0^0/90^0/0^0$)	Present	4.708	6.772	7.611	7.886
		Mantari and Canales [44]	4.673	6.757	-	-
		Khdeir and Reddy [110]	4.708	6.772	-	-
	($0^0/90^0$)	Present	1.236	1.324	1.349	1.356
		Aydogdu [48]	1.235	-	-	-
		Mantari and Canales [44]	1.221	1.311	-	-
C-C	($0^0/90^0/0^0$)	Present	11.652	34.453	75.328	114.398
		Mantari and Canales [44]	11.502	34.365	-	-
		Khdeir and Reddy [110]	11.652	34.453	-	-
	($0^0/90^0$)	Present	8.674	15.626	19.768	21.372
		Mantari and Canales [44]	8.509	15.468	-	-

Tables 2.7-2.9 report the fundamental frequencies and critical buckling loads of ($0^0/90^0/0^0$) and ($0^0/90^0$) composite beams with different boundary conditions. The present solutions are validated by comparison with those derived from HOBTs [21, 24, 44, 48, 100, 101, 110]. Excellent agreements between solutions from the present model and previous ones are observed while a slight deviation with those from Mantari and Canales [44] is found for L/h = 5.

Table 2.8. Normalized critical buckling loads of ($0^0/90^0/0^0$) and ($0^0/90^0$) composite beams with simply-supported boundary conditions (MAT I.2 and II.2, E_1/E_2 = 10).

Lay-ups	Theory	L/h			
		5	10	20	50
MAT I.2					
($0^0/90^0/0^0$)	Present	4.727	6.814	7.666	7.945
	Aydogdu [48]	4.726	-	7.666	-
	Vo and Thai [21]	4.709	6.778	7.620	7.896
($0^0/90^0$)	Present	1.920	2.168	2.241	2.262
	Aydogdu [48]	1.919	-	2.241	-
	Vo and Thai [21]	1.910	2.156	2.228	2.249
MAT II.2					
($0^0/90^0/0^0$)	Present	3.728	6.206	7.460	7.909
	Aydogdu [48]	3.728	-	7.459	-
	Vo and Thai [21]	3.717	6.176	7.416	7.860
($0^0/90^0$)	Present	1.766	2.116	2.227	2.260
	Aydogdu [48]	1.765	-	2.226	-
	Vo and Thai [21]	1.758	2.104	2.214	2.247

The first three mode shapes of ($0^0/90^0/0^0$) and ($0^0/90^0$) composite beams (L/h = 10) with MAT I.2 and $E_1 / E_2 = 40$ is plotted in Fig. 2.4. It can be seen that the symmetric beam exhibits double coupled vibration (w_0 , u_1) whereas the anti-symmetric one presents triply coupled vibration (u_0, w_0, u_1).

Table 2.9. Normalized fundamental frequencies of $(0^0/90^0/0^0)$ and $(0^0/90^0)$ composite beams (MAT I.2, $E_1/E_2 = 25$).

BC	Lay-ups	Theory	L/h			
			5	10	20	50
S-S	$(0^0/90^0/0^0)$	Present	9.208	13.614	16.338	17.462
		Murthy et al. [24]	9.207	13.611	-	-
		Khdeir and Reddy [101]	9.208	13.614	-	-
		Aydogdu [100]	9.207	-	16.337	-
		Vo and Thai [21]	9.206	13.607	16.327	-
		Mantari and Canales [44]	9.208	13.610	-	-
	$(0^0/90^0)$	Present	6.128	6.945	7.219	7.302
		Murthy et al. [24]	6.045	6.908	-	-
		Khdeir and Reddy [101]	6.128	6.945	-	-
		Aydogdu [100]	6.144	-	7.218	-
		Vo and Thai [21]	6.058	6.909	7.204	7.296
		Mantari and Canales [44]	6.109	6.913	-	-
C-F	$(0^0/90^0/0^0)$	Present	4.234	5.498	6.070	6.267
		Murthy et al. [24]	4.230	5.491	-	-
		Khdeir and Reddy [101]	4.234	5.495	-	-
		Aydogdu [100]	4.234	-	6.070	-
		Mantari and Canales [44]	4.221	5.490	-	-
	$(0^0/90^0)$	Present	2.383	2.543	2.591	2.605
		Murthy et al. [24]	2.378	2.541	-	-
		Khdeir and Reddy [101]	2.386	2.544	-	-
		Aydogdu [100]	2.384	-	2.590	-
		Mantari and Canales [44]	2.375	2.532	-	-
C-C	$(0^0/90^0/0^0)$	Present	11.607	19.728	29.695	37.679
		Murthy et al. [24]	11.602	19.719	-	-
		Khdeir and Reddy [101]	11.603	19.712	-	-
		Aydogdu [100]	11.637	-	26.926	-
		Mantari and Canales [44]	11.486	19.652	-	-
	$(0^0/90^0)$	Present	10.027	13.670	15.661	16.429
		Murthy et al. [24]	10.011	13.657	-	-
		Khdeir and Reddy [101]	10.026	13.660	-	-
		Aydogdu [100]	10.102	-	15.688	-
		Mantari and Canales [44]	9.974	13.628	-	-

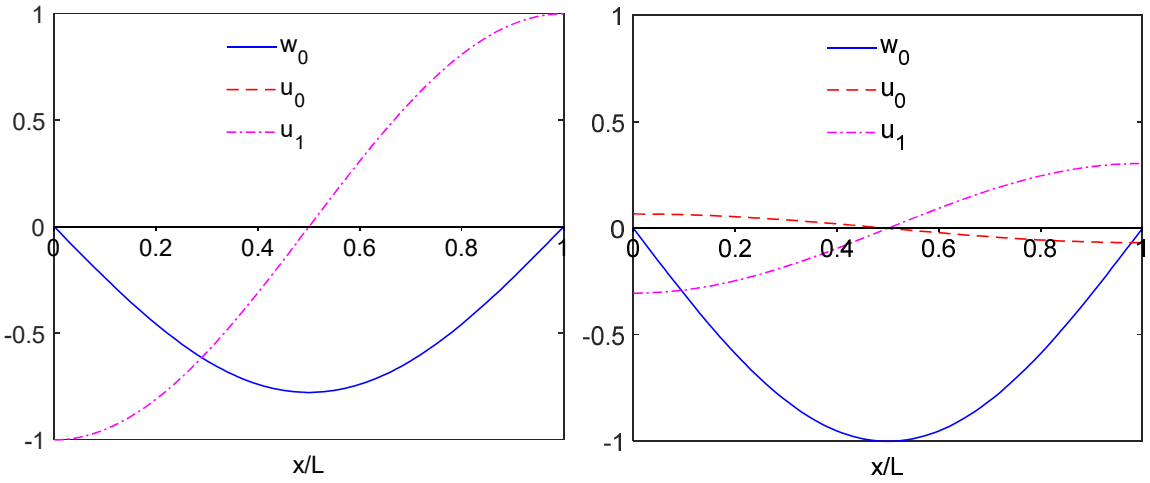

a. $\bar{\omega}_1 = 13.6136$ $(0^0/90^0/0^0)$ b. $\bar{\omega}_1 = 6.9451$ $(0^0/90^0)$

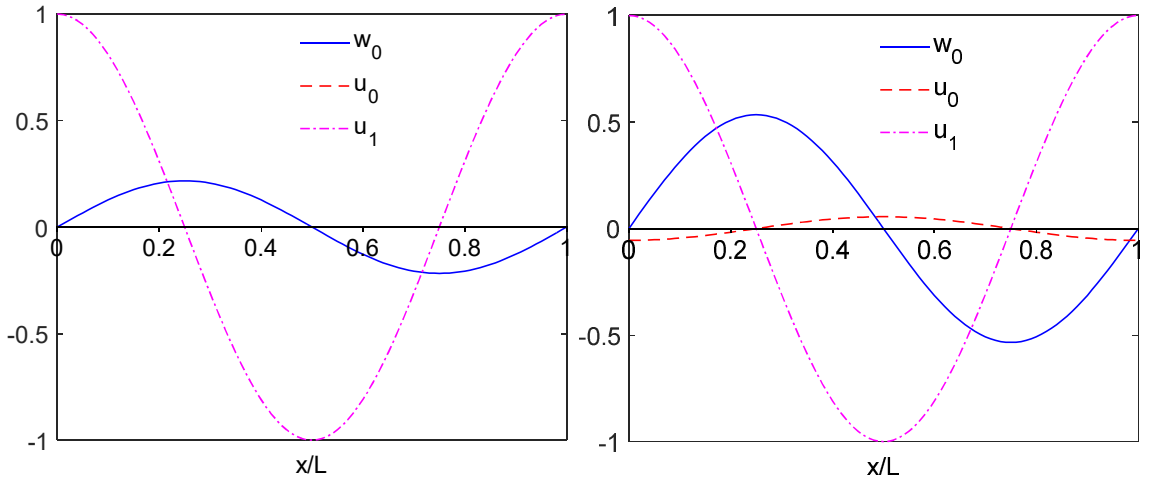

c. $\bar{\omega}_2 = 36.8334$ $(0^0/90^0/0^0)$ d. $\bar{\omega}_2 = 24.5139$ $(0^0/90^0)$

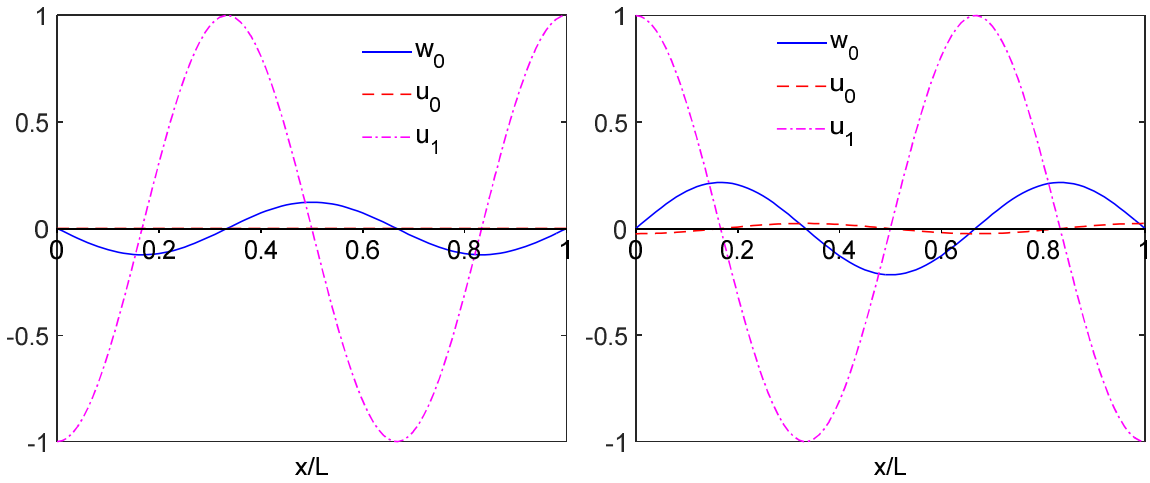

e. $\bar{\omega}_3 = 60.8686$ $(0^0/90^0/0^0)$ f. $\bar{\omega}_3 = 47.5396$ $(0^0/90^0)$

Figure 2.4.The first three mode shapes of $(0^0/90^0/0^0)$ and $(0^0/90^0)$ composite beams with simply-supported boundary conditions (L/h = 10, MAT I.2, E_1/E_2 = 40).

The effect of the ratio of material anisotropy on the fundamental frequencies and critical buckling loads is plotted in Fig. 2.5. Obviously, the results increase with E_1 / E_2

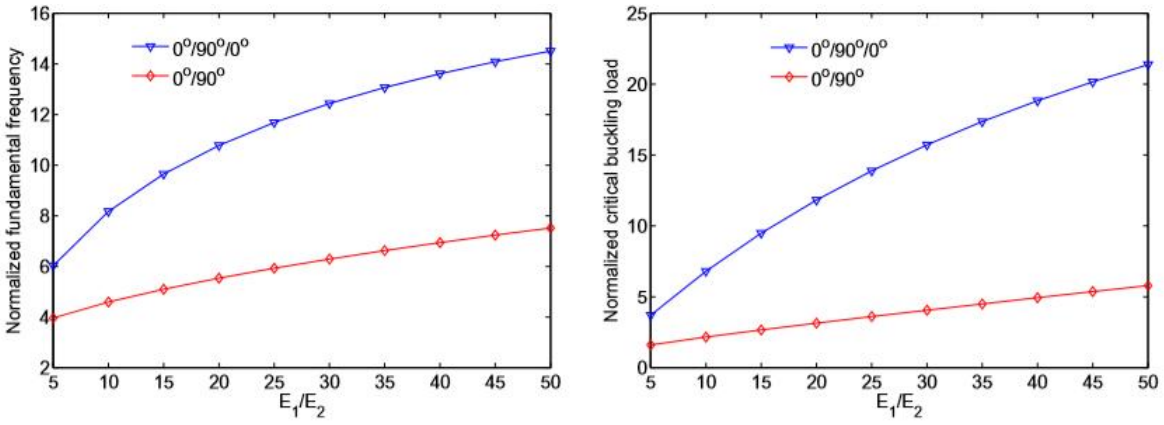

a. b.

Figure 2.5. Effects of material anisotropy on the normalized fundamental frequencies and critical buckling loads of $(0^0/90^0/0^0)$ and $(0^0/90^0)$ composite beams with simplysupported boundary conditions ($L / h = 10$, MAT I.2).

Finally, $(\theta / -\theta)_S$ composite beams (L/h = 15) with MAT III.2 are analysed. The effects of fibre angle variation on the fundamental frequencies and critical buckling loads are illustrated in Table 2.10 and Fig. 2.6. It can be seen that the results decrease with an increase of fibre angle. A good agreement between the present solutions and those obtained from [27] is observed. It should be noted that there exist slight deviations between the present solution and Chandrashekhara et al. [27] with those from previous studies [21, 47, 84]. The $(30^0 / -30^0)_S$ composite beams with S-S, C-F and C-C boundary conditions are chosen to investigate the effect of the length-to-height ratio on the fundamental frequencies and critical buckling loads (Fig. 2.7). It can be seen that the results increase with the increase of L/h. The effect of the length-to-height ratio is effectively significant for C-C boundary condition when $L/h < 20$.

Table 2.10. Normalized fundamental frequencies of $(\theta/-\theta)_s$ composite beams with respect to the fibre angle change ($L/h=15$ MAT III.2).

BC	Reference	Angle-ply (θ)			
		0^0	30^0	60^0	90^0
S-S	Present	2.6563	2.1033	1.0121	0.7317
	Aydogdu [47]	2.6510	1.1410	0.7360	0.7290
	Chandrashekhara et al. [78]	2.6560	2.1032	1.0124	0.7320
	Vo and Thai [21]	2.6494	1.5540	0.7361	0.7295
C-F	Present	0.9832	0.7683	0.3631	0.2618
	Aydogdu [47]	0.9810	0.4140	0.2620	0.2600
	Chandrashekhara et al. [78]	0.9820	0.7678	0.3631	0.2619
	Vo and Thai [21]	0.9801	0.3678	0.3631	0.2619
C-C	Present	4.9116	4.1307	2.2019	1.6205
	Aydogdu [47]	4.9730	2.1950	1.6690	1.6190
	Chandrashekhara et al. [78]	4.8487	4.0981	2.1984	1.6200
	Vo and Thai [21]	4.8969	3.2355	1.6309	1.6152
	Chen et al. [84]	4.8575	2.3445	1.6711	1.6237

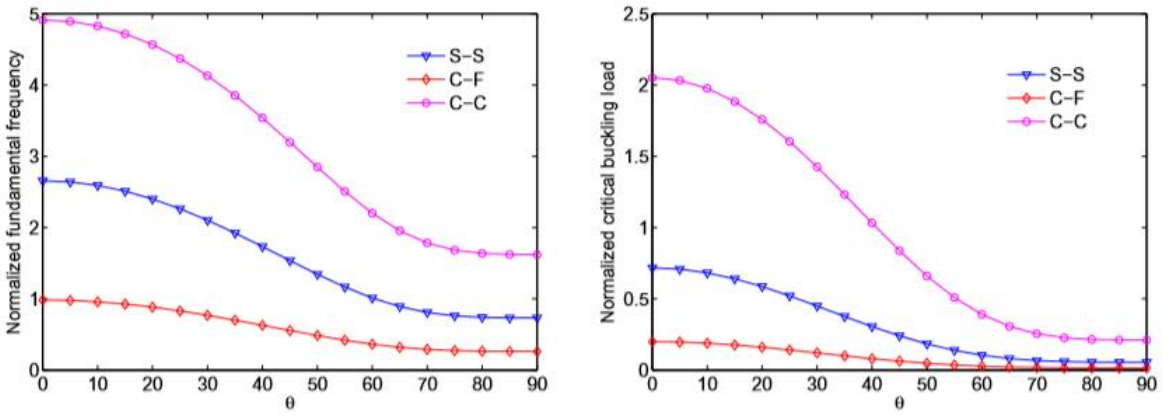

a. b.

Figure 2.6. Effects of the fibre angle change on the normalized fundamental frequencies and critical buckling loads of $(\theta/-\theta)_s$ composite beams ($L/h=15$, MAT III.2)

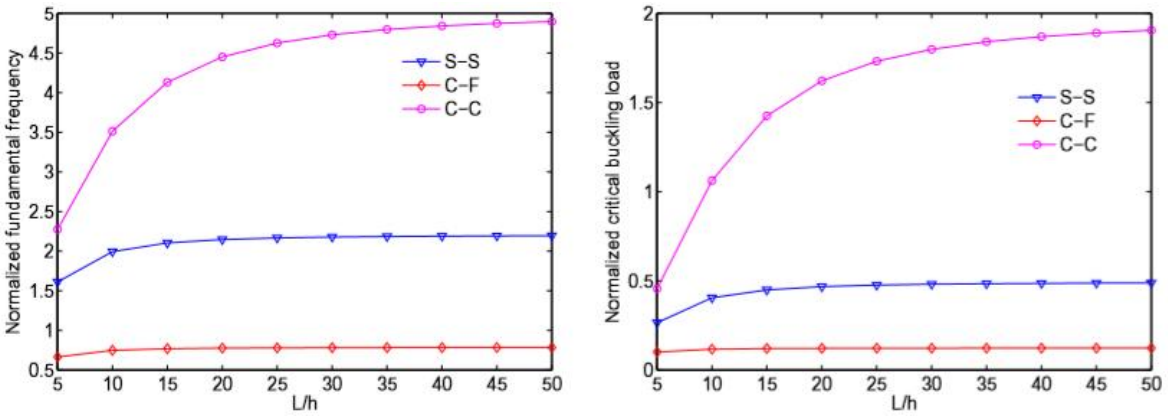

Figure 2.7. Effects of the length-to-height ratio on the normalized fundamental frequencies and critical buckling loads of $(30/-30)_s$ composite beams ($L/h=15$, MAT III.2)

2.4. Conclusion

The new analytical solution is proposed for static, buckling and vibration analysis of laminated composite beams based on a HOBT. This solution based on trigonometric series is developed for various boundary conditions. Numerical results are obtained to compare with previous studies and to investigate effects of fibre angle and material anisotropy on the deflections, stresses, natural frequencies, critical buckling loads and corresponding mode shapes. The obtained results show that:

- Beam model is suitable for free vibration, buckling and bending analysis of laminated composite beams.
- The proposed series solution converges quickly for buckling analysis.
- The present solution is found to simple and efficient in analysis of laminated composite beams with various boundary conditions.

Chapter 3. VIBRATION AND BUCKLING ANALYSIS OF LAMINATED COMPOSITE BEAMS UNDER THERMO-MECHANICAL LOAD [4]

3.1. Introduction

The laminated composite beam has been widely used in multi-physics environments such as construction, transportation, nuclear, etc. In this context, the analysis of thermal and mechanical behaviours of laminated composite beams has attracted a number of researchers who employed various analytical and numerical approaches to accurately predict the behaviour of laminated composite beams. Among numerical approaches, finite element method is the most popular one used for the analysis of laminated composite beams. For example, Mathew et al. [113] investigated the thermal buckling behaviour of composite beams based on the first-order shear deformation theory, whilst Lee [114] examined the thermal buckling response of composite beams based on a layerwise theory. Murthy et al. [24] and Vo and Thai [22] used a higher-order shear deformation beam theory to predict the bending behaviour of laminated composite beams. Vo and Thai [21] also applied the HOBT to analyse the mechanical buckling and vibration of laminated composite beams. For analytical approaches, Kant et al. [115] studied the dynamic responses of laminated composite beams based on a refined HOBT and Navier solution procedure. Emam and Eltaher [116] investigated buckling and postbuckling behaviours of laminated composite beams in hygrothermal environment. For the laminated composite beam with various boundary conditions, Khdeir and Reddy ([101], [117]) used a state-space approach and various beam theories for the vibration and buckling analysis of cross-ply laminated composite beams. The thermal buckling behaviour of laminated composite beams was also investigated by Khdeir [118] based on various beam theories including the CBT, FOBT and HOBT. Moreover, Abramovich [119] predicted thermal buckling load of laminated composite beams based on the FOBT and an analytical solution for different boundary conditions. Based on Ritz method and the HOBT, Aydogdu examined the free vibration [100], mechanical buckling

[4] A slightly different version of this chapter has been published in Composite Structures in 2018

[48] and thermal buckling [120] of laminated composite beams with different boundary conditions. Wattanasakulpong et al. [121] used polynomial functions to determine thermal buckling load and free vibration of functionally graded beams. Mantari and Canales [44] also used Ritz method to predict mechanical buckling and vibration responses of laminated composite beams. Asadi et al. [122] analysed the nonlinear vibration and thermal stability of shape memory alloy hybrid laminated composite beams based on Galerkin method. Warminska et al. [123] analysed the vibration of composite beams under thermal and mechanical loadings based on the FOBT. Jun et al. [124] applied dynamic stiffness method to analyse the vibration and buckling of laminated composite beams. Vosoughi et al. [125] adopted the differential quadrature method and the FOBT to study the thermal buckling and postbuckling behaviours of laminated composite beams with temperature-dependent properties. It can be seen that Ritz method has not been widely used to analyse laminated composite beams under thermal and mechanical loadings.

The objective of this Chapter is to develop a Ritz solution for thermo-mechanical buckling and vibration of laminated composite beams. In the present solution, new approximation functions are proposed. The displacement field of the present study is based on the HOBT. Verification study is carried out throughout numerical examples to illustrate the accuracy of the present solution. Parametric study is also performed to examine the influences of length-to-height ratio, boundary conditions, material anisotropy and temperature changes on the buckling and vibration of laminated composite beams under mechanical and thermal loads.

3.2. Theoretical formulation

A laminated composite beam, which is defined in Chapter Two (Fig. 2.1), is supposed to be embedded in thermal environment with a uniform temperature rise through the beam thickness as:

$$T = T_0 + \Delta T \tag{3.1}$$

where T_0 is reference temperature which is supposed to be one at the bottom surface of the beam.

3.2.1. Beam model based on the HOBT

The displacement field and constitutive equations of composite beams are based on the HOBT [89, 90] as in Chapter Two. Therefore, the strain energy Π_E and the kinetic energy Π_K of beams are also determined as Eq. (2.7) and (2.11), respectively.

The work done Π_W by thermal and mechanical loads can be written as:

$$\Pi_W = -\frac{1}{2}\int_0^L N_x^{0m}(w_{0,x})^2 b dx - \frac{1}{2}\int_0^L N_x^{0t}(w_{0,x})^2 b dx \tag{3.2}$$

where N_x^{0m} and N_x^{0t} are the axial mechanical load and axial thermal stress resultant, respectively. For a temperature rise $(T - T_0)$, the thermal axial stress resultant is given by:

$$N_x^{0t} = \sum_{k=1}^{n}\int_{z_k}^{z_{k+1}} \left(\overline{Q}_{11}\alpha_x + \overline{Q}_{12}\alpha_y + \overline{Q}_{16}\alpha_{xy}\right)(T - T_0)\, dz \tag{3.3}$$

where α_x, α_y and α_{xy} are the transformed thermal expansion coefficients in global coordinates (see Appendix A for more details).

The total energy Π of beams is obtained as:

$$\Pi = \Pi_E + \Pi_W - \Pi_K$$

$$\Pi = \frac{1}{2}\int_0^L \Big[A(u_{0,x})^2 - 2Bu_{0,x}w_{0,xx} + D(w_{0,xx})^2 + 2B^s u_{0,x}u_{1,x} - 2D^s w_{0,xx}u_{1,x} + H^s(u_{1,x})^2 + A^s(u_1)^2 \Big] dx$$

$$-\frac{1}{2}\int_0^L N_x^{0m}(w_{0,x})^2 b dx - \frac{1}{2}\int_0^L N_x^{0t}(w_{0,x})^2 b dx$$

$$-\frac{1}{2}\int_0^L \Big[I_0\dot{u}_0^2 - 2I_1\dot{u}_0\dot{w}_{0,x} + I_2\left(\dot{w}_{0,x}\right)^2 + 2J_1\dot{u}_1\dot{u}_0 - 2J_2\dot{u}_1\dot{w}_{0,x} + K_2\dot{u}_1^2 + I_0\dot{w}_0^2 \Big] dx \tag{3.4}$$

3.2.2. Solution procedure

Ritz solution is used to approximate the displacement field as:

$$u_0(x,t) = \sum_{j=1}^{m}\psi_j(x)u_{0j}e^{i\omega t} \tag{3.5}$$

$$w_0(x,t) = \sum_{j=1}^{m}\varphi_j(x)w_{0j}e^{i\omega t} \tag{3.6}$$

$$u_1(x,t) = \sum_{j=1}^{m} \xi_j(x) u_{1j} e^{i\omega t} \tag{3.7}$$

where ω is the frequency, $i^2 = -1$ the imaginary unit; u_{0j}, w_{0j}, u_{1j} are values to be determined; $\psi_j(x)$, $\varphi_j(x)$ and $\xi_j(x)$ are approximation functions. This Chapter proposed new hybrid approximation functions reported in Table 3.1. They are combinations of exponential and admissible functions which satisfy simply-supported (S-S), hinged-hinged (H-H), clamped-free (C-F), clamped-simply suppoeted (C-S), clamped-hinged (C-H) and clamped-clamped (C-C) boundary conditions.

Table 3.1. Approximation functions and kinematic BC of the beams.

BC	Position	$\frac{\psi_j(x)}{e^{-jx/L}}$	$\frac{\varphi_j(x)}{e^{-jx/L}}$	$\frac{\xi_j(x)}{e^{-jx/L}}$	Value
S-S	x=0	$(L-2x)$	$x(L-x)$	$(L-2x)$	$w_0 = 0$
	x=L				$w_0 = 0$
H-H	x=0	$x(L-x)$	$x(L-x)$	1	$u_0 = 0, w_0 = 0$
	x=L				$u_0 = 0, w_0 = 0$
C-F	x=0	x	x^2	x	$u_0 = 0, w_0 = 0, w_{0,x} = 0, u_1 = 0$
	x=L				
C-S	x=0	x	$x^2(L-x)$	x	$u_0 = 0, w_0 = 0, w_{0,x} = 0, u_1 = 0$
	x=L				$w_0 = 0$
C-H	x=0	$x(L-x)$	$x^2(L-x)$	x	$u_0 = 0, w_0 = 0, w_{0,x} = 0, u_1 = 0$
	x=L				$u_0 = 0, w_0 = 0$
C-C	x=0	$x(L-x)$	$x^2(L-x)^2$	$x(L-x)$	$u_0 = 0, w_0 = 0, w_{0,x} = 0, u_1 = 0$
	x=L				$u_0 = 0, w_0 = 0, w_{0,x} = 0, u_1 = 0$

By substituting Eqs. (3.5, 3.6 and 3.7) into Eq. (3.4) and using Lagrange's equations Eq. (3.8)

$$\frac{\partial \Pi}{\partial p_j} - \frac{d}{dt}\frac{\partial \Pi}{\partial \dot{p}_j} = 0 \tag{3.8}$$

with p_j representing the values of (u_{0j}, w_{0j}, u_{1j}), the thermo-mechanical buckling and vibration responses of laminated composite beams can be obtained from the following equations

$$\left(\begin{bmatrix} \mathbf{K}^{11} & \mathbf{K}^{12} & \mathbf{K}^{13} \\ {}^{T}\mathbf{K}^{12} & \mathbf{K}^{22} & \mathbf{K}^{23} \\ {}^{T}\mathbf{K}^{13} & {}^{T}\mathbf{K}^{23} & \mathbf{K}^{33} \end{bmatrix} - \omega^2 \begin{bmatrix} \mathbf{M}^{11} & \mathbf{M}^{12} & \mathbf{M}^{13} \\ {}^{T}\mathbf{M}^{12} & \mathbf{M}^{22} & \mathbf{M}^{23} \\ {}^{T}\mathbf{M}^{13} & {}^{T}\mathbf{M}^{23} & \mathbf{M}^{33} \end{bmatrix} \right) \begin{Bmatrix} \mathbf{u_0} \\ \mathbf{w_0} \\ \mathbf{u_1} \end{Bmatrix} = \begin{Bmatrix} \mathbf{0} \\ \mathbf{0} \\ \mathbf{0} \end{Bmatrix} \tag{3.9}$$

where the components of stiffness matrix **K** and mass matrix **M** are given by:

$$K_{ij}^{11} = A\int_0^L \psi_{i,x}\psi_{j,x}dx,\ K_{ij}^{12} = -B\int_0^L \psi_{i,x}\varphi_{j,xx}dx,\ K_{ij}^{13} = B^s\int_0^L \psi_{i,x}\xi_{j,x}dx$$

$$K_{ij}^{22} = D\int_0^L \varphi_{i,xx}\varphi_{j,xx}dx - N_x^{0m}\int_0^L \varphi_{i,x}\varphi_{j,x}dx - N_x^{0t}\int_0^L \varphi_{i,x}\varphi_{j,x}dx,\ K_{ij}^{23} = -D^s\int_0^L \varphi_{i,xx}\xi_{j,x}dx,$$

$$K_{ij}^{33} = -H^s\int_0^L \xi_{i,x}\xi_{j,x}dx + A^s\int_0^L \xi_i\xi_j dx,$$

$$M_{ij}^{11} = I_0\int_0^L \psi_i\psi_j dx,\ M_{ij}^{12} = -I_1\int_0^L \psi_i\varphi_{j,x}dx\ M_{ij}^{13} = -J_1\int_0^L \psi_i\xi_j dx,$$

$$M_{ij}^{22} = I_0\int_0^L \varphi_i\varphi_j dx + I_2\int_0^L \varphi_{i,x}\varphi_{j,x}dx,\ M_{ij}^{23} = -J_2\int_0^L \varphi_{i,x}\xi_j dx,\ M_{ij}^{33} = K_2\int_0^L \xi_i\xi_j dx \tag{3.10}$$

The critical buckling loads and natural frequencies of composite beams can be determined by solving Eq.(3.9).

3.3. Numerical results

Each lamina of laminated composite beams has the same thicknesses and it is made from the orthotropic materials as given in Table 3.2. The beam is supposed to be embedded in thermal environments with a uniform temperature rise in the depth of the beam. Moreover, it is assumed that $T_0 = 0^0\mathrm{C}$ in the examples. For convenience, the following nondimensional terms are used:

$$\bar{\omega} = \frac{\omega L^2}{h}\sqrt{\frac{\rho}{E_2}},\ \overline{N}_{cr} = N_{cr}\frac{L^2}{E_2 b h^3},\ \overline{T}_{cr} = T_{cr}\frac{L^2\alpha_1}{h^2}\ \text{for Material I.3 (MAT I.3)} \tag{3.11}$$

Table 3.2. Material properties of laminated composite beams.

Material properties	MAT I.3 [100]	MAT II.3 [124]
E_1 (GPa)	E_1/E_2=open	*138*
$E_2=E_3$(GPa)	-	6.9
$G_{12}=G_{13}$ (GPa)	$0.6E_2$	4.14
G_{23} (GPa)	$0.5E_2$	3.45
$\nu_{12}=\nu_{13}$	0.25	0.25
ρ (kg/m^2)	-	1550.1
L (m)	L/h=open	*0.381*
h (m)	-	0.0381
b (m)	-	1
$\alpha_1^*(1/^0C)$	$\alpha_2^*/\alpha_1^*=$ open	$6\text{x}10^{-6}$
$\alpha_2^*(1/^0C)$	-	$18\text{x}10^{-6}$

3.3.1. Convergence study

For purpose of testing the convergence of the present solutions, laminated composite beams (MAT I.3, $0^0/90^0/0^0$, $L/h=5$, $E_1/E_2=40$) with different boundary conditions subjected to mechanical loads are considered. The variations of nondimensional fundamental frequencies and critical buckling loads with respect to the series number m are given in Table 3.3. The results show that $m=12$ is the convergence point for the natural frequency and buckling load for all BCs. Therefore, this number of series terms will be used in the following numerical examples.

Table 3.3. Convergence study of nondimensional critical buckling load and fundamental frequency of ($0^0/90^0/0^0$) beams (MAT I.3, $L/h = 5$, $E_1/E_2 = 40$).

BC	*m*						
	2	4	6	8	10	12	14
Fundamental frequency							
S-S	9.6543	9.2186	9.2088	9.2084	9.2084	9.2084	9.2084
H-H	9.8795	9.2195	9.2088	9.2084	9.2084	9.2084	9.2084
C-F	4.2776	4.2383	4.2319	4.2316	4.2315	4.2315	4.2315
C-S	10.5759	10.2712	10.2397	10.2393	10.2393	10.2393	10.2393
C-H	10.5759	10.2712	10.2397	10.2393	10.2393	10.2393	10.2393
C-C	12.2770	11.7198	11.6292	11.6074	11.6044	11.6048	11.6045
Critical buckling load							
S-S	9.3219	8.6261	8.6139	8.6132	8.6132	8.6132	8.6132
H-H	9.1156	8.6272	8.6138	8.6132	8.6132	8.6132	8.6132
C-F	5.0327	4.7085	4.7080	4.7080	4.7080	4.7080	4.7080
C-S	9.9534	9.8257	9.8138	9.8138	9.8138	9.8138	9.8138
C-H	9.9534	9.8257	9.8138	9.8138	9.8138	9.8138	9.8138
C-C	12.0368	11.6687	11.6520	11.6518	11.6518	11.6518	11.6518

3.3.2. Vibration analysis

The first example is to analyse free vibration of symmetric ($0^0/90^0/0^0$) and unsymmetric ($0^0/90^0$) cross-ply beams (MAT I.3) with various length-to-height ratios and BCs. The nondimensional fundamental frequencies are compared with those from previous works in Tables 3.4 and 3.5. It is clear that the obtained results agree well with earlier works. For symmetric composite beams, the nondimensional fundamental frequencies of S-S and C-S BCs are the similar to those of H-H and C-H BCs, respectively.

Table 3.4. Nondimensional fundamental frequency of ($0^0/90^0/0^0$) beams (MAT I.3, $E_1/E_2 = 40$).

L/h	Reference	BC					
		S-S	H-H	C-F	C-S	C-H	C-C
5	Present	9.208	9.208	4.232	10.239	10.239	11.605
	Murthy et al. [24]	9.207	-	4.230	10.238	-	11.602
	Khdeir and Reddy [101]	9.208	-	4.234	10.239	-	11.603
	Aydogdu [100]	9.207	-	4.234	10.236	-	11.637
	Vo and Thai [21]	9.206	-	-	-	-	-
	Mantari and Canales [44]	9.208	-	4.221	10.520	-	11.486
10	Present	13.614	13.614	5.494	16.599	16.599	19.727
	Murthy et al. [24]	13.611	-	5.491	16.600	-	19.719
	Khdeir and Reddy [101]	13.614	-	5.495	16.599	-	19.712
	Vo and Thai [21]	13.607	-	-	-	-	-
	Mantari and Canales [21]	13.610	-	5.490	17.225	-	19.652
20	Present	16.338	16.338	6.067	22.850	22.850	29.677
	Aydogdu [100]	16.337	-	6.070	22.907	-	29.926
	Vo and Thai [21]	16.327	-	-	-	-	-
50	Present	17.462	17.462	6.267	26.669	26.669	37.686
	Vo and Thai [21]	17.449	-	-	-	-	-

Table 3.5. Nondimensional fundamental frequency of ($0^0/90^0$) beams (MAT I.3, $E_1/E_2 = 40$).

L/h	Reference	BC					
		S-S	H-H	C-F	C-S	C-H	C-C
5	Present	6.129	7.620	2.383	8.033	8.548	10.030
	Murthy et al. [24]	6.045	-	2.378	8.033	-	10.011
	Khdeir and Reddy [101]	6.128	-	2.386	8.033	-	10.026
	Aydogdu [100]	6.144	-	2.384	8.068	-	10.102
	Vo and Thai [21]	6.058	-	-	-	-	-
	Mantari and Canales [44]	6.109	-	2.375	8.268	-	9.974
10	Present	6.945	9.653	2.543	10.130	11.039	13.668
	Murthy et al. [24]	6.908	-	2.541	10.124	-	13.657
	Khdeir and Reddy [101]	6.945	-	2.544	10.129	-	13.660
	Vo and Thai [21]	6.909	-	-	-	-	-
	Mantari and Canales [44]	6.913	-	2.532	10.239	-	13.628
20	Present	7.219	10.528	2.591	11.051	12.194	15.663
	Aydogdu [100]	7.218	-	2.590	11.060	-	15.688
	Vo and Thai [21]	7.204	-	-	-	-	-
50	Present	7.302	10.835	2.605	11.369	12.604	16.430
	Vo and Thai [21]	7.296	-	-	-	-	-

In the second example, the ($0^0/90^0/0^0$) and ($0^0/90^0$) composite beams with MAT II.3 under uniform temperature rise (UTR) is considerd. The fundamental frequencies are reported in Table 3.6 for various BCs. Again, the obtained results are close to those given by Jun et al. [124]. Fig. 3.2a and 3.2b display the effects of UTR on the

fundamental frequency of beams. Obviously, the result decreases with the increase of ΔT up to critical temperatures at which the fundamental frequencies vanish.

Table 3.6. The fundamental frequency (Hz) of $(0^0/90^0/0^0)$ and $(0^0/90^0)$ beams with various boundary conditions (MAT II.3).

Lay-up	ΔT (^{0}C)	Reference	BC		
			H-H	C-H	C-C
$(0^0/90^0/0^0)$	0	Present	950.2	1245.3	1552.4
	100		913.5	1215.6	1522.4
	-100		985.6	1274.3	1571.1
$(0^0/90^0)$	0	Present	664.3	783.8	1001.2
		Jun et al. [124]	663.4	783.1	999.6
	100	Present	621.2	743.8	968.4
		Jun et al. [124]	621.7	744.5	968.1
	-100	Present	704.8	821.7	1032.8
		Jun et al. [124]	702.5	819.7	1030.0

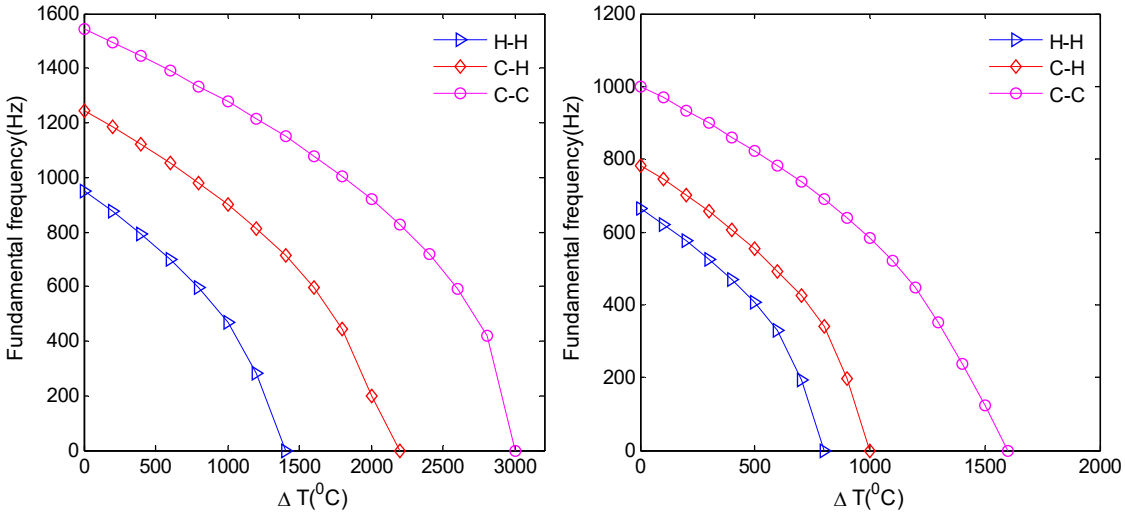

a. $0^0/90^0/0^0$ b. $0^0/90^0$

Figure 3.1. Variation of fundamental frequency of $(0^0/90^0/0^0)$ and $(0^0/90^0)$ beams (MAT II.3) with respect to uniform temperature rise ΔT.

3.3.3. Buckling analysis

In the first example, the buckling of laminated composite beam under mechanical loads is considered. Tables 3.7, 3.8 and 7.9 presented the critical buckling load of cross-ply ($0^0/90^0/0^0$; $0^0/90^0$) and angle-ply composite beams (MAT I.3) with various length-to-height ratios and BCs. The present results are very close with published results.

Table 3.7. Nondimensional critical buckling load of ($0^0/90^0/0^0$) beams (MAT I.3, $E_1/E_2 = 40$).

L/h	Reference	BC					
		S-S	H-H	C-F	C-S	C-H	C-C
5	Present	8.613	8.613	4.708	9.814	9.814	11.652
	Mantari and Canales [44]	8.585	-	4.673	10.192	-	11.502
	Khdeir and Reddy [117]	8.613	-	4.708	9.814	-	11.602
10	Present	18.832	18.832	6.772	25.857	25.857	34.453
	Mantari and Canales [44]	18.796	-	6.757	27.090	-	34.365
	Khdeir and Reddy [117]	18.832	-	6.772	25.857	-	34.453
50	Present	30.906	30.906	7.886	61.174	61.174	114.398

Table 3.8. Nondimensional critical buckling load of ($0^0/90^0$) beams (MAT I.3, $E_1/E_2 = 40$).

L/h	Reference	BC					
		S-S	H-H	C-F	C-S	C-H	C-C
5	Present	3.907	5.923	1.236	5.985	6.772	8.674
	Aydogdu [48]	3.906	-	1.235	5.984	-	-
	Mantari and Canales [44]	3.856	-	1.221	6.127	-	8.509
10	Present	4.942	9.379	1.324	9.105	10.982	15.626
	Mantari and Canales [44]	4.887	-	1.311	-	-	15.468
50	Present	5.406	11.623	1.356	11.005	13.816	21.372

Table 3.9. Nondimensional critical buckling load of angle-ply beams (MAT I.3, $E_1/E_2 = 40$).

L/h	Lay-up	Reference	BC			
			S-S	C-F	C-S	C-C
5	$0^0/30^0/0^0$	Present	9.1024	4.8990	10.4293	12.4407
		Mantari and Canales [44]	9.0718	4.8633	10.8326	12.2267
		Canales and Mantari [126]	9.0658	4.5551	10.2878	12.0767
	$0^0/45^0/0^0$	Present	8.9391	4.8267	10.2236	12.1725
		Mantari and Canales [44]	7.6533	4.7909	10.6209	12.0091
		Canales and Mantari [126]	8.8846	4.4885	10.0813	11.8078
	$0^0/60^0/0^0$	Present	8.7762	4.7632	10.0184	11.9091
		Mantari and Canales [44]	8.7473	4.7275	10.4074	11.7534
		Canales and Mantari [126]	8.7340	4.4295	9.8755	11.5503
	$0^0/45^0/-45^0/0^0$	Present	8.7744	4.6402	10.0513	11.9418
		Mantari and Canales [44]	8.7439	4.6034	10.4632	11.7924
		Canales and Mantari [126]	8.7382	4.3211	9.9177	11.5436
	$0^0/60^0/-60^0/0^0$	Present	8.5432	4.5228	9.7627	11.5639
		Mantari and Canales [44]	8.5136	4.4857	10.1696	11.4270
		Canales and Mantari [126]	8.5092	4.2103	9.6311	11.1619
10	$0^0/30^0/0^0$	Present	19.5961	6.9620	27.1507	36.4094
		Mantari and Canales [44]	19.5591	6.9473	28.4236	36.3133
		Canales and Mantari [126]	19.6135	6.8824	27.1649	36.2597
	$0^0/45^0/0^0$	Present	19.3066	6.8743	26.7009	35.7563
		Mantari and Canales [44]	19.2700	6.8596	27.9582	35.6626
		Canales and Mantari [126]	19.3191	6.7956	26.7074	35.5977
	$0^0/60^0/0^0$	Present	19.0527	6.8110	26.2707	35.1049
		Mantari and Canales [44]	19.0166	6.7569	27.5149	35.0138
		Canales and Mantari [126]	19.0597	6.7324	26.2652	34.9327
	$0^0/45^0/-45^0/0^0$	Present	18.5607	6.4894	25.9949	35.0977
		Mantari and Canales [44]	18.5228	6.4746	27.1980	35.0019
		Canales and Mantari [126]	18.5976	6.4208	26.0510	35.0047
	$0^0/60^0/-60^0/0^0$	Present	18.0910	6.3255	25.3249	34.1726
		Mantari and Canales [44]	18.0533	6.3106	26.5014	34.0797
		Canales and Mantari [126]	18.1286	6.2593	25.3793	34.0846

The next example is to examine the critical buckling temperature of symmetric and unsymmetric composite beam with MAT I.3, $E_1 / E_2 = 10$, $\alpha_2^* / \alpha_1^* = 3$. Tables 3.10 and 3.11 indicate that the present results are in good agreement with those given by Aydogdu [120] and Wattanasakulpong et al. [121].

Table 3.10. Nondimensional critical buckling temperature of ($0^0/90^0/0^0$) beams (MAT I.3, $E_1/E_2 = 40$, $\alpha_2^* / \alpha_1^* = 3$).

L/h	Reference	BC		
		H-H	C-H	C-C
5	Present	0.450	0.551	0.682
	Khdeir [118]	0.468	0.573	0.710
10	Present	0.791	1.230	1.798
	Khdeir [118]	0.823	1.280	1.871
	Aydogdu [120]	0.790	1.230	1.797
	Wattanasakulpong et al. [121]	0.791	1.230	1.800
20	Present	0.979	1.823	3.163
	Khdeir [118]	1.019	1.897	3.292
50	Present	1.049	2.111	4.032
	Khdeir [118]	1.092	2.265	4.196
	Aydogdu [120]	1.049	2.110	4.030

Table 3.11. Nondimensional critical buckling temperature of unsymmetric C-C beams (MAT I.3, $E_1/E_2 = 20$, $\alpha_2^* / \alpha_1^* = 3$)

L/h	Reference	Number of layers		
		2 ($0^0/90^0$)	4 ($0^0/90^0/0^0/90^0$)	10 ($0^0/90^0/\ldots$)
5	Present	0.558	0.678	0.725
	Aydogdu [120]	0.557	0.677	0.723
	Khdeir [118]	0.583	0.708	0.756
10	Present	0.887	1.466	1.616
	Aydogdu [120]	0.885	1.463	1.513
	Khdeir [118]	0.926	1.530	1.687
20	Present	1.045	2.089	2.369

	Aydogdu [120]	1.092	2.079	2.182
	Khdeir [118]	1.090	2.180	2.472
50	Present	1.100	2.374	2.727
	Aydogdu [120]	1.098	2.372	2.721
	Khdeir [118]	1.148	2.477	2.846

Finally, the effect of α_2^* / α_1^* and E_1 / E_2 ratios on the critical buckling temperature is investigated. The nondimensional critical buckling temperature of of ($0^0/90^0/0^0$) and ($0^0/90^0$) composite beams are showed in Table 3.12 and 3.13, respectively. It can be seen that a good agreement between the results are found.

Table 3.12. Nondimensional critical buckling temperature of ($0^0/90^0$) composite beams (MAT I.3, $L / h = 10$).

BC	E_1 / E_2	α_2^* / α_1^*				
		3	10	20	50	100
H-H	3	0.435	0.193	0.108	0.046	0.024
	10	0.497	0.306	0.198	0.096	0.051
	20	0.476	0.349	0.253	0.138	0.079
	40	0.427	0.356	0.288	0.183	0.114
C-H	3	0.757	0.337	0.188	0.081	0.041
	10	0.674	0.415	0.268	0.130	0.070
	20	0.587	0.430	0.311	0.170	0.097
	40	0.498	0.416	0.336	0.213	0.133
C-C	3	1.368	0.608	0.339	0.146	0.075
	10	1.090	0.671	0.433	0.210	0.113
	20	0.887	0.650	0.471	0.257	0.147
	40	0.709	0.592	0.478	0.304	0.189

Figure 3.3 plots the variation of nondimensional critical buckling temperature with respect to α_2^* / α_1^* of ($0^0/90^0/0^0$) laminated composite beams with MAT I.3, $E_1 / E_2 = 20$, $L / h = 10$. It is found that the results decrease with the increase of α_2^* / α_1^*

Table 3.13. Nondimensional critical buckling temperature of ($0^0/90^0/0^0$) composite beams (MAT I.3, $L/h=10$)

BC	E_1/E_2	Reference	α_2^*/α_1^*				
			3	10	20	50	100
H-H	3	Present	0.637	0.322	0.171	0.084	0.044
		Aydogdu [120]	0.637	0.323	0.189	0.293	0.153
	10	Present	0.821	0.576	0.404	0.213	0.119
		Aydogdu [120]	0.820	0.576	0.404	0.213	0.119
	20	Present	0.791	0.641	0.504	0.307	0.186
		Aydogdu [120]	0.791	0.640	0.523	0.307	0.185
		Khdeir [118]	0.823	0.708	0.590	0.393	0.253
	40	Present	0.666	0.592	0.512	0.363	0.245
		Aydogdu [120]	0.666	0.593	0.592	0.363	0.245
C-H	3	Present	1.226	0.620	0.364	0.162	0.084
		Aydogdu [120]	1.226	0.619	0.362	0.162	0.207
	10	Present	1.419	0.996	0.699	0.369	0.206
		Aydogdu [120]	1.420	0.996	0.698	0.368	0.206
	20	Present	1.230	0.997	0.784	0.478	0.289
		Aydogdu [120]	1.234	0.997	0.783	0.477	0.289
		Khdeir [118]	1.280	1.101	0.918	0.612	0.393
	40	Present	0.914	0.813	0.703	0.499	0.336
		Aydogdu [120]	0.918	0.816	0.705	0.500	0.337
C-C	3	Present	2.212	1.119	0.656	0.293	0.152
		Aydogdu [120]	1.994	1.007	0.590	0.263	0.137
	10	Present	2.278	1.599	1.122	0.592	0.331
		Aydogdu [120]	2.090	1.467	1.028	0.542	0.302
	20	Present	1.798	1.456	1.145	0.698	0.423
		Aydogdu [120]	1.804	1.462	1.148	0.699	0.423
		Khdeir [118]	1.871	1.609	1.341	0.894	0.575
	40	Present	1.218	1.083	0.936	0.665	0.448
		Aydogdu [120]	1.229	1.092	0.944	0.670	0.451

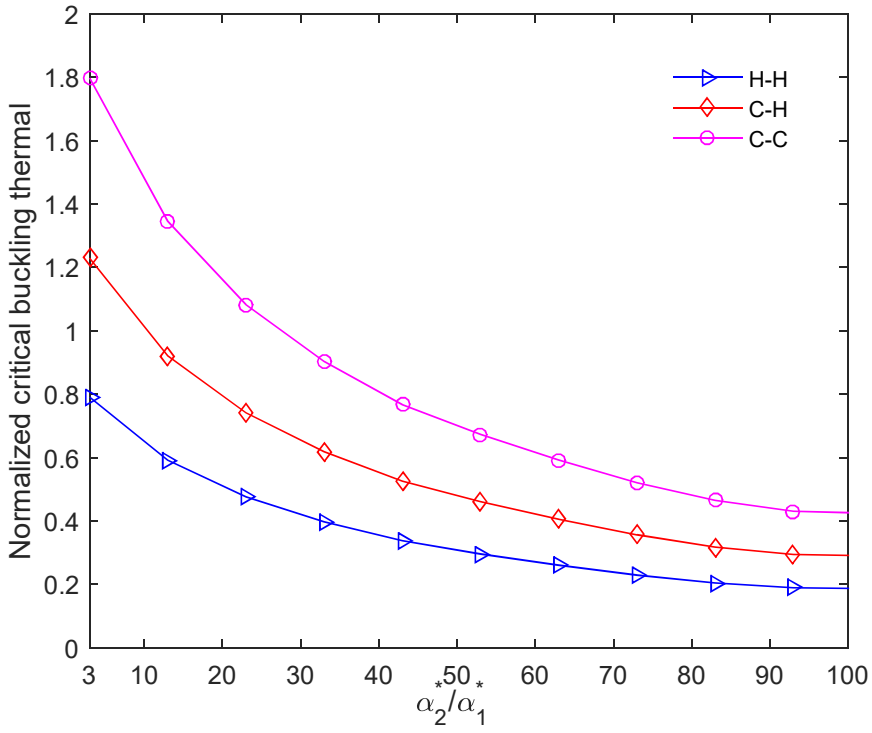

Figure 3.2. Effect of α_2^*/α_1^* ratio on nondimensional critical buckling temperature of $(0^0/90^0/0^0)$ composite beams (MAT I.3, $E_1/E_2 = 20,\ L/h = 10$).

3.4. Conclusions

The new hybrid approximation functions are proposed to study the mechanical and thermal buckling and free vibration behaviours of laminated composite beams using a HOBT. Numerical results for different boundary conditions are obtained to examine the effects of material anisotropy, length-to-height ratio, thermal expansion ratio and temperature changes on the buckling load and buckling temperature as well as natural frequencies of composite beams. The results indicate as followings:

- Thermal load is significant to behaviours of buckling and vibration of lamianated composite beams. The increase of temperatures makes beams be more flexible. Therefore, the fundamental frequency and critical buckling load reduce.
- The proposed solution is not only good convergence but also simple and effecient for the buckling and vibration analysis of laminated composite beams under thermal and mechanical loadings.

Chapter 4. EFFECT OF TRANSVERSE NORMAL STRAIN ON BEHAVIOURS OF LAMINATED COMPOSITE BEAMS [5]

4.1. Introduction

In Chapter Two and Three, HOBT is used to analyse bending, buckling and vibration behaviours of laminated composite beams under mechanical and thermal loadings. Although HOBT has attracted huge attention for the researchers [69, 79-82], it neglected transverse normal strain. For this reason, quasi-3D theories [36, 83-85] were developed based on higher-order variations of both in-plane and out-of-plane displacements.

For computational methods, many analytical and numerical approaches have been proposed to analyse behaviours of laminated composite beams and only some of them are mentioned here. Zenkour [36] used Navier solution for bending analysis of cross-ply laminated and sandwich beams. Aydogdu [47, 48, 100] developed Ritz method for buckling and vibration analysis of laminated composite beams. Mantari and Canales [44, 126] also analysed the vibration and buckling of laminated beams by using the Ritz method. Khdeir and Reddy [101, 117] developed state space approach for the vibration and buckling analysis of cross-ply laminated beams. Finite element method has widely used to analyse static, dynamic and buckling of composite beams [19-28, 33]. In addition, dynamic stiffness matrix method was used by Jun et al. [32] for the vibration analysis of composite beams. Shao et al. [127] used the method of reverberation ray matrix to analyse free vibration of laminated beams with general boundary conditions. Natural frequency of laminated composite beams was also examined by experiments ([128], [129]).

Although Ritz method is efficient to analyse the behaviours of composite beams with various boundary conditions, the available literature indicate that the number of researches used the Ritz method is still limited. Among them, only few research investigated the effect of transverse normal strain on static, vibration and buckling of

[5] A slightly different version of this chapter has been published in International Journal of Structural Stability and Dynamics in 2018

laminated composite beams. On the other hand, most of above studies focused on cross-ply composite beams, which is a special case of the general laminated ones. Unlike the cross-ply laminated beams, angle-ply laminated beams have the coupling between out-of-plane stresses and strains. Therefore, the study of composite beams with arbitrary lay-ups is necessary and has practical significance.

The objective of this Chapter is to propose new Ritz-method-based analytical solutions for static, vibration and buckling analysis of general laminated composite beams based on a quasi-3D theory which accounts for a higher-order variation of the axial and transverse displacements. The governing equations of motion are derived by using Lagrange's equations. The convergence and verification studies are carried out to demonstrate the accuracy of the present study. Numerical results are presented to investigate the effects of transverse normal strain, length-to-height ratio, fibre angle, Poisson's ratio and material anisotropy on the deflections, stresses, natural frequencies and buckling loads of laminated composite beams.

4.2. Theoretical formulation

4.2.1. Kinetic, strain and stress relations

Consider a laminated composite beam, which is defined in Chapter Two (Fig. 2.1). The displacement field of composite beams is given by [36]:

$$u(x,z,t) = u_0(x,t) + zu_1(x,t) - \frac{1}{2}z^2\frac{\partial w_1}{\partial x} + z^3\left[-\frac{4}{3h^2}\left(\frac{\partial w_0}{\partial x} + u_1(x,t)\right) - \frac{1}{3}\frac{\partial w_2}{\partial x}\right] \tag{4.1}$$

$$w(x,z,t) = w_0(x,t) + zw_1(x,t) + z^2w_2(x,t) \tag{4.2}$$

where $u_0(x,t)$ and $w_0(x,t)$ are the axial and transverse displacements of mid-plan of the beam, respectively; $u_1(x,t)$ is the rotation of a transverse normal about the *y*-axis; $w_1(x,t)$ and $w_2(x,t)$ are additional higher-order terms. The present theory therefore holds five variables to be determined.

The strain field of beams is given by:

$$\varepsilon_x = \frac{\partial u}{\partial x} = \varepsilon_x^{(0)} + z\varepsilon_x^{(1)} + z^2\varepsilon_x^{(2)} + z^3\varepsilon_x^{(3)} \tag{4.3}$$

$$\varepsilon_z = \frac{\partial w}{\partial z} = \varepsilon_z^{(0)} + z\varepsilon_z^{(1)} \tag{4.4}$$

$$\gamma_{xz} = \frac{\partial u}{\partial z} + \frac{\partial w}{\partial x} = \gamma_{xz}^{(0)} + z^2\gamma_{xz}^{(2)} \tag{4.5}$$

where

$$\varepsilon_x^{(0)} = \frac{\partial u_0}{\partial x},\ \varepsilon_x^{(1)} = \frac{\partial u_1}{\partial x},\ \varepsilon_x^{(2)} = -\frac{1}{2}\frac{\partial^2 w_1}{\partial x^2},\ \varepsilon_x^{(3)} = \left[-\frac{4}{3h^2}\left(\frac{\partial^2 w_0}{\partial x^2} + \frac{\partial u_1}{\partial x}\right) - \frac{1}{3}\frac{\partial^2 w_2}{\partial x^2}\right] \tag{4.6}$$

$$\varepsilon_z^{(0)} = w_1,\ \varepsilon_z^{(1)} = 2w_2,\ \gamma_{xz}^{(0)} = u_1 + \frac{\partial w_0}{\partial x},\ \gamma_{xz}^{(2)} = -\frac{4}{h^2}\left(u_1 + \frac{\partial w_0}{\partial x}\right) \tag{4.7}$$

The elastic strain and stress relations of k^{th}-layer of quasi-3D theory are given by:

$$\begin{Bmatrix}\sigma_x\\ \sigma_z\\ \sigma_{xz}\end{Bmatrix}^{(k)} = \begin{pmatrix}\overline{\overline{C}}_{11} & \overline{\overline{C}}_{13} & 0\\ \overline{\overline{C}}_{13} & \overline{\overline{C}}_{33} & 0\\ 0 & 0 & \overline{\overline{C}}_{55}\end{pmatrix}^{(k)} \begin{Bmatrix}\varepsilon_x\\ \varepsilon_z\\ \gamma_{xz}\end{Bmatrix} \tag{4.8}$$

where $\overline{\overline{C}}_{11}, \overline{\overline{C}}_{13}, \overline{\overline{C}}_{33}, \overline{\overline{C}}_{55}$ are indicated in Appendix A. If the transverse normal stress is omitted ($\sigma_z = 0$), the strain and stress relations of HOBT are recovered as:

$$\begin{Bmatrix}\sigma_x\\ \sigma_{xz}\end{Bmatrix}^{(k)} = \begin{pmatrix}\overline{\overline{C}}^{*}_{11} & 0\\ 0 & \overline{\overline{C}}^{*}_{55}\end{pmatrix}^{(k)} \begin{Bmatrix}\varepsilon_x\\ \gamma_{xz}\end{Bmatrix} \tag{4.9}$$

where $\overline{\overline{C}}^{*}_{11}$ and $\overline{\overline{C}}^{*}_{55}$ are showed in Appendix A. It should be noted that for HOBT, the higher-order terms ($w_1(x,t)$ and $w_2(x,t)$) will be vanished.

4.2.2. Variational formulation

The strain energy Π_E of beam is given by:

$$\Pi_E = \frac{1}{2}\int_V \left(\sigma_x\varepsilon_x + \sigma_z\varepsilon_z + \sigma_{xz}\gamma_{xz}\right)dV$$

$$= \frac{1}{2}\int_0^L \Bigg[A_{11}(u_{0,x})^2 + \left(2B_{11} - \frac{8}{3h^2}E_{11}\right)u_{0,x}u_{1,x} - \frac{8}{3h^2}E_{11}u_{0,x}w_{0,xx} - D_{11}u_{0,x}w_{1,xx} + 2A_{13}u_{0,x}w_1 + 4B_{13}u_{0,x}w_2$$

$$-\frac{2}{3}E_{11}u_{0,x}w_{2,xx} + \left(D_{11} + \frac{16}{9h^4}H_{11} - \frac{8}{3h^2}F_{11}\right)(u_{1,x})^2 + \left(A_{55} - \frac{8}{h^2}B_{55} + \frac{16}{h^4}D_{55}\right)u_1^2$$

$$+\left(\frac{32}{9h^4}H_{11}-\frac{8}{3h^2}F_{11}\right)u_{1,x}w_{0,xx}+2\left(A_{55}-\frac{8}{h^2}B_{55}+\frac{16}{h^4}D_{55}\right)u_1w_{0,x}+\left(\frac{4}{3h^2}G_{11}-E_{11}\right)u_{1,x}w_{1,xx}$$

$$+\left(2B_{13}-\frac{8}{3h^2}E_{13}\right)u_{1,x}w_1+\left(\frac{8}{9h^2}H_{11}-\frac{2}{3}F_{11}\right)u_{1,x}w_{2,xx}+\left(4D_{13}-\frac{16}{3h^2}F_{13}\right)u_{1,x}w_2+\frac{16}{9h^4}H_{11}(w_{0,xx})^2$$

$$+\left(A_{55}-\frac{8}{h^2}B_{55}+\frac{16}{h^4}D_{55}\right)(w_{0,x})^2+\frac{4}{3h^2}G_{11}w_{0,xx}w_{1,xx}-\frac{8}{3h^2}E_{13}w_{0,xx}w_1+\frac{8}{9h^2}H_{11}w_{0,xx}w_{2,xx}$$

$$-\frac{16}{3h^2}F_{13}w_{0,xx}w_2+\frac{1}{4}F_{11}(w_{1,xx})^2-D_{13}w_{1,xx}w_1+A_{33}w_1^2+\frac{1}{3}G_{11}w_{1,xx}w_{2,xx}-2E_{13}w_{1,xx}w_2$$

$$-\frac{2}{3}E_{13}w_{2,xx}w_1+4B_{33}w_1w_2+\frac{1}{9}H_{11}(w_{2,xx})^2-\frac{4}{3}F_{13}w_{2,xx}w_2+4D_{33}w_2^2\Bigg]dx \tag{4.10}$$

where the stiffness coefficients of the beam are determined as follows:

$$\left(A_{11},B_{11},D_{11},E_{11},F_{11},G_{11},H_{11}\right)=\sum_{k=1}^{n}\int_{z_k}^{z_{k+1}}\overline{\overline{C}}_{11}\left(1,z,z^2,z^3,z^4,z^5,z^6\right)bdz \tag{4.11}$$

$$\left(A_{13},B_{13},D_{13},E_{13},F_{13}\right)=\sum_{k=1}^{n}\int_{z_k}^{z_{k+1}}\overline{\overline{C}}_{13}\left(1,z,z^2,z^3,z^4\right)bdz \tag{4.12}$$

$$\left(A_{33},B_{33},D_{33}\right)=\sum_{k=1}^{n}\int_{z_k}^{z_{k+1}}\overline{\overline{C}}_{33}\left(1,z,z^2\right)bdz \tag{4.13}$$

$$\left(A_{55},B_{55},D_{55}\right)=\sum_{k=1}^{n}\int_{z_k}^{z_{k+1}}\overline{\overline{C}}_{55}\left(1,z^2,z^4\right)bdz \tag{4.14}$$

The work done Π_W by compression load N_0 and transverse load q applied on the beam bottom surface is given by:

$$\Pi_W=\frac{1}{2}\int_0^L N_0\left(w_{0,x}^2+\frac{h^2}{6}w_{0,x}w_{2,x}+\frac{h^2}{12}w_{1,x}^2+\frac{h^4}{80}w_{2,x}^2\right)dx-\int_0^L q\left(w_0-\frac{h}{2}w_1+\frac{h^2}{4}w_2\right)bdx \tag{4.15}$$

The kinetic energy Π_K of beam is written by:

$$\Pi_K=\frac{1}{2}\int_V\rho(z)\left(\dot{u}^2+\dot{w}^2\right)dV$$

$$=\frac{1}{2}\int_0^L\Bigg[I_1\dot{u}_0^2-I_3\dot{u}_0\dot{w}_{1'x}+\left(I_3+\frac{16}{9h^4}I_7-\frac{8}{3h^2}I_5\right)\dot{u}_1^2+\left(\frac{32}{9h^4}I_7-\frac{8}{3h^2}I_5\right)\dot{u}_1\dot{w}_{0,x}+\left(\frac{8}{9h^2}I_7-\frac{2}{3}I_5\right)\dot{u}_1\dot{w}_{2,x}$$

$$+\frac{16}{9h^4}I_7\dot{w}_{0,x}^2+I_1\dot{w}_0^2+\frac{8}{9h^2}I_7\dot{w}_{0,x}\dot{w}_{2,x}+2I_3\dot{w}_0\dot{w}_2+\frac{1}{4}I_5\dot{w}_{1,x}^2+I_3\dot{w}_1^2+\frac{1}{9}I_7\dot{w}_{2,x}^2+I_5\dot{w}_2^2)\Bigg]dx \tag{4.16}$$

where dot-superscript denotes the differentiation with respect to the time t; ρ is the mass density of each layer, and I_1, I_3, I_5, I_7 are the inertia coefficients defined by:

$$\left(I_1, I_3, I_5, I_7\right) = \sum_{k=1}^{n} \int_{z_k}^{z_{k+1}} \rho\left(1, z^2, z^4, z^6\right) b dz \tag{4.17}$$

The total potential energy of system is expressed by:

$$\Pi = \Pi_E + \Pi_W - \Pi_K \tag{4.18}$$

Based on the Ritz method, the displacement field in Eq. (4.1 and 4.2) is approximated in the following forms:

$$u_0(x,t) = \sum_{j=1}^{m} \varphi_{j,x}(x) u_{0j} e^{i\omega t} \tag{4.19}$$

$$u_1(x,t) = \sum_{j=1}^{m} \varphi_{j,x}(x) u_{1j} e^{i\omega t} \tag{4.20}$$

$$w_0(x,t) = \sum_{j=1}^{m} \varphi_j(x) w_{0j} e^{i\omega t} \tag{4.21}$$

$$w_1(x,t) = \sum_{j=1}^{m} \varphi_j(x) w_{1j} e^{i\omega t} \tag{4.22}$$

$$w_2(x,t) = \sum_{j=1}^{m} \varphi_j(x) w_{2j} e^{i\omega t} \tag{4.23}$$

where ω is the frequency; $i^2 = -1$ the imaginary unit; u_{0j}, u_{1j}, w_{0j}, w_{1j}, w_{2j} are unknown values to be determined; $\varphi_j(x)$ are the approximation functions. The approximation functions of Ritz method should satisfy the specified essential boundary conditions [1]. In this Chapter, the new approximation functions which combine polynomial and exponential functions are proposed. These approximation functions are given in Table 4.1 for S-S, C-C and C-F boundary conditions.

Table 4.1. Approximation functions and kinematic BCs of beams.

BC	Position	$\varphi_j(x)$	Value
S-S	x=0	$x(L-x)e^{\frac{x}{jL}}$	$w_0=0, w_1=0, w_2=0$
	x=L		$w_0=0, w_1=0, w_2=0$
C-F	x=0	$x^2 e^{\frac{x}{jL}}$	$u_0=0, u_1=0, w_0=0, w_1=0, w_2=0,$ $w_{0,x}=0, w_{1,x}=0, w_{2,x}=0$
	x=L		
C-C	x=0	$x^2(L-x)^2 e^{\frac{x}{jL}}$	$u_0=0, u_1=0, w_0=0, w_1=0, w_2=0,$ $w_{0,x}=0, w_{1,x}=0, w_{2,x}=0$
	x=L		$u_0=0, u_1=0, w_0=0, w_1=0, w_2=0,$ $w_{0,x}=0, w_{1,x}=0, w_{2,x}=0$

The governing equations of motion can be obtained by substituting Eqs. (4.19-4.23) into Eq. (4.18) and using Lagrange's equations:

$$\frac{\partial \Pi}{\partial q_j}-\frac{d}{dt}\frac{\partial \Pi}{\partial \dot{q}_j}=0 \tag{4.24}$$

with q_j representing the values of $(u_{0j}, u_{1j}, w_{0j}, w_{1j}, w_{2j})$, that leads to:

$$\left(\begin{bmatrix} \mathbf{K}^{11} & \mathbf{K}^{12} & \mathbf{K}^{13} & \mathbf{K}^{14} & \mathbf{K}^{15} \\ {}^T\mathbf{K}^{12} & \mathbf{K}^{22} & \mathbf{K}^{23} & \mathbf{K}^{24} & \mathbf{K}^{25} \\ {}^T\mathbf{K}^{13} & {}^T\mathbf{K}^{23} & \mathbf{K}^{33} & \mathbf{K}^{34} & \mathbf{K}^{35} \\ {}^T\mathbf{K}^{14} & {}^T\mathbf{K}^{24} & {}^T\mathbf{K}^{34} & \mathbf{K}^{44} & \mathbf{K}^{45} \\ {}^T\mathbf{K}^{15} & {}^T\mathbf{K}^{25} & {}^T\mathbf{K}^{35} & {}^T\mathbf{K}^{45} & \mathbf{K}^{55} \end{bmatrix} - \omega^2 \begin{bmatrix} \mathbf{M}^{11} & \mathbf{0} & \mathbf{0} & \mathbf{M}^{14} & \mathbf{0} \\ \mathbf{0} & \mathbf{M}^{22} & \mathbf{M}^{23} & \mathbf{0} & \mathbf{M}^{25} \\ \mathbf{0} & {}^T\mathbf{M}^{23} & \mathbf{M}^{33} & \mathbf{0} & \mathbf{M}^{35} \\ {}^T\mathbf{M}^{14} & \mathbf{0} & \mathbf{0} & \mathbf{M}^{44} & \mathbf{0} \\ \mathbf{0} & {}^T\mathbf{M}^{25} & {}^T\mathbf{M}^{35} & \mathbf{0} & \mathbf{M}^{55} \end{bmatrix}\right)\begin{Bmatrix} \mathbf{u_0} \\ \mathbf{u_1} \\ \mathbf{w_0} \\ \mathbf{w_1} \\ \mathbf{w_2} \end{Bmatrix} = \begin{Bmatrix} \mathbf{0} \\ \mathbf{0} \\ \mathbf{F_0} \\ \mathbf{F_1} \\ \mathbf{F_2} \end{Bmatrix} \tag{4.25}$$

where the components of stiffness matrix **K**, mass matrix **M** and load vector **F** are given by:

$$K_{ij}^{11}=A_{11}\int_0^L \varphi_{i,xx}\varphi_{j,xx}dx,\ K_{ij}^{12}=\left(B_{11}-\frac{4}{3h^2}E_{11}\right)\int_0^L \varphi_{i,xx}\varphi_{j,xx}dx,\ K_{ij}^{13}=-\frac{4}{3h^2}E_{11}\int_0^L \varphi_{i,xx}\varphi_{j,xx}dx$$

$$K_{ij}^{14}=-\frac{1}{2}D_{11}\int_0^L \varphi_{i,xx}\varphi_{j,xx}dx+A_{13}\int_0^L \varphi_{i,xx}\varphi_j dx,\ K_{ij}^{15}=-\frac{1}{3}E_{11}\int_0^L \varphi_{i,xx}\varphi_{j,xx}dx+2B_{13}\int_0^L \varphi_{i,xx}\varphi_j dx$$

$$K_{ij}^{22}=\left(D_{11}-\frac{8}{3h^2}F_{11}+\frac{16}{9h^4}H_{11}\right)\int_0^L \varphi_{i,xx}\varphi_{j,xx}dx+\left(A_{55}-\frac{8}{h^2}B_{55}+\frac{16}{h^4}D_{55}\right)\int_0^L \varphi_{i,x}\varphi_{j,x}dx$$

$$K_{ij}^{23}=\left(-\frac{4}{3h^2}F_{11}+\frac{16}{9h^4}H_{11}\right)\int_0^L\varphi_{i,xx}\varphi_{j,xx}dx+\left(A_{55}-\frac{8}{h^2}B_{55}+\frac{16}{h^4}D_{55}\right)\int_0^L\varphi_{i,x}\varphi_{j,x}dx$$

$$K_{ij}^{24}=\left(-\frac{1}{2}E_{11}+\frac{2}{3h^2}G_{11}\right)\int_0^L\varphi_{i,xx}\varphi_{j,xx}dx+\left(B_{13}-\frac{4}{3h^2}E_{13}\right)\int_0^L\varphi_{i,xx}\varphi_{j}dx$$

$$K_{ij}^{25}=\left(-\frac{1}{3}F_{11}+\frac{4}{9h^2}H_{11}\right)\int_0^L\varphi_{i,xx}\varphi_{j,xx}dx+\left(2D_{13}-\frac{8}{3h^2}F_{13}\right)\int_0^L\varphi_{i,xx}\varphi_{j}dx$$

$$K_{ij}^{33}=\frac{16}{9h^4}H_{11}\int_0^L\varphi_{i,xx}\varphi_{j,xx}dx+\left(A_{55}-\frac{8}{h^2}B_{55}+\frac{16}{h^4}D_{55}\right)\int_0^L\varphi_{i,x}\varphi_{j,x}dx+N_0\int_0^L\varphi_{i,x}\varphi_{j,x}dx$$

$$K_{ij}^{34}=\frac{2}{3h^2}H_{11}\int_0^L\varphi_{i,xx}\varphi_{j,xx}dx-\frac{4}{3h^2}E_{13}\int_0^L\varphi_{i,xx}\varphi_{j}dx$$

$$K_{ij}^{35}=\frac{4}{9h^2}H_{11}\int_0^L\varphi_{i,xx}\varphi_{j,xx}dx-\frac{8}{3h^2}F_{13}\int_0^L\varphi_{i,xx}\varphi_{j}dx+\frac{h^2}{12}N_0\int_0^L\varphi_{i,x}\varphi_{j,x}dx$$

$$K_{ij}^{44}=\frac{1}{4}F_{11}\int_0^L\varphi_{i,xx}\varphi_{j,xx}dx-D_{13}\int_0^L\varphi_{i,xx}\varphi_{j}dx+A_{33}\int_0^L\varphi_{i}\varphi_{j}dx+\frac{h^2}{12}N_0\int_0^L\varphi_{i,x}\varphi_{j,x}dx$$

$$K_{ij}^{45}=\frac{1}{6}G_{11}\int_0^L\varphi_{i,xx}\varphi_{j,xx}dx-E_{13}\int_0^L\varphi_{i,xx}\varphi_{j}dx-\frac{1}{3}E_{13}\int_0^L\varphi_{i}\varphi_{j,xx}dx+2B_{33}\int_0^L\varphi_{i}\varphi_{j}dx$$

$$K_{ij}^{55}=\frac{1}{9}H_{11}\int_0^L\varphi_{i,xx}\varphi_{j,xx}dx-\frac{4}{3}F_{13}\int_0^L\varphi_{i,xx}\varphi_{j}dx+4D_{33}\int_0^L\varphi_{i}\varphi_{j}dx+\frac{h^4}{80}N_0\int_0^L\varphi_{i,x}\varphi_{j,x}dx$$

$$M_{ij}^{11}=I_1\int_0^L\varphi_{i,x}\varphi_{j,x}dx,\ M_{ij}^{14}=-\frac{1}{2}I_3\int_0^L\varphi_{i,x}\varphi_{j,x}dx,\ M_{ij}^{22}=\left(I_3-\frac{8}{3h^2}I_5+\frac{16}{9h^4}I_7\right)\int_0^L\varphi_{i,x}\varphi_{j,x}dx$$

$$M_{ij}^{23}=\left(-\frac{4}{3h^2}I_5+\frac{16}{9h^4}I_7\right)\int_0^L\varphi_{i,x}\varphi_{j,x}dx,\ M_{ij}^{25}=\left(-\frac{1}{3}I_5+\frac{4}{9h^2}I_7\right)\int_0^L\varphi_{i,x}\varphi_{j,x}dx$$

$$M_{ij}^{33}=I_1\int_0^L\varphi_{i}\varphi_{j}dx+\frac{16}{9h^4}I_7\int_0^L\varphi_{i,x}\varphi_{j,x}dx,\ M_{ij}^{35}=I_3\int_0^L\varphi_{i}\varphi_{j}dx+\frac{4}{9h^2}I_7\int_0^L\varphi_{i,x}\varphi_{j,x}dx$$

$$M_{ij}^{44}=I_3\int_0^L\varphi_{i}\varphi_{j}dx+\frac{1}{4}I_5\int_0^L\varphi_{i,x}\varphi_{j,x}dx,\ M_{ij}^{55}=I_5\int_0^L\varphi_{i}\varphi_{j}dx+\frac{1}{9}I_7\int_0^L\varphi_{i,x}\varphi_{j,x}dx$$

$$F_{0i}=\int_0^L q\varphi_i dx,\ F_{1i}=-\frac{h}{2}\int_0^L q\varphi_i dx,\ F_{2i}=\frac{h^2}{4}\int_0^L q\varphi_i dx \tag{4.26}$$

Finally, the static, vibration and buckling responses of composite beams can be determined by solving Eq. (4.25).

4.3. Numerical results

In this section, convergence and verification studies are carried out to demonstrate the accuracy of the present study. For static analysis, the beam is subjected to a uniformly distributed load with density q, applied on the surface $z=-h/2$ in the z-direction. Laminates are supposed to have equal thicknesses and made of the same orthotropic materials whose properties are given in Table 4.2. For convenience, the following nondimensional terms are used:

$$\bar{w}=\frac{100w_0E_2bh^3}{qL^4},\ \bar{\sigma}_x=\frac{bh^2}{qL^2}\sigma_x\left(\frac{L}{2},\frac{h}{2}\right),\ \bar{\sigma}_z=\frac{b}{q}\sigma_z\left(\frac{L}{2},\frac{h}{2}\right),\ \bar{\sigma}_{xz}=\frac{bh}{qL}\sigma_{xz}\left(0,0\right) \tag{4.27}$$

$$\bar{N}_{cr}=\frac{N_{cr}L^2}{bE_2h^3} \tag{4.28}$$

$$\bar{\omega}=\frac{\omega L^2}{h}\sqrt{\frac{\rho}{E_2}}\ \text{for Material (MAT) I.4 and}\ \bar{\omega}=\frac{\omega L^2}{h}\sqrt{\frac{\rho}{E_1}}\ \text{for MAT IV.4} \tag{4.29}$$

Table 4.2. Material properties of laminated composite beams.

Material properties	MAT I.4 [100]	MAT II.4 [69]	MAT III.4 [84, 128]	MAT IV.4 [78]
E_1 (GPa)	E_1/E_2=open	E_1/E_2=25	129.11	144.8
$E_2=E_3$(GPa)	-	-	9.408	9.65
$G_{12}=G_{13}$ (GPa)	$0.6E_2$	$0.5E_2$	5.1568	4.14
G_{23} (GPa)	$0.5E_2$	$0.2E_2$	3.45	3.45
$\nu_{12}=\nu_{13}=\nu_{23}$	0.25	0.25	0.3	0.3
ρ (kg/m^3)	-	-	1550.1	-
L (m)	L/h=open	L/h=open	0.1905	L/h=15
h (m)	-	-	0.003175	-
b (m)	-	-	0.0127	-

The composite beams (MAT I.4, $0^0/90^0$, $L/h=5$, $E_1/E_2=40$) with different BCs are considered to evaluate the convergence. The nondimensional fundamental

frequencies, critical buckling loads and mid-span displacements with respect to the series number m are given in Table 4.3. It can be seen that the present results converge at $m=12$ for natural frequency and critical buckling load, and $m=14$ for deflection. Thus, these numbers of series terms are chosen for analysis.

Table 4.3. Convergence studies for the nondimensional fundamental frequencies, critical buckling loads and mid-span displacements of $(0^0/90^0)$ composite beams (MAT I.4, $L/h=5$, $E_1/E_2=40$).

BC	m						
	2	4	6	8	10	12	14
a. Fundamental frequency							
S-S	6.3764	6.1406	6.1400	6.1400	6.1400	6.1400	6.1400
C-F	2.5879	2.3927	2.3845	2.3824	2.3820	2.3819	2.3819
C-C	10.3078	10.0566	9.9881	9.9650	9.9519	9.9435	9.9382
b. Critical buckling load							
S-S	4.1943	3.9217	3.9211	3.9211	3.9211	3.9211	3.9211
C-F	1.2668	1.2365	1.2341	1.2334	1.2333	1.2333	1.2333
C-C	8.8169	8.6247	8.6167	8.6160	8.6156	8.6154	8.6153
c. Deflection							
S-S	3.0041	3.2540	3.2481	3.2490	3.2488	3.2488	3.2488
C-F	6.9948	10.3704	10.4354	10.5022	10.4986	10.5079	10.5056
C-C	1.1999	1.2008	1.2440	1.2369	1.2473	1.2442	1.2455

4.3.1. Cross-ply beams

The symmetric $(0^0/90^0/0^0)$ and un-symmetric $(0^0/90^0)$ beams with different length-to-height ratios and BCs are considered in this example. The nondimensional fundamental frequencies, critical buckling loads and mid-span displacements $\left(x=L/2, z=0\right)$ of beams are presented in Tables 4.4, 4.5 and 4.6, respectively. The present results are compared with those from previous works using the HOBT [21, 24, 48, 69, 100, 101, 117] and the quasi-3D theories [20, 36, 44, 83]. It can be seen that the present results comply with earlier ones for both theories. It is also observed

that there are differences of the results predicted by HOBT and quasi-3D, especially for un-symmetric and thick beams ($L/h=5$). For slender beams ($L/h=50$), however, the predictions by HOBT and quasi-3D are close to each other.

Table 4.4. Nondimensional fundamental frequencies of ($0^0/90^0/0^0$) and ($0^0/90^0$) composite beams (MAT I.4, $E_1/E_2 = 40$).

Theory	Reference	$0^0/90^0/0^0$		$0^0/90^0$	
		L/h=5	50	*L/h*=5	50
a. S-S boundary condition					
HOBT	Present	9.206	17.449	6.125	7.297
	Khdeir and Reddy [101]	9.208	-	6.128	-
	Vo and Thai [21]	9.206	17.449	6.058	7.296
	Murthy et al. [24]	9.207	-	6.045	-
	Aydogdu [100]	9.207	-	6.144	-
Quasi-3D	Present	9.208	17.449	6.140	7.297
	Mantari and Canales [44]	9.208	-	6.109	-
	Matsunaga [83]	9.200	-	5.662	-
b. C-F boundary condition					
HOBT	Present	4.230	6.262	2.381	2.603
	Khdeir and Reddy [101]	4.234	-	2.386	-
	Murthy et al. [24]	4.230	-	2.378	-
	Aydogdu [100]	4.234	-	2.384	-
Quasi-3D	Present	4.223	6.262	2.382	2.604
	Mantari and Canales [44]	4.221	-	2.375	-
c. C-C boundary condition					
HOBT	Present	11.601	37.629	10.019	16.414
	Khdeir and Reddy [101]	11.603	-	10.026	-
	Murthy et al. [24]	11.602	-	10.011	-
	Aydogdu [100]	11.637	-	10.103	-
Quasi-3D	Present	11.499	37.633	9.944	16.432
	Mantari and Canales [44]	11.486	-	9.974	-

Table 4.5. Nondimensional critical buckling loads of ($0^0/90^0/0^0$) and ($0^0/90^0$) composite beams (MAT I.4, $E_1/E_2 = 40$).

Theory	Reference	$0^0 / 90^0 / 0^0$		$0^0 / 90^0$	
		L/h=5	50	*L/h*=5	50
a. S-S boundary condition					
HOBT	Present	8.609	30.859	3.902	5.398
	Khdeir and Reddy [117]	8.613	-	-	-
	Aydogdu [48]	8.613	-	3.906	-
Quasi-3D	Present	8.613	30.860	3.921	5.398
	Mantari and Canales [44]	8.585	-	3.856	-
b. C-F boundary condition					
HOBT	Present	4.704	7.873	1.234	1.353
	Khdeir and Reddy [117]	4.708	-	-	-
	Aydogdu [48]	4.708	-	1.236	-
Quasi-3D	Present	4.699	7.874	1.233	1.354
	Mantari and Canales [44]	4.673	-	1.221	-
c. C-C boundary condition					
HOBT	Present	11.648	114.237	8.668	21.339
	Khdeir and Reddy [117]	11.652	-	-	-
Quasi-3D	Present	11.652	114.260	8.615	21.371
	Mantari and Canales [44]	11.502	-	8.509	-

Table 4.6. Nondimensional mid-span displacements of ($0^0/90^0/0^0$) and ($0^0/90^0$) composite beams under a uniformly distributed load (MAT II.4).

Theory	Reference	$0^0/90^0/0^0$			$0^0/90^0$		
		L/h=5	10	50	*L/h*=5	10	50
a. S-S boundary condition							
HOBT	Present	2.414	1.098	0.666	4.785	3.697	3.345
	Murthy et al. [24]	2.398	1.090	0.661	4.750	3.668	3.318
	Khdeir and Reddy [69]	2.412	1.096	0.666	4.777	3.688	3.336
Quasi-3D	Present	2.405	1.097	0.666	4.764	3.694	3.345
	Zenkour [36]	2.405	1.097	0.666	4.828	3.763	3.415
	Mantari and Canales [20]	-	1.097	-	-	3.731	-
b. C-F boundary condition							
HOBT	Present	6.830	3.461	2.257	15.308	12.371	11.365
	Murthy et al. [24]	6.836	3.466	2.262	15.334	12.398	11.392
	Khdeir and Reddy [69]	6.824	3.455	2.251	15.279	12.343	11.337
Quasi-3D	Present	6.844	3.451	2.256	15.260	12.339	11.343
	Mantari and Canales [20]	-	3.459	-	-	12.475	-
c. C-C boundary condition							
HOBT	Present	1.538	0.532	0.147	1.924	1.007	0.680
	Khdeir and Reddy [69]	1.537	0.532	0.147	1.922	1.005	0.679
Quasi-3D	Present	1.543	0.532	0.147	1.916	1.005	0.679
	Mantari and Canales [20]	-	0.532	-	-	1.010	-

The nondimensional axial, transverse shear, and transverse normal stresses of simply supported beams with $L/h = 5, 50$ are presented in Table 4.7, and compared

to the solutions obtained by Vo and Thai [22] using HOBT and Mantari and Canales [20], Zenkour [36] using quasi-3D theory. Good agreements with the previous models are also found.

Table 4.7. Nondimensional stresses of ($0^0/90^0/0^0$) and ($0^0/90^0$) composite beams with S-S boundary condition under a uniformly distributed load (MAT II.4).

Theory	Reference	$0^0/90^0/0^0$		$0^0/90^0$	
		L/h=5	50	L/h=5	50
a. Normal axial stress					
HOBT	Present	1.0669	0.8705	0.2361	0.2336
	Zenkour [36]	1.0669	0.7805	0.2362	0.2336
	Vo and Thai [22]	1.0670	-	0.2361	-
Quasi-3D	Present	1.0732	0.7806	0.2380	0.2336
	Zenkour [36]	1.0732	0.7806	0.2276	0.2236
b. Shear stress					
HOBT	Present	0.4057	0.4523	0.9205	0.9878
	Zenkour [36]	0.4057	0.4514	0.9211	0.9860
	Vo and Thai [22]	0.4057	-	0.9187	-
Quasi-3D	Present	0.4013	0.4521	0.9052	0.9869
	Zenkour [36]	0.4013	0.4509	0.9038	0.9814
c. Transverse normal stress					
Quasi-3D	Present	0.1833	0.1804	0.2966	0.3046
	Zenkour [36]	0.1833	0.1804	0.2988	0.2983

The distribution of nondimensional transverse displacements across the thickness direction for $L/h = 5,10,50$ is displayed in Figs. 4.1-4.3. It is observed that the nonlinear variation of transverse displacement is clearly displayed for thick beams ($L/h = 5$) with all BCs.

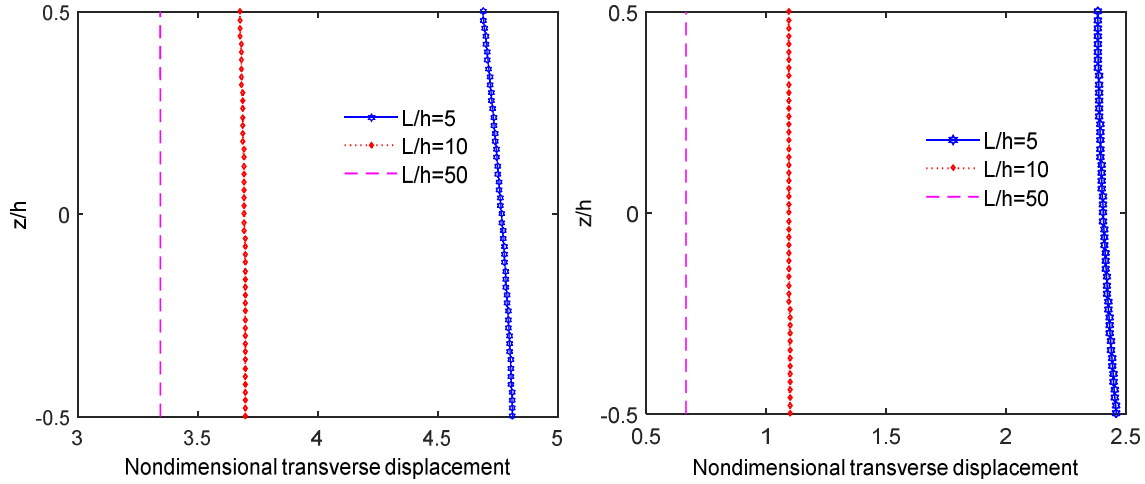

a. $0^0/90^0$ b. $0^0/90^0/0^0$

Figure 4.1. Distribution of nondimensional transverse displacement through the thickness of ($0^0/90^0$) and ($0^0/90^0/0^0$) composite beams with S-S boundary condition (MAT II.4).

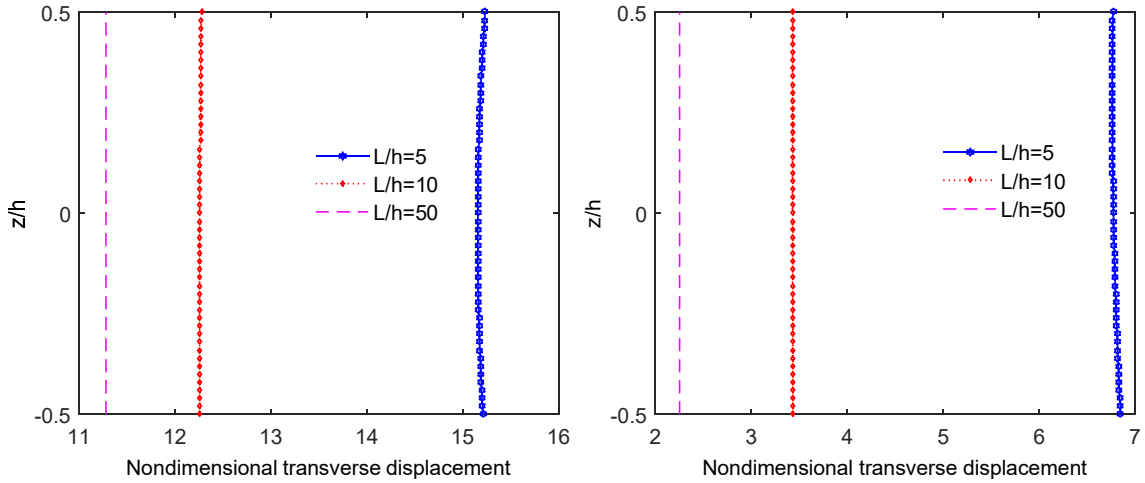

a. $0^0/90^0$ b. $0^0/90^0/0^0$

Figure 4.2. Distribution of nondimensional transverse displacement through the thickness of ($0^0/90^0$) and ($0^0/90^0/0^0$) composite beams with C-F boundary condition (MAT II.4).

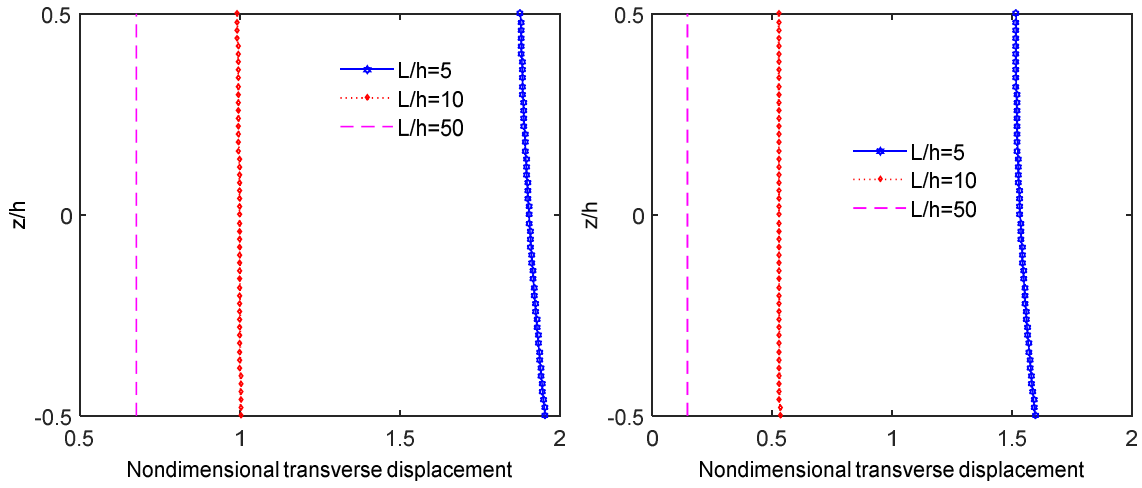

a. $0^0/90^0$ b. $0^0/90^0/0^0$

Figure 4.3. Distribution of nondimensional transverse displacement through the thickness of $(0^0/90^0)$ and $(0^0/90^0/0^0)$ composite beams with C-C boundary condition (MAT II.4).

4.3.2. Angle-ply beams

This example is extended from previous one. The $(0^0/\theta/0^0)$ and $(0^0/\theta)$ beams are considered. Tables 4.8, 4.9, 4.10 and 4.11 present variation of nondimensional fundamental frequencies, critical buckling loads, mid-span displacements $(x = L/2, z = 0)$ and stresses of beams used Quasi-3D theory respect to the angle-ply of beams. It can be seen that the present results in Table 4.10 and 4.11 are close with those of Vo et al. [19].

Table 4.8. Nondimensional fundamental frequencies of ($0^0/\theta\ /0^0$) and ($0^0/\theta$) composite beams (MAT I.4, $E_1/E_2 = 40$).

Lay-up	BC	*L/h*	Angle-ply (θ)			
			0^0	30^0	60^0	90^0
$0^0/\theta/0^0$	S-S	5	9.5498	9.4487	9.2831	9.2083
		10	13.9976	13.8130	13.6729	13.6099
		50	17.7844	17.4788	17.4558	17.4493
	C-F	5	4.3628	4.3047	4.2484	4.2231
		10	5.6259	5.5403	5.5059	5.4909
		50	6.3803	6.2697	6.2635	6.2622
	C-C	5	12.0240	11.8341	11.6020	11.4992
		10	20.4355	20.1923	19.8335	19.6723
		50	38.4410	37.8172	37.6863	37.6333
$0^0/\theta$	S-S	5	9.5498	6.8336	6.2215	6.1400
		10	13.9976	7.9772	7.0561	6.9475
		50	17.7844	8.5069	7.4191	7.2971
	C-F	5	4.3628	2.7077	2.4173	2.3819
		10	5.6259	2.9428	2.5837	2.5428
		50	6.3803	3.0359	2.6474	2.6043
	C-C	5	12.0240	10.4823	10.0347	9.9435
		10	20.4355	15.0934	13.8389	13.6637
		50	38.4410	19.0914	16.6995	16.4323

Table 4.9. Nondimensional critical buckling loads of ($0^0/\theta/0^0$) and ($0^0/\theta$) composite beams (MAT I.4, $E_1/E_2 = 40$).

Lay-up	BC	*L/h*	Angle-ply (θ)			
			0^0	30^0	60^0	90^0
$0^0/\theta/0^0$	S-S	5	9.2665	9.0709	8.7542	8.6131
		10	19.9125	19.3911	18.9974	18.8217
		50	32.0563	30.9641	30.8826	30.8596
	C-F	5	4.9708	4.8413	4.7432	4.6994
		10	7.0644	6.8417	6.7856	6.7622
		50	8.1715	7.8897	7.8762	7.8739
	C-C	5	12.7118	12.3736	11.8718	11.6517
		10	37.0660	36.2838	35.0169	34.4524
		50	119.0990	115.2235	114.5322	114.2601
$0^0/\theta$	S-S	5	9.2665	4.8298	4.0242	3.9211
		10	19.9125	6.5116	5.1007	4.9455
		50	32.0563	7.3361	5.5800	5.3981
	C-F	5	4.9708	1.6246	1.2717	1.2333
		10	7.0644	1.7845	1.3672	1.3236
		50	8.1715	1.8418	1.3998	1.3543
	C-C	5	12.7118	9.6517	8.7780	8.6154
		10	37.0660	19.3221	16.1028	15.6927
		50	119.0990	28.8970	22.0782	21.3712

Table 4.10. Nondimensional mid-span displacements of ($0^0/\theta\ /0^0$) and ($0^0/\theta$) composite beams under a uniformly distributed load (MAT II.4).

Lay-up	BC	*L/h*	Reference	Angle-ply (θ)			
				0^0	30^0	60^0	90^0
$0^0/\theta/0^0$	S-S	5	Present	1.7930	2.0140	2.3030	2.4049
			Vo et al. [19]	1.7930	2.0140	2.3030	2.4049
		10	Present	0.9222	0.9946	1.0700	1.0965
			Vo et al. [19]	0.9222	0.9946	1.0700	1.0965
		50	Present	0.6370	0.6608	0.6650	0.6661
			Vo et al. [19]	0.6370	0.6608	0.6650	0.6661
	C-F	5	Present	5.2683	5.8705	6.5930	6.8442
			Vo et al. [19]	5.2774	5.8804	6.6029	6.8541
		10	Present	2.9647	3.1810	3.3871	3.4511
			Vo et al. [19]	2.9663	3.1828	3.3889	3.4605
		50	Present	2.1599	2.2402	2.2529	2.2562
			Vo et al. [19]	2.1602	2.2405	2.2531	2.2565
	C-C	5	Present	1.0866	1.2616	1.4711	1.5431
			Vo et al. [19]	1.0998	1.2670	1.4766	1.5487
		10	Present	0.3958	0.4459	0.5098	0.5323
			Vo et al. [19]	0.3968	0.4469	0.5108	0.5332
		50	Present	0.1367	0.1431	0.1462	0.1473
			Vo et al. [19]	0.1367	0.1431	0.1462	0.1472
$0^0/\theta$	S-S	5	Present	1.7930	3.6681	4.6312	4.7645
			Vo et al. [19]	1.7930	3.6634	4.6135	4.7346
		10	Present	0.9222	2.7463	3.6070	3.6942
			Vo et al. [19]	0.9222	2.7403	3.5871	3.6626
		50	Present	0.6370	2.4454	3.2725	3.3446
			Vo et al. [19]	0.6370	2.4406	3.2540	3.3147
	C-F	5	Present	5.2683	11.6981	14.8708	15.2595

Lay-up	BC	*L/h*	Reference	Angle-ply (θ)			
				0^0	30^0	60^0	90^0
			Vo et al. [19]	5.2774	11.6830	14.8020	15.1540
		10	Present	2.9647	9.1667	12.0630	12.3387
			Vo et al. [19]	2.9663	9.1499	12.0020	12.2440
		50	Present	2.1599	8.3044	11.1059	11.3428
			Vo et al. [19]	2.1602	8.2916	11.0540	11.2580
	C-C	5	Present	1.0866	1.5673	1.8524	1.9164
			Vo et al. [19]	1.0998	1.5755	1.8575	1.9193
		10	Present	0.3958	0.7797	0.9771	1.0050
			Vo et al. [19]	0.3968	0.7783	0.9726	0.9983
		50	Present	0.1367	0.4987	0.6646	0.6790
			Vo et al. [19]	0.1367	0.4974	0.6608	0.6733

Table 4.11. Nondimensional stresses of ($0^0/\theta/0^0$) and ($0^0/\theta$) composite beams with S-S boundary condition under a uniformly distributed load (MAT II.4).

Lay-up	*L/h*	Reference	Angle-ply (θ)			
			0^0	30^0	60^0	90^0
a. Normal axial stress						
$0^0/\theta/0^0$	5	Present	0.9556	1.0062	1.0556	1.0732
		Vo et al. [19]	0.9498	1.0010	1.0500	1.0670
	10	Present	0.7998	0.8325	0.8459	0.8504
		Vo et al. [19]	0.8002	0.8326	0.8459	0.8502
	50	Present	0.7520	0.7785	0.7803	0.7806
		Vo et al. [19]	0.7523	0.7788	0.7806	0.7809
$0^0/\theta$	5	Present	0.9556	0.3736	0.2476	0.2380
		Vo et al. [19]	0.9498	0.3746	0.2510	0.2428
	10	Present	0.7998	0.3655	0.2445	0.2346

Lay-up	*L/h*	Reference	Angle-ply (θ)			
			0^0	30^0	60^0	90^0
		Vo et al. [19]	0.8002	0.3661	0.2464	0.2375
	50	Present	0.7520	0.3631	0.2436	0.2336
		Vo et al. [19]	0.7523	0.3633	0.2449	0.2358
b. Shear stress						
$0^0/\theta/0^0$	5	Present	0.6668	0.5721	0.4456	0.4013
		Vo et al. [19]	0.6679	0.5729	0.4462	0.4017
	10	Present	0.7078	0.6070	0.4751	0.4286
		Vo et al. [19]	0.7100	0.6088	0.4762	0.4295
	50	Present	0.7439	0.6377	0.5006	0.4521
		Vo et al. [19]	0.7434	0.6373	0.5003	0.4518
$0^0/\theta$	5	Present	0.6668	0.7545	0.8646	0.9052
		Vo et al. [19]	0.6679	0.7598	0.8703	0.9117
	10	Present	0.7078	0.7902	0.9046	0.9476
		Vo et al. [19]	0.7100	0.7913	0.9039	0.9474
	50	Present	0.7439	0.8234	0.9418	0.9869
		Vo et al. [19]	0.7434	0.7434	0.8085	0.8481

Figs. 4.4-4.6 show the displacements of the ($0^0/\theta/0^0$) and ($0^0/\theta$) thick beams $(L/h=3)$ increase with the increase of angle-ply θ. There are significant differences between the results of HOBT and quasi-3D solutions.

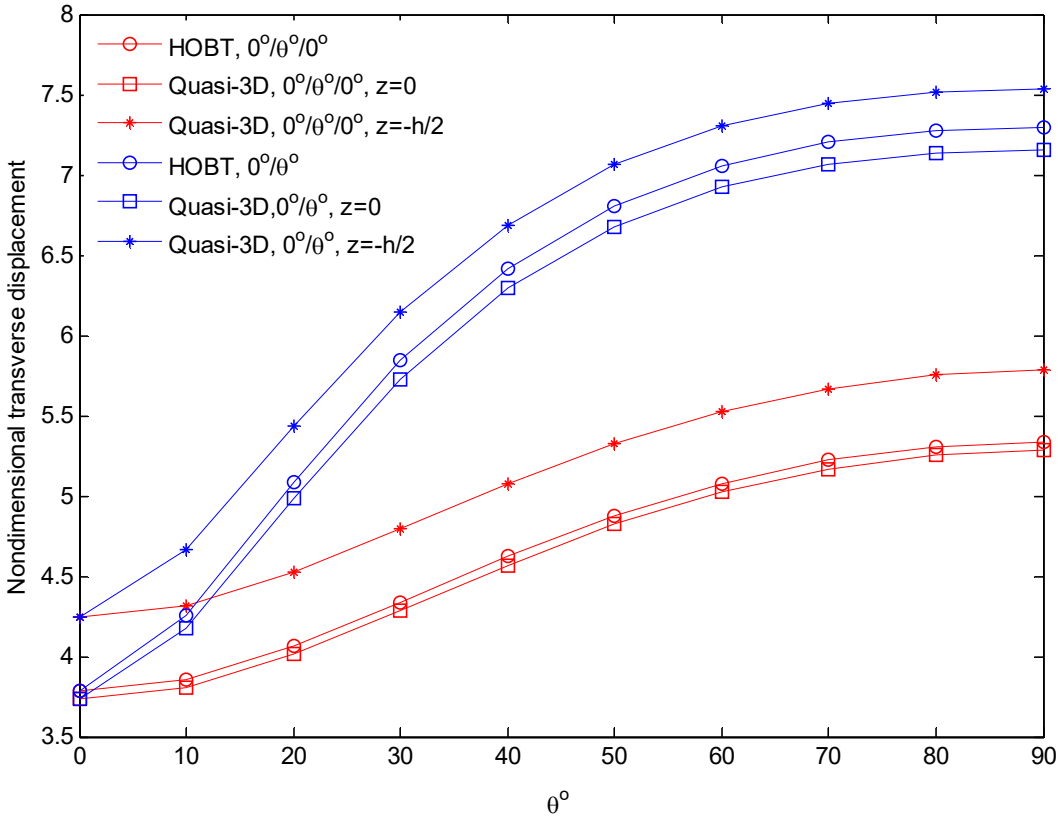

Figure 4.4. The nondimensional mid-span transverse displacement with respect to the fiber angle change of composite beams with S-S boundary condition ($L/h=3$, MAT II.4).

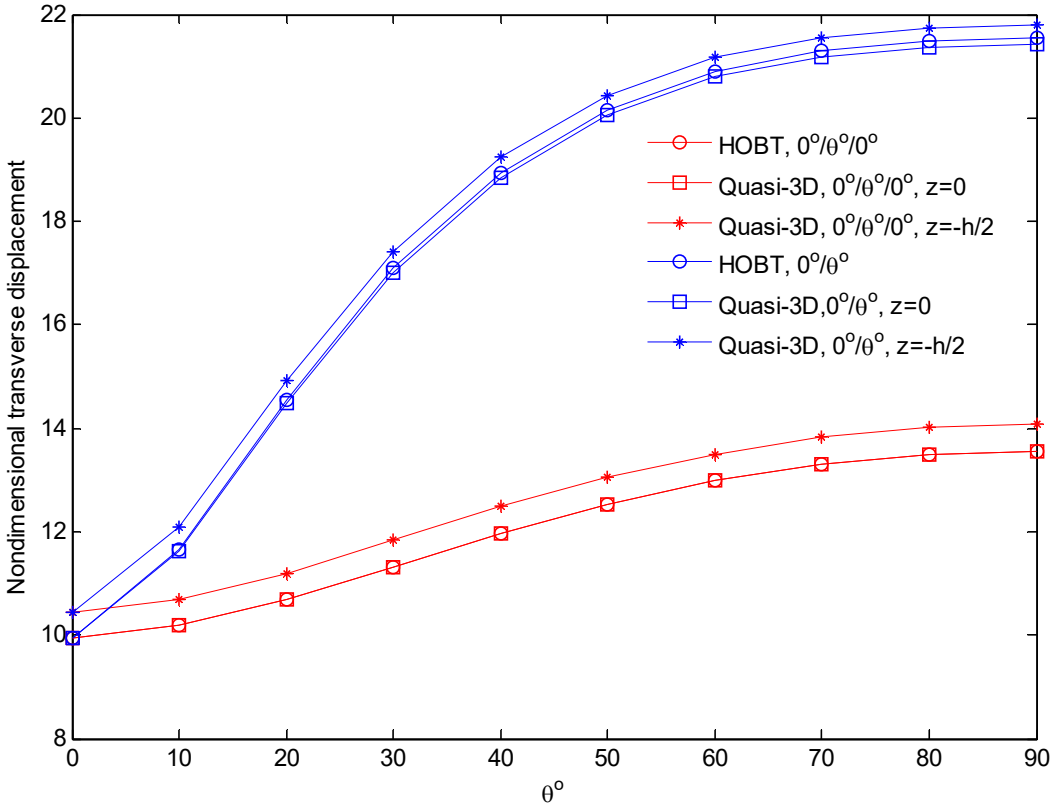

Figure 4.5. The nondimensional mid-span transverse displacement with respect to the fiber angle change of composite beams with C-F boundary condition ($L / h = 3$, MAT II.4).

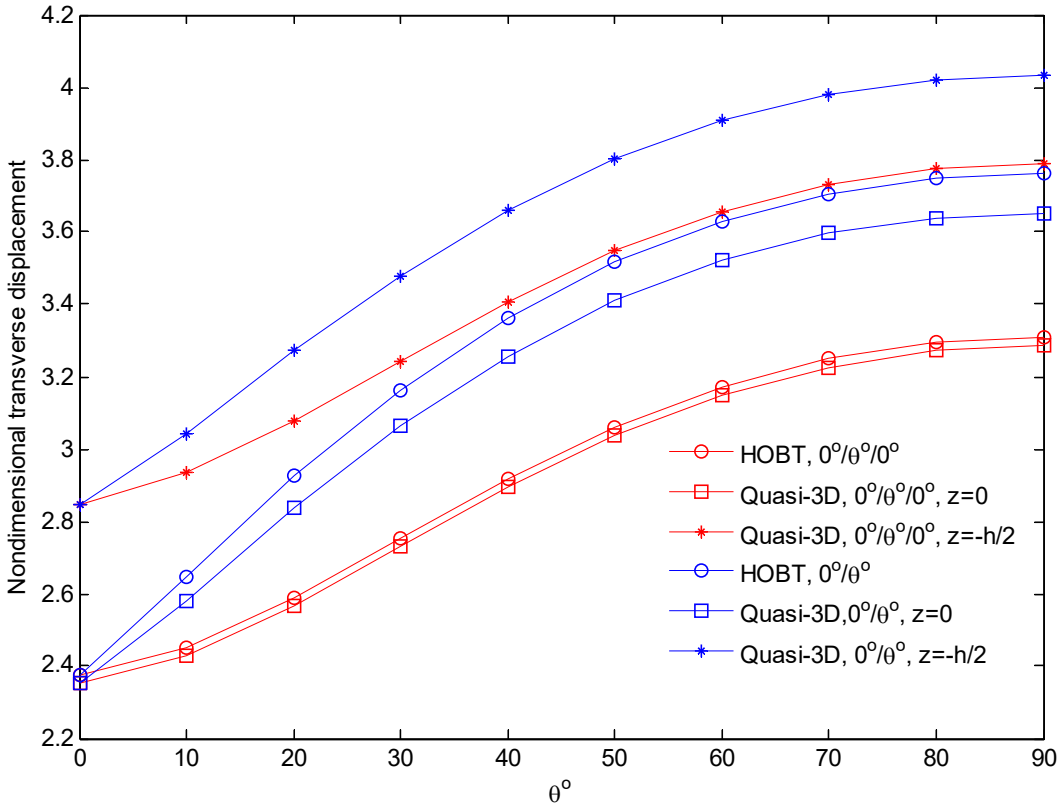

Figure 4.6. The nondimensional mid-span transverse displacement with respect to the fiber angle change of composite beams with C-C boundary condition ($L/h=3$, MAT II.4).

4.3.3. Arbitrary-ply beams

The example aims to analyse behaviours of composite beams with arbitrary-ply. The first, the symmetric single-layered C-F beams of 15^0 and 30^0 ply (MAT III.4) are considered. Their first four natural frequencies are displayed in Table 4.12 and compared with those from Chen et al. [84] and experiment results of Abarcar and Cunniff [128]. It is seen that there is consistency between present results and those from [84] and [128], especially the first mode of vibration.

Table 4.12. Fundamental frequencies (Hz) of single-layer composite beam with C-F boundary condition (MAT III.4).

Lay-up	Theory	Reference	Mode			
			1	2	3	4
15^0	HOBT	Present	82.19	512.86	1426.29	-
	Quasi-3D	Present	82.22	513.09	1427.12	-
		Chen et al. [84]	82.55	515.68	1437.02	-
	Experiment	Abarcar and Cunniff [128]	82.50	511.30	1423.40	1526.90*
30^0	HOBT	Present	52.63	329.13	918.51	1791.22
	Quasi-3D	Present	52.67	329.43	919.48	1793.62
		Chen et al. [84]	52.73	330.04	922.45	1803.01
	Experiment	Abarcar and Cunniff [128]	52.70	331.80	924.70	1766.90

Note: '' denotes: the results are the torsional mode*

Table 4.13. Nondimensional fundamental frequencies of arbitrary-ply laminated composite beams (MAT IV.4).

Lay-up	Theory	Reference	BC		
			S-S	C-F	C-C
$45^0/-45^0/45^0/-45^0$	HOBT	Present	0.7961	0.2849	1.7592
		Chandrashekhara and Bangera [27]	0.8278	0.2962	1.9807
	Quasi-3D	Present	0.7962	0.2852	1.7629
		Chen et al. [84]	0.7998	0.2969	1.8446
$30^0/-50^0/50^0/-30^0$	HOBT	Present	0.9726	0.3486	2.1255
	Quasi-3D	Present	0.9728	0.3489	2.1281
		Chen et al. [84]	0.9790	0.3572	2.2640

Next, the un-symmetric ($45^0/-45^0/45^0/-45^0$) and ($30^0/-50^0/50^0/-30^0$) beams (MAT IV.4) with various BCs are considered, and their responses on fundamental frequencies are reported in Table 4.13. Good agreements of the present theory and

previous studies are again found. Finally, the symmetric $(\theta/-\theta)_s$ composite beams (MAT IV.4) are considered.

The effects of angle-ply variation on the frequency, buckling and displacement are again illustrated in Table 4.14. In addition, the nondimensional fundamental frequencies are also shown in Fig. 4.7. It can be seen that the present frequencies are closer to those of [47, 84] and smaller than to those of [78, 130] which neglected the Poisson's effect, especially for beams with arbitrary-ply. This phenomenon can be explained as follows. In present study, Poisson's effect is incorporated in the constitutive equations by assuming $\sigma_y = \sigma_{xy} = \sigma_{yz} = 0$. It means that the strains (ε_y, γ_{yz}, γ_{xy}) are nonzero. For beams with arbitrary-ply (30^0), when the Poisson's effect is considered, the beam's stiffness constants are much smaller than when the Poisson's effect is neglected. This causes beams more flexible [85]. It leads to the conclusion that the Poisson's effect is quite significant to the arbitrary-ply laminated beams, and that the neglect of this effect is only suitable for the cross-ply laminated beams. It should be also noted that there is deviation between the present critical buckling load and those from Wang et al. [33]. This situation occurred because Wang et al. [33] mentioned the rotation of the normal to the mid-plane in y-direction in displacement field.

Table 4.14. Nondimensional fundamental frequencies, critical buckling loads and mid-span displacements of $(\theta/-\theta)_s$ composite beams (MAT IV.4).

BC	Theory	Reference	Angle-ply (θ)			
			0^0	30^0	60^0	90^0
a. Fundamental frequency						
S-S	HOBT	Present	2.649	0.999	0.731	0.729
		Aydogdu [47]	2.651	1.141	0.736	0.729
		Nguyen et al. [130]	2.656	2.103	1.012	0.732
	FOBT	Chandrashekhara et al. [78]	2.656	2.103	1.012	0.732
	Quasi-3D	Present	2.650	0.999	0.731	0.730

BC	Theory	Reference	Angle-ply (θ)			
			0^0	30^0	60^0	90^0
C-F	HOBT	Present	0.980	0.358	0.261	0.261
		Aydogdu [47]	0.981	0.414	0.262	0.260
		Nguyen et al. [130]	0.983	0.768	0.363	0.262
	FOBT	Chandrashekhara et al. [78]	0.982	0.768	0.363	0.262
	Quasi-3D	Present	0.980	0.358	0.262	0.262
C-C	HOBT	Present	4.897	2.180	1.620	1.615
		Aydogdu [47]	4.973	2.195	1.669	1.619
		Nguyen et al. [130]	4.912	4.131	2.202	1.621
	FOBT	Chandrashekhara et al. [78]	4.849	4.098	2.198	1.620
	Quasi-3D	Present	4.901	2.183	1.626	1.625
		Chen et al. [84]	4.858	2.345	1.671	1.623
b. Critical buckling load						
S-S	HOBT	Present	10.709	1.522	0.816	0.813
	Quasi-3D		10.713	1.523	0.816	0.813
C-F	HOBT	Present	2.973	0.386	0.206	0.205
	Quasi-3D		2.974	0.387	0.206	0.206
	FOBT	Wang et al. [33]	2.971	0.712	0.208	0.205
C-C	HOBT	Present	30.689	5.747	3.154	3.136
	Quasi-3D		30.726	5.758	3.168	3.160
	FOBT	Wang et al. [33]	30.592	10.008	3.187	3.136
c. Mid-span displacement						
S-S	HOBT	Present	1.196	8.437	15.745	15.811
	Quasi-3D		1.195	8.432	15.733	15.796
C-F	HOBT		3.987	28.611	53.452	53.675
	Quasi-3D		3.983	28.570	53.170	53.208
C-C	HOBT		0.355	1.815	3.289	3.308
	Quasi-3D		0.355	1.812	3.272	3.276

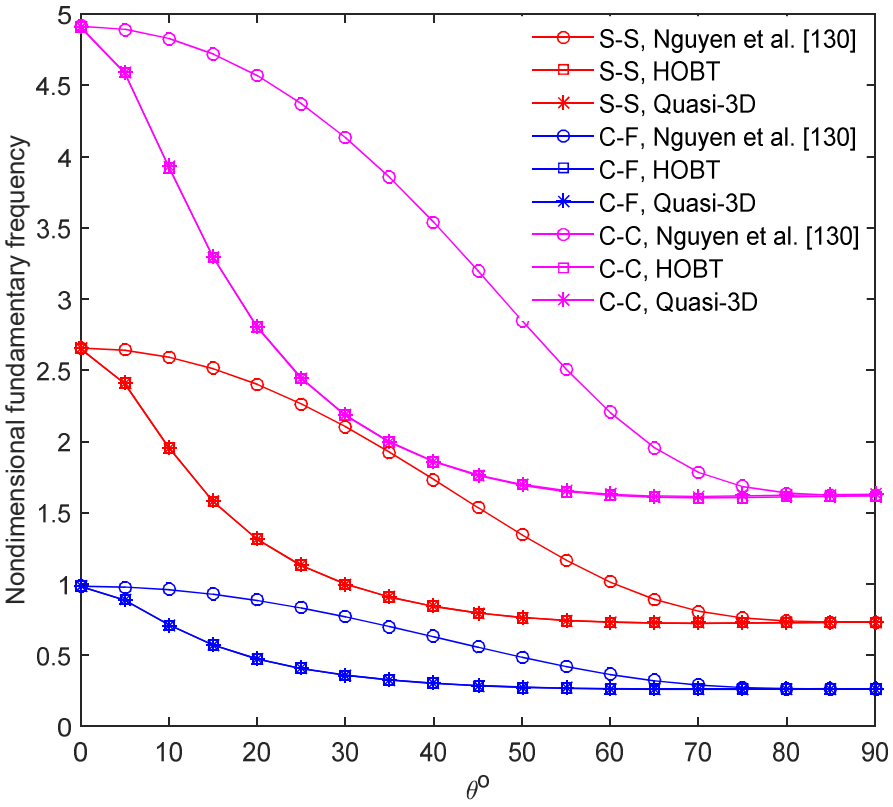

Figure 4.7. Effects of the fibre angle change on the nondimensional fundamental frequency of $(\theta/-\theta)_s$ composite beams (MAT IV.4).

4.4. Conclusions

The new approximation functions which combined polynomial and exponential functions are presented to study the free vibration, buckling and static behaviours of laminated composite beams. The displacement field is based on a quasi-3D theory accounting for a higher-order variation of both axial and transverse displacements. Poisson's effect is incorporated in beam model. Numerical results for different BCs are obtained to compare with previous studies and investigate effects of material anisotropy, Poisson's ratio and angle-ply on the natural frequencies, buckling loads, displacements and stresses of composite beams. The obtained results show that:

- The transverse normal strain effects are significant for un-symmetric and thick beams.

- The Poisson's effect is quite significant to the laminated beams with arbitrary lay-up, and the neglect of this effect is only suitable for the cross-ply laminated beams.
- The present model is found to be appropriate for vibration, buckling and bending analysis of cross-ply and arbitrary-ply composite beams.

Chapter 5. SIZE DEPENDENT BEHAVIOURS OF MICRO GENERAL LAMINATED COMPOSITE BEAMS BASED ON MODIFIED COUPLE STRESS THEORY [6]

5.1. Introduction

In Chapters Two, Three and Four, the macro composite beams are analysed using classical continuum mechanics theories. However, the use of composite materials with microstructure in micro-electro-mechanical systems such as microswitches and microrobots has recently motivated many researchers [131-133] to study the behaviour materials in order of micron and sub-micron. The results obtained by these studies show that the classical continuum mechanics theories can not describe the behaviour of such micro-structures due to their size dependencies.

A review of non-classical continuum mechanics models for size-dependent analysis of small-scale structures can be found in [134]. These models for size-dependent analysis can be divided into three groups: nonlocal elasticity theory, micro continuum theory and strain gradient family. Nonlocal elasticity theory was proposed by Eringen [3, 135], Eringen and Edelen [136], and its recent applications can be found in [137-140]. In this theory, the stress at a reference point is considered as a function of strain field at all points of the body, and thus the size effect is captured by means of constitutive equations using a nonlocal parameter. Micro continuum theory in which each particle can rotate and deform independently regardless of the motion of the centroid of the particle was developed by Eringen [141-143]. The strain gradient family is composed of the strain gradient theory [133, 144], the modified strain gradient theory [131], the couple stress theories [4-6] and the modified couple stress theory (MCST) [145]. In the strain gradient family, both strains and gradient of strains are considered in the strain energy. The size effect is accounted for using material length scale parameters (MLSP). The MCST introduced an equilibrium condition of moments of couples to enforce the couple stress tensor to be symmetric. Consequently, MCST needs only one MLSP instead of two as the couple stress

[6] A slightly different version of this chapter has been published in Composite Structures in 2018

theories, or three as the modified strain gradient theory. This feature makes the MCST easier to use and more preferable to capture the size effect because the determination of MLSP is a challenging task.

Chen et al. [12, 146] developed Timoshenko and Reddy beam models to analyse the static behaviours of cross-ply simply supported microbeams. Chen and Si [147] suggested an anisotropic constitutive relation for the MCST and used global-local theory to analyse Reddy beams using Navier solutions. By using a meshless method, Roque et al. [10] analysed the static bending response of micro laminated Timoshenko beams. A size-dependent zigzag model was also proposed by Yang et al. [7] for the bending analysis of cross-ply microbeams. Abadi and Daneshmehr [148] analysed the buckling of micro composite beams using Euler-Bernoulli and Timoshenko models. Mohammadabadi et al. [37] also predicted the thermal effect on size-dependent buckling behaviour of micro composite beams. The generalized differential quadrature method was used to solve with different boundary conditions (BCs). Chen and Li [149] predicted dynamic behaviours of micro laminated Timoshenko beams. Mohammad-Abadi and Daneshmehr [8] used the MCST to analyse free vibration of cross-ply microbeams by using Euler-Bernoulli, Timoshenko and Reddy beam models. Ghadiri et al. [150] analysed the thermal effect on dynamics of thin and thick microbeams with different BCs. Most of the above-mentioned studies mainly focused on cross-ply microbeams. Therefore, the study of micro general laminated composite beams (MGLCB) with arbitrary lay-ups is necessary.

Despite the fact that numerical approaches are used increasingly [10, 21, 50, 137, 138, 151], Ritz method is still efficient to analyse structural behaviours of beams [44, 45, 48, 130, 152-155]. In Ritz method, the accuracy and efficiency of solution strictly depends on the choice of approximation functions. An inappropriate choice of the approximation functions may cause slow convergence rates and numerical instabilities [48]. The approximation functions should satisfy the specified essential BCs [1]. If this requirement is not satisfied, the Lagrangian multipliers and penalty

method can be used to handle arbitrary BCs [44, 126, 156]. However, this approach leads to an increase in the dimension of the stiffness and mass matrices and causing computational costs. Therefore, the objective of this Chapter is to propose approximation functions for Ritz type solutions that give fast convergence rate, numerical stability and satisfy the specified BCs.

In this Chapter, new exponential approximation functions are proposed for the size-dependent analysis of MGLCB based on the MCST using a refined shear deformation theory. Lagrange's equations are used to obtain the governing equations of motion. The accuracy of the present model is demonstrated by verification studies. Numerical results are presented to investigate the effects of MLSP, length-to-height ratio and fibre angle on the deflections, stresses, natural frequencies and critical buckling loads of micro composite beams with arbitrary lay-ups.

5.2. Theoretical formulation

A MGLCB with rectangular cross-section shown in Fig. 5.1 is considered. L ,b and h denote are the length, width and thickness of the beam, respectively. It is composed of n plies of orthotropic materials in different fibre angles with respect to the x-axis.

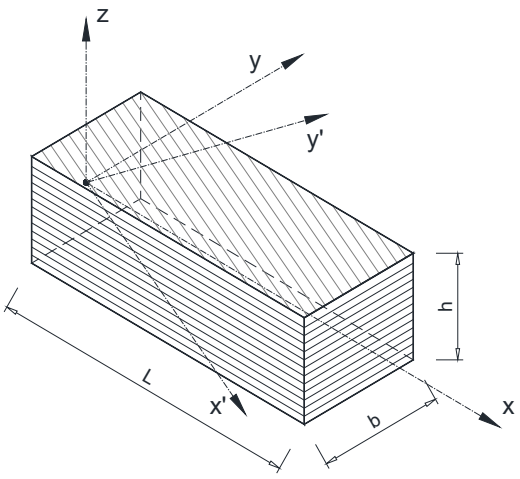

Figure 5.1. Geometry and coordinate of a laminated composite beam.

5.2.1. Kinematics

The beam theory used in this Chapter based on HOBT ([89, 90]). The displacement field accounts a higher-order variation of axial displacement and meets

the traction-free boundary conditions of the transvese shear stress on the top and bottom surfaces of the beams:

$$u(x,z,t)=u_0(x,t)-z\frac{\partial w_0(x,t)}{\partial x}+\left(\frac{5z}{4}-\frac{5z^3}{3h^2}\right)u_1(x,t)=u_0(x,t)-zw_{0,x}+f(z)u_1(x,t) \quad (5.1)$$

$$v(x,z,t)=0 \quad (5.2)$$

$$w(x,z,t)=w_0(x,t) \quad (5.3)$$

where $u_0(x,t)$ and $w_0(x,t)$ are the axial and transverse displacements of a point on the beam mid-plane along the x- and z-directions, respectively; $u_1(x,t)$ is the rotation of the cross-section about the y-axis and $f(z)=\frac{5z}{4}-\frac{5z^3}{3h^2}$ is the shape function. The comma indicates a partial differentiation with respect to the corresponding subscript coordinate.

Based on the MCST [145, 149], the rotation displacement about the x-, y-, z-axes are determined by:

$$\theta_x(x,z,t)=\frac{1}{2}\left(w_{,y}-v_{,z}\right)=0 \quad (5.4)$$

$$\theta_y(x,z,t)=\frac{1}{2}\left(u_{,z}-w_{,x}\right)=\frac{1}{2}\left(f_{,z}u_1-2w_{0,x}\right) \quad (5.5)$$

$$\theta_z(x,z,t)=\frac{1}{2}\left(v_{,x}-u_{,y}\right)=0 \quad (5.6)$$

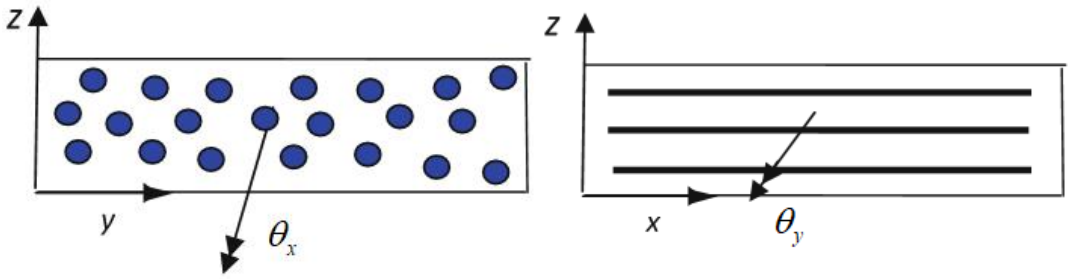

a. y-z plane fiber cross-section b. Fiber within x-z plane

Figure 5.2. Rotation displacement about the x-, y-axes

The strain and curvature-strain fields of beams are obtained as [37]:

$$\varepsilon_x = \frac{\partial u}{\partial x} = u_{0,x} - zw_{0,xx} + fu_{1,x} \tag{5.7}$$

$$\gamma_{xz} = \frac{\partial u}{\partial z} + \frac{\partial w}{\partial x} = f_{,z}u_1 \tag{5.8}$$

$$\chi_{xy} = \frac{\partial \theta_y}{\partial x} + \frac{\partial \theta_x}{\partial y} = \frac{1}{2}\left(f_{,z}u_{1,x} - 2w_{0,xx}\right) \tag{5.9}$$

$$\chi_{zy} = \frac{\partial \theta_y}{\partial z} + \frac{\partial \theta_z}{\partial y} = \frac{1}{2}f_{,zz}u_1 \tag{5.10}$$

5.2.2. Constitutive relations

The stress-strain relations for the k^{th}-ply of a laminated beam in global coordinate system are expressed as [85]:

$$\begin{Bmatrix} \sigma_x \\ \sigma_{xz} \end{Bmatrix}^{(k)} = \begin{pmatrix} \bar{\bar{C}}^*_{11} & 0 \\ 0 & \bar{\bar{C}}^*_{55} \end{pmatrix}^{(k)} \begin{Bmatrix} \varepsilon_x \\ \gamma_{xz} \end{Bmatrix} \tag{5.11}$$

The couple stress moments-curvature relation for the k^{th}-ply of a laminated beam can be given by [37]:

$$\begin{Bmatrix} m_{xy} \\ m_{zy} \end{Bmatrix}^{k} = \begin{bmatrix} \bar{\bar{C}}^*_{44} & 0 \\ 0 & \bar{\bar{C}}^*_{66} \end{bmatrix}^{k} \begin{Bmatrix} \chi_{xy} \\ \chi_{zy} \end{Bmatrix} \tag{5.12}$$

where:

$$\bar{\bar{C}}^*_{44} = \xi^2_{kb}C_{55}m^2\left(m^2 - n^2\right) - \xi^2_{km1}C_{44}n^2\left(m^2 - n^2\right) + 2m^2n^2\left(\xi^2_{kb}C_{44} + \xi^2_{km1}C_{55}\right) \tag{5.13}$$

$$\bar{\bar{C}}^*_{66} = \xi^2_{km2}\left(C_{55}m^2 + C_{44}n^2\right) \tag{5.14}$$

In the above formulas, C_{ij} are elastic coefficients of orthotropic material [1]; m_{xy} and m_{zy} are the couple stress moments which are caused by rotation displacement; ξ_{kb}, ξ_{km1} and ξ_{km2} are respectively the MLSPs in x-, y- and z-directions. In term of physical meaning, ξ_{kb} represents the micro-scale material parameter of the fiber rotating in the $y-z$ plane where the fiber cross-section and the matrix interact, and the fiber are viewed as the impurity affecting the rotational equilibrium. ξ_{km1} and ξ_{km2} represent the micro-scale material parameter within the matrix rotating about the

impurity in the $x'-z$ and $x'-y'$ plane, respectively [6, 149]; $m=\cos\theta^k$, $n=\sin\theta^k$, θ^k is a fiber angle with respect to the x-axis.

5.2.3. Variational formulation

The strain energy, work done and kinetic energy are denoted by Π_E, Π_W and Π_K respectively. The strain energy Π_E of the beam is given by:

$$\begin{aligned}\Pi_E &= \frac{1}{2}\int_V \left(\sigma_x\varepsilon_x+\sigma_{xz}\gamma_{xz}+m_{xy}\chi_{xy}+m_{zy}\chi_{zy}\right)dV \\ &= \frac{1}{2}\int_0^L \Big[A\left(u_{0,x}\right)^2 - 2Bu_{0,x}w_{0,xx} + 2B^s u_{0,x}u_{1,x} + \left(A^m+D\right)\left(w_{0,xx}\right)^2 \\ &-2\left(\frac{B^m}{2}+D^s\right)w_{0,xx}u_{1,x} + \left(\frac{D^m}{4}+H^s\right)(u_{1,x})^2 + \left(A^s+\frac{H^m}{4}\right)(u_1)^2 \Big] dx\end{aligned} \tag{5.15}$$

where the stiffness coefficients of the beam are determined as follows:

$$\left(A,B,D,B^s,D^s,H^s\right)=\sum_{k=1}^{n}\int_{z_k}^{z_{k+1}}\bar{\bar{C}}_{11}^{*}\left(1,z,z^2,f,zf,f^2\right)bdz \tag{5.16}$$

$$A^s=\sum_{k=1}^{n}\int_{z_k}^{z_{k+1}}\bar{\bar{C}}_{55}^{*}f_{,z}^2 bdz \tag{5.17}$$

$$\left(A^m,B^m,D^m\right)=\sum_{k=1}^{n}\int_{z_k}^{z_{k+1}}\bar{\bar{C}}_{44}^{*}\left(1,f_{,z},f_{,z}^2\right)bdz \tag{5.18}$$

$$H^m=\sum_{k=1}^{n}\int_{z_k}^{z_{k+1}}\bar{\bar{C}}_{66}^{*}f_{,zz}^2 bdz \tag{5.19}$$

The work done Π_W by axially compressive load N_0 and transverse load q is given by:

$$\Pi_W=-\frac{1}{2}\int_0^L N_0(w_{0,x})^2 bdx+\int_0^L qw_0 bdx \tag{5.20}$$

The kinetic energy Π_K of the beam is written by:

$$\begin{aligned}\Pi_K &= \frac{1}{2}\int_V \rho(z)\left(\dot{u}^2+\dot{v}^2+\dot{w}^2\right)dV \\ &= \frac{1}{2}\int_0^L \Big[I_0\dot{u}_0^2 - 2I_1\dot{u}_0\dot{w}_{0,x} + I_2\left(\dot{w}_{0,x}\right)^2 + 2J_1\dot{u}_1\dot{u}_0 - 2J_2\dot{u}_1\dot{w}_{0,x} + K_2\dot{u}_1^2 + I_0\dot{w}_0^2 \Big] dx\end{aligned} \tag{5.21}$$

where the dot-superscript denotes the differentiation with respect to the time t; ρ is the mass density of each layer; I_0, I_1, I_2, J_1, J_2, K_2 are the inertia coefficients determined by:

$$\left(I_0, I_1, I_2, J_1, J_2, K_2\right) = \sum_{k=1}^{n} \int_{z_k}^{z_{k+1}} \rho^{(k)} \left(1, z, z^2, f, zf, f^2\right) b dz \tag{5.22}$$

The total potential energy of system is expressed by:

$$\Pi = \Pi_E + \Pi_W - \Pi_K$$

$$\begin{aligned}\Pi = \frac{1}{2}\int_0^L \Bigg[& A\left(u_{0,x}\right)^2 - 2Bu_{0,x}w_{0,xx} + 2B^s u_{0,x}u_{1,x} + \left(A^m + D\right)\left(w_{0,xx}\right)^2 - 2\left(\frac{B^m}{2} + D^s\right) w_{0,xx}u_{1,x} \\ & + \left(\frac{D^m}{4} + H^s\right)(u_{1,x})^2 + \left(A^s + \frac{H^m}{4}\right)(u_1)^2 \Bigg] dx + \frac{1}{2}\int_0^L N_0 (w_{0,x})^2 b dx - \int_0^L q w_0 b dx \\ & - \frac{1}{2}\int_0^L \left[I_0 \dot{u}_0^2 - 2I_1 \dot{u}_0 \dot{w}_{0,x} + I_2 \left(\dot{w}_{0,x}\right)^2 + 2J_1 \dot{u}_1 \dot{u}_0 - 2J_2 \dot{u}_1 \dot{w}_{0,x} + K_2 \dot{u}_1^2 + I_0 \dot{w}_0^2 \right] dx\end{aligned} \tag{5.23}$$

5.2.4. Ritz solution

By using Ritz method, the displacement field in Eq. (5.23) is approximated by:

$$u_0(x,t) = \sum_{j=1}^{m} \varphi_{j,x}(x) u_{0j} e^{i\omega t} \tag{5.24}$$

$$w_0(x,t) = \sum_{j=1}^{m} \varphi_j(x) w_{0j} e^{i\omega t} \tag{5.25}$$

$$u_1(x,t) = \sum_{j=1}^{m} \varphi_{j,x}(x) u_{1j} e^{i\omega t} \tag{5.26}$$

where ω is the frequency, $i^2 = -1$ the imaginary unit; u_{0j}, w_{0j} and u_{1j} are unknown and need to be determined; $\varphi_j(x)$ are approximation functions. In this Chapter, new exponential approximation functions for Ritz solution reported in Table 5.1 are proposed for three typical BCs including S-S, C-F and C-C.

By substituting Eq. (5.24-5.26) into Eq. (5.23) and using Lagrange's equations:

$$\frac{\partial \Pi}{\partial p_j} - \frac{d}{dt}\frac{\partial \Pi}{\partial \dot{p}_j} = 0 \tag{5.27}$$

with p_j representing the values of $\left(u_{0j}, w_{0j}, u_{1j}\right)$, the static, vibration and buckling behaviour of MGLCB can be obtained by solving the following equations:

$$\left(\begin{bmatrix} \mathbf{K}^{11} & \mathbf{K}^{12} & \mathbf{K}^{13} \\ {}^{T}\mathbf{K}^{12} & \mathbf{K}^{22} & \mathbf{K}^{23} \\ {}^{T}\mathbf{K}^{13} & {}^{T}\mathbf{K}^{23} & \mathbf{K}^{33} \end{bmatrix} - \omega^2 \begin{bmatrix} \mathbf{M}^{11} & \mathbf{M}^{12} & \mathbf{M}^{13} \\ {}^{T}\mathbf{M}^{12} & \mathbf{M}^{22} & \mathbf{M}^{23} \\ {}^{T}\mathbf{M}^{13} & {}^{T}\mathbf{M}^{23} & \mathbf{M}^{33} \end{bmatrix}\right) \begin{Bmatrix} \mathbf{u_0} \\ \mathbf{w_0} \\ \mathbf{u_1} \end{Bmatrix} = \begin{Bmatrix} \mathbf{0} \\ \mathbf{F} \\ \mathbf{0} \end{Bmatrix} \tag{5.28}$$

Table 5.1. Approximation functions and essential BCs of beams

BC	$\varphi_j(x)$	x=0	x=L
S-S	$\left(1-e^{\frac{-jx}{L}}\right)\left(1-e^{-j\left(1-\frac{x}{L}\right)}\right)$	$w_0=0$	$w_0=0$
C-F	$\left(1-\frac{jx}{L}-e^{\frac{-jx}{L}}\right)$	$u_0=0, w_0=0,$ $u_1=0, w_{0,x}=0$	
C-C	$\left(1-e^{\frac{-jx}{L}}\right)^2\left(1-e^{-j\left(1-\frac{x}{L}\right)}\right)^2$	$u_0=0, w_0=0,$ $u_1=0, w_{0,x}=0$	$u_0=0, w_0=0,$ $u_1=0, w_{0,x}=0$

where the components of stiffness matrix $\mathbf{K}$, mass matrix $\mathbf{M}$ and load vector $\mathbf{F}$ are given by:

$$K_{ij}^{11} = A\int_0^L \varphi_{i,xx}\varphi_{j,xx}dx,\ K_{ij}^{12} = -B\int_0^L \varphi_{i,xx}\varphi_{j,xx}dx,\ K_{ij}^{13} = B^s\int_0^L \varphi_{i,xx}\varphi_{j,xx}dx,$$

$$K_{ij}^{22} = \left(A^m + D\right)\int_0^L \varphi_{i,xx}\varphi_{j,xx}dx + N_0\int_0^L \varphi_{i,x}\varphi_{j,x}dx,\ K_{ij}^{23} = -\left(\frac{B^m}{2} + D^s\right)\int_0^L \varphi_{i,xx}\varphi_{j,xx}dx,$$

$$K_{ij}^{33} = \left(\frac{D^m}{4} + H^s\right)\int_0^L \varphi_{i,xx}\varphi_{j,xx}dx + \left(\frac{H^m}{4} + A^s\right)\int_0^L \varphi_{i,x}\varphi_{j,x}dx, M_{ij}^{11} = I_0\int_0^L \varphi_{i,x}\varphi_{j,x}dx,$$

$$M_{ij}^{12} = -I_1\int_0^L \varphi_{i,x}\varphi_{j,x}dx, M_{ij}^{13} = J_1\int_0^L \varphi_{i,x}\varphi_{j,x}dx, M_{ij}^{22} = I_0\int_0^L \varphi_i\varphi_j dx + I_2\int_0^L \varphi_{i,x}\varphi_{j,x}dx,$$

$$M_{ij}^{23} = -J_2\int_0^L \varphi_{i,x}\varphi_{j,x}dx,\ M_{ij}^{33} = K_2\int_0^L \varphi_{i,x}\varphi_{j,x}dx,\ F_i = \int_0^L q\varphi_i dx. \tag{5.29}$$

5.3. Numerical results

5.3.1. Convergence and accuracy studies

Convergence and verification studies are conducted to demonstrate the accuracy of the present study. Laminates, which are made of the same orthotropic materials, have equal thicknesses with material properties in Table 5.2. The beam is under a uniformly distributed load $q = q_0$ or a sinusoidal load $q = q_0 \sin\left(\frac{\pi x}{L}\right)$. Unless otherwise stated, the following non-dimensional terms are used:

$$\bar{w} = \frac{100 w_0 E_2 b h^3}{q_0 L^4},\ \bar{\sigma}_x = \frac{bh^2}{q_0 L^2}\sigma_x\left(\frac{L}{2}, z\right),\ \bar{\sigma}_{xz} = \frac{bh}{q_0 L}\sigma_{xz}(0, z),\ \bar{N}_{cr} = N_{cr}\frac{L^2}{E_2 b h^3} \tag{5.30}$$

$$\bar{\omega} = \frac{\omega L^2}{h}\sqrt{\frac{\rho}{E_2}} \text{ for Material (MAT) I.5 and } \bar{\omega} = \frac{\omega L^2}{h}\sqrt{\frac{\rho}{E_1}} \text{ for MAT III.5} \tag{5.31}$$

The numerical results of marco composite beams can be achieved by setting $\xi_{kb} = \xi_{km1} = \xi_{km2} = 0$. It should be noted that turning the composite laminated beam around the fiber direction is easier than turning around the normal to the fiber direction. The MLSP in the fiber direction is greater than that in other directions, i.e. $\xi_{kb} >> \left(\xi_{km1}, \xi_{km2}\right)$. Therefore, only the MLSP in the fiber direction is considered in this study, i.e. $\left(\xi_{kb} = \xi_b\right)$ and $\xi_{km1} = \xi_{km2} = 0$. The value of the MLSP is referred from [7, 8, 37, 146, 148, 150].

Table 5.2. Material properties of laminated composite beams considered in this study.

Material properties	MAT I.5 [48]	MAT II.5 [7]	MAT III.5 [78]
E_2=E_3 (GPa)	*6.98*	*10^{-3}*	9.65
E_1 (GPa)	*$25E_2$*	*$25E_2$*	144.8
G_{12}=G_{13} (GPa)	$0.5E_2$	$0.5E_2$	4.14
G_{23} (GPa)	$0.2E_2$	$0.2E_2$	3.45
ν_{12}	0.25	0.25	0.3
ν_{13}	0.25	0.25	0.3
ν_{23}	0.25	0.25	0.3
h (μm)	4	$2\text{x}10^3$	25
b (μm)	8	$1\text{x}10^3$	25

Composite beams (MAT I.5, $0^0/90^0/0^0$, $L/h=5$) with various BCs are considered to evaluate the convergence. The non-dimensional fundamental frequencies, critical buckling loads and mid-span displacements with respect to the series number m are given in Table 5.3. The results indicate that $m=6$ is the convergence point for natural frequency, critical buckling load and displacement, respectively. Thus, this number of series terms is used hereafter. It can be stated that the convergence of present solution appears to be faster than that of the solution from [152] ($m=12$). This is advantage of proposed approximation function.

Table 5.3. Convergence studies for ($0^0/90^0/0^0$) composite beams (MAT I.5, $L/h=5$).

BC	ξ_b/h	m				
		2	4	6	8	10
Fundamental frequency						
S-S	0	7.1811	7.1796	7.1796	7.1796	7.1796
	1	8.4006	8.3979	8.3979	8.3979	8.3979
C-F	0	3.3711	3.3163	3.3111	3.3108	3.3108
	1	3.8675	3.8433	3.8416	3.8415	3.8415
C-C	0	9.0547	9.0359	9.0359	9.0359	9.0359
	1	13.0536	13.0530	13.0530	13.0530	13.0530
Critical buckling load						
S-S	0	5.2373	5.2354	5.2354	5.2354	5.2354
	1	7.1639	7.1599	7.1599	7.1599	7.1599
C-F	0	2.9459	2.8950	2.8945	2.8945	2.8945
	1	3.3750	3.5088	3.5082	3.5082	3.5082
C-C	0	7.0582	7.0564	7.0564	7.0564	7.0564
	1	13.7654	13.7555	13.7555	13.7555	13.7555
Mid-span displacement						
S-S	0	2.4216	2.4144	2.4141	2.4141	2.4141
	1	1.7870	1.7827	1.7826	1.7826	1.7826
C-F	0	6.1552	6.8006	6.8309	6.8301	6.8306
	1	4.3796	4.6111	4.6061	4.6060	4.6061
C-C	0	1.5127	1.5375	1.5378	1.5378	1.5378
	1	0.7551	0.7556	0.7556	0.7556	0.7556

In order to verify the accuracy of the present solution, the simply supported beams are investigated. Since there is no published data for the micro composite beams with arbitrary lay-ups, the verifications are only focused on cross-ply beams. The critical buckling loads and fundamental frequencies of $\left(90^0/0^0/90^0\right)$ and $\left(0^0/90^0/0^0\right)$ beams (MAT I.5) with $\xi_b = h$ are shown in Figs. 5.3 and 5.4, and compared with those from analytical solution of Abadi and Daneshmehr [148], Mohammad-Abadi and Daneshmehr [8]. It can be seen that the present results are in good agreements with previous results for Timoshenko and Reddy beam models.

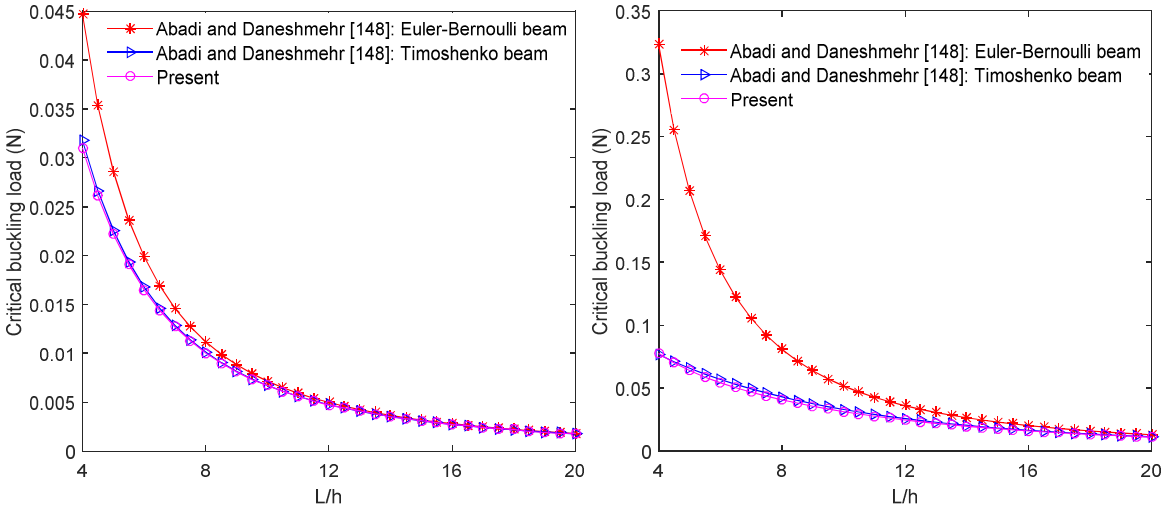

a. $90^0/0^0/90^0$ b. $0^0/90^0/0^0$

Figure 5.3. Comparison of critical buckling loads of S-S beams (MAT I.5).

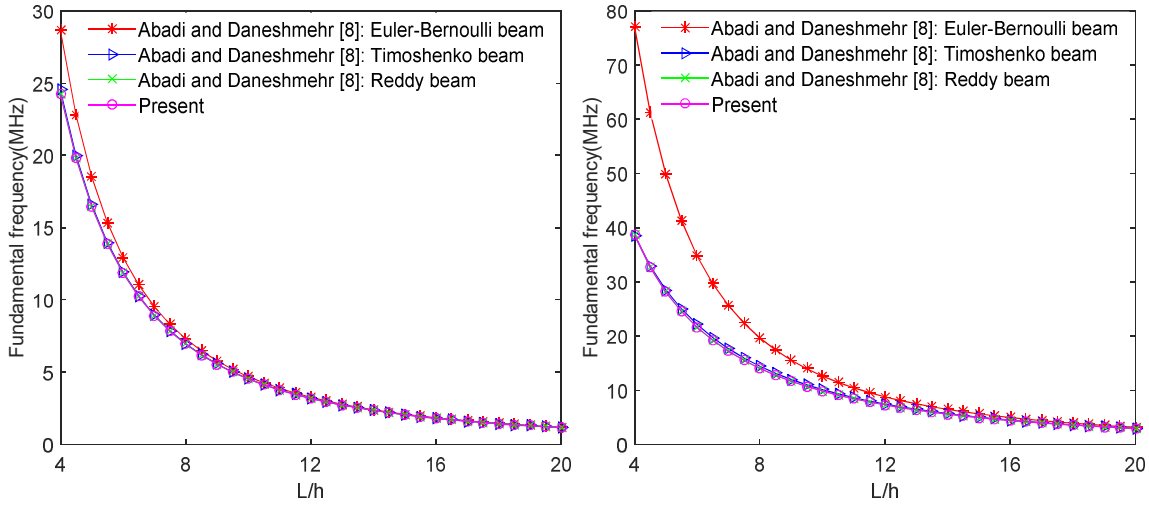

a. $90^0/0^0/90^0$ b. $0^0/90^0/0^0$

Figure 5.4. Comparison of fundamental frequencies of S-S beams (MAT I.5).

Further verification is illustrated in Fig. 5.5 for $\left(90^0/0^0/90^0\right)$ beams (MAT II.5) with $\xi_b = h$ and L=4h, subjected to sinusoidal loads $q = q_0 \sin\left(\frac{\pi x}{L}\right)$. It should be noted that the non-dimensional forms of the displacement and axial stress are $\bar{w} = 100 w_0 E_2 b h^3 / q_0 L^4$ and $\bar{\sigma}_x = \sigma_x\left(\frac{L}{2}, z\right)/q_0$, respectively. There is a slight discrepancy between the present results and those of Yang et al. [7].

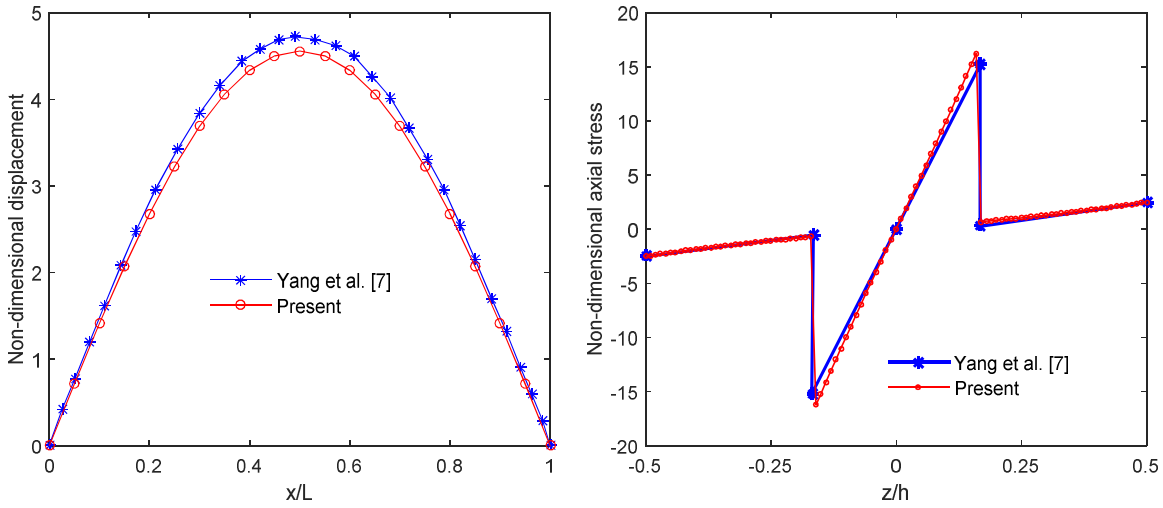

a. Non-dimensional displacement b. Non-dimensional normal stress

Figure 5.5. Comparison of displacement and normal stress of $\left(90^0/0^0/90^0\right)$ S-S beams (MAT II.5).

5.3.2. Static analysis

The static behaviours of the MGLCB with various BCs and length-to-height ratios are considered in this section. The non-dimensional mid-span displacements of beams (MAT II.5) subjected to a uniformly load $\left(q = q_0\right)$ with $\xi_b = 0, h/4, h/2, h$ are shown in Tables 5.4-5.6. It can be seen that the displacements of beams decrease as ξ_b increases for all BCs and span-to-thickness ratios. In the case of $\xi_b = 0$, the results of marco beams are recovered and agree well with those of Vo et al. [19], which obtained from finite element model and higher-order beam theory.

Table 5.4. Displacement of S-S beams (MAT II.5).

L/h	Lay-ups	θ	Vo et al. [19]	Present			
				$\xi_b = 0$	$\xi_b = h/4$	$\xi_b = h/2$	$\xi_b = h$
5	$0^0/\theta/0^0$	0^0	1.7930	1.8021	1.7622	1.6523	1.3240
		30^0	2.0140	2.0233	1.9799	1.8596	1.4959
		60^0	2.3030	2.3122	2.2642	2.1303	1.7197
		90^0	2.4049	2.4141	2.3627	2.2195	1.7826
	$0^0/\theta$	0^0	1.7930	1.8021	1.7622	1.6523	1.3240
		30^0	3.6634	3.6836	3.5127	3.0870	2.1039
		60^0	4.6135	4.6511	4.4605	3.9759	2.7980
		90^0	4.7346	4.7852	4.5895	4.0917	2.8814
10	$0^0/\theta/0^0$	0^0	0.9222	0.9236	0.9086	0.8664	0.7320
		30^0	0.9946	0.9961	0.9814	0.9398	0.8047
		60^0	1.0700	1.0715	1.0577	1.0186	0.8875
		90^0	1.0965	1.0980	1.0838	1.0436	0.9089
	$0^0/\theta$	0^0	0.9222	0.9236	0.9086	0.8664	0.7320
		30^0	2.7402	2.7482	2.6290	2.3274	1.6024
		60^0	3.5871	3.6094	3.4687	3.1064	2.1985
		90^0	3.6626	3.6966	3.5529	3.1829	2.2545
50	$0^0/\theta/0^0$	0^0	0.6370	0.6370	0.6276	0.6008	0.5135
		30^0	0.6608	0.6609	0.6523	0.6279	0.5462
		60^0	0.6650	0.6650	0.6580	0.6380	0.5687
		90^0	0.6651	0.6661	0.6592	0.6394	0.5706
	$0^0/\theta$	0^0	0.6370	0.6370	0.6276	0.6008	0.5135
		30^0	2.4406	2.4458	2.3415	2.0759	1.4283
		60^0	3.2540	3.2727	3.1465	2.8204	1.9940
		90^0	3.3147	3.3446	3.2161	2.8836	2.0403

Table 5.5. Displacement of C-F beams (MAT II.5).

L/h	Lay-ups	θ	Vo et al. [19]	Present			
				$\xi_b = 0$	$\xi_b = h/4$	$\xi_b = h/2$	$\xi_b = h$
5	$0^0/\theta/0^0$	0^0	5.2774	5.2572	5.0746	4.6404	3.5800
		30^0	5.8804	5.8586	5.6504	5.1624	3.9877
		60^0	6.6029	6.5800	6.3435	5.7916	4.4792
		90^0	6.8541	6.8309	6.5778	5.9896	4.6061
	$0^0/\theta$	0^0	5.2774	5.2572	5.0746	4.6404	3.5800
		30^0	11.6830	11.7047	11.0919	9.6451	6.4689
		60^0	14.8020	14.8997	14.2305	12.5869	8.7400
		90^0	15.1540	15.3084	14.6211	12.9334	8.9841
10	$0^0/\theta/0^0$	0^0	2.9663	2.9653	2.9082	2.7550	2.2981
		30^0	3.1828	3.1817	3.1236	2.9687	2.5060
		60^0	3.3889	3.3882	3.3307	3.1786	2.7245
		90^0	3.4605	3.4601	3.4001	3.2425	2.7753
	$0^0/\theta$	0^0	2.9663	2.9653	2.9082	2.7550	2.2981
		30^0	9.1499	9.1716	8.7662	7.7464	5.3131
		60^0	12.0020	12.0801	11.6027	10.3782	7.3237
		90^0	12.2440	12.3673	11.8797	10.6288	7.5061
50	$0^0/\theta/0^0$	0^0	2.1602	2.1598	2.1278	2.0372	1.7408
		30^0	2.2405	2.2401	2.2110	2.1282	1.8512
		60^0	2.2531	2.2526	2.2289	2.1610	1.9262
		90^0	2.2565	2.2559	2.2325	2.1652	1.9322
	$0^0/\theta$	0^0	2.1602	2.1598	2.1278	2.0372	1.7408
		30^0	8.2916	8.3096	7.9551	7.0528	4.8524
		60^0	11.0540	11.1202	10.6915	9.5833	6.7754
		90^0	11.2580	11.3645	10.9277	9.7980	6.9325

Table 5.6. Displacement of C-C beams (MAT II.5).

L/h	Lay-ups	θ	Vo et al. [19]	Present			
				$\xi_b = 0$	$\xi_b = h/4$	$\xi_b = h/2$	$\xi_b = h$
5	$0^0/\theta/0^0$	0^0	1.0998	1.0908	1.0239	0.8756	0.5709
		30^0	1.2670	1.2569	1.1767	1.0008	0.6442
		60^0	1.4766	1.4658	1.3699	1.1587	0.7339
		90^0	1.5487	1.5378	1.4341	1.2067	0.7556
	$0^0/\theta$	0^0	1.0998	1.0908	1.0239	0.8756	0.5709
		30^0	1.5755	1.5707	1.4497	1.1960	0.7345
		60^0	1.8575	1.8582	1.7414	1.4806	0.9599
		90^0	1.9193	1.9236	1.8025	1.5320	0.9927
10	$0^0/\theta/0^0$	0^0	0.3968	0.3957	0.3831	0.3527	0.2750
		30^0	0.4469	0.4457	0.4315	0.3973	0.3104
		60^0	0.5108	0.5096	0.4934	0.4547	0.3563
		90^0	0.5332	0.5319	0.5147	0.4734	0.3690
	$0^0/\theta$	0^0	0.3968	0.3957	0.3831	0.3527	0.2750
		30^0	0.7783	0.7799	0.7392	0.6431	0.4326
		60^0	0.9726	0.9782	0.9343	0.8266	0.5754
		90^0	0.9983	1.0068	0.9617	0.8509	0.5927
50	$0^0/\theta/0^0$	0^0	0.1367	0.1367	0.1346	0.1287	0.1097
		30^0	0.1431	0.1430	0.1411	0.1356	0.1176
		60^0	0.1462	0.1461	0.1445	0.1399	0.1240
		90^0	0.1472	0.1472	0.1456	0.1409	0.1251
	$0^0/\theta$	0^0	0.1367	0.1367	0.1346	0.1287	0.1097
		30^0	0.4974	0.4989	0.4776	0.4233	0.2913
		60^0	0.6608	0.6654	0.6397	0.5733	0.4054
		90^0	0.6733	0.6803	0.6541	0.5864	0.4150

In the next example, micro composite beams under sinusoidal loads, $q = q_0 \sin\left(\frac{\pi x}{L}\right)$ (MAT II.5, $L/h = 4$), are investigated. Their deflections with various MLSP are plotted in Figs. 5.6-5.8. It can be seen that they decrease with the increase of ξ_b. Fig. 5.9 shows mid-span displacements of $\left(0^0/30^0/0^0\right)$ and $\left(0^0/30^0\right)$ beams with different BCs. It is interesting to see that as ξ_b/h increases, the variation of the beams' displacement depends on BC. The C-F beam has the biggest variation.

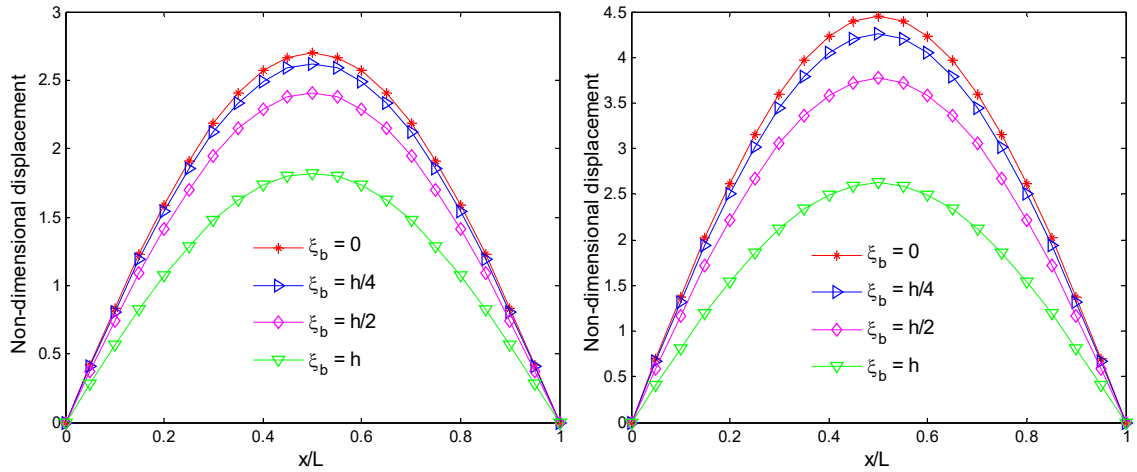

a. $0^0/90^0/0^0$ b. $0^0/90^0$

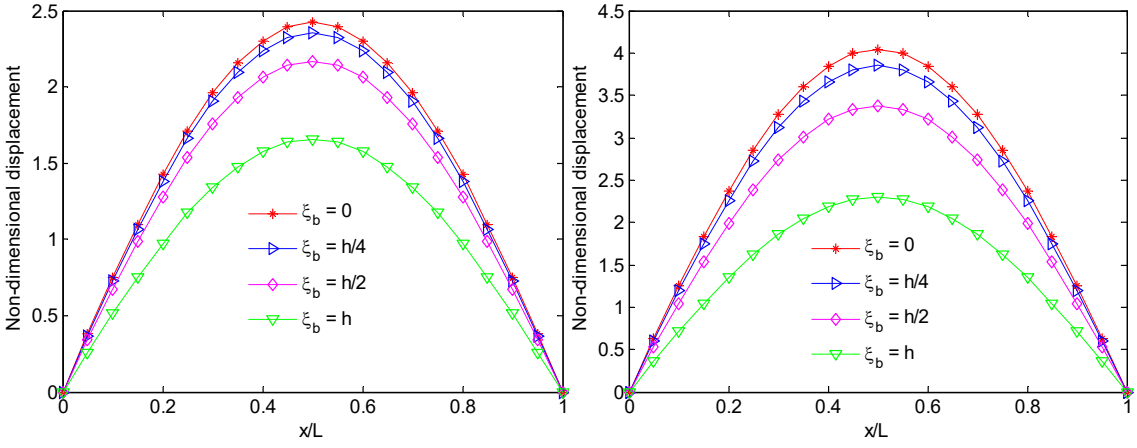

c. $0^0/45^0/0^0$ d. $0^0/45^0$

Figure 5.6. Effect of MLSP on displacements of S-S beams (MAT II.5, $L/h = 4$).

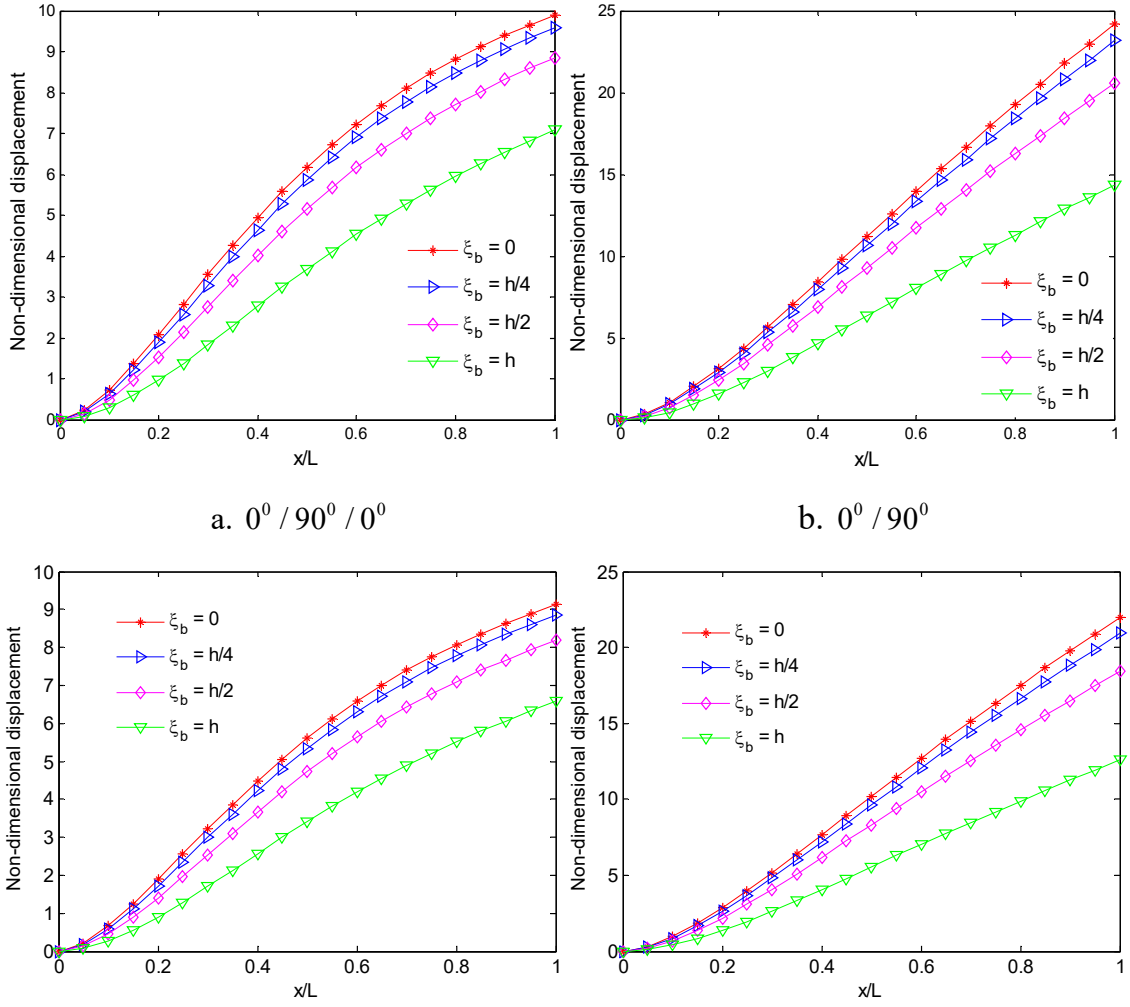

a. $0^0 / 90^0 / 0^0$ b. $0^0 / 90^0$

c. $0^0 / 45^0 / 0^0$ d. $0^0 / 45^0$

Figure 5.7. Effect of MLSP on displacements of C-F beams (MAT II.5, $L / h = 4$).

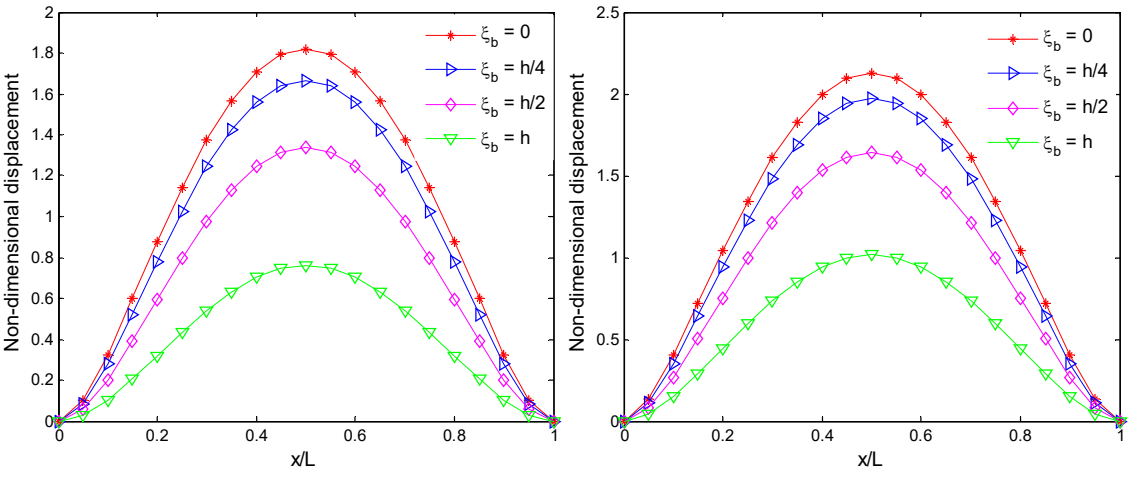

a. $0^0 / 90^0 / 0^0$ b. $0^0 / 90^0$

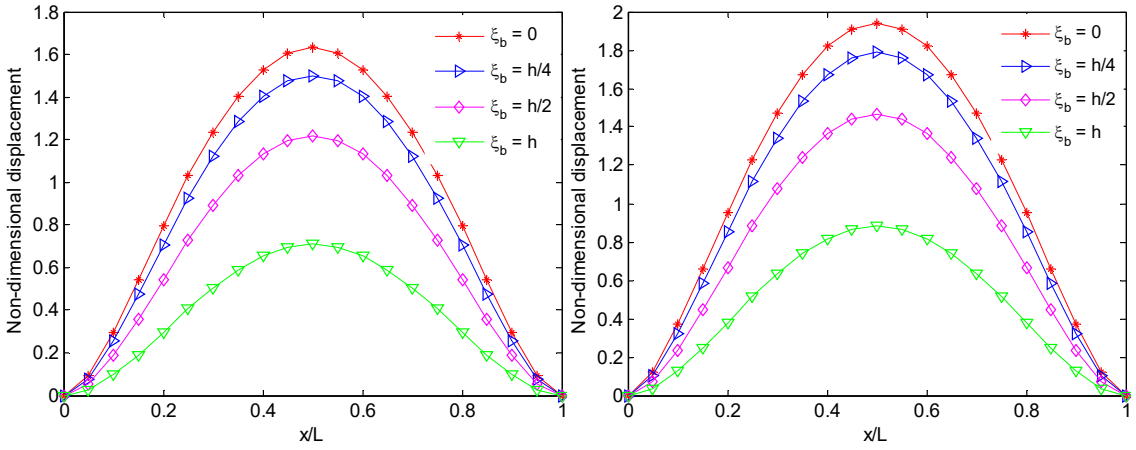

c. $0^0 / 45^0 / 0^0$ d. $0^0 / 45^0$

Figure 5.8. Effect of MLSP on displacements of C-C beams (MAT II, $L/h = 4$).

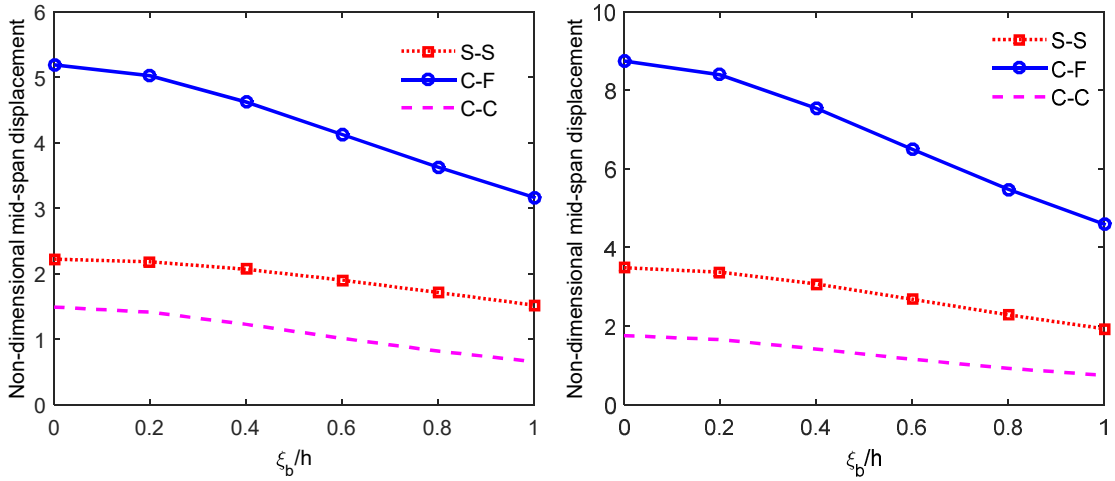

a. $0^0 / 30^0 / 0^0$ b. $0^0 / 30^0$

Figure 5.9. Effect of MLSP on displacements of beams with various BCs (MAT II.5, $L/h = 4$)

The axial and shear stresses of $\left(0^0 / 60^0 / 0^0\right)$ and $\left(0^0 / 60^0\right)$ simply supported beams are shown in Figs. 5.10 and 5.11. Similar to the displacement, the stress also reduces as the MLSP increases.

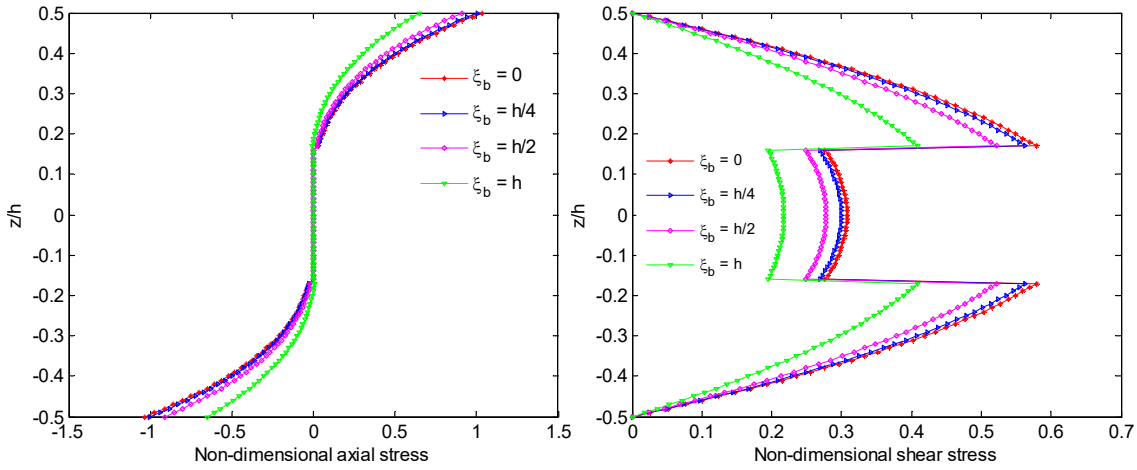

a. $\bar{\sigma}_{xx}$ b. $\bar{\sigma}_{xz}$

Figure 5.10. Effect of MLSP on through-thickness distribution of stresses of $(0^0/60^0/0^0)$ S-S beams (MAT II.5, $L/h=4$).

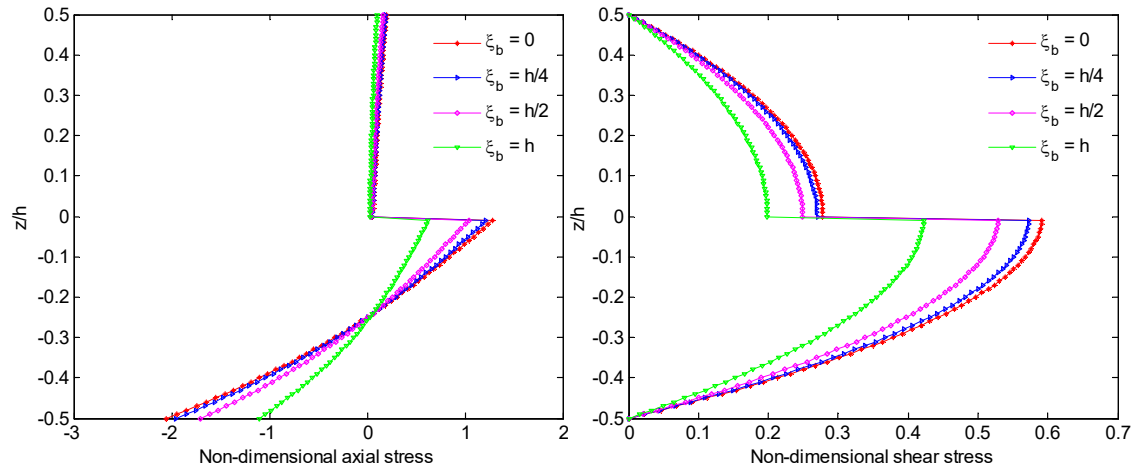

a. $\bar{\sigma}_{xx}$ b. $\bar{\sigma}_{xz}$

Figure 5.11. Effect of MLSP on through-thickness distribution of stresses of $(0^0/60^0)$ S-S beams (MAT II.5, $L/h=4$).

5.3.3. Vibration and buckling analysis

The non-dimensional fundamental frequencies and critical buckling loads of the MGLCB with various BCs and length-to-height are given in Tables 5.7-5.10. For macro composite beams ($\xi_b=0$), the present results again agree well with those of Vo et al. [157] and Chen et al. [84] (Tables 5.7 and 5.8). Some new results for micro composite beams are shown to serve as benchmarks for future studies. It can be seen

that the results are increased as ξ_b increases. This response can be expected because an increase in the MLSP leads to an increase in the beams' stiffness.

Table 5.7. Fundamental frequencies of ($\theta/-\theta$) beams (MAT III.5).

BC	L/h	θ	Chen et al. [84]	Vo et al. [157]	Present			
					$\xi_b = 0$	$\xi_b = h/4$	$\xi_b = h/2$	$\xi_b = h$
S-S	5	0^0	-	-	1.8492	1.8766	1.9559	2.2383
		30^0	-	-	0.9185	0.9727	1.1181	1.5555
		60^0	-	-	0.6912	0.7121	0.7712	0.9700
		90^0	-	-	0.6886	0.6886	0.6886	0.6886
	15	0^0	-	-	2.6494	2.6785	2.7637	3.0789
		30^0	-	-	0.9986	1.0556	1.2105	1.6914
		60^0	-	-	0.7310	0.7527	0.8143	1.0239
		90^0	-	-	0.7295	0.7295	0.7295	0.7295
C-F	5	0^0	-	-	0.7956	0.8083	0.8427	0.9580
		30^0	-	-	0.3435	0.3636	0.4177	0.5829
		60^0	-	-	0.2545	0.2621	0.2837	0.3569
		90^0	-	-	0.2538	0.2538	0.2538	0.2538
	15	0^0	-	-	0.9803	0.9910	1.0224	1.1386
		30^0	-	-	0.3580	0.3784	0.4339	0.6067
		60^0	-	-	0.2615	0.2692	0.2913	0.3663
		90^0	-	-	0.2610	0.2610	0.2610	0.2610
C-C	5	0^0	-	2.4448	2.4605	2.5572	2.8013	3.5424
		30^0	-	1.6668	1.6642	1.7942	2.1076	2.9612
		60^0	-	1.3546	1.3452	1.3944	1.5252	1.9389
		90^0	-	1.3477	1.3342	1.3342	1.3342	1.3342
	15	0^0	4.8575	4.9004	4.8968	4.9697	5.1701	5.8566
		30^0	2.3016	2.1832	2.1802	2.3077	2.6502	3.6930
		60^0	1.6686	1.6249	1.6201	1.6688	1.8065	2.2718
		90^0	1.6237	1.6227	1.6153	1.6153	1.6153	1.6153

Table 5.8. Fundamental frequencies of ($0^0/\theta$) beams (MAT III.5).

BC	L/h	θ	Chen et al. [84]	Vo et al. [157]	Present			
					$\xi_b = 0$	$\xi_b = h/4$	$\xi_b = h/2$	$\xi_b = h$
S-S	5	0^0	-	-	1.8492	1.8766	1.9559	2.2383
		30^0	-	-	1.3198	1.3612	1.4771	1.8575
		60^0	-	-	1.1754	1.2096	1.3061	1.6275
		90^0	-	-	1.1722	1.2011	1.2833	1.5631
	15	0^0	-	-	2.6494	2.6785	2.7637	3.0789
		30^0	-	-	1.5437	1.5886	1.7160	2.1489
		60^0	-	-	1.3329	1.3698	1.4749	1.8346
		90^0	-	-	1.3314	1.3626	1.4521	1.7639
C-F	5	0^0	-	-	0.7956	0.8083	0.8427	0.9580
		30^0	-	-	0.5140	0.5300	0.5745	0.7219
		60^0	-	-	0.4500	0.4631	0.4997	0.6226
		90^0	-	-	0.4492	0.4602	0.4914	0.5983
	15	0^0	-	-	0.9803	0.9910	1.0224	1.1386
		30^0	-	-	0.5571	0.5733	0.6192	0.7758
		60^0	-	-	0.4797	0.4929	0.5307	0.6604
		90^0	-	-	0.4792	0.4904	0.5226	0.6349
C-C	5	0^0	-	2.4448	2.4605	2.5572	2.8013	3.5424
		30^0	-	2.1200	2.1245	2.2319	2.5015	3.2864
		60^0	-	1.9999	1.9968	2.0804	2.2975	2.9511
		90^0	-	1.9935	1.9860	2.0570	2.2441	2.8211
	15	0^0	4.8575	4.9004	4.8968	4.9697	5.1701	5.8566
		30^0	3.3548	3.2489	3.2406	3.3408	3.6201	4.5414
		60^0	2.9491	2.8669	2.8500	2.9320	3.1629	3.9364
		90^0	2.8012	2.8709	2.8443	2.9136	3.1103	3.7828

Table 5.9. Buckling loads of ($\theta/-\theta$) beams (MAT III.5).

BC	L/h	θ	Present			
			$\xi_b = 0$	$\xi_b = h/4$	$\xi_b = h/2$	$\xi_b = h$
S-S	5	0^0	5.2343	5.3899	5.8533	7.6577
		30^0	1.3140	1.4730	1.9443	3.7485
		60^0	0.7464	0.7921	0.9287	1.4671
		90^0	0.7408	0.7408	0.7408	0.7408
	15	0^0	10.7087	10.9449	11.6521	14.4607
		30^0	1.5224	1.7013	2.2370	4.3671
		60^0	0.8160	0.8651	1.0124	1.6007
		90^0	0.8125	0.8125	0.8125	0.8125
C-F	5	0^0	2.2972	2.3501	2.5082	3.1323
		30^0	0.3714	0.4152	0.5462	1.0633
		60^0	0.2011	0.2132	0.2496	0.3945
		90^0	0.2001	0.2001	0.2001	0.2001
	15	0^0	2.9724	3.0375	3.2298	3.9974
		30^0	0.3864	0.4316	0.5675	1.1099
		60^0	0.2058	0.2182	0.2553	0.4037
		90^0	0.2050	0.2050	0.2050	0.2050
C-C	5	0^0	7.9859	8.4589	9.8645	15.3013
		30^0	3.6046	4.1007	5.5445	10.7495
		60^0	2.3211	2.4736	2.9260	4.6610
		90^0	2.2856	2.2856	2.2856	2.2856
	15	0^0	30.6893	31.4445	33.6981	42.5424
		30^0	5.7473	6.4294	8.4636	16.4222
		60^0	3.1536	3.3446	3.9166	6.1887
		90^0	3.1360	3.1360	3.1360	3.1360

Table 5.10. Buckling loads of ($0^0/\theta$) beams (MAT III.5).

BC	L/h	θ	Present			
			$\xi_b = 0$	$\xi_b = h/4$	$\xi_b = h/2$	$\xi_b = h$
S-S	5	0^0	5.2343	5.3899	5.8533	7.6577
		30^0	2.7128	2.8843	3.3929	5.3424
		60^0	2.1645	2.2915	2.6688	4.1269
		90^0	2.1523	2.2589	2.5763	3.8086
	15	0^0	10.7087	10.9449	11.6521	14.4607
		30^0	3.6429	3.8579	4.5015	7.0582
		60^0	2.7174	2.8700	3.3273	5.1471
		90^0	2.7115	2.8400	3.2250	4.7581
C-F	5	0^0	2.2972	2.3501	2.5082	3.1323
		30^0	0.8641	0.9156	1.0693	1.6752
		60^0	0.6531	0.6900	0.8004	1.2367
		90^0	0.6513	0.6823	0.7752	1.1431
	15	0^0	2.9734	3.0375	3.2298	3.9974
		30^0	0.9412	0.9965	1.1623	1.8241
		60^0	0.6961	0.7351	0.8521	1.3192
		90^0	0.6949	0.7278	0.8263	1.2196
C-C	5	0^0	7.9859	8.4589	9.8645	15.3013
		30^0	5.9147	6.4082	7.8569	13.2243
		60^0	5.1933	5.5641	6.6547	10.7226
		90^0	5.1373	5.4483	6.3659	9.8223
	15	0^0	30.6893	31.4445	33.6981	42.5424
		30^0	12.9047	13.6837	16.0053	25.0737
		60^0	9.9157	10.4806	12.1667	18.7882
		90^0	9.8793	10.3542	11.7730	17.3589

Figs. 5.12 and 5.13 show variation of the natural frequencies and critical buckling loads with respect to ξ_b / h ratio of $\left(0^0/30^0/0^0\right)$ and $\left(0^0/30^0\right)$ beams. It is clear that as ξ_b / h increases, their variation depend on BC. The C-C beam has the biggest variation.

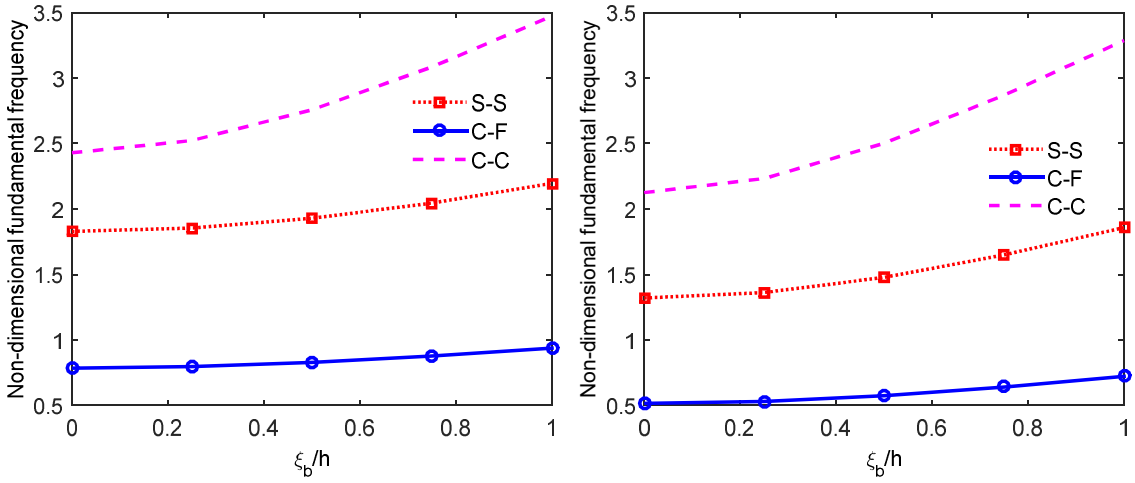

a. $0^0/30^0/0^0$ b. $0^0/30^0$

Figure 5.12. Effect of MLSP on frequencies of beams with various BC (MAT III.5, $L/h=5$)

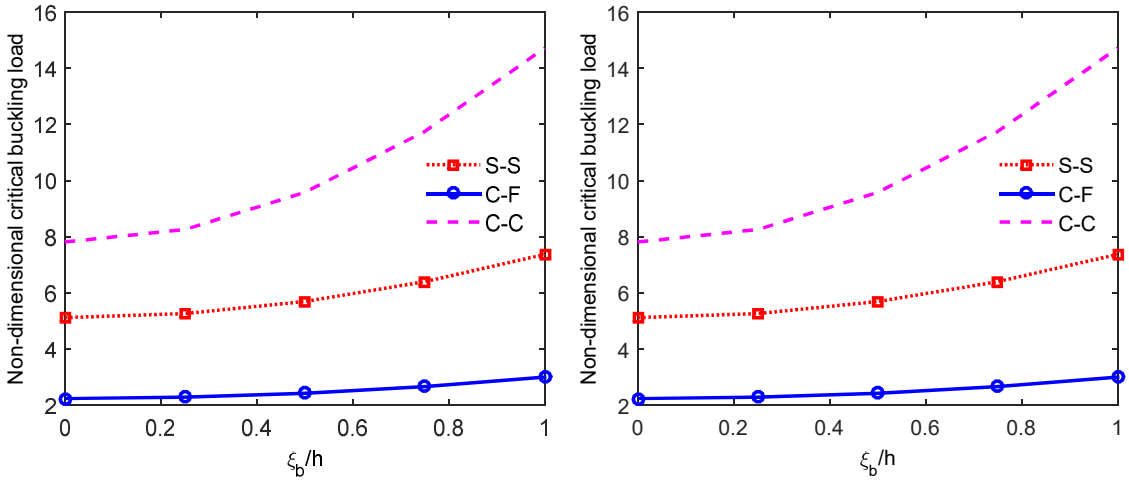

a. $0^0/30^0/0^0$ b. $0^0/30^0$

Figure 5.13. Effect of MLSP on buckling loads of beams with various BCs (MAT III.5, $L/h=5$)

5.4. Conclusions

The size effect, which is included by the modified couple stress theory, on bending, vibration and buckling behaviours of micro composite beams with arbitrary

lay-ups is investigated in this Chapter. This is the first times Poisson's effect is incorporated in constitutive equations for analysing the micro composite beams with arbitrary lay-ups. The governing equations of motion are derived from Lagrange's equations. New approximation functions are developed to solve problems. The frequencies, critical buckling loads, displacements and stresses of micro composite beams with various BCs are obtained. The obtained results indicate that:

- The size effect is significant for bending, buckling and free vibration analysis of micro laminated composite beams.
- Beam model and constitutive behaviours used in this Chapter are suitable for analysis of micro laminated composite beams with arbitrary lay-ups.
- The proposed functions are simple and efficient for predicting behaviours of micro laminated composite beams.

Chapter 6. ANALYSIS OF THIN-WALLED LAMINATED COMPOSITE BEAMS BASED ON FIRST-ORDER BEAM THEORY [7]

6.1. Introduction

Composite and functionally graded materials are commonly used in many fields of mechanical, aeronautical and civil engineering. The most well-known advantages of these materials are high stiffness-to-weight and strength-to-weight ratios, low thermal expansion, enhanced fatigue life and good corrosive resistance. In addition to their extensive use in practice, the available literatures indicate that a large number of studies have been conducted to analyse behaviours of these materials [103, 158, 159] in which thin-walled composite and functionally graded (FG) sandwich structures have been considered ([160-167]). Thin-walled beam theories have been presented by Vlasov [168] and Gjelsvik [169]. Bauld and Lih-Shyng [15] then extended Vlasov's thin-walled beam theory of isotropic material to the composite one. Pandey et al. [170] used Galerkin's method to solve the equilibrium differential equation for analysing of the flexural-torsional buckling of thin-walled composite I-beams. Buckling and free vibration of these beams were presented by Lee and Kim [17, 18] based on the finite element method (FEM) and classical beam theory. The FEM was used by Rajasekaran and Nalinaa [171] to investigate static, buckling and vibration behaviours of thin-walled composite beams with generic section. Maddur and Chaturvedi [172, 173] presented a Vlasov-type modified FOBT and analysed the dynamic responses of thin-walled composite open sections beams. Qin and Librescu [174] used an extended Galerkin's method to investigate natural frequencies and static responses of anisotropic thin-walled beams which account for shear deformation effects. A beam element based on the FOBT was developed by Lee [175] for the bending analysis of laminated composite I-beams under uniformly distributed loads. Machado and Cortinez [176] presented a stability analysis of thin-walled composite beams with open and closed sections considering shear deformation effects. Vo and Lee [177] extended previous research [175] to study vibration and

[7] A slightly different version of this chapter has been published in Composite Part B in 2019

buckling of thin-walled open section composite beams. Dynamic stiffness matrix method were also used in the studies [178-181] to analyse vibration and buckling of the thin-walled composite beams. Silvestre and Camotim [182] used shear deformable generalised beam theory for buckling behaviours of lipped channel columns. Prokic et al. [183] proposed an analytical solution for free vibration of simply-supported thin-walled composite beams by using Vlasov's beam theory and classical lamination theory. Based on the Carrera Unified Formulation (CUF), Carrera et al. [184-188] analysed static, vibration and elastoplastic thin-walled composite structures. By using FEM, Sheikh et al. [189] conducted the study of free vibration of thin-walled composite beams having open and closed sections to investigate the shear effects. Li et al. [190] investigated hygrothermal effects on free vibration of simply-supported thin-walled composite beams by using Galerkin's method. Recently, the thin-walled FG beams have caught interests of many researchers. Nguyen et al. [191, 192] analysed vibration and lateral buckling of the thin-walled FG beams by FEM. Lanc et al. [193] analysed nonlinear buckling responses of thin-walled FG open section beams based on Euler-Bernoulli-Vlasov theory. Kim and Lee [194, 195] investigated the shear effects on free vibration and buckling behaviours of the thin-walled FG beam by three different types of finite beam elements, namely, linear, quadratic and cubic elements. The studies on the effects of shear deformation on buckling and vibration behaviours of thin-walled FG beams are still limited. On the other hand, Ritz method is simple and efficient to analyse the behaviours of composite beams with various boundary conditions [44, 47, 48, 130, 196, 197], however, it has not been used for thin-walled composite and FG sandwich beams.

The main novelty of this Chapter is to develop a Ritz solution for the vibration, buckling and bending analyses of thin-walled composite and FG beams by using the FOBT. The governing equations of motion are derived by using Lagrange's equations. Results of the present element are compared with those in available literature to show its accuracy of the present solution. Parametric study is also

performed to investigate the effects of shear deformation, length-to-height ratio, fibre angle, material anisotropy and material distribution on natural frequencies, critical buckling loads and deflection of the thin-walled composite and FG sandwich beams.

6.2. Theoretical formulation

6.2.1. Kinematics

In this section, a kinematic field of the thin-walled composite and FG beams is presented. The theoretical development requires three sets of coordinate systems as shown in Fig. 6.1. The first coordinate system is the orthogonal Cartesian coordinate system (x, y, z), for which the *y*- and *z*-axes lie in the plane of the cross-section and the *x* axis parallel to the longitudinal axis of the beam. The second coordinate system is the local plate coordinate (n, s, x), wherein the *n* axis is normal to the middle surface of a plate element, the *s* axis is tangent to the middle surface and is directed along the contour line of the cross-section. θ_s is an angle of orientation between (n, s, x) and (x, y, z) coordinate systems. The pole P, which has coordinate (y_P, z_P), is called the shear center [198].

The following assumptions are made:

a. Strains are small and contour of section does not deform in its own plane.
b. Shear strains $\gamma_{yx}^0, \gamma_{zx}^0$ and warping shear γ_{ϖ}^0 are uniform over the section.
c. Local buckling and pre-buckling deformation are not considered.
d. Poisson's coefficient is constant.

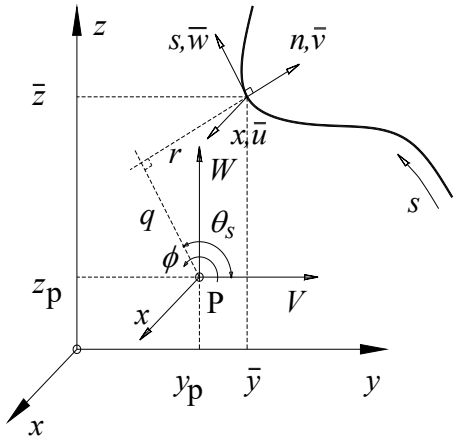

Figure 6.1. Thin-walled coordinate systems

Relation of the mid-surface displacements ($\bar{u},\bar{v},\bar{w}$) at a point in the contour coordinate system and global beam displacements (U, V,W) is given by ([175]):

$$\bar{v}(s,x,t)=V(x,t)\sin\theta_s(s)-W(x,t)\cos\theta_s(s)-\phi(x,t)q(s) \tag{6.1}$$

$$\bar{w}(s,x,t)=V(x,t)\cos\theta_s(s)+W(x,t)\sin\theta_s(s)+\phi(x,t)r(s) \tag{6.2}$$

$$\bar{u}(s,x,t)=U(x,t)+\psi_z(x,t)y(s)+\psi_y(x,t)z(s)+\psi_\varpi(x,t)\varpi(s) \tag{6.3}$$

where U, V and W are displacement of P in the $x-$, $y-$ and $z-$ direction, respectively; ϕ is the rotation angle about pole axis; ψ_y,ψ_z and ψ_ϖ denote rotations of the cross-section with respect to y, z and ϖ:

$$\psi_z=\gamma_{yx}^0-V_{,x} \tag{6.4}$$

$$\psi_y=\gamma_{zx}^0-W_{,x} \tag{6.5}$$

$$\psi_\varpi=\gamma_\varpi^0-\phi_{,x} \tag{6.6}$$

where ϖ is warping function given by:

$$\varpi(s)=\int_{s_0}^{s} r(s)ds \tag{6.7}$$

The displacements (u,v,w) at any generic point on section are expressed by the mid-surface displacements ($\bar{u},\bar{v},\bar{w}$) as:

$$v(n,s,x,t)=\bar{v}(s,x,t) \tag{6.8}$$

$$w(n,s,x,t)=\bar{w}(s,x,t)+n\bar{\psi}_s(s,x,t) \tag{6.9}$$

$$u(n,s,x,t)=\bar{u}(s,x,t)+n\bar{\psi}_x(s,x,t) \tag{6.10}$$

where $\bar{\psi}_s$ and $\bar{\psi}_x$ are determined by ([177]):

$$\bar{\psi}_x=\psi_z\sin\theta_s-\psi_y\cos\theta_s-\psi_\varpi q \tag{6.11}$$

$$\bar{\psi}_s(s,x,t)=-\frac{\partial\bar{v}}{\partial s} \tag{6.12}$$

The strain fields are defined as:

$$\varepsilon_s(n,s,x,t)=\bar{\varepsilon}_s(s,x,t)+n\bar{\kappa}_s(s,x,t) \tag{6.13}$$

$$\varepsilon_x(n,s,x,t)=\bar{\varepsilon}_x(s,x,t)+n\bar{\kappa}_x(s,x,t) \tag{6.14}$$

$$\gamma_{sx}\left(n,s,x,t\right)=\overline{\gamma}_{sx}\left(s,x,t\right)+n\overline{\kappa}_{sx}\left(s,x,t\right) \tag{6.15}$$

$$\gamma_{nx}\left(n,s,x,t\right)=\overline{\gamma}_{nx}\left(s,x,t\right)+n\overline{\kappa}_{nx}\left(s,x,t\right) \tag{6.16}$$

where

$$\overline{\varepsilon}_{s}=0 \tag{6.17}$$

$$\overline{\varepsilon}_{x}=\frac{\partial\overline{u}}{\partial x}=\varepsilon_{x}^{0}+y\kappa_{z}+z\kappa_{y}+\varpi\kappa_{\varpi} \tag{6.18}$$

$$\overline{\kappa}_{s}=0 \tag{6.19}$$

$$\overline{\kappa}_{x}=\frac{\partial\overline{\psi}_{x}}{\partial x}=\kappa_{z}\sin\theta_{s}-\kappa_{y}\cos\theta_{s}-\kappa_{\varpi}q \tag{6.20}$$

$$\overline{\kappa}_{sx}=\kappa_{sx} \tag{6.21}$$

$$\overline{\kappa}_{nx}=0 \tag{6.22}$$

$$\varepsilon_{x}^{0}=U_{,x} \tag{6.23}$$

$$\kappa_{y}=\psi_{y,x} \tag{6.24}$$

$$\kappa_{z}=\psi_{z,x} \tag{6.25}$$

$$\kappa_{\varpi}=\psi_{\varpi,x} \tag{6.26}$$

$$\kappa_{sx}=\phi_{,x}-\psi_{\varpi} \tag{6.27}$$

$$\varepsilon_{x}=\varepsilon_{x}^{0}+\left(y+n\sin\theta_{s}\right)\kappa_{z}+\left(z-n\cos\theta_{s}\right)\kappa_{y}+\left(\varpi-nq\right)\kappa_{\varpi} \tag{6.28}$$

$$\gamma_{sx}=\gamma_{yx}^{0}\cos\theta_{s}+\gamma_{zx}^{0}\sin\theta_{s}+\gamma_{\varpi}^{0}r+n\kappa_{sx} \tag{6.29}$$

$$\gamma_{nx}=\gamma_{yx}^{0}\sin\theta_{s}-\gamma_{zx}^{0}\cos\theta_{s}-\gamma_{\varpi}^{0}q \tag{6.30}$$

6.2.2. Constitutive relations

6.2.2.1. Thin-walled composite beam

The composite beam is constituted by a finite number of orthotropic layers. The constitutive relations at the k^{th} – layer in (n,s,x) coordinate systems can be expressed as:

$$\begin{Bmatrix}\sigma_{x}\\ \sigma_{sx}\\ \sigma_{nx}\end{Bmatrix}^{(k)}=\begin{pmatrix}\overline{Q}_{11}^{*} & \overline{Q}_{16}^{*} & 0\\ \overline{Q}_{16}^{*} & \overline{Q}_{66}^{*} & 0\\ 0 & 0 & \overline{Q}_{55}^{*}\end{pmatrix}^{(k)}\begin{Bmatrix}\varepsilon_{x}\\ \gamma_{sx}\\ \gamma_{nx}\end{Bmatrix} \tag{6.31}$$

where

$$\bar{Q}_{11}^{*} = \bar{Q}_{11} - \frac{\bar{Q}_{12}^{2}}{\bar{Q}_{22}} \tag{6.32}$$

$$\bar{Q}_{16}^{*} = \bar{Q}_{16} - \frac{\bar{Q}_{12}\bar{Q}_{26}}{\bar{Q}_{22}} \tag{6.33}$$

$$\bar{Q}_{66}^{*} = \bar{Q}_{66} - \frac{\bar{Q}_{26}^{2}}{\bar{Q}_{22}} \tag{6.34}$$

$$\bar{Q}_{55}^{*} = \bar{Q}_{55} \tag{6.35}$$

where $\bar{Q}_{ij}$ are the transformed reduced stiffnesses, see Appendix A for more details.

6.2.2.2. Thin-walled functionally graded (FG) sandwich beam

The constitutive relations of the FG sandwich beams can be written as follows:

$$\begin{Bmatrix} \sigma_x \\ \sigma_{sx} \\ \sigma_{nx} \end{Bmatrix} = \begin{pmatrix} \bar{Q}_{11}^{*} & 0 & 0 \\ 0 & \bar{Q}_{66}^{*} & 0 \\ 0 & 0 & \bar{Q}_{55}^{*} \end{pmatrix} \begin{Bmatrix} \varepsilon_x \\ \gamma_{sx} \\ \gamma_{nx} \end{Bmatrix} \tag{6.36}$$

where

$$\bar{Q}_{11}^{*} = E(n) \tag{6.37}$$

$$\bar{Q}_{66}^{*} = \bar{Q}_{55}^{*} = \frac{E(n)}{2(1+\nu)} \tag{6.38}$$

$E(n)$ is Young's modulus; ν is Poisson's coefficient. The effective mass density ρ and Young's modulus E of the thin-walled FG sandwich beam are approximated by:

$$\rho = \rho_c V_c + \rho_m (1 - V_c) \tag{6.39}$$

$$E = E_c V_c + E_m (1 - V_c) \tag{6.40}$$

where the subscripts c and m are used to indicate the ceramic and metal constituents, respectively; V_c is the volume fraction of ceramic material. Two type of material distributions are considered in this Chapter:

Type A (for the flange, see Fig. 6.2a):

$$V_c = \left[\frac{n + 0.5h}{(1-\alpha)h} \right]^{p}, \; -0.5h \le n \le (0.5 - \alpha)h \tag{6.41}$$

$$V_c = 1, \; (0.5 - \alpha)h \le n \le 0.5h \tag{6.42}$$

where h (h_1,h_2), p , α (α_1,α_2) are the thickness of the flange, material parameter and thickness ratio of ceramic material of the flange, respectively.

Type B (for the web, see Fig. 6.2b):

$$V_c = \left[\frac{-|n|+0.5h}{0.5(1-\beta)h}\right]^p, \ -0.5h \le n \le -0.5\beta h \ \text{ or } \ 0.5\beta h \le n \le 0.5h \tag{6.43}$$

$$V_c = 1, \ -0.5\beta h \le n \le 0.5\beta h \tag{6.44}$$

where $h = h_3$ is the thickness of the web; β is thickness ratio of the ceramic material of the web.

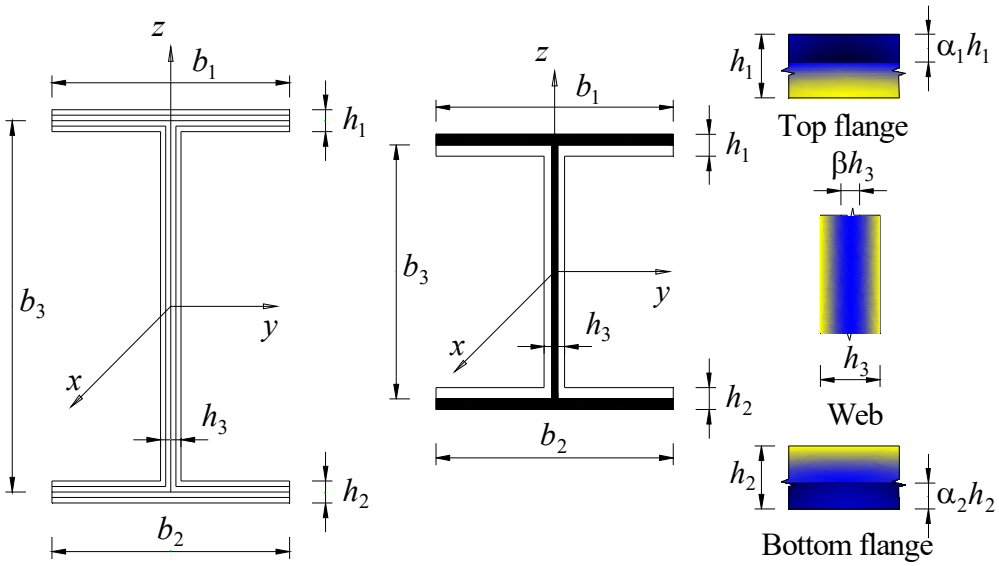

a. Composite I-beams b. FG sandwich I-beams

Figure 6.2. Geometry of thin-walled I-beams

6.2.3. Variational formulation

The strain energy Π_E of the thin-walled beams is defined by:

$$\Pi_E = \frac{1}{2}\int_\Omega \left(\sigma_x\varepsilon_x + \sigma_{sx}\gamma_{sx} + k^s\sigma_{nx}\gamma_{nx}\right)d\Omega \tag{6.45}$$

where k^s and Ω are shear correction factor and volume of beam, respectively. It is well-known that the models based on the FOBT require a correct value of the shear correction factors. Several authors made contributions in order to improve the models used for the FOBT. Nguyen et al. [199] proposed shear correction factors for analysis

of functionally graded beams and plates. Hutchinson [200], Gruttmann and Wagner [201], and Barbero et al. [202] presented formulas in order to compute the shear factors of different cross-sections of a Timoshenko's beam. In this Chapter, the shear factor is assumed to be a unity, which was suggested by some previous authors ([174, 175, 177]). Substituting Eqs. (6.28), (6.29), (6.30), (6.31) and (6.36) into Eq. (6.45) leads to:

$$\begin{aligned}
\Pi_E = \frac{1}{2}\int_0^L \Big[& E_{11}\left(U_{,x}\right)^2 + 2E_{16}U_{,x}V_{,x} + 2E_{17}U_{,x}W_{,x} + 2\left(E_{15}+E_{18}\right)U_{,x}\phi_{,x} \\
& + 2E_{12}U_{,x}\psi_{z,x} + 2E_{16}U_{,x}\psi_z + 2E_{13}U_{,x}\psi_{y,x} + 2E_{17}U_{,x}\psi_y + 2E_{14}U_{,x}\psi_{\varpi,x} \\
& + 2\left(E_{18}-E_{15}\right)U_{,x}\psi_{\varpi} + E_{66}\left(V_{,x}\right)^2 + 2E_{67}V_{,x}W_{,x} + 2\left(E_{56}+E_{68}\right)V_{,x}\phi_{,x} + 2E_{26}V_{,x}\psi_{z,x} \\
& + 2E_{66}V_{,x}\psi_z + 2E_{36}V_{,x}\psi_{y,x} + 2E_{67}V_{,x}\psi_y + 2E_{46}V_{,x}\psi_{\varpi,x} + 2\left(E_{68}-E_{56}\right)V_{,x}\psi_{\varpi} + E_{77}\left(W_{,x}\right)^2 \\
& + 2\left(E_{57}+E_{78}\right)W_{,x}\phi_{,x} + 2E_{27}W_{,x}\psi_{z,x} + 2E_{67}W_{,x}\psi_z + 2E_{37}W_{,x}\psi_{y,x} + 2E_{77}W_{,x}\psi_y + 2E_{47}W_{,x}\psi_{\varpi,x} \\
& + 2\left(E_{78}-E_{57}\right)W_{,x}\psi_{\varpi} + \left(E_{55}+2E_{58}+E_{88}\right)\left(\phi_{,x}\right)^2 + 2\left(E_{25}+E_{28}\right)\phi_{,x}\psi_{z,x} + 2\left(E_{56}+E_{68}\right)\phi_{,x}\psi_z \\
& + 2\left(E_{35}+E_{38}\right)\phi_{,x}\psi_{y,x} + 2\left(E_{57}+E_{78}\right)\phi_{,x}\psi_y + 2\left(E_{45}+E_{48}\right)\phi_{,x}\psi_{\varpi,x} + 2\left(E_{88}-E_{55}\right)\phi_{,x}\psi_{\varpi} \\
& + E_{22}\left(\psi_{z,x}\right)^2 + 2E_{26}\psi_{z,x}\psi_z + E_{66}\psi_z^2 + 2E_{23}\psi_{z,x}\psi_{y,x} + 2E_{27}\psi_{z,x}\psi_y + 2E_{36}\psi_z\psi_{y,x} + 2E_{67}\psi_z\psi_y \\
& + 2E_{24}\psi_{z,x}\psi_{\varpi,x} + 2\left(E_{28}-E_{25}\right)\psi_{z,x}\psi_{\varpi} + 2E_{46}\psi_z\psi_{\varpi,x} + 2\left(E_{68}-E_{56}\right)\psi_z\psi_{\varpi} + E_{33}\left(\psi_{y,x}\right)^2 \\
& + 2E_{37}\psi_{y,x}\psi_y + E_{77}\psi_y^2 + 2E_{34}\psi_{y,x}\psi_{\varpi,x} + 2\left(E_{38}-E_{35}\right)\psi_{y,x}\psi_{\varpi} + 2E_{47}\psi_y\psi_{\varpi,x} \\
& + 2\left(E_{78}-E_{57}\right)\psi_y\psi_{\varpi} + E_{44}\left(\psi_{\varpi,x}\right)^2 + 2\left(E_{48}-E_{45}\right)\psi_{\varpi,x}\psi_{\varpi} + \left(E_{88}-2E_{58}+E_{55}\right)\psi_{\varpi}^2 \Big] dx
\end{aligned} \tag{6.46}$$

where the stiffness coefficients E_{ij} are given in Appendix B [177], L is length of beam.

The potential energy Π_W of thin-walled beam subjected to axial compressive load N_0 and transverse load q can be expressed as:

$$\begin{aligned}
\Pi_W &= -\frac{1}{2}\int_\Omega \frac{N_0}{A}\left(\left(v_{,x}\right)^2 + \left(w_{,x}\right)^2\right) d\Omega + \int_\Omega qw d\Omega \\
&= -\frac{1}{2}\int_0^L N_0\left(\left(V_{,x}\right)^2 + \left(W_{,x}\right)^2 + 2z_p V_{,x}\phi_{,x} - 2y_p W_{,x}\phi_{,x} + \frac{I_P}{A}\left(\phi_{,x}\right)^2\right) dx + \int_0^L qW dx
\end{aligned} \tag{6.47}$$

where A is the cross-sectional area, I_P is polar moment of inertia of the cross-section about the centroid defined by:

$$I_P = I_y + I_z \tag{6.48}$$

where I_y and I_z are second moment of inertia with respect to $y-$ and $z-$ axis, defined by:

$$I_y = \int_A z^2 dA \tag{6.49}$$

$$I_z = \int_A y^2 dA \tag{6.50}$$

The kinetic energy Π_K of the thin-walled beam is given by:

$$\begin{aligned}
\Pi_K &= \frac{1}{2}\int_\Omega \rho(n)\left(\dot{u}^2 + \dot{v}^2 + \dot{w}^2\right) d\Omega \\
&= \frac{1}{2}\int_0^L \Big[m_0\dot{U}^2 + 2m_s\dot{U}\dot{\psi}_z - 2m_c\dot{U}\dot{\psi}_y + 2\left(m_\varpi - m_q\right)\dot{U}\dot{\psi}_\varpi + m_0\dot{V}^2 + 2\left(m_c + m_0 z_P\right)\dot{V}\dot{\phi} \\
&+ m_0\dot{W}^2 + 2\left(m_s - m_0 y_p\right)\dot{W}\dot{\phi} + \left(m_p + m_2 + 2m_r\right)\dot{\phi}^2 + \left(m_{x2} + 2m_{xs} + m_{s2}\right)\dot{\psi}_z^2 \\
&+ 2\left(m_{xycs} - m_{cs}\right)\dot{\psi}_z\dot{\psi}_y + 2\left(m_{x\varpi} + m_{x\varpi qs} - m_{qs}\right)\dot{\psi}_z\dot{\psi}_\varpi + \left(m_{y2} - 2m_{yc} + m_{c2}\right)\dot{\psi}_y^2 \\
&+ 2\left(m_{y\varpi} - m_{y\varpi qc} + m_{qc}\right)\dot{\psi}_y\dot{\psi}_\varpi + \left(m_{\varpi 2} - 2m_{q\varpi} + m_{q2}\right)\dot{\psi}_\varpi^2 \Big] dx
\end{aligned} \tag{6.51}$$

where dot-superscript denotes the differentiation with respect to the time t, $\rho(n)$ is the mass density and the inertia coefficients are given in Appendix B [177].

The total potential energy of thin-walled beam is expressed by:

$$\Pi = \Pi_E + \Pi_W - \Pi_K \tag{6.52}$$

6.2.4. Ritz solution

By using the Ritz method, the displacement field is approximated by:

$$U(x,t) = \sum_{j=1}^{m} \varphi_j'(x) U_j e^{i\omega t} \tag{6.53}$$

$$V(x,t) = \sum_{j=1}^{m} \varphi_j(x) V_j e^{i\omega t} \tag{6.54}$$

$$W(x,t) = \sum_{j=1}^{m} \varphi_j(x) W_j e^{i\omega t} \tag{6.55}$$

$$\phi(x,t) = \sum_{j=1}^{m} \varphi_j(x) \phi_j e^{i\omega t} \tag{6.56}$$

$$\psi_z(x,t) = \sum_{j=1}^{m} \varphi_j'(x) \psi_{zj} e^{i\omega t} \tag{6.57}$$

$$\psi_y(x,t)=\sum_{j=1}^{m}\varphi_j^{'}(x)\psi_{yj}e^{i\omega t} \tag{6.58}$$

$$\psi_{\varpi}(x,t)=\sum_{j=1}^{m}\varphi_j^{'}(x)\psi_{\varpi j}e^{i\omega t} \tag{6.59}$$

where ω is the frequency, $i^2=-1$ the imaginary unit; U_j, V_j, W_j, ϕ_j, ψ_{zj}, ψ_{yj} and $\psi_{\varpi j}$ are unknown and need to be determined; $\varphi_j(z)$ are approximation functions. It is clear that these approximation functions in Table 6.1 satisfy the various BCs such as S-S, C-F and C-C.

Table 6.1. Approximation functions and essential BCs of thin-walled beams.

BC	$\dfrac{\varphi_j(x)}{e^{\frac{-jx}{L}}}$	x=0	x=L
S-S	$\dfrac{x}{L}\left(1-\dfrac{x}{L}\right)$	$V=W=\phi=0$	$V=W=\phi=0$
C-F	$\left(\dfrac{x}{L}\right)^2$	$V=W=\phi=0$ $V_{,x}=W_{,x}=\phi_{,x}=0$ $U=\psi_z=\psi_y=\psi_{\varpi}=0$	
C-C	$\left(\dfrac{x}{L}\right)^2\left(1-\dfrac{x}{L}\right)^2$	$V=W=\phi=0$ $V_{,x}=W_{,x}=\phi_{,x}=0$ $U=\psi_z=\psi_y=\psi_{\varpi}=0$	$V=W=\phi=0$ $V_{,x}=W_{,x}=\phi_{,x}=0$ $U=\psi_z=\psi_y=\psi_{\varpi}=0$

By substituting Eqs. (6.53-6.59) into Eq. (6.52) and using Lagrange's equations:

$$\frac{\partial\Pi}{\partial p_j}-\frac{d}{dt}\frac{\partial\Pi}{\partial\dot{p}_j}=0 \tag{6.60}$$

with p_j representing the values of $\left(U_j,V_j,W_j,\phi_j,\psi_{zj},\psi_{yj},\psi_{\varpi j}\right)$, the vibration, buckling and bending behaviours of the thin-walled beam can be obtained by solving the following equations:

$$\left(\begin{bmatrix} \mathbf{K}^{11} & \mathbf{K}^{12} & \mathbf{K}^{13} & \mathbf{K}^{14} & \mathbf{K}^{15} & \mathbf{K}^{16} & \mathbf{K}^{17} \\ {}^{T}\mathbf{K}^{12} & \mathbf{K}^{22} & \mathbf{K}^{23} & \mathbf{K}^{24} & \mathbf{K}^{25} & \mathbf{K}^{26} & \mathbf{K}^{27} \\ {}^{T}\mathbf{K}^{13} & {}^{T}\mathbf{K}^{23} & \mathbf{K}^{33} & \mathbf{K}^{34} & \mathbf{K}^{35} & \mathbf{K}^{36} & \mathbf{K}^{37} \\ {}^{T}\mathbf{K}^{14} & {}^{T}\mathbf{K}^{24} & {}^{T}\mathbf{K}^{34} & \mathbf{K}^{44} & \mathbf{K}^{45} & \mathbf{K}^{46} & \mathbf{K}^{47} \\ {}^{T}\mathbf{K}^{15} & {}^{T}\mathbf{K}^{25} & {}^{T}\mathbf{K}^{35} & {}^{T}\mathbf{K}^{45} & \mathbf{K}^{55} & \mathbf{K}^{56} & \mathbf{K}^{57} \\ {}^{T}\mathbf{K}^{16} & {}^{T}\mathbf{K}^{26} & {}^{T}\mathbf{K}^{36} & {}^{T}\mathbf{K}^{46} & {}^{T}\mathbf{K}^{56} & \mathbf{K}^{66} & \mathbf{K}^{67} \\ {}^{T}\mathbf{K}^{17} & {}^{T}\mathbf{K}^{27} & {}^{T}\mathbf{K}^{37} & {}^{T}\mathbf{K}^{47} & {}^{T}\mathbf{K}^{57} & {}^{T}\mathbf{K}^{67} & \mathbf{K}^{77} \end{bmatrix} \right.$$
$$\left. -\omega^2 \begin{bmatrix} \mathbf{M}^{11} & \mathbf{0} & \mathbf{0} & \mathbf{0} & \mathbf{M}^{15} & \mathbf{M}^{16} & \mathbf{M}^{17} \\ \mathbf{0} & \mathbf{M}^{22} & \mathbf{0} & \mathbf{M}^{24} & \mathbf{0} & \mathbf{0} & \mathbf{0} \\ \mathbf{0} & \mathbf{0} & \mathbf{M}^{33} & \mathbf{M}^{34} & \mathbf{0} & \mathbf{0} & \mathbf{0} \\ \mathbf{0} & {}^{T}\mathbf{M}^{24} & {}^{T}\mathbf{M}^{34} & \mathbf{M}^{44} & \mathbf{0} & \mathbf{0} & \mathbf{0} \\ {}^{T}\mathbf{M}^{15} & \mathbf{0} & \mathbf{0} & \mathbf{0} & \mathbf{M}^{55} & \mathbf{M}^{56} & \mathbf{M}^{57} \\ {}^{T}\mathbf{M}^{16} & \mathbf{0} & \mathbf{0} & \mathbf{0} & {}^{T}\mathbf{M}^{56} & \mathbf{M}^{66} & \mathbf{M}^{67} \\ {}^{T}\mathbf{M}^{17} & \mathbf{0} & \mathbf{0} & \mathbf{0} & {}^{T}\mathbf{M}^{57} & {}^{T}\mathbf{M}^{67} & \mathbf{M}^{77} \end{bmatrix} \right) \begin{Bmatrix} \mathbf{u} \\ \mathbf{v} \\ \mathbf{w} \\ \mathbf{\Phi} \\ \boldsymbol{\psi}_z \\ \boldsymbol{\psi}_y \\ \boldsymbol{\psi}_{\varpi} \end{Bmatrix} = \begin{Bmatrix} \mathbf{0} \\ \mathbf{0} \\ \mathbf{F} \\ \mathbf{0} \\ \mathbf{0} \\ \mathbf{0} \\ \mathbf{0} \end{Bmatrix} \tag{6.61}$$

where the stiffness matrix **K**, mass matrix **M** and load vector **F** are expressed by:

$$K_{ij}^{11} = E_{11}\int_0^L \varphi_{i,xx}\varphi_{j,xx}dx,\ K_{ij}^{12} = E_{16}\int_0^L \varphi_{i,xx}\varphi_{j,x}dx,\ K_{ij}^{13} = E_{17}\int_0^L \varphi_{i,xx}\varphi_{j,x}dx,$$

$$K_{ij}^{14} = \left(E_{15}+E_{18}\right)\int_0^L \varphi_{i,xx}\varphi_{j,x}dx,$$

$$K_{ij}^{15} = E_{12}\int_0^L \varphi_{i,xx}\varphi_{j,xx}dx + E_{16}\int_0^L \varphi_{i,x}\varphi_{j}dx,\ K_{ij}^{16} = E_{13}\int_0^L \varphi_{i,xx}\varphi_{j,xx}dx + E_{17}\int_0^L \varphi_{i,xx}\varphi_{j,x}dx,$$

$$K_{ij}^{17} = E_{14}\int_0^L \varphi_{i,xx}\varphi_{j,xx}dx + \left(E_{18}-E_{15}\right)\int_0^L \varphi_{i,xx}\varphi_{j,x}dx \quad , \quad K_{ij}^{22} = E_{66}\int_0^L \varphi_{i,x}\varphi_{j,x}dx + N_0\int_0^L \varphi_{i,x}\varphi_{j,x}dx \quad ,$$

$$K_{ij}^{23} = E_{67}\int_0^L \varphi_{i,x}\varphi_{j,x}dx,$$

$$K_{ij}^{24} = \left(E_{56}+E_{68}\right)\int_0^L \varphi_{i,x}\varphi_{j,x}dx + N_0 z_p\int_0^L \varphi_{i,x}\varphi_{j,x}dx,\ K_{ij}^{25} = E_{26}\int_0^L \varphi_{i,x}\varphi_{j,xx}dx + E_{66}\int_0^L \varphi_{i,x}\varphi_{j,x}dx,$$

$$K_{ij}^{26} = E_{36}\int_0^L \varphi_{i,x}\varphi_{j,xx}dx + E_{67}\int_0^L \varphi_{i,x}\varphi_{j,x}dx,\ K_{ij}^{27} = E_{46}\int_0^L \varphi_{i,x}\varphi_{j,xx}dx + \left(E_{68}-E_{56}\right)\int_0^L \varphi_{i,x}\varphi_{j,x}dx,$$

$$K_{ij}^{33} = E_{77}\int_0^L \varphi_{i,x}\varphi_{j,x}dx + N_0\int_0^L \varphi_{i,x}\varphi_{j,x}dx,\ K_{ij}^{34} = \left(E_{57}+E_{78}\right)\int_0^L \varphi_{i,x}\varphi_{j,x}dx - N_0 y_p\int_0^L \varphi_{i,x}\varphi_{j,x}dx,$$

$$K_{ij}^{35}=E_{27}\int_0^L\varphi_{i,x}\varphi_{j,xx}dx+E_{67}\int_0^L\varphi_{i,x}\varphi_{j,x}dx\,,\ K_{ij}^{36}=E_{37}\int_0^L\varphi_{i,x}\varphi_{j,xx}dx+E_{77}\int_0^L\varphi_{i,x}\varphi_{j,x}dx\,,$$

$$K_{ij}^{37}=E_{47}\int_0^L\varphi_{i,x}\varphi_{j,xx}dx+\left(E_{78}-E_{57}\right)\int_0^L\varphi_{i,x}\varphi_{j,x}dx\,,$$

$$K_{ij}^{44}=\left(E_{55}+2E_{58}+E_{88}\right)\int_0^L\varphi_{i,x}\varphi_{j,x}dx+\frac{N_0I_p}{A}\int_0^L\varphi_{i,x}\varphi_{j,x}dx\,,$$

$$K_{ij}^{45}=\left(E_{25}+E_{28}\right)\int_0^L\varphi_{i,x}\varphi_{j,xx}dx+\left(E_{56}+E_{68}\right)\int_0^L\varphi_{i,x}\varphi_{j,x}dx\,,$$

$$K_{ij}^{46}=\left(E_{35}+E_{38}\right)\int_0^L\varphi_{i,x}\varphi_{j,xx}dx+\left(E_{57}+E_{78}\right)\int_0^L\varphi_{i,x}\varphi_{j,x}dx\,,$$

$$K_{ij}^{47}=\left(E_{45}+E_{48}\right)\int_0^L\varphi_{i,x}\varphi_{j,xx}dx+\left(E_{88}-E_{55}\right)\int_0^L\varphi_{i,x}\varphi_{j,x}dx\,,$$

$$K_{ij}^{55}=E_{22}\int_0^L\varphi_{i,xx}\varphi_{j,xx}dx+E_{26}\int_0^L\left(\varphi_{i,xx}\varphi_{j,x}+\varphi_{i,x}\varphi_{j,xx}\right)dx+E_{66}\int_0^L\varphi_{i,x}\varphi_{j,x}dx\,,$$

$$K_{ij}^{56}=E_{23}\int_0^L\varphi_{i,xx}\varphi_{j,xx}dx+E_{27}\int_0^L\varphi_{i,xx}\varphi_{j,x}dx+E_{36}\int_0^L\varphi_{i,x}\varphi_{j,xx}dx+E_{67}\int_0^L\varphi_{i,x}\varphi_{j,x}dx\,,$$

$$K_{ij}^{57}=E_{24}\int_0^L\varphi_{i,xx}\varphi_{j,xx}dx+\left(E_{28}-E_{25}\right)\int_0^L\varphi_{i,xx}\varphi_{j,x}dx+E_{46}\int_0^L\varphi_{i,x}\varphi_{j,xx}dx+\left(E_{68}-E_{56}\right)\int_0^L\varphi_{i,x}\varphi_{j,x}dx\,,$$

$$K_{ij}^{66}=E_{33}\int_0^L\varphi_{i,xx}\varphi_{j,xx}dx+E_{37}\int_0^L\left(\varphi_{i,xx}\varphi_{j,x}+\varphi_{i,x}\varphi_{j,xx}\right)dx+E_{77}\int_0^L\varphi_{i,x}\varphi_{j,x}dx\,,$$

$$K_{ij}^{67}=E_{34}\int_0^L\varphi_{i,xx}\varphi_{j,xx}dx+\left(E_{38}-E_{35}\right)\int_0^L\varphi_{i,xx}\varphi_{j,x}dx+E_{47}\int_0^L\varphi_{i,x}\varphi_{j,xx}dx+\left(E_{78}-E_{57}\right)\int_0^L\varphi_{i,x}\varphi_{j,x}dx\,,$$

$$K_{ij}^{77}=E_{44}\int_0^L\varphi_{i,xx}\varphi_{j,xx}dx+\left(E_{48}-E_{45}\right)\int_0^L\left(\varphi_{i,xx}\varphi_{j,x}+\varphi_{i,x}\varphi_{j,xx}\right)dx+\left(E_{88}-2E_{58}+E_{55}\right)\int_0^L\varphi_{i,x}\varphi_{j,x}dx\,,$$

$$M_{ij}^{11}=m_0\int_0^L\varphi_{i,x}\varphi_{j,x}dx\,,\ M_{ij}^{15}=m_s\int_0^L\varphi_{i,x}\varphi_{j,x}dx\,,\ M_{ij}^{16}=-m_c\int_0^L\varphi_{i,x}\varphi_{j,x}dx\,,$$

$$M_{ij}^{17}=\left(m_{\varpi}-m_q\right)\int_0^L\varphi_{i,x}\varphi_{j,x}dx\,,$$

$$M_{ij}^{22}=m_0\int_0^L\varphi_i\varphi_jdx\,,\ M_{ij}^{24}=\left(m_c+m_0y_p\right)\int_0^L\varphi_i\varphi_jdx\,,\ M_{ij}^{33}=m_0\int_0^L\varphi_i\varphi_jdx\,,$$

$$M_{ij}^{34}=\left(m_s-m_0y_p\right)\int_0^L\varphi_i\varphi_j dx\ ,\ M_{ij}^{44}=\left(m_p+m_2+2m_r\right)\int_0^L\varphi_i\varphi_j dx\ ,$$

$$M_{ij}^{55}=\left(m_{x2}+2m_{xs}+m_{s2}\right)\int_0^L\varphi_{i,x}\varphi_{j,x}dx\ ,\ M_{ij}^{56}=\left(m_{xycs}-m_{cs}\right)\int_0^L\varphi_{i,x}\varphi_{j,x}dx\ ,$$

$$M_{ij}^{57}=\left(m_{x\varpi}+m_{x\varpi qs}-m_{qs}\right)\int_0^L\varphi_{i,x}\varphi_{j,x}dx\ ,\ M_{ij}^{66}=\left(m_{y2}-2m_{yc}+m_{c2}\right)\int_0^L\varphi_{i,x}\varphi_{j,x}dx\ ,$$

$$M_{ij}^{67}=\left(m_{y\varpi}-m_{y\varpi qc}+m_{qc}\right)\int_0^L\varphi_{i,x}\varphi_{j,x}dx\ ,\ M_{ij}^{77}=\left(m_{\varpi 2}-2m_{q\varpi}+m_{q2}\right)\int_0^L\varphi_{i,x}\varphi_{j,x}dx$$

$$F_i=\int_0^L q\varphi_i dx \tag{6.62}$$

If the shear effect is ignored, Eq. (6.1-6.3) degenerate to $\psi_z=-V_{,x}$, $\psi_y=-W_{,x}$, $\psi_\varpi=-\phi_{,x}$ By setting $\gamma_{yx}^0=\gamma_{zx}^0=\gamma_\varpi^0=0$ into the above equations, the number of unknown variables reduces to four (U,V,W,ϕ) as the Euler-Bernoulli-Vlasov beam model. Finally, the natural frequencies, critical buckling loads and deflections of the thin-walled beams without shear effects can be found:

$$\left(\begin{bmatrix} {}_{NS}\mathbf{K}^{11} & {}_{NS}\mathbf{K}^{12} & {}_{NS}\mathbf{K}^{13} & {}_{NS}\mathbf{K}^{14} \\ {}_{NS}^{T}\mathbf{K}^{12} & {}_{NS}\mathbf{K}^{22} & {}_{NS}\mathbf{K}^{23} & {}_{NS}\mathbf{K}^{24} \\ {}_{NS}^{T}\mathbf{K}^{13} & {}_{NS}^{T}\mathbf{K}^{23} & {}_{NS}\mathbf{K}^{33} & {}_{NS}\mathbf{K}^{34} \\ {}_{NS}^{T}\mathbf{K}^{14} & {}_{NS}^{T}\mathbf{K}^{24} & {}_{NS}^{T}\mathbf{K}^{34} & {}_{NS}\mathbf{K}^{44} \end{bmatrix}-\omega^2\begin{bmatrix} {}_{NS}\mathbf{M}^{11} & \mathbf{0} & \mathbf{0} & \mathbf{0} \\ \mathbf{0} & {}_{NS}\mathbf{M}^{22} & \mathbf{0} & {}_{NS}\mathbf{M}^{24} \\ \mathbf{0} & \mathbf{0} & {}_{NS}\mathbf{M}^{33} & {}_{NS}\mathbf{M}^{34} \\ \mathbf{0} & {}_{NS}^{T}\mathbf{M}^{24} & {}_{NS}^{T}\mathbf{M}^{34} & {}_{NS}\mathbf{M}^{44} \end{bmatrix}\right)\begin{Bmatrix}\mathbf{u}\\ \mathbf{v}\\ \mathbf{w}\\ \mathbf{\Phi}\end{Bmatrix}=\begin{Bmatrix}\mathbf{0}\\ \mathbf{0}\\ \mathbf{F}\\ \mathbf{0}\end{Bmatrix} \tag{6.63}$$

where the stiffness matrix **K**, mass matrix **M** and load vector **F** are given by:

$${}_{NS}K_{ij}^{11}=E_{11}\int_0^L\varphi_{i,xx}\varphi_{j,xx}dx\ ,\ {}_{NS}K_{ij}^{12}=-E_{12}\int_0^L\varphi_{i,xx}\varphi_{j,xx}dx\ ,\ {}_{NS}K_{ij}^{13}=-E_{13}\int_0^L\varphi_{i,xx}\varphi_{j,xx}dx\ ,$$

$${}_{NS}K_{ij}^{14}=2E_{15}\int_0^L\varphi_{i,xx}\varphi_{j,x}dx-E_{14}\int_0^L\varphi_{i,xx}\varphi_{j,xx}dx\quad ,\quad {}_{NS}K_{ij}^{22}=E_{22}\int_0^L\varphi_{i,xx}\varphi_{j,xx}dx+N_0\int_0^L\varphi_{i,x}\varphi_{j,x}dx\quad ,$$

$${}_{NS}K_{ij}^{23}=E_{23}\int_0^L\varphi_{i,xx}\varphi_{j,xx}dx\ ,$$

$${}_{NS}K_{ij}^{24}=E_{24}\int_0^L\varphi_{i,xx}\varphi_{j,xx}dx-2E_{25}\int_0^L\varphi_{i,xx}\varphi_{j,x}dx+N_0z_p\int_0^L\varphi_{i,x}\varphi_{j,x}dx\ ,\ {}_{NS}K_{ij}^{33}=E_{33}\int_0^L\varphi_{i,xx}\varphi_{j,xx}dx\ ,$$

$$_{NS}K_{ij}^{34} = E_{34}\int_0^L \varphi_{i,xx}\varphi_{j,xx}dx - 2E_{35}\int_0^L \varphi_{i,xx}\varphi_{j,x}dx - N_0 y_p \int_0^L \varphi_{i,x}\varphi_{j,x}dx,$$

$$_{NS}K_{ij}^{44} = E_{44}\int_0^L \varphi_{i,xx}\varphi_{j,xx}dx - 2E_{45}\int_0^L \left(\varphi_{i,xx}\varphi_{j,x} + \varphi_{i,x}\varphi_{j,xx}\right)dx + 4E_{55}\int_0^L \varphi_{i,x}\varphi_{j,x}dx + \frac{N_0 I_p}{A}\int_0^L \varphi_{i,x}\varphi_{j,x}dx,$$

$$_{NS}M_{ij}^{11} = m_0\int_0^L \varphi_{i,x}\varphi_{j,x}dx,\ _{NS}M_{ij}^{22} = m_0\int_0^L \varphi_i\varphi_j dx,\ _{NS}M_{ij}^{24} = \left(m_c + m_0 y_p\right)\int_0^L \varphi_i\varphi_j dx,$$

$$_{NS}M_{ij}^{33} = m_0\int_0^L \varphi_i\varphi_j dx,\ _{NS}M_{ij}^{34} = \left(m_s - m_0 y_p\right)\int_0^L \varphi_i\varphi_j dx,\ _{NS}M_{ij}^{44} = \left(m_p + m_2 + 2m_\varpi\right)\int_0^L \varphi_i\varphi_j dx$$

$$F_i = \int_0^L q\varphi_i dx \tag{6.64}$$

6.3. Numerical results

Results for natural frequencies, critical buckling loads and deflection of thin-walled composite and FG sandwich beams with various configurations including boundary conditions, lay-ups and thickness ratio of the ceramic material are presented in this section. Convergence and comparison with the available literature are made to show the accuracy of the present solution. In addition, some new results, which may be used as reference data for future, are presented. The material properties and geometry of thin-walled beams are given in Table 6.2 and Fig.6.2. The effect of the fiber angle, shear deformation, material parameter, length-to-height ratio and thickness ratio of ceramic material on vibration, buckling and bending behaviours of the thin-walled beams are investigated. The shear effect is defined by $\left(R_{NS} - R_s\right)/R_{NS}\times 100\%$ where R_S and R_{NS} denote the results with and without the shear effects, respectively.

Unless otherwise stated, the following non-dimensional terms are used:

$$\text{For composite beams: } \bar{\omega} = \frac{\omega L^2}{b_3}\sqrt{\frac{\rho}{E_2}},\ \bar{N}_{cr} = \frac{N_{cr}L^2}{hE_2 b_3^3} \tag{6.65}$$

$$\text{For FG sandwich beams: } \bar{\omega} = \frac{\omega L^2}{b_3}\sqrt{\frac{\rho_m}{E_m}},\ \bar{N}_{cr} = \frac{N_{cr}L^2}{hE_m b_3^3} \tag{6.66}$$

Table 6.2. Material properties of thin-walled beams.

Material properties	MAT I.6	MAT II.6	MAT III.6	MAT IV.6	MAT V.6
E_1 , E_c (GPa)	*53.78*	25	*380*	*320.7*	*141.9*
E_2=E_3 , E_m (GPa)	17.93	1	70	101.69	9.78
G_{12}=G_{13} (GPa)	8.96	0.6	-	-	6.13
G_{23} (GPa)	3.45	0.6	-	-	4.8
ν, ν_{12}= ν_{13}	0.25	0.25	0.30	0.3	0.42
ρ (kg/m^3)	1968.90	-	-	-	1445
ρ_c (kg/m^3)	-	-	3960	-	-
ρ_m (kg/m^3)	-	-	2702	-	-

6.3.1. Convergence study

For purpose of testing convergence of present solution, the composite I-beams (MAT I.6, $b_1 = b_2 = b_3 = 5$ cm, $h_1 = h_2 = h_3 = 0.208$ cm and $L = 40b_3$), FG sandwich I-beams (MAT III.6, $b_1 = b_2 = 15$ cm, $b_3 = 20$ cm, $h_1 = h_2 = h_3 = 0.5$ cm, $\alpha_1 = \alpha_2 = \beta = 0.1$, $p = 5$ and $L = 10b_3$) with the various BCs are considered. It is noted that both flanges and web of composite I-beams are assumed to be symmetrically laminated angle-ply $[45/-45]_{4s}$ with respect to its mid-plane. The fundamental frequencies, critical buckling loads and deflections of thin-walled I-beams are presented in Table 6.3 and 6.4 with various series number m. As can be seen, a rapid convergence is obtained and $m = 10$ is sufficient to guarantee the numerical convergence

Table 6.3. Convergence studies for thin-walled composite I-beams.

BC		*m*					
		2	4	6	8	10	12
a. Fundamental frequency (Hz)							
S-S	Shear	16.763	16.544	16.482	16.481	16.481	16.481
	No shear	16.773	16.553	16.491	16.490	16.490	16.490
C-F	Shear	5.958	5.878	5.873	5.873	5.873	5.873
	No shear	5.959	5.880	5.875	5.875	5.875	5.875
C-C	Shear	37.433	37.307	37.304	37.303	37.302	37.301
	No shear	37.502	37.382	37.382	37.382	37.382	37.382
b. Critical buckling load (kN)							
S-S	Shear	2.752	2.690	2.671	2.671	2.671	2.671
	No shear	2.755	2.692	2.673	2.673	2.673	2.673
C-F	Shear	0.706	0.668	0.668	0.668	0.668	0.668
	No shear	0.706	0.668	0.668	0.668	0.668	0.668
C-C	Shear	10.797	10.678	10.657	10.657	10.657	10.657
	No shear	10.832	10.712	10.691	10.691	10.691	10.691
c. Deflection at mid-span under uniformly distributed load of 1kN (cm)							
S-S	Shear	5.320	5.483	5.518	5.516	5.516	5.516
	No shear	5.301	5.464	5.499	5.497	5.497	5.497
C-F	Shear	18.137	18.697	18.748	18.745	18.746	18.746
	No shear	18.089	18.645	18.692	18.690	18.690	18.690
C-C	Shear	1.109	1.116	1.117	1.118	1.118	1.118
	No shear	1.104	1.100	1.100	1.100	1.100	1.100

Table 6.4. Convergence studies for thin-walled FG sandwich I-beams.

BC		*m*					
		2	4	6	8	10	12
a. Fundamental frequency (Hz)							
S-S	Shear	92.715	91.522	91.184	91.180	91.180	91.180
	No shear	93.701	92.474	92.127	92.122	92.122	92.122
C-F	Shear	33.137	32.690	32.663	32.660	32.660	32.660
	No shear	33.291	32.846	32.820	32.818	32.818	32.818
C-C	Shear	201.801	200.434	200.127	199.973	199.885	199.830
	No shear	209.499	208.830	208.828	208.828	208.828	208.828
b. Critical buckling load (MN)							
S-S	Shear	1.036	1.013	1.006	1.006	1.006	1.006
	No shear	1.055	1.031	1.024	1.024	1.024	1.024
C-F	Shear	0.269	0.255	0.255	0.255	0.255	0.255
	No shear	0.271	0.256	0.256	0.256	0.256	0.256
C-C	Shear	3.867	3.827	3.820	3.820	3.820	3.820
	No shear	4.150	4.104	4.096	4.096	4.096	4.096
c. Deflection at mid-span uniformly distributed load of 1kN (mm)							
S-S	Shear	0.080	0.082	0.083	0.083	0.083	0.083
	No shear	0.074	0.077	0.077	0.077	0.077	0.077
C-F	Shear	0.269	0.278	0.279	0.279	0.279	0.279
	No shear	0.254	0.261	0.262	0.262	0.262	0.262
C-C	Shear	0.020	0.021	0.021	0.021	0.021	0.021
	No shear	0.015	0.015	0.015	0.015	0.015	0.015

6.3.2. Composite I-beams

6.3.2.1. Verification

The first example demonstrates accuracy and validity of present solutions. The symmetric angle-ply I-beams (MAT I.6) with the various BCs are considered. The flanges and web are 0.208 cm thickness, and made of symmetric laminates that consist of 16 layers ($[\eta/-\eta]_{4S}$). The first natural frequencies of S-S I-beams ($b_1 = b_2 = b_3 = 5$ cm and $L = 40b_3$), C-F I-beams ($b_1 = b_2 = 4$ cm, $b_5 = 5$ cm and $L = 20b_3$)

and C-C I-beams ($b_1 = b_2 = b_3 = 5$ cm and $L = 40b_3$) are showed in Table 6.5 and Fig. 6.3. It can be seen that the present results are coincided with existing ones.

Table 6.5. The fundamental frequency (Hz) of thin-walled S-S and C-F I-beams

BC	Reference	Lay-up			
		$[0]_{16}$	$\begin{bmatrix}30/\\-30\end{bmatrix}_{4s}$	$\begin{bmatrix}60/\\-60\end{bmatrix}_{4s}$	$\begin{bmatrix}90/\\-90\end{bmatrix}_{4s}$
S-S	Present (Shear)	24.169	19.806	14.660	13.964
	Present (No shear)	24.198	19.820	14.668	13.972
	Vo and Lee [177] (Shear)	24.150	19.776	14.627	13.937
	Sheikh et al. [189] (Shear)	24.160	19.800	14.660	13.960
	Kim et al. [179] (No shear)	24.194	19.816	14.666	13.970
C-F	Present (Shear)	26.479	21.699	16.063	15.299
	Present (No shear)	26.514	21.717	16.072	15.309
	Kim and Lee [165] (Shear)	26.460	21.700	16.060	15.300
	Kim and Lee [165] (No shear)	26.510	21.710	16.070	15.310

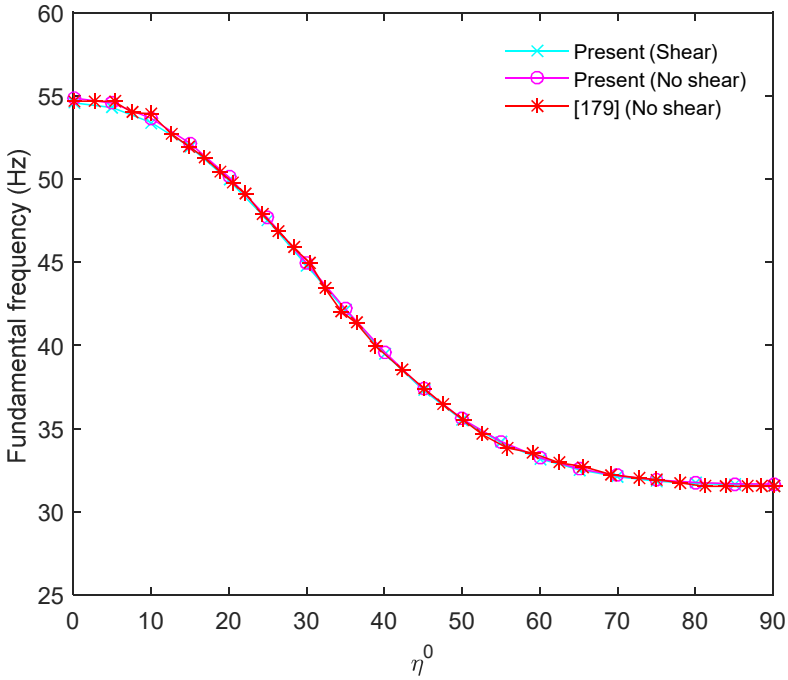

Figure 6.3. Variation of the fundamental frequencies (Hz) of thin-walled C-C I-beams with respect to fiber angle.

The critical buckling loads of S-S I-beams ($b_1 = b_2 = b_3 = 5$ cm and $L = 80b_3$), C-F I-beams ($b_1 = b_2 = b_3 = 5$ cm and $L = 20b_3$) and C-C I-beams ($b_1 = b_2 = b_3 = 5$ cm, $L = 80b_3$) are displayed in Table 6.6 and Fig. 6.4, respectively. Good agreements between the present results and those of Vo and Lee [177], Kim et al. [180, 181] are found again. It is also stated that there are not much differences between shear and no shear results because these beams are slender.

Table 6.6. Critical buckling load (N) of thin-walled S-S and C-F I-beams

BC	Reference	Lay-up			
		$[0]_{16}$	$\begin{bmatrix}30/\\-30\end{bmatrix}_{4s}$	$\begin{bmatrix}60/\\-60\end{bmatrix}_{4s}$	$\begin{bmatrix}0/\\90\end{bmatrix}_{4s}$
S-S	Present (Shear)	1438.1	965.0	528.6	959.0
	Present (No shear)	1438.8	965.2	528.7	959.3
	Kim et al. [180] (No shear)	1438.8	965.2	528.7	964.4
C-F	Present (Shear)	5743.3	3856.8	2113.2	3831.4
	Present (No shear)	5755.2	3861.0	2114.7	3837.3
	Vo and Lee [177] (Shear)	5741.5	3854.5	2111.3	3829.8
	Kim et al. [180] (No shear)	5755.2	3861.0	2114.7	3857.8

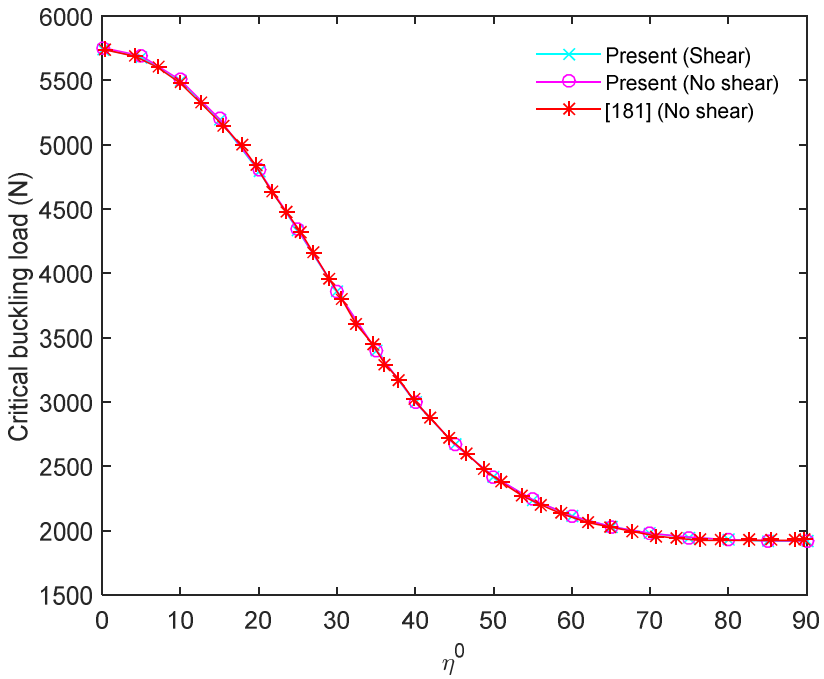

Figure 6.4. Variation of the critical buckling loads (N) of thin-walled C-C I-beams with respect to fiber angle.

The deflection at mid-span of I-beams ($b_1 = b_2 = b_3 = 5$ cm and $L = 50b_3$) with various different BCs under uniformly distributed load of 1 kN/m are displayed in Table 6.7. Good agreements between the present solution and other results are also found.

Table 6.7. Deflections (cm) at mid-span of thin-walled I-beams

BC	Reference	Lay-up			
		$[0]_{16}$	$\begin{bmatrix} 30/ \\ -30 \end{bmatrix}_{4s}$	$\begin{bmatrix} 60/ \\ -60 \end{bmatrix}_{4s}$	$\begin{bmatrix} 0/ \\ 90 \end{bmatrix}_{4s}$
S-S	Present (Shear)	6.261	9.317	16.998	9.384
	Present (No shear)	6.233	9.290	16.962	9.349
	Lee and Lee [203] (No shear)	6.233	9.290	16.962	9.299
	Lee [175] (Shear)	6.259	9.314	16.992	9.381
C-F	Present (Shear)	21.274	31.666	57.777	31.889
	Present (No shear)	21.191	31.587	57.670	31.785
C-C	Present (Shear)	1.274	1.884	3.427	1.904
	Present (No shear)	1.247	1.858	3.392	1.870

6.3.2.2. Shear deformation effect

This example is to investigate the effects of shear deformation on the vibration and buckling behaviors of I-beams. The composite I-beams (MAT II.6, $b_1 = b_2 = 20$ cm, $b_3 = 30$ cm, $h_1 = h_2 = h_3 = 1$ cm and $L = 20b_3$) are considered. The top and bottom flanges are angle-ply lay-up $[\eta / -\eta]$ and the web is unidirectional one. The results of I-beams with different BCs are displayed in Tables 6.8-6.10. From these tables, it can be seen that the present results comply with those of Vo and Lee [177], and both natural frequencies and critical buckling loads decrease as the fiber angle increases for all BCs.

Table 6.8. Non-dimensional natural frequency of thin-walled S-S I-beams

BC	Reference	Lay-up			
		$[0]$	$\begin{bmatrix}30/\\-30\end{bmatrix}$	$\begin{bmatrix}60/\\-60\end{bmatrix}$	$\begin{bmatrix}90/\\-90\end{bmatrix}$
Present (Shear)	ω_1	7.107	3.755	1.627	1.468
	ω_2	8.189	5.137	2.967	2.645
	ω_3	19.140	12.904	6.495	5.860
	ω_4	27.542	14.957	8.577	7.685
	ω_5	30.741	17.791	9.976	9.817
Present (No shear)	ω_1	7.186	3.761	1.628	1.469
	ω_2	8.303	5.145	2.970	2.648
	ω_3	20.856	13.404	6.513	5.876
	ω_4	28.743	15.043	8.606	7.713
	ω_5	32.408	17.917	10.213	10.045

Table 6.9. Non-dimensional natural frequency of thin-walled C-F I-beams

Reference	Frequency	Lay-up			
		$[0]$	$\begin{bmatrix}30/\\-30\end{bmatrix}$	$\begin{bmatrix}60/\\-60\end{bmatrix}$	$\begin{bmatrix}90/\\-90\end{bmatrix}$
Present (Shear)	ω_1	2.547	1.339	0.580	0.523
	ω_2	3.174	2.423	1.572	1.400
	ω_3	7.123	4.746	3.597	3.272
	ω_4	15.492	8.357	3.627	3.540
	ω_5	17.559	10.755	5.780	5.162
Present (No shear)	ω_1	2.560	1.340	0.580	0.523
	ω_2	3.197	2.426	1.574	1.401
	ω_3	7.430	4.835	3.635	3.280
	ω_4	16.043	8.396	3.637	3.578
	ω_5	18.333	10.811	5.796	5.177

Table 6.10. Non-dimensional natural frequency of thin-walled C-C I-beams

Reference	Frequency	Lay-up			
		$[0]$	$\begin{bmatrix}30/\\-30\end{bmatrix}$	$\begin{bmatrix}60/\\-60\end{bmatrix}$	$\begin{bmatrix}90/\\-90\end{bmatrix}$
Present (Shear)	ω_1	15.480	8.474	3.682	3.322
	ω_2	17.239	10.104	4.839	4.332
	ω_3	34.221	23.221	10.121	9.131
	ω_4	40.918	25.221	12.265	11.004
	ω_5	44.983	27.483	19.739	17.804
Present (No shear)	ω_1	16.289	8.525	3.691	3.330
	ω_2	18.362	10.172	4.854	4.346
	ω_3	44.902	23.499	10.175	9.180
	ω_4	47.279	26.604	12.342	11.079
	ω_5	50.406	31.022	19.946	17.996
Vo and Lee [177] (Shear)	ω_1	15.460	8.471	3.678	3.319
	ω_2	17.211	10.092	4.836	4.330
	ω_3	33.996	23.209	10.147	9.152
	ω_4	40.271	25.126	12.286	11.022
	ω_5	44.134	27.457	19.855	17.905
Vo and Lee [177] (No shear)	ω_1	16.289	8.525	3.691	3.330
	ω_2	18.362	10.172	4.854	4.346
	ω_3	44.903	23.499	10.175	9.180
	ω_4	47.279	26.604	12.342	11.079
	ω_5	50.406	31.022	19.946	17.996

Table 6.11. Non-dimensional critical buckling load of thin-walled composite I-beams

BC	Reference	Lay-up			
		$[0]$	$\begin{bmatrix}30/\\-30\end{bmatrix}$	$\begin{bmatrix}60/\\-60\end{bmatrix}$	$\begin{bmatrix}90/\\-90\end{bmatrix}$
S-S	Present (Shear)	11.947	3.336	0.626	0.510
	Present (No shear)	12.208	3.344	0.627	0.510
C-F	Present (Shear)	3.035	0.835	0.157	0.128
	Present (No shear)	3.052	0.836	0.157	0.128
C-C	Present (Shear)	44.914	13.249	2.498	2.034
	Present (No shear)	48.830	13.374	2.507	2.041

The shear effects of I-beams with $[15/-15]$ angle-ply in flanges for various BCs are conducted. Figs. 6.5 and 6.6 show the shear effects of fundamental frequencies and critical buckling load with respect to length-to-height's ratio, respectively. It can be seen that the shear effects are biggest for beams with C-C BC, and are significant for beams with small length-to-height's ratio.

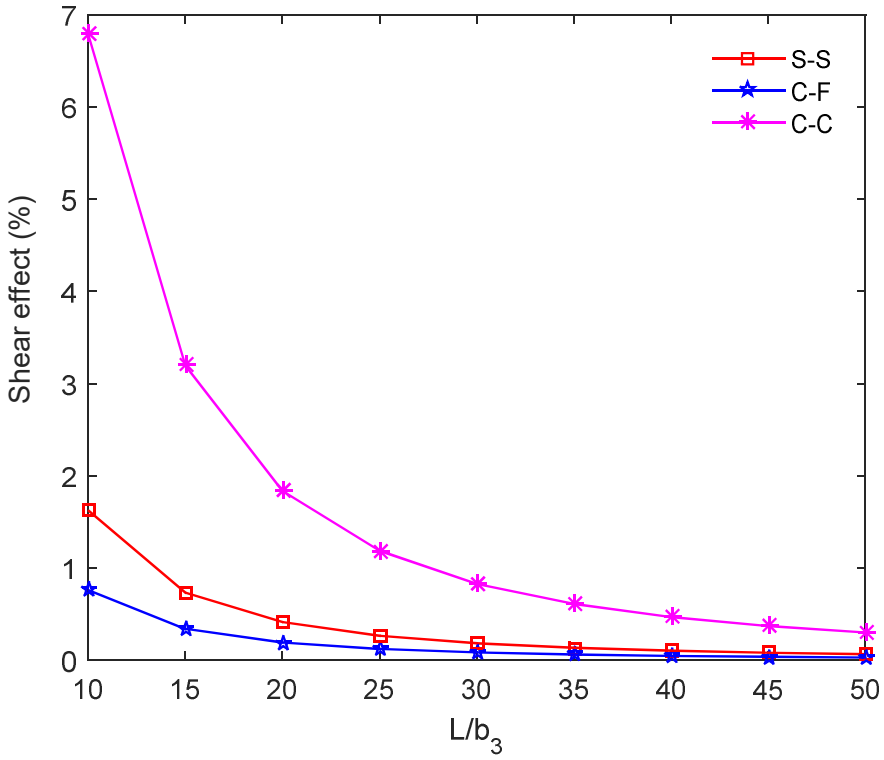

Figure 6.5. Shear effect on the fundamental frequency for various BCs

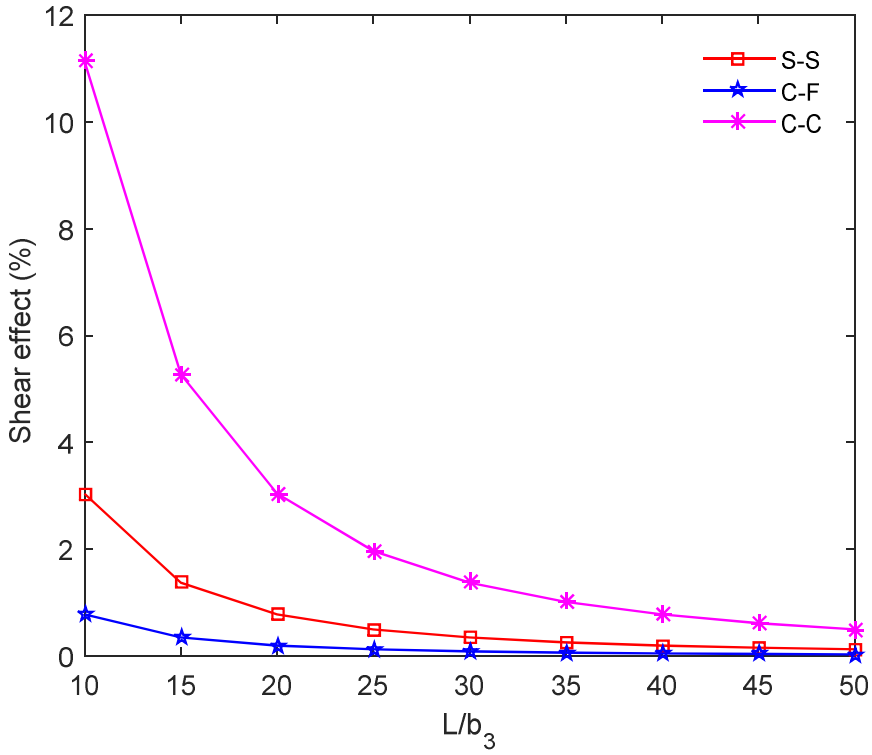

Figure 6.6. Shear effect on the critical buckling loads for various BCs

In order to clearly investigate the shear effects and fibre angle to the natural frequencies, the above composite I-beams with different geometry and material properties (MAT I, $b_1 = b_2 = b_3 = 30$ cm , $h_1 = h_2 = h_3 = 2$ cm and $L = 10b_3$) are considered. Fig. 6.7 displays the shear effects on first three frequencies of beams for C-C BC. It is clear to see that the shear effects are significant for high modes. It is also interesting to see that the shear effects on third mode (mode V) are smallest at fiber angle 55^0. This phenomenon can be explained in Fig. 6.8 which shows the ratio of flexural rigidity (E_{33}) to shear rigidity (E_{77}) with respect to η. It is observed that the ratio of E_{33} / E_{77} is the smallest at this angle (55^0).

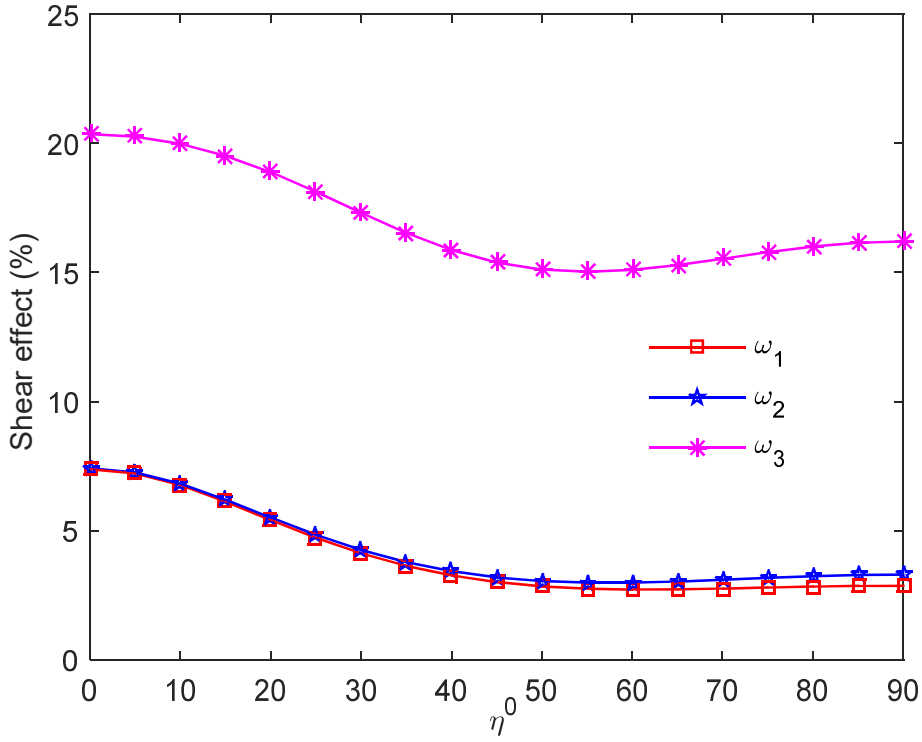

Figure 6.7. Shear effect on first three natural frequencies of thin-walled C-C I-beams

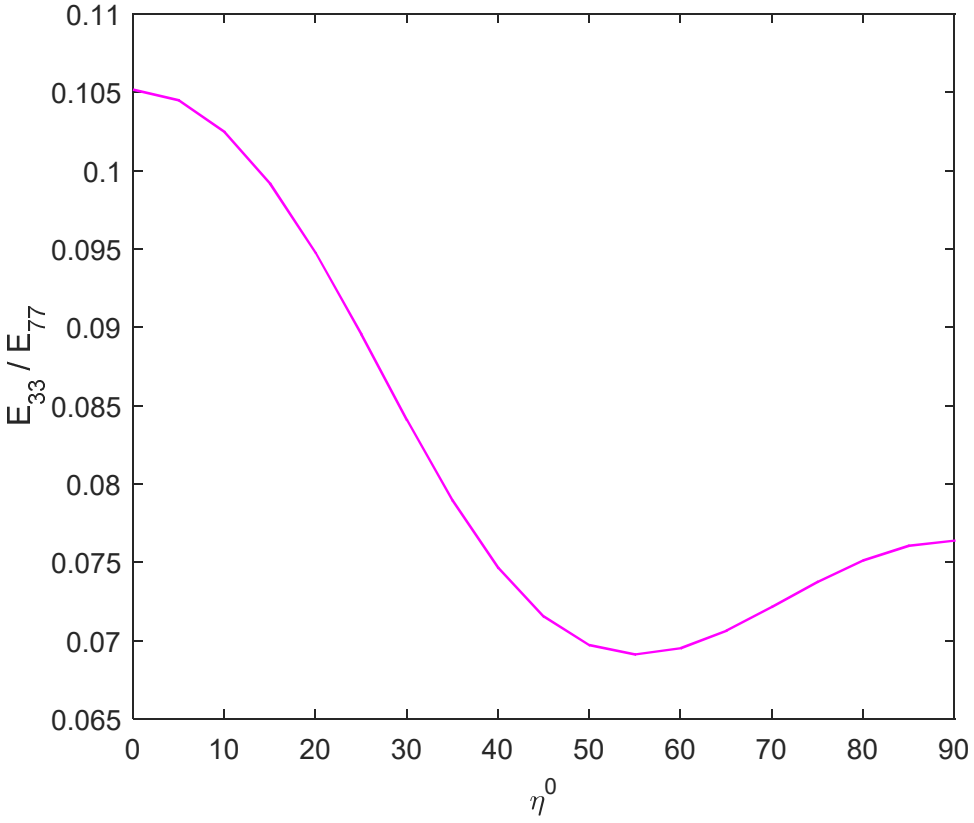

Figure 6.8. Variation of E_{33} / E_{77} ratio with respect to η

Figs. 6.9-6.11 also show first three mode shapes of C-C I-beams with $[45/-45]$ angle-ply in flanges with shear and without shear effect. It can be seen that the vibration modes 1, 2 and 3 are first flexural mode in $x-$direction (mode U), torsional mode (mode ϕ) and flexural mode in $y-$direction (mode V), respectively.

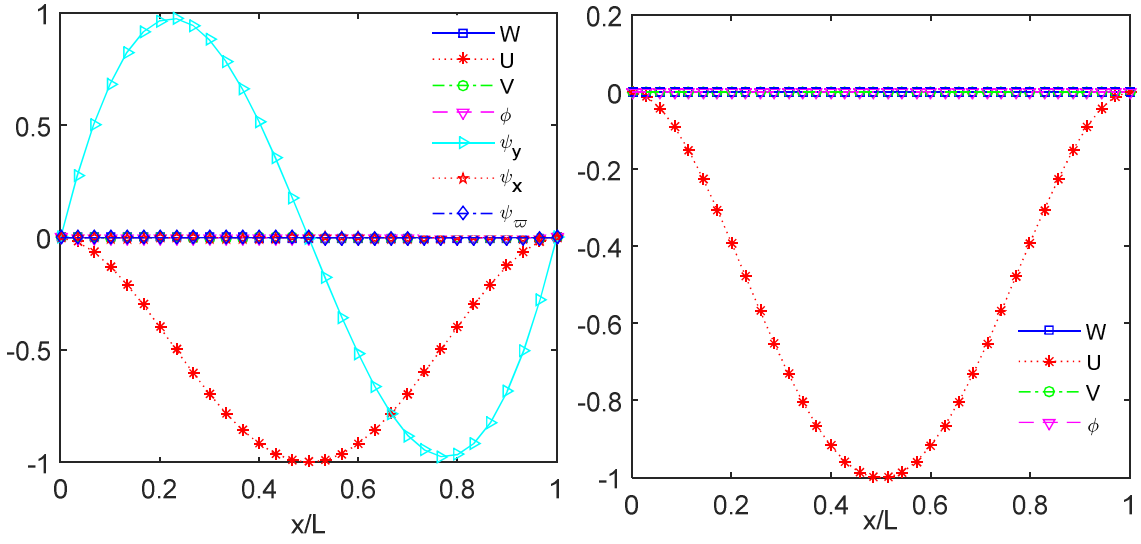

a. $\bar{\omega}_1 = 6.049$ (Shear) b. $\bar{\omega}_1 = 6.239$ (No shear)

Figure 6.9. Mode shape 1 of thin-walled C-C I-beams

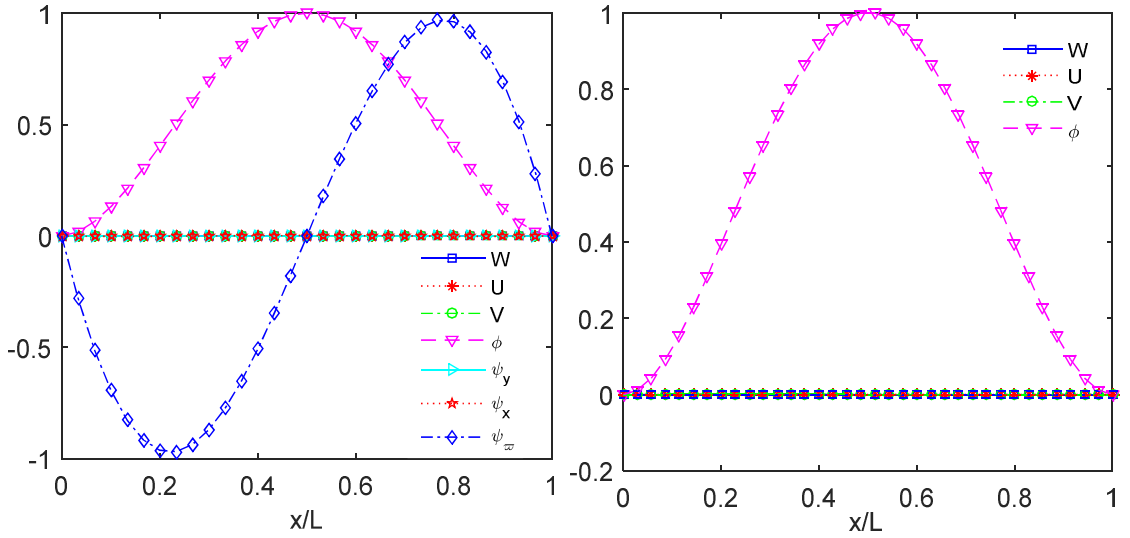

a. $\bar{\omega}_2 = 6.383$ (Shear) b. $\bar{\omega}_2 = 6.596$ (No shear)

Figure 6.10. Mode shape 2 of thin-walled C-C I-beams

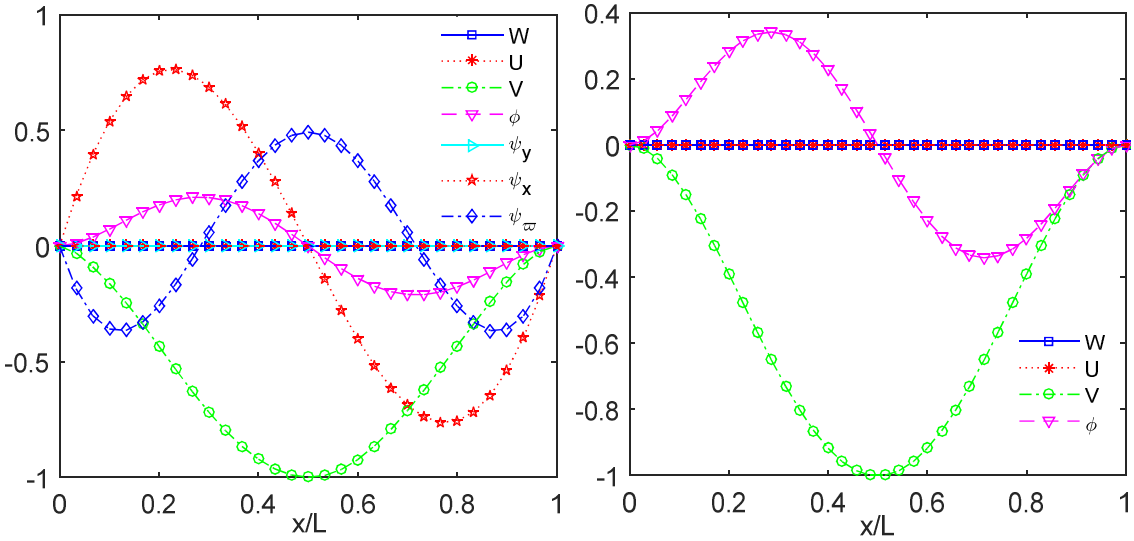

a. $\bar{\omega}_3 = 10.607$ (Shear) b. $\bar{\omega}_3 = 12.555$ (No shear)

Figure 6.11. Mode shape 3 of thin-walled C-C I-beams

6.3.2.3. Anisotropic effect

The third example investigates the effect of modulus ratio E_1 / E_2 on natural frequencies and critical buckling loads of composite I- beams (MAT II.6, $b_1 = b_2 = 20$ cm , $b_3 = 30$ cm , $h_1 = h_2 = h_3 = 1$ cm and $L = 20b_3$) with various BCs. The flanges are symmetric cross-ply $[0/90]_s$ lay-up and the web is unidirectional one. The variation of fundamental frequencies and critical buckling loads in case of including shear effects with respect to the ratio of E_1 / E_2 is displayed in Figs. 6.12 and 6.13. It is observed that the results increase as E_1 / E_2 increases for all BCs, and the beams with C-C BC have the biggest variation.

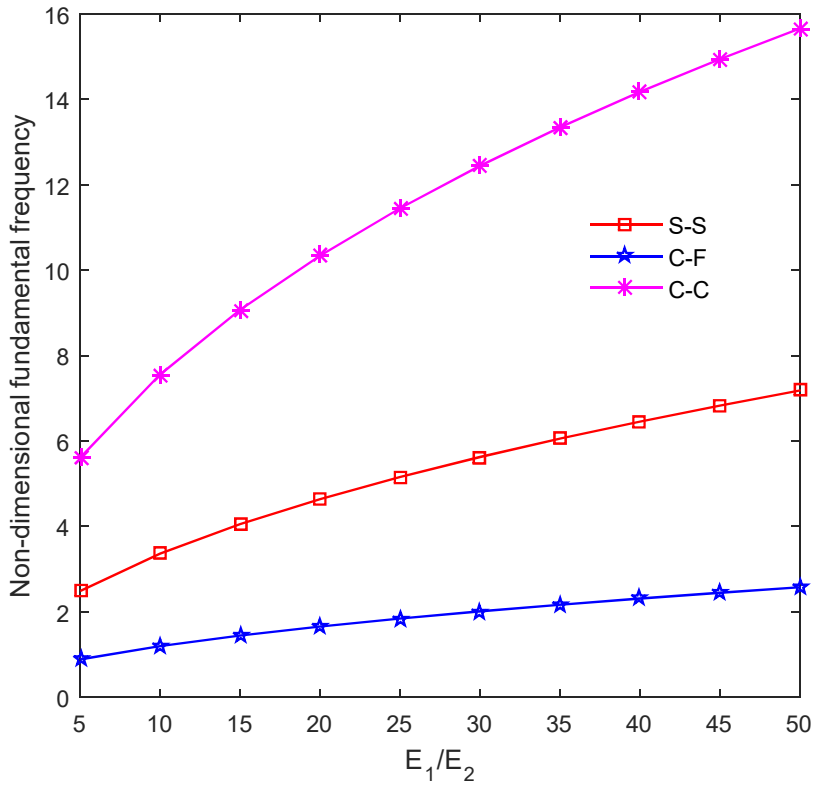

Figure 6.12. Non-dimensional fundamental frequency for various BCs

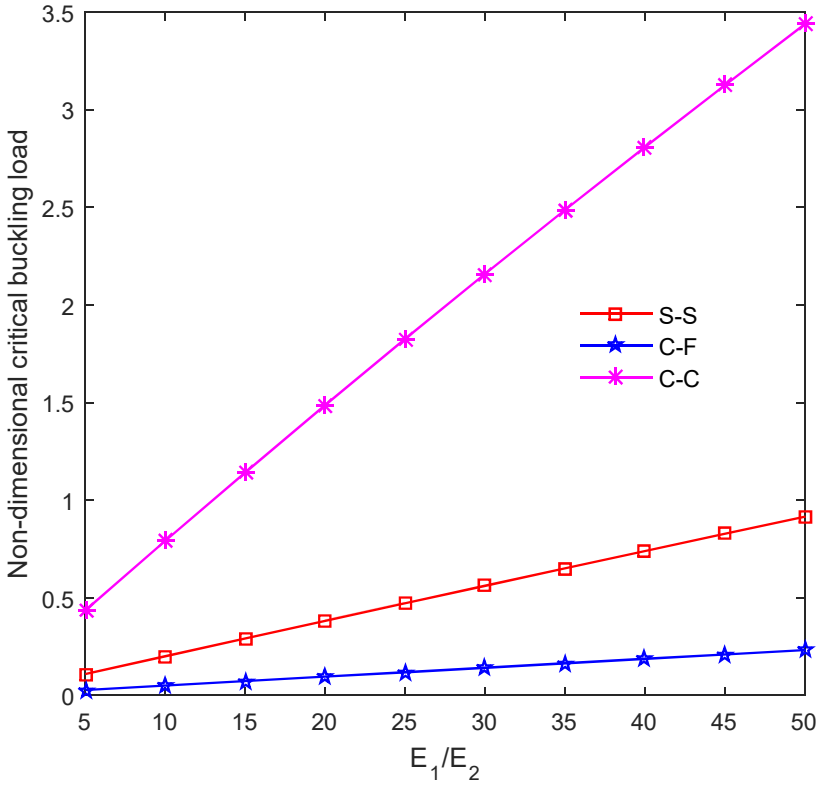

Figure 6.13. Non-dimensional critical buckling load for various BCs

6.3.3. Functionally graded sandwich I-beams.

6.3.3.1. Verification

This example assesses the accuracy and efficiency of the present solution for thin-walled FG sandwich I-beams. Non-dimensional fundamental frequencies of S-S beams (MAT III.6, $b_1 = 20h$, $b_2 = 10h$, $b_3 = 40h$, $h_1 = h_2 = h_3 = h$, $\alpha_1 = 0.1$, $\alpha_2 = 0.9$ and $L = 40b_3$) with $p = 1$ and $p = 5$ are displayed in Fig 14. The critical buckling load of I-beams (MAT IV.6, $b_1 = b_2 = 10$ cm , $b_3 = 20$ cm , $h_1 = h_2 = h_3 = 0.5$ cm , $\alpha_1 = \alpha_2 = 0.7$, $\beta = 0.4$ and $L = 12.5b_3$) with different BCs is printed in Table 6.12. It can be found that the present solutions are in good agreements with previous results of Nguyen et al. [192], Lanc et al. [193] and Kim and Lee [194]. Results in Table 6.12 also indicated that the critical buckling loads decrease as material parameter p increases.

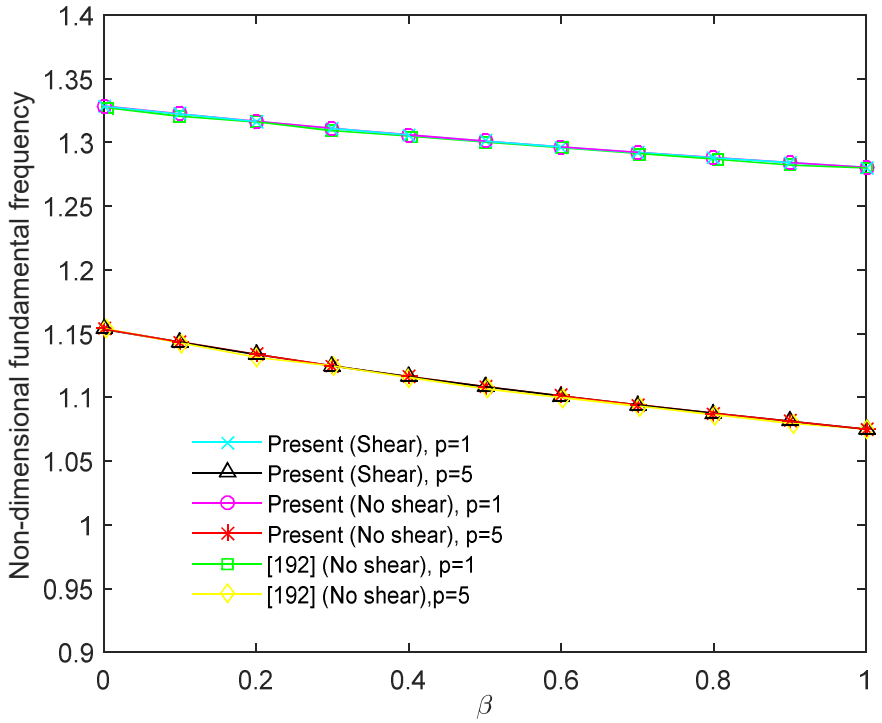

Figure 6.14. Non-dimensional fundamental frequency of thin-walled FG sandwich I-beams.

Table 6.12. The critical buckling load (N) of FG sandwich I-beams

BC	p	Reference				
		Present		Kim and Lee [194]		Lanc et al. [193]
		Shear	No shear	Shear	No shear	No shear
S-S	0	421633	423079	422359	423083	423296
	0.25	404154	405602	405208	405933	406130
	0.5	392508	393960	393783	394515	394692
	1	377958	379420	379533	380286	380412
	2	363420	364899	365280	366056	366150
	5	348899	350404	351058	351825	351914
	10	342305	343826	344601	345333	345451
	20	338539	340070	340906	341605	341762
C-F	0	105679	105770	105725	105771	105773
	0.25	101310	101401	101435	101483	101484
	0.5	98399	98490	98577	98629	98626
	1	94763	94855	95013	95072	95057
	2	91132	91225	91448	91514	91494
	5	87507	87601	87891	87957	87936
	10	85861	85957	86277	86334	86321
	20	84922	85018	85353	85403	85400
C-C	0	1669413	1692317	1680840	1692352	1705050
	0.25	1599491	1622408	1612410	1623751	1635900
	0.5	1552860	1575838	1566830	1578078	1589830
	1	1494551	1517678	1509950	1521156	1532310
	2	1436213	1459595	1453060	1464229	1474860
	5	1377838	1401613	1396270	1407293	1417520
	10	1351288	1375299	1370490	1381317	1391480
	20	1336111	1360275	1355730	1366399	1376630

6.3.3.2. Parameter study

In order to investigate the effects of thickness ratio of ceramic material on free vibration and buckling behaviours, the FG sandwich I-beams (MAT III.6, $b_1 = b_2 = 30h$, $b_3 = 40h$, $h_1 = h_2 = h_3 = h$ and $L = 10b_3$) are considered. Figs. 6.15 and 6.16 show the effect of ceramic thickness ratio in flanges on the non-dimensional fundamental frequencies and critical buckling loads of beams with $\beta = 0.3$ and $p = 10$ for the different BCs. It can be seen that frequencies and critical buckling load significantly increase as ceramic thickness ratio increases.

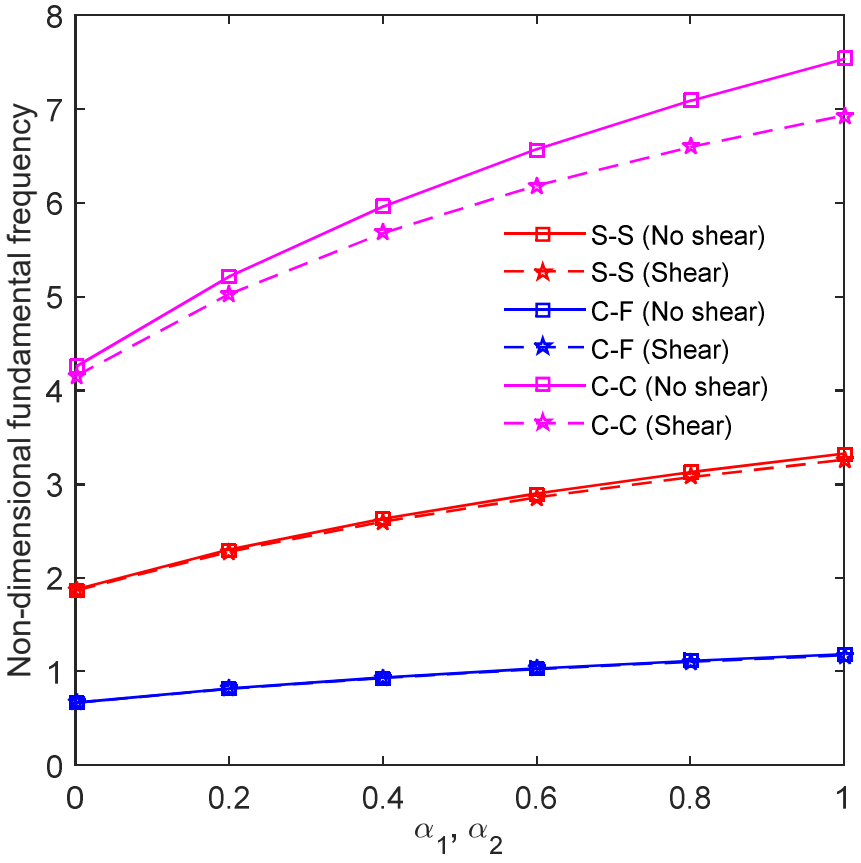

Figure 6.15. Non-dimensional fundamental frequency with respect to α_1, α_2 ($\alpha_1 = \alpha_2$, $\beta = 0.3$ and $p = 10$)

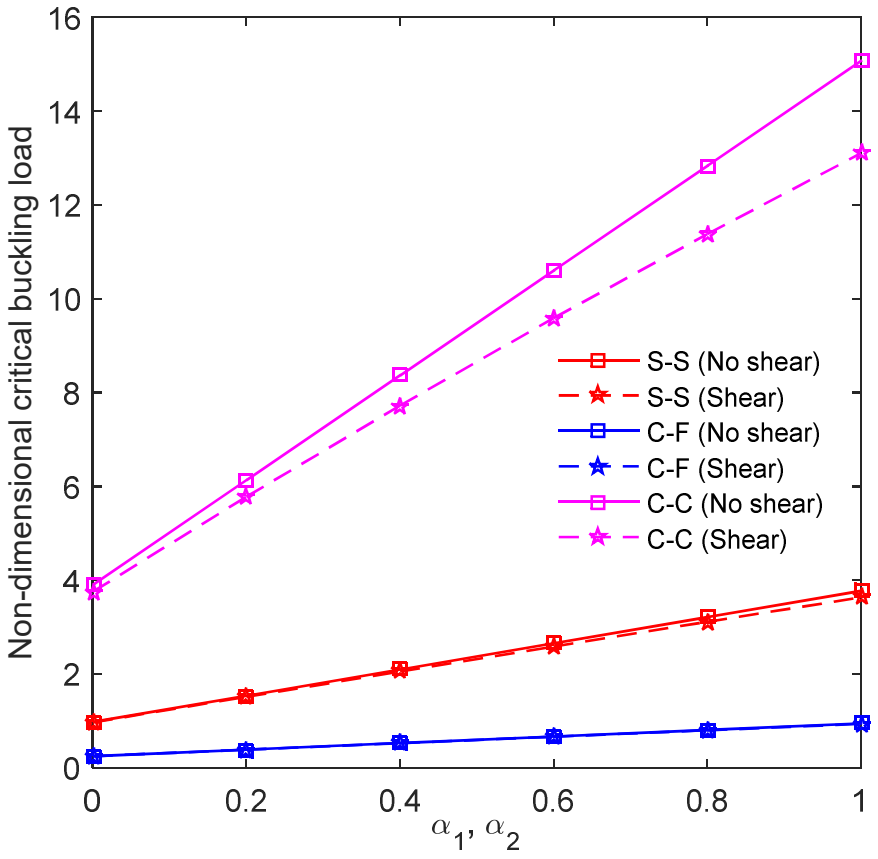

Figure 6.16. Non-dimensional critical buckling load with respect to α_1, α_2 ($\beta = 0.3$ and $p = 10$)

Figs. 6.17 and 6.18 show the non-dimensional fundamental frequencies and critical buckling loads of beams ($\alpha_1 = \alpha_2 = 0.1$ and $p = 10$) with respect to the ceramic thickness ratio in web for different BCs. It is observed that increasing of ceramic thickness ratio in web causes slightly decrease fundamental frequencies, and slightly increase critical loads.

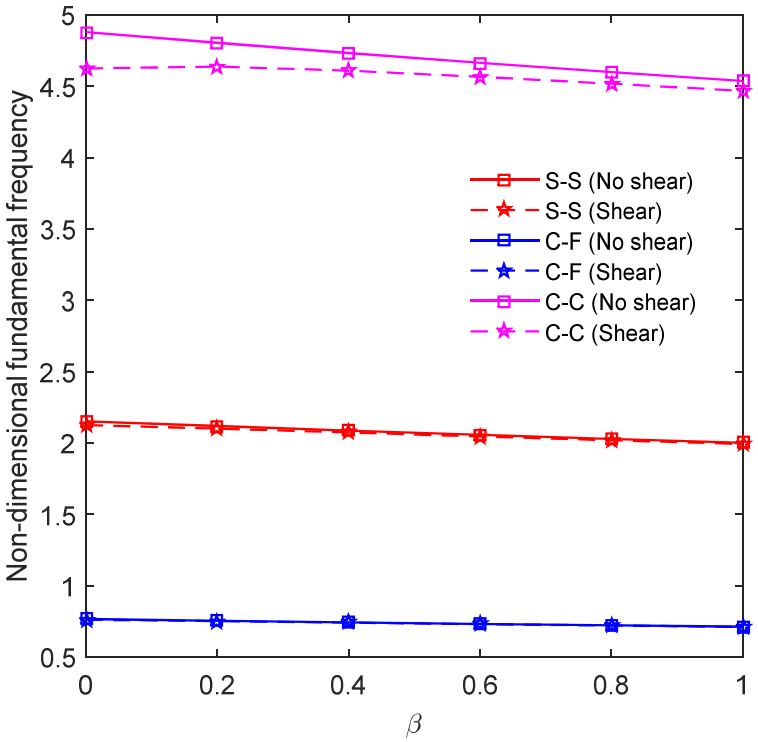

Figure 6.17. Non-dimensional fundamental frequency with respect to β ($\alpha_1 = \alpha_2 = 0.1$, and $p = 10$)

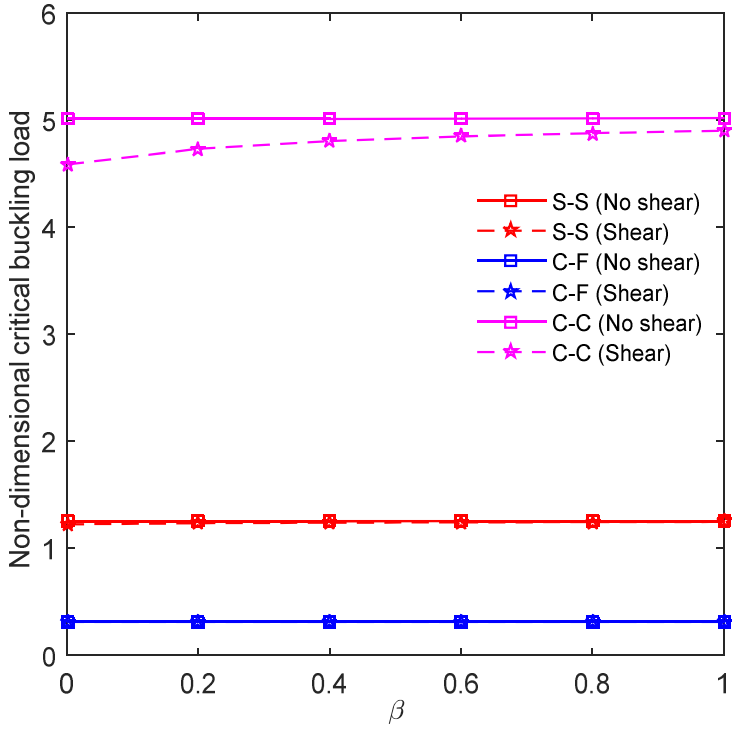

Figure 6.18. Non-dimensional critical buckling load with respect to β ($\alpha_1 = \alpha_2 = 0.1$, and $p = 10$)

6.3.3.3. Shear deformation effect

The FG sandwich I-beams (MAT III.6, $b_1 = b_2 = b_3 = 20h$, $h_1 = h_2 = h_3 = h$, $\alpha_1 = \alpha_2 = \beta = 0.1$) are considered to investigate the effects of shear deformation. Figs. 6.19 and 6.20 show shear effect on fundamental frequencies and critical buckling loads of beams with $p = 1$ and with respect to the length-to-height ratio. From these figures, it can be seen that the shear effects decrease as the length-to-height ratio increases as expected. Effects of the material parameter on the shear effects of the C-C I-beams with $L = 10b_3$ are indicated in Fig. 6.21. It can be seen that the shear effect is significant with high modes, and is not effected by the material parameter for first three vibration modes.

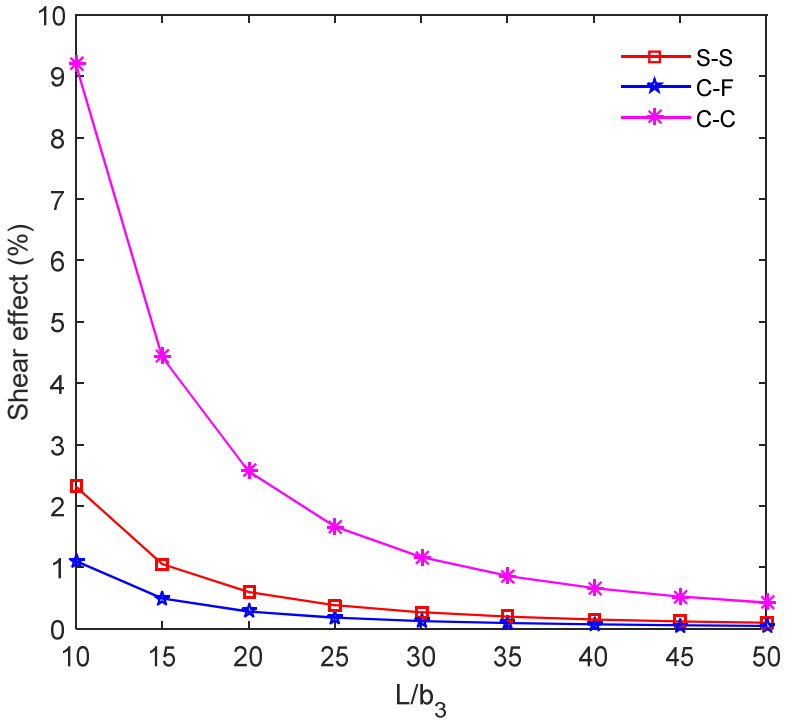

Figure 6.19. Shear effect on fundamental frequency for various BCs

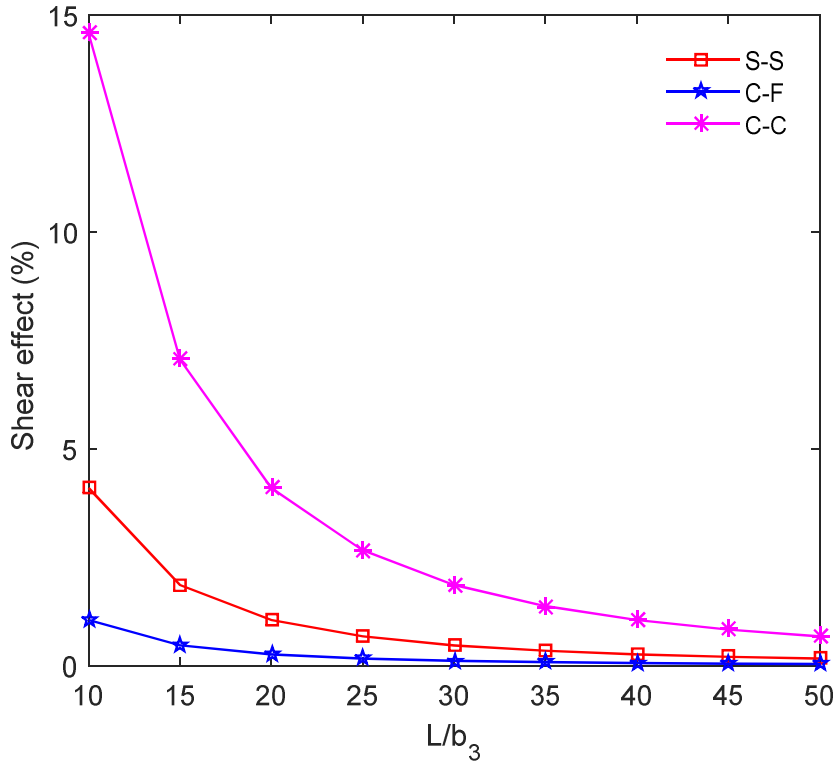

Figure 6.20. Shear effect on critical buckling load for various BCs

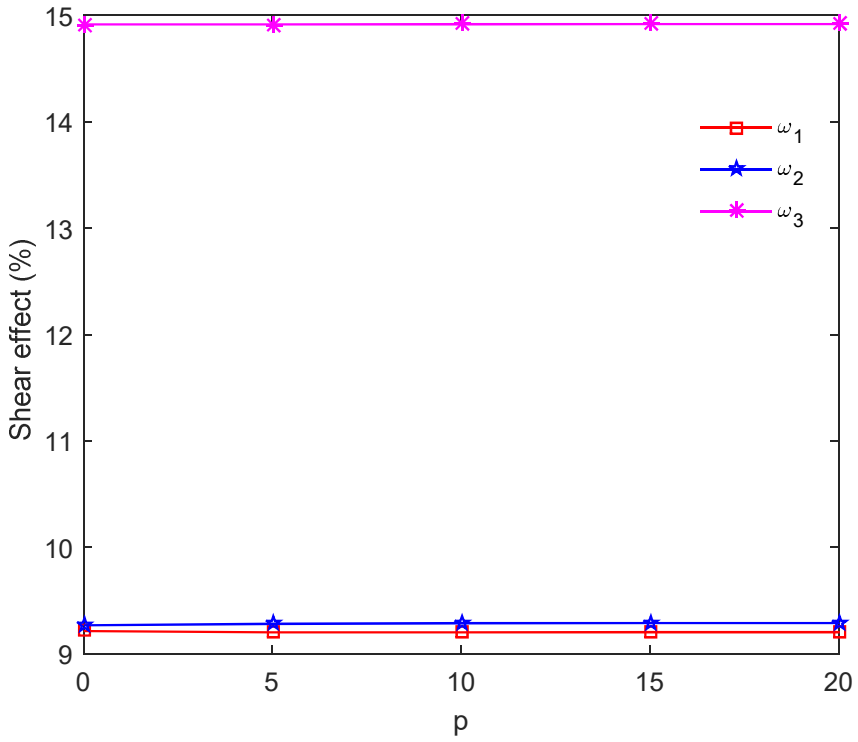

Figure 6.21. Shear effect on first three frequency of C-C I-beams with respect to material parameter

6.3.4. Composite channel-beams

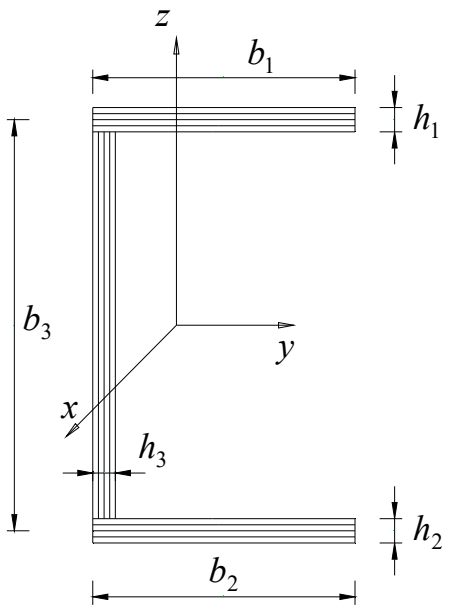

Figure 6.22. Geometry of thin-walled composite channel beams

The following section aims to present the results of composite channel beams. Firstly, the symmetric angle-ply channel beams (MAT IV.6) with the various BCs are considered. The flanges and web are 0.0762 cm thickness, and made of asymmetric laminates that consist of 6 layers ($[\eta/-\eta]_3$). The first five natural frequencies of channel beams ($b_1 = b_2 = 0.6$ cm, $b_3 = 2.0$ cm and $L = 100b_3$) in case of no shear are showed in Table 6.13. It can be seen that the present results are coincided with existing ones. Secondly, the buckling load and deflection at mid-span of composite channel beams (MAT.6 V $b_1 = b_2 = b_3 = 10$cm, $h_1 = h_2 = h_3 = 1.0$ cm and $L = 20b_3$) are showed in Table 6.14 and compared with Cortinez and Piovan [204]. Good agreement are also found. Finally, the effects of shear deformation are investigated by considering composite channel beams (MAT III.6, $b_1 = b_2 = b_3 = 10$cm, $h_1 = h_2 = h_3 = 1.0$ cm). Figs. 6.23 and 6.24 show shear effect on fundamental frequencies and critical buckling loads of beams with respect to the length-to-height ratio. From these figures, it can be seen that the shear effects are the biggest for beams with C-C BC, and are significant for beams with small length-to-height's ratio as expected.

Table 6.13. First five frequencies (Hz) of thin-walled channel beams

Reference	Frequency	Lay-up						
		$[0]$	$\begin{bmatrix}15/\\-15\end{bmatrix}$	$\begin{bmatrix}30/\\-30\end{bmatrix}$	$\begin{bmatrix}45/\\-45\end{bmatrix}$	$\begin{bmatrix}60/\\-60\end{bmatrix}$	$\begin{bmatrix}75/\\-75\end{bmatrix}$	$\begin{bmatrix}90/\\-90\end{bmatrix}$
a. S-S BC								
Present	ω_1	7.031	6.327	4.291	2.723	2.087	1.889	1.846
	ω_2	24.460	25.013	17.098	10.872	8.345	7.774	7.384
	ω_3	28.125	25.678	17.911	11.436	8.777	7.940	7.758
	ω_4	36.119	43.319	38.512	24.471	18.779	16.997	16.614
	ω_5	59.497	56.746	47.443	40.503	33.370	30.220	29.099
b. C-F BC								
Present	ω_1	2.505	2.250	1.525	0.969	0.743	0.673	0.658
	ω_2	10.061	9.488	6.462	4.101	3.142	2.840	2.773
	ω_3	15.698	14.093	9.555	6.070	4.658	4.216	4.121
	ω_4	16.616	21.506	23.900	16.997	13.043	11.806	11.539
	ω_5	43.954	39.451	26.753	20.358	16.982	15.118	14.536
c. C-C BC								
Present	ω_1	15.939	14.324	9.707	6.165	4.730	4.281	4.184
	ω_2	32.704	39.350	26.752	16.993	13.038	11.801	11.535
	ω_3	43.937	41.325	37.226	25.020	19.365	17.494	17.066
	ω_4	71.670	68.160	52.443	33.313	25.560	23.135	22.613
	ω_5	73.718	77.287	55.748	44.633	36.871	32.659	31.342
Sheikh et al. [189]	ω_1	15.931	14.345	9.781	6.174	4.708	4.281	4.121
	ω_2	32.692	39.532	26.959	17.018	12.977	11.802	11.359
	ω_3	43.890	40.662	37.271	25.031	19.262	17.485	16.798
	ω_4	71.641	68.182	52.854	33.367	25.444	23.140	22.272
	ω_5	73.098	77.480	55.454	44.278	36.631	32.689	30.903

Table 6.14. Buckling load (N) and deflection (mm) at mid-span under uniformly load of 1 kN of thin-walled channel beams

BC	Reference	Lay-up	
		$(0^0/0^0/0^0/0^0)$	$(0^0/90^0/90^0/0^0)$
a. Buckling load (10^5N)			
S-S	Present	2.617	1.595
	Cortinez and Piovan [204]	2.674	1.635
C-F	Present	0.929	0.656
	Cortinez and Piovan [204]	0.947	0.670
C-C	Present	9.310	5.240
	Cortinez and Piovan [204]	9.503	5.371
b. Deflection (mm)			
S-S	Present	0.247	0.463
C-F		0.841	1.573
C-C		0.049	0.093

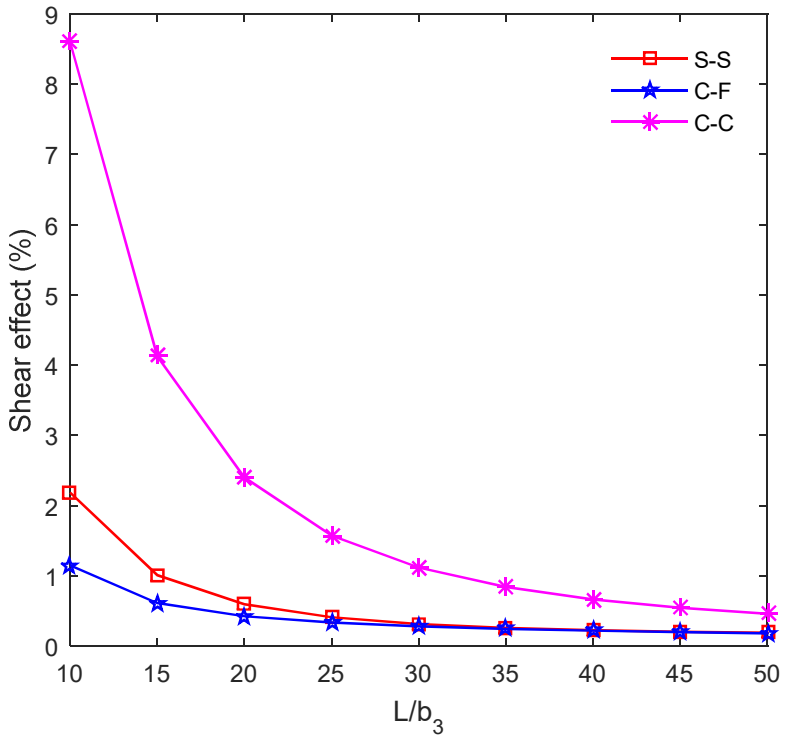

Figure 6.23. Shear effect on fundamental frequency for various BCs

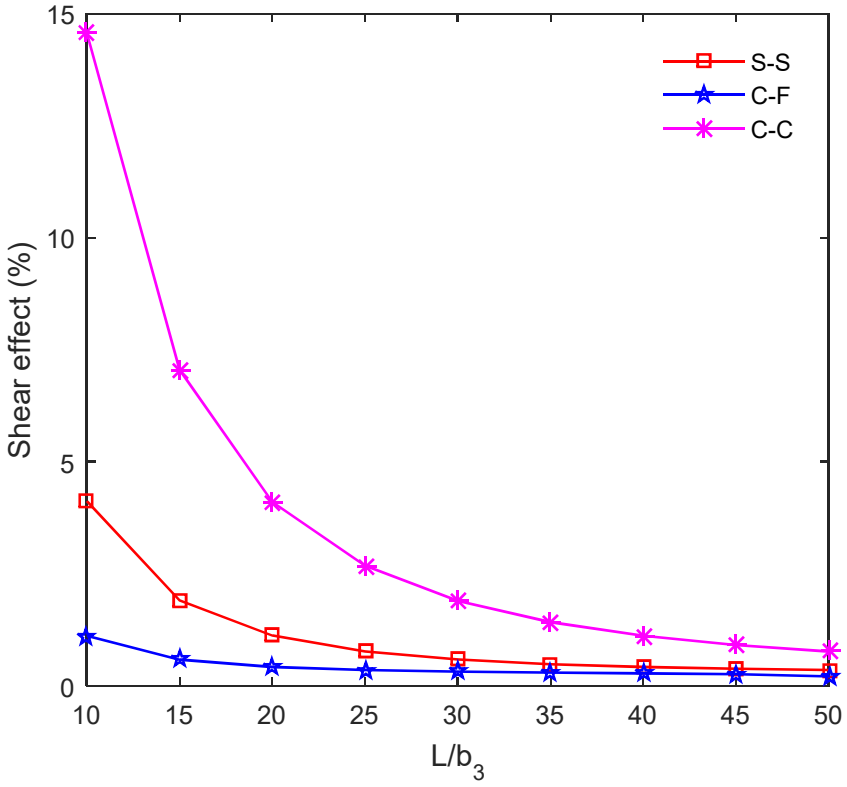

Figure 6.24. Shear effect on critical buckling load for various BCs

6.4. Conclusions

Ritz method is developed to analyse buckling, vibration and bending of thin-walled composite and FG sandwich thin-walled beams in this Chapter. The theory is based on the FOBT. The governing equations of motion are derived from Lagrange's equations. The natural frequencies, critical buckling loads and deflection of thin-walled composite and FG sandwich beams with various BCs are obtained and compared with those of the previous works. The results indicate that:

- The shear effects become significant for higher degrees and lower length-to-height ratio of thin-wall beams.
- The shear effects are the biggest for thin-walled beams with clamped-clamped boundary conditions.
- The effects of fiber orientation are significant for bending, buckling and free vibration behaviours of thin-walled beams.

- The proposed functions are found to be appropriate and efficient in analysing buckling, free vibration and bending problems of thin-walled beams with various cross-sections

Chapter 7. CONVERGENCY, ACCURARY AND NUMERICAL STABILITY OF RITZ METHOD

7.1. Introduction

In Chapter Two to Six, the author proposed Ritz functions to analyse behaviours of laminated composite beams with various cross-sections. It can be seen that the proposed methods are very simple and effective. It is also stated that convergency, accuracy and numerical stability of Ritz method depends on approximation functions. Therefore, it is very essential to study their characteristics. In this Chapter, four approximation functions which used in previous Chapters (Table 7.1 and 7.2) for S-S and C-C boundary condition are considered. For comparison purposes, orthogonal polynomials (OP) function, which is well-known and used in a large number of work, is considered. Numerical results are presented for laminated composite beams ($0^0/90^0/0^0$) with rectangular section based on HOBT as indicated in Eqs. (2.1 and 2.2). The computations are carried out in an Intel® Core™ i7 with 4 cores at 3.4 GHz, 8 GB of RAM, and calculations in MATLAB R2015a. The governing equations of motion are given below:

$$\left(\begin{bmatrix} \mathbf{K}^{11} & \mathbf{K}^{12} & \mathbf{K}^{13} \\ {}^{T}\mathbf{K}^{12} & \mathbf{K}^{22} & \mathbf{K}^{23} \\ {}^{T}\mathbf{K}^{13} & {}^{T}\mathbf{K}^{23} & \mathbf{K}^{33} \end{bmatrix} - \omega^2 \begin{bmatrix} \mathbf{M}^{11} & \mathbf{M}^{12} & \mathbf{M}^{13} \\ {}^{T}\mathbf{K}^{12} & \mathbf{M}^{22} & \mathbf{M}^{23} \\ {}^{T}\mathbf{K}^{13} & {}^{T}\mathbf{M}^{23} & \mathbf{M}^{33} \end{bmatrix}\right) \begin{Bmatrix} \mathbf{u_0} \\ \mathbf{w_0} \\ \mathbf{u_1} \end{Bmatrix} = \begin{Bmatrix} \mathbf{0} \\ \mathbf{F} \\ \mathbf{0} \end{Bmatrix} \tag{7.1}$$

where the components of stiffness matrix **K**, mass matrix **M** and **F** are given by:

$$K_{ij}^{11} = A\int_0^L \psi_{i,x}\psi_{j,x}dx,\ K_{ij}^{12} = -B\int_0^L \psi_{i,x}\varphi_{j,xx}dx,\ K_{ij}^{13} = B^s\int_0^L \psi_{i,x}\xi_{j,x}dx$$

$$K_{ij}^{22} = D\int_0^L \varphi_{i,xx}\varphi_{j,xx}dx - N_0\int_0^L \varphi_{i,x}\varphi_{j,x}dx,\ K_{ij}^{23} = -D^s\int_0^L \varphi_{i,xx}\xi_{j,x}dx,$$

$$K_{ij}^{33} = -H^s\int_0^L \xi_{i,x}\xi_{j,x}dx + A^s\int_0^L \xi_i\xi_j dx,\ M_{ij}^{11} = I_0\int_0^L \psi_i\psi_j dx,\ M_{ij}^{12} = -I_1\int_0^L \psi_i\varphi_{j,x}dx$$

$$M_{ij}^{13} = -J_1\int_0^L \psi_i\xi_j dx, M_{ij}^{22} = I_0\int_0^L \varphi_i\varphi_j dx + I_2\int_0^L \varphi_{i,x}\varphi_{j,x}dx,\ M_{ij}^{23} = -J_2\int_0^L \varphi_{i,x}\xi_j dx,$$

$$M_{ij}^{33} = K_2 \int_0^L \xi_i \xi_j dx\,, \quad F_i = \int_0^L q\varphi_i dx \tag{7.2}$$

It is stated that for H1, H2 and EX functions, owing to $\psi_i = \xi_i = \varphi_{i,x}$, the number of integral calculated will be reduced from thirteen to three. Therefore, the components of stiffness matrix **K**, mass matrix **M** can be writen:

$$K_{ij}^{11} = A\int_0^L IT_1 dx\,,\ K_{ij}^{12} = -B\int_0^L IT_1 dx\,,\ K_{ij}^{13} = B^s \int_0^L IT_1 dx$$

$$K_{ij}^{22} = D\int_0^L IT_1 dx - N_0 \int_0^L IT_2 dx\,,\ K_{ij}^{23} = -D^s \int_0^L IT_1 dx\,,$$

$$K_{ij}^{33} = -H^s \int_0^L IT_1 dx + A^s \int_0^L IT_2 dx\,,\ M_{ij}^{11} = I_0 \int_0^L IT_2 dx\,,\ M_{ij}^{12} = -I_1 \int_0^L IT_2 dx$$

$$M_{ij}^{13} = -J_1 \int_0^L IT_2 dx\,, M_{ij}^{22} = I_0 \int_0^L IT_3 dx + I_2 \int_0^L IT_2 dx\,,\ M_{ij}^{23} = -J_2 \int_0^L IT_2 dx\,,$$

$$M_{ij}^{33} = K_2 \int_0^L IT_2 dx \tag{7.3}$$

where $IT_1 = \varphi_{i,xx}\varphi_{j,xx}$, $IT_2 = \varphi_{i,x}\varphi_{j,x}$, $IT_3 = \varphi_i\varphi_j$.

The orthotropic material and normalized terms are used as followings:

$$E_1 / E_2 = 25\,,\ G_{12} = G_{13} = 0.5E_2\,,\ G_{23} = 0.2E_2\,,\ \upsilon_{12} = 0.25 \tag{7.4}$$

$$\overline{w} = \frac{100 w_0 E_2 b h^3}{qL^4} \tag{7.5}$$

$$\overline{\omega} = \frac{\omega L^2}{h}\sqrt{\frac{\rho}{E_2}} \tag{7.6}$$

$$\overline{N}_{cr} = N_{cr}\frac{L^2}{E_2 b h^3} \tag{7.7}$$

Table 7.1. Approximation functions for S-S boundary condition

Function	$\varphi_j(x)$	$\psi_j(x)$	$\xi_j(x)$	Name
Orthogonal polynomials [100]	$\left(\frac{x}{L}\right)^j\left(\frac{x}{L}-1\right)$	$\left(\frac{x}{L}\right)^{j-1}\left(\frac{x}{L}-1\right)$	$\left(\frac{x}{L}\right)^{j-1}\left(\frac{x}{L}-1\right)$	OP-S
Trigonometric (Chapter Two) [130]	$\sin\left(\frac{j\pi x}{L}\right)$	$\cos\left(\frac{j\pi x}{L}\right)$	$\cos\left(\frac{j\pi x}{L}\right)$	TR-S
Hybric function (Chapter Four) [196]	$x(L-x)e^{\frac{x}{jL}}$	$\varphi_{j,x}(x)$	$\varphi_{j,x}(x)$	H1-S
Exponential function (Chapter Five) [197]	$\left(1-e^{\frac{-jx}{L}}\right)\left(1-e^{-j\left(1-\frac{x}{L}\right)}\right)$	$\varphi_{j,x}(x)$	$\varphi_{j,x}(x)$	EX-S
Hybric function (Chpater Six) [205]	$\frac{x}{L}\left(1-\frac{x}{L}\right)e^{\frac{-jx}{L}}$	$\varphi_{j,x}(x)$	$\varphi_{j,x}(x)$	H2-S

Table 7.2. Approximation functions for C-C boundary condition

Function	$\varphi_j(x)$	$\psi_j(x)$	$\xi_j(x)$	Name
Orthogonal polynomials [100]	$\left(\frac{x}{L}\right)^2\left(\frac{x}{L}-1\right)^2\left(\frac{x}{L}\right)^{j-1}$	$\left(\frac{x}{L}\right)\left(\frac{x}{L}-1\right)^2\left(\frac{x}{L}\right)^{j-1}$	$\left(\frac{x}{L}\right)\left(\frac{x}{L}-1\right)^2\left(\frac{x}{L}\right)^{j-1}$	OP-C
Trigonometric (Chapter Two) [130]	$\sin^2\left(\frac{j\pi x}{L}\right)$	$\sin\left(\frac{2j\pi x}{L}\right)$	$\sin\left(\frac{2j\pi x}{L}\right)$	TR-C
Hybric function (Chapter Four) [196]	$x^2(L-x)^2 e^{\frac{x}{jL}}$	$\varphi_{j,x}(x)$	$\varphi_{j,x}(x)$	H1-C
Exponential function (Chapter Five) [197]	$\left(1-e^{\frac{-jx}{L}}\right)^2\left(1-e^{-j\left(1-\frac{x}{L}\right)}\right)^2$	$\varphi_{j,x}(x)$	$\varphi_{j,x}(x)$	EX-C
Hybric function (Chapter Six) [205]	$\left(\frac{x}{L}\right)^2\left(1-\frac{x}{L}\right)^2 e^{\frac{-jx}{L}}$	$\varphi_{j,x}(x)$	$\varphi_{j,x}(x)$	H2-C

7.2. Results of comparative study

7.2.1. Convergence

To study the convergence of approximation functions, the reference distance is defined as:

$$d_f = R_{i+1} - R_i \tag{7.8}$$

where R_i and R_{i+1} are results of fundamental frequency, critical buckling load or deflection of beams at m_i and m_{i+1}, respectively.

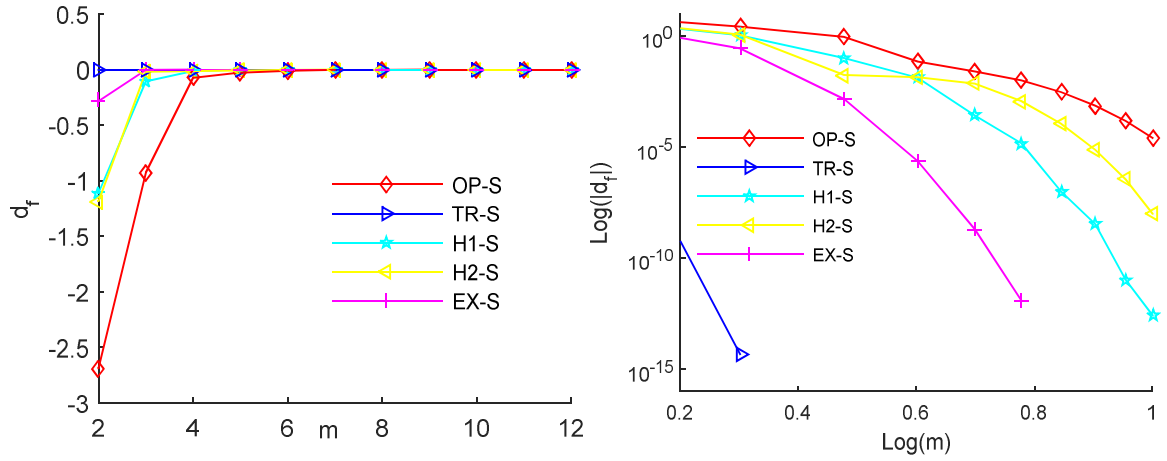

a. S-S boundary condition

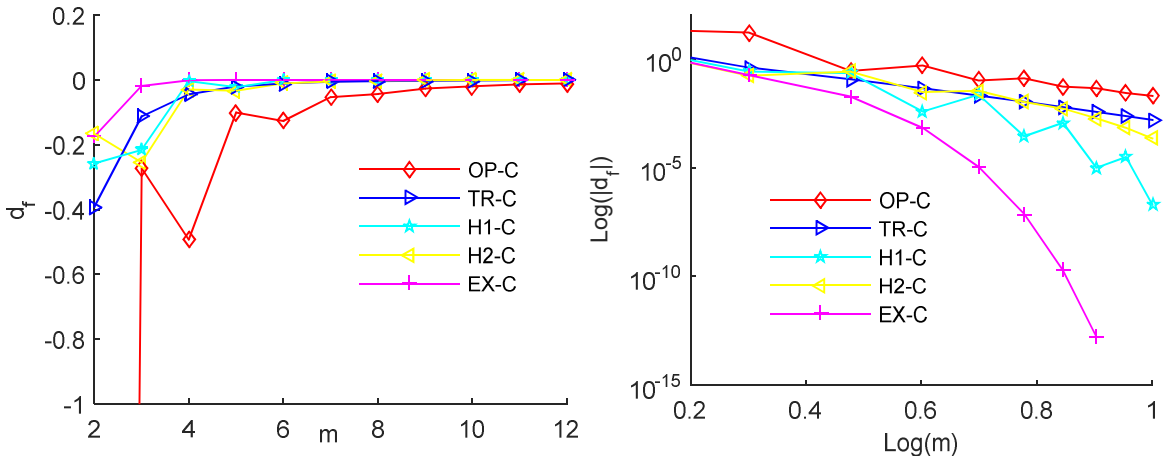

b. C-C boundary condition

Figure 7.1. Distance of fundamental frequency

Fig. 7.1 shows convergence of approximation functions for vibration analysis. It can be seen that for S-S boundary condition, TR function has the best convergence. OP function has the lowest convergence for both S-S and C-C boundary conditions. EX function converges better than H1 and H2 functions for both S-S and C-C boundary conditions.

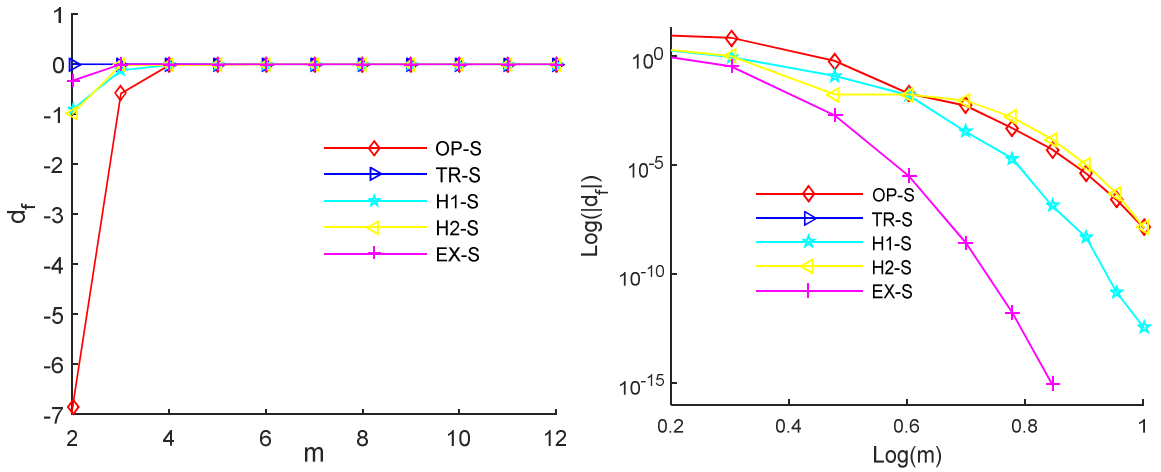

a. S-S boundary condition

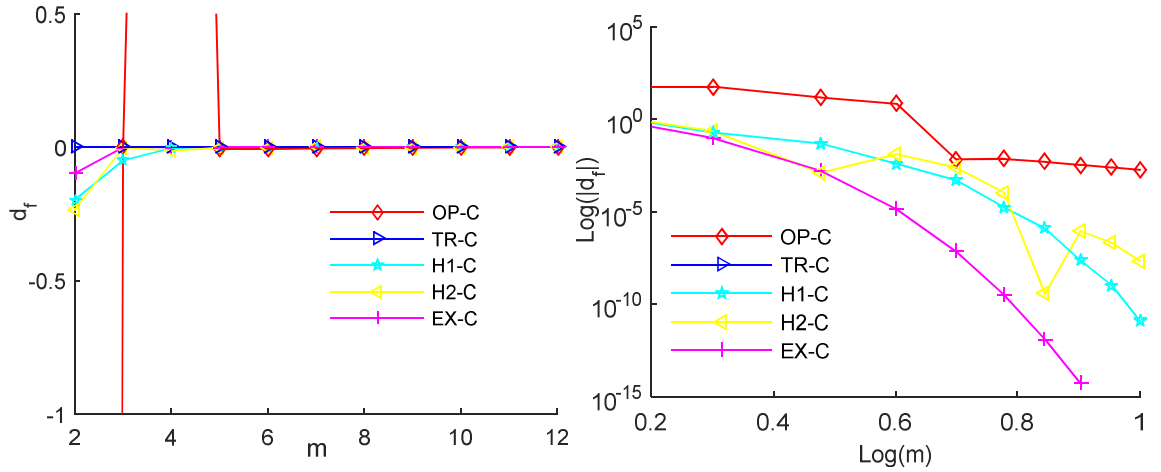

b. C-C boundary condition

Figure 7.2. Distance of critical buckling load

Convergence of approximation functions for buckling analysis is displayed in Fig. 7.2. TR function has the best convergence rate, and OP function has the lowest convergence for both S-S and C-C boundary conditions. Again, EX function converges better than H1 and H2 functions for both S-S and C-C boundary conditions.

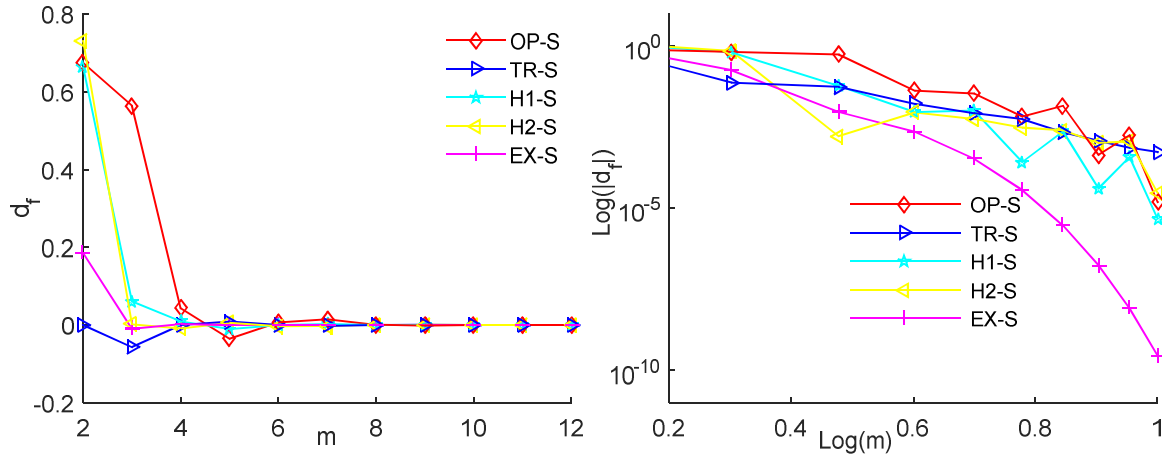

a. S-S boundary condition

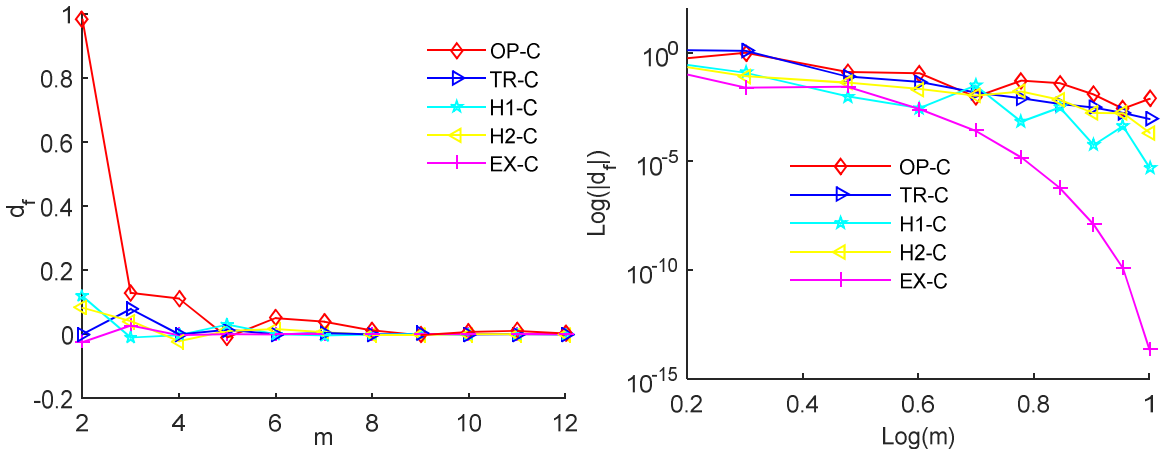

b. C-C boundary condition

Figure 7.3. Distance of deflection

Fig. 7.3 displays convergence rate of approximation functions for static analysis. It can be stated that EX function has the best convergence rate whisle OP and TR functions have low covergence for both S-S and C-C boundary conditions.

Table 7.3 shows convergence point (m) of approximation functions. It can be seen that for S-S boundary conditions, presented functions converge faster than published functions for both vibration and buckling analysis. For C-C boundary condition, present results converge faster than those of Nguyen et al.[98] and Mantari and Canales [44], but lower than those of Aydogdu [100].

Table 7.3. Convergence studies of approximation functions

Reference	m	
	S-S	C-C
1.Vibration analysis		
Present (TR)	2	12
Present (H1)	6	12
Present (H2)	6	10
Present (EX)	6	6
Aydogdu (Orthogonal polynomials) [100]	8	8
Nguyen et al. (Polynomials) [98]	14	14
Mantari and Canales (Hybrid) [44]	30	80
2. Buckling analysis		
Present (TR)	2	2
Present (H1)	6	12
Present (H2)	6	10
Present (EX)	6	6
Aydogdu (Orthogonal polynomials) [48]	8	-
Nguyen et al. (Polynomials) [98]	14	14
Mantari and Canales (Hybrid) [44]	12	12

7.2.2. Computational time

Computational time for frequency, critical buckling load and deflection of beams are shown in Figs. 7.4-7.6.

For S-S boundary condition: H1 function is less computational cost than other fuctions for both bending, buckling and vibration analysis; H2 and EX functions have low computational cost for bending and buckling analysis, but are the highest for vibration analysis; TR function is the highest computational cost for bending and buckling analysis.

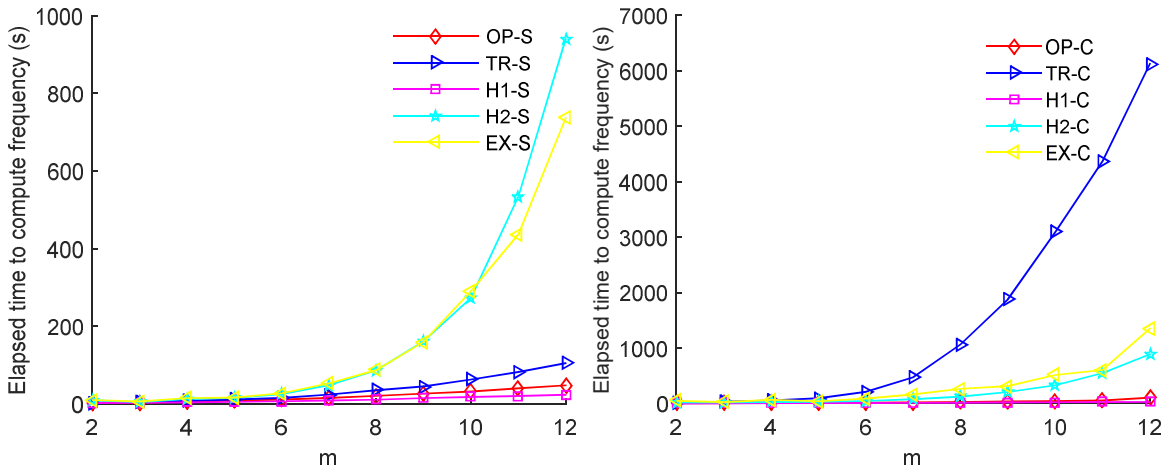

a. S-S boundary condition b. C-C boundary condition

Figure 7.4. Elapsed time to compute frequency

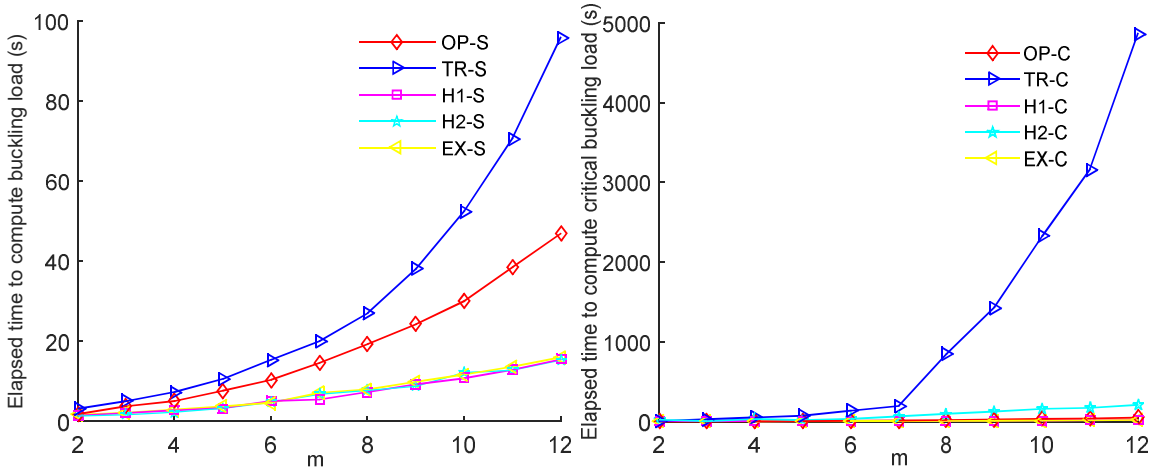

a. S-S boundary condition b. C-C boundary condition

Figure 7.5. Elapsed time to compute critical buckling load

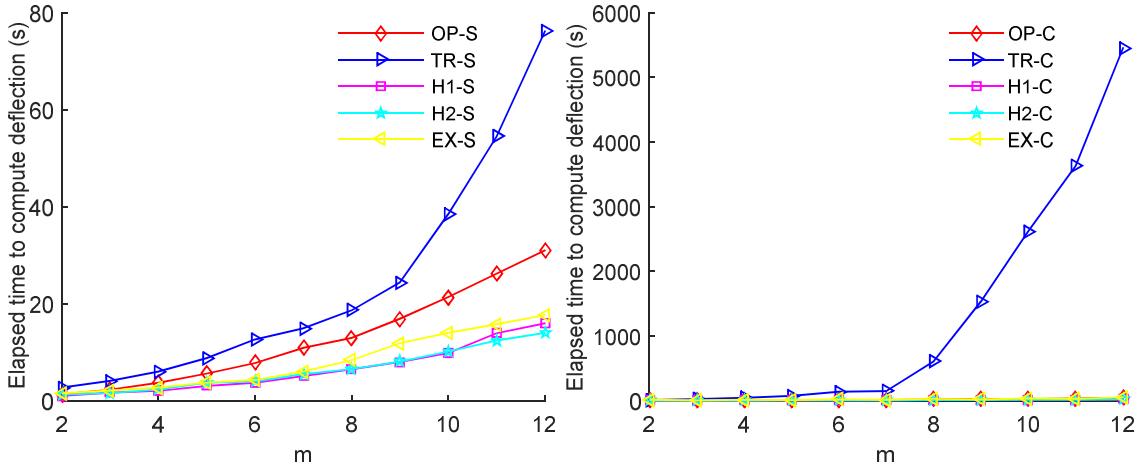

a. S-S boundary condition b. C-C boundary condition

Figure 7.6. Elapsed time to compute deflection

For C-C boundary condition: TR function is the highest computational cost for bending, buckling and vibration analysis.

It can be seen that C-C boundary condition has more computational cost than S-S boundary condition for all functions.

7.2.3. Numerical stability

One of method to assess the numerical stability is to consider the coefficient maximum eigenvalue/minimum eigenvalue. This coefficient increases linearly as evidence for the numerical stability [206, 207]. The results can be seen in Fig. 7.7. It can be seen that the coefficient is monotonically increasing for OP, TR, H1 and H2 functions. EX function has parabolic shape. From Fig.7.7, it can be stated that TR is the best for numerical stability term.

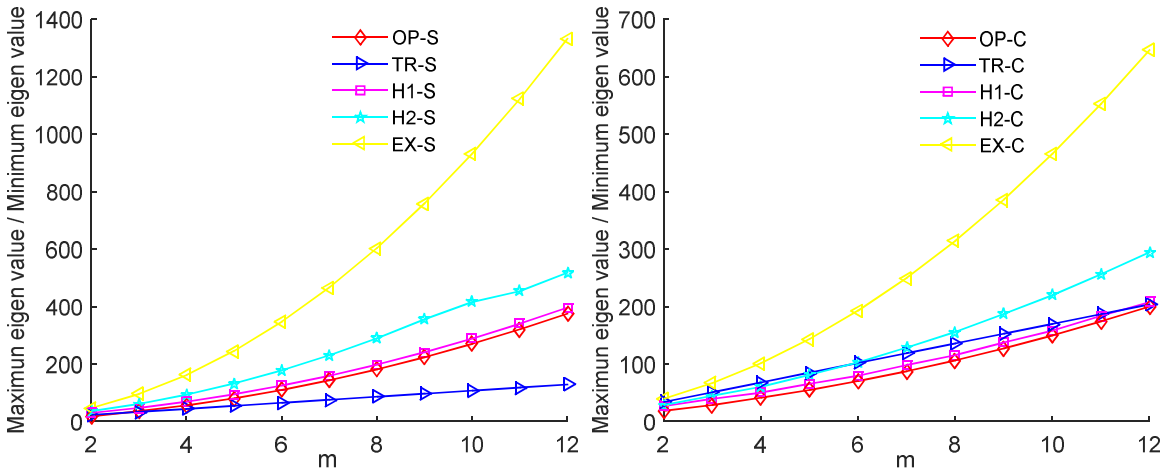

a. S-S boundary condition b. C-C boundary condition

Figure 7.7. Maximun eigen value-to-Minimun eigen value ratio

7.3. Conclusions

Five approximation functions for S-S and C-C boundary conditions were tested to study their performance in terms of convergence, computational time and stability. All proposed functions are suitable for predicting behaviours of laminated composite beams. Some conclusions are as follows:

- In terms of computational cost, H1 function is recommended for bending, buckling and vibration analysis of beams. H2 and EX functions are also

recommended for bending, buckling analysis, and to be limited use in vibration analysis. OP function can be also recommended for vibration analysis because computational cost is just more than H1 function. TR function is recommened to be limited use in C-C boundary condition.

- Regarding the convergence, TR function is recommended for buckling analysis. EX function is also better than remaining functions for all behaviours and boundary conditions. OP function is not recommended due to low convergence rate, especially bending analysis.
- All functions present evidences of numerical stability. The TR function has very good numerical behavior.
- Considering all the three numerical features, the H1 function is recommended for bending, buckling and vibration analysis, TR function is suitable for buckling, vibration analysis, and can be used with some necessary cautions about the numerical stability. While EX function should be discarded as appropriate for the computation of higher natural frequencies.

Chapter 8. CONCLUSIONS AND RECOMMENDATIONS

8.1. Conclusions

In this thesis, the new approximation functions are proposed to analyse free vibration, buckling and bending of of laminated composite beams with various cross-section such as rectangular and thin-walled beams. FOBT, HOBT and quasi-3D theories combined with modified couple stress theory are used for macro beams and microbeams. The governing equations of motion are derived by using Lagrange equations. The convergence and verification studies are carried out to demonstrate the accuracy of the proposed solution. Poisson's effect is considered in constitutive equations. Numerical results are presented to investigate the effects of length-to-height ratio, fibre angle and material anisotropy on the deflections, stresses, natural frequencies and critical buckling loads of composite beams. According to the results of the present work, the following conclusions can be drawn:

- The new approximation functions are simple and effective for analysis both retangular and thin-walled laminated composite beams.
- The effects of length-to-height ratio, fibre angle and material anisotropy on the deflections, stresses, natural frequencies and critical buckling load are significant.
- The Poisson's effects are important, which cannot be ignored, on behaviours of arbitary angle beams but less significant on cross-ply ones.
- The shear deformation effects become significant for lower length-to-height ratio, higher degrees of anisotropy of thin-walled composite beams.

8.2. Recommendations

The following are recommendations concerning the extension of the proposed for the future research:

- The new approximation functions can be applied to analyse behaviours of composite plates.

- The present method can be combined with Lagrange multiplier, penalty method and finite element method to achieve 3D solutions and more complex geometrices and boundary conditions.
- Analysis of curved composite beams can be developed by extending present methods.
- A nonlinear model based on large displacements, rotations and Ritz method should be considered for analysis of rectangular and thin-walled composite beams.

APPENDIX A

The coefficients in Eq. (1.19)

$$C_{11}=\frac{1-\nu_{23}\nu_{32}}{E_2E_3\Delta},\ C_{12}=\frac{\nu_{21}+\nu_{31}\nu_{23}}{E_2E_3\Delta}=\frac{\nu_{12}+\nu_{32}\nu_{13}}{E_1E_3\Delta},\ C_{13}=\frac{\nu_{31}+\nu_{21}\nu_{32}}{E_2E_3\Delta}=\frac{\nu_{13}+\nu_{12}\nu_{23}}{E_1E_2\Delta} \tag{A.1}$$

$$C_{22}=\frac{1-\nu_{13}\nu_{31}}{E_1E_3\Delta},\ C_{23}=\frac{\nu_{32}+\nu_{12}\nu_{31}}{E_1E_3\Delta}=\frac{\nu_{23}+\nu_{21}\nu_{13}}{E_1E_2\Delta},\ C_{33}=\frac{1-\nu_{12}\nu_{21}}{E_1E_2\Delta},\ C_{44}=G_{23},\ C_{55}=G_{13} \tag{A.2}$$

$$C_{66}=G_{12},\Delta=\frac{1-\nu_{12}\nu_{21}-\nu_{23}\nu_{32}-\nu_{31}\nu_{13}-2\nu_{21}\nu_{32}\nu_{13}}{E_1E_2E_3} \tag{A.3}$$

The coefficients in Eq. (1.20)

$$Q_{11}=\frac{E_1}{1-\nu_{12}\nu_{21}},\ Q_{12}=\frac{\nu_{12}E_2}{1-\nu_{12}\nu_{21}},\ Q_{22}=\frac{E_2}{1-\nu_{12}\nu_{21}},\ Q_{44}=G_{23},\ Q_{55}=G_{13},\ Q_{66}=G_{12} \tag{A.4}$$

The coefficients in Eqs. (1.21) and (1.22)

$$\bar{Q}_{11}=Q_{11}\cos^4\theta+2\left(Q_{12}+2Q_{66}\right)\sin^2\theta\cos^2\theta+Q_{22}\sin^4\theta \tag{A.5}$$

$$\bar{Q}_{12}=\left(Q_{11}+Q_{22}-4Q_{66}\right)\sin^2\theta\cos^2\theta+Q_{12}\left(\sin^4\theta+\cos^4\theta\right) \tag{A.6}$$

$$\bar{Q}_{16}=\left(Q_{11}-Q_{12}-2Q_{66}\right)\sin\theta\cos^3\theta+\left(Q_{12}-Q_{22}+2Q_{66}\right)\sin^3\theta\cos\theta \tag{A.7}$$

$$\bar{Q}_{22}=Q_{11}\sin^4\theta+2\left(Q_{12}+2Q_{66}\right)\sin^2\theta\cos^2\theta+Q_{22}\cos^4\theta \tag{A.8}$$

$$\bar{Q}_{26}=\left(Q_{11}-Q_{12}-2Q_{66}\right)\sin^3\theta\cos\theta+\left(Q_{12}-Q_{22}+2Q_{66}\right)\sin\theta\cos^3\theta \tag{A.9}$$

$$\bar{Q}_{44}=Q_{44}\cos^2\theta+Q_{55}\sin^2\theta,\ \bar{Q}_{45}=\left(Q_{55}-Q_{44}\right)\sin\theta\cos\theta,\ \bar{Q}_{55}=Q_{44}\sin^2\theta+Q_{55}\cos^2\theta \tag{A.10}$$

$$\bar{Q}_{66}=\left(Q_{11}+Q_{22}-2Q_{12}-2Q_{66}\right)\sin^2\theta\cos^2\theta+Q_{66}\left(\sin^4\theta+\cos^4\theta\right) \tag{A.11}$$

The coefficients in Eq. (1.23)

$$\bar{C}_{11}=C_{11}\cos^4\theta+2\left(C_{12}+2C_{66}\right)\sin^2\theta\cos^2\theta+C_{22}\sin^4\theta \tag{A.12}$$

$$\bar{C}_{12}=\left(C_{11}+C_{22}-4C_{66}\right)\sin^2\theta\cos^2\theta+C_{12}\left(\sin^4\theta+\cos^4\theta\right) \tag{A.13}$$

$$\bar{C}_{13}=C_{13}\cos^2\theta+C_{23}\sin^2\theta \tag{A.14}$$

$$\bar{C}_{16}=\left(C_{11}-C_{12}-2C_{66}\right)\sin\theta\cos^3\theta+\left(C_{12}-C_{22}+2C_{66}\right)\sin^3\theta\cos\theta \tag{A.15}$$

$$\bar{C}_{22}=C_{11}\sin^4\theta+2\left(C_{12}+2C_{66}\right)\sin^2\theta\cos^2\theta+C_{22}\cos^4\theta \tag{A.16}$$

$$\bar{C}_{23}=C_{13}\sin^2\theta+C_{23}\cos^2\theta \tag{A.17}$$

$$\bar{C}_{26}=\left(C_{11}-C_{12}-2C_{66}\right)\sin^3\theta\cos\theta+\left(C_{12}-C_{22}+2C_{66}\right)\sin\theta\cos^3\theta,\ \bar{C}_{33}=C_{33} \tag{A.18}$$

$$\overline{C}_{36} = \left(C_{13} - C_{23}\right)\sin\theta\cos\theta\,,\ \overline{C}_{44} = C_{44}\cos^2\theta + C_{55}\sin^2\theta \tag{A.19}$$

$$\overline{C}_{45} = \left(C_{55} - C_{44}\right)\sin\theta\cos\theta\,,\ \overline{C}_{55} = C_{44}\sin^2\theta + C_{55}\cos^2\theta \tag{A.20}$$

$$\overline{C}_{66} = \left(C_{11} + C_{22} - 2C_{12}\right)\sin^2\theta\cos^2\theta + C_{66}\left(\cos^2\theta - \sin^2\theta\right)^2 \tag{A.21}$$

The coefficients in Eq. (1.24)

$$\overline{\overline{C}}_{11} = \overline{C}_{11} + \frac{\overline{C}_{16}^{\,2}\overline{C}_{22} - 2\overline{C}_{12}\overline{C}_{16}\overline{C}_{26} + \overline{C}_{12}^{\,2}\overline{C}_{66}}{\overline{C}_{26}^{\,2} - \overline{C}_{22}\overline{C}_{66}} \tag{A.22}$$

$$\overline{\overline{C}}_{13} = \overline{C}_{13} + \frac{\overline{C}_{16}\overline{C}_{22}\overline{C}_{36} + \overline{C}_{12}\overline{C}_{23}\overline{C}_{66} - \overline{C}_{16}\overline{C}_{23}\overline{C}_{26} - \overline{C}_{12}\overline{C}_{26}\overline{C}_{36}}{\overline{C}_{26}^{\,2} - \overline{C}_{22}\overline{C}_{66}} \tag{A.23}$$

$$\overline{\overline{C}}_{33} = \overline{C}_{33} + \frac{\overline{C}_{36}^{\,2}\overline{C}_{22} - 2\overline{C}_{23}\overline{C}_{26}\overline{C}_{36} + \overline{C}_{23}^{\,2}\overline{C}_{66}}{\overline{C}_{26}^{\,2} - \overline{C}_{22}\overline{C}_{66}} \tag{A.24}$$

$$\overline{\overline{C}}_{55} = \overline{C}_{55} - \frac{\overline{C}_{45}^{\,2}}{\overline{\overline{C}}_{44}} \tag{A.25}$$

The coefficients in Eq. (1.25)

$$\overline{\overline{C}}_{11}^{*} = \overline{\overline{C}}_{11} - \frac{\overline{\overline{C}}_{13}^{\,2}}{\overline{\overline{C}}_{33}},\ \overline{\overline{C}}_{55}^{*} = \overline{\overline{C}}_{55} \tag{A.26}$$

The coefficients in Eq. (3.3)

$$\alpha_x = \alpha_1^* \cos^2\theta + \alpha_2^* \sin^2\theta \tag{A.27}$$

$$\alpha_y = \alpha_1^* \sin^2\theta + \alpha_2^* \cos^2\theta \tag{A.28}$$

$$\alpha_{xy} = \left(\alpha_2^* - \alpha_1^*\right)\sin\theta\cos\theta \tag{A.29}$$

APPENDIX B

The coefficients in Eq. (6.48)

$$E_{11}=\int_s A_{11}ds,\ E_{12}=\int_s\left(A_{11}y+B_{11}\sin\theta\right)ds\ ,E_{13}=\int_s\left(A_{11}z-B_{11}\cos\theta\right)ds \tag{B.1}$$

$$E_{14}=\int_s\left(A_{11}\varpi-B_{11}q\right)ds\,,E_{15}=\int_s B_{16}ds\,,\ E_{16}=\int_s A_{16}\cos\theta ds\,,\ E_{17}=\int_s A_{16}\sin\theta ds \tag{B.2}$$

$$E_{18}=\int_s A_{16}rds\,,E_{22}=\int_s\left(A_{11}y^2+2B_{11}y\sin\theta+D_{11}\sin^2\theta\right)ds \tag{B.3}$$

$$E_{23}=\int_s\left(A_{11}yz+B_{11}\left(z\sin\theta-y\cos\theta\right)-D_{11}\sin\theta\cos\theta\right)ds \tag{B.4}$$

$$E_{24}=\int_s\left(A_{11}y\varpi+B_{11}\left(\varpi\sin\theta-qy\right)-D_{11}q\sin\theta\right)ds\,,\ E_{25}=\int_s\left(B_{16}y+D_{16}\sin\theta\right)ds \tag{B.5}$$

$$E_{26}=\int_s\left(A_{16}y+B_{16}\sin\theta\right)\cos\theta ds\,,E_{27}=\int_s\left(A_{16}y+B_{16}\sin\theta\right)\sin\theta ds \tag{B.6}$$

$$E_{28}=\int_s\left(A_{16}y+B_{16}\sin\theta\right)rds\,,E_{33}=\int_s\left(A_{11}z^2-2B_{11}z\cos\theta+D_{11}\cos^2\theta\right)ds \tag{B.7}$$

$$E_{34}=\int_s\left(A_{11}z\varpi-B_{11}\left(\varpi\cos\theta+qz\right)+D_{11}q\cos\theta\right)ds\,,E_{35}=\int_s\left(B_{16}z-D_{16}\cos\theta\right)ds \tag{B.8}$$

$$E_{36}=\int_s\left(A_{16}z-B_{16}\cos\theta\right)\cos\theta ds\,,E_{37}=\int_s\left(A_{16}z-B_{16}\cos\theta\right)\sin\theta ds \tag{B.9}$$

$$E_{38}=\int_s\left(A_{16}z-B_{16}\cos\theta\right)rds\,,E_{44}=\int_s\left(A_{11}\varpi^2-2B_{11}\varpi q+D_{11}q^2\right)ds \tag{B.10}$$

$$E_{45}=\int_s\left(B_{16}\varpi-D_{16}q\right)ds\,,E_{46}=\int_s\left(A_{16}\varpi-B_{16}q\right)\cos\theta ds\,,E_{47}=\int_s\left(A_{16}\varpi-B_{16}q\right)\sin\theta ds \tag{B.11}$$

$$E_{48}=\int_s\left(A_{16}\varpi-B_{16}q\right)rds\ E_{55}=\int_s D_{66}ds\,,\ E_{56}=\int_s B_{66}\cos\theta ds\,,\ E_{57}=\int_s B_{66}\sin\theta ds \tag{B.12}$$

$$E_{58}=\int_s B_{66}rds\,,\ E_{58}=\int_s B_{66}rds\,,\ E_{66}=\int_s\left(A_{66}\cos^2\theta+A_{55}\sin^2\theta\right)ds \tag{B.13}$$

$$E_{67}=\int_s\left(\left(A_{66}-A_{55}\right)\sin\theta\cos\theta\right)ds\,,\ E_{68}=\int_s\left(A_{66}r\cos\theta-A_{55}q\sin\theta\right)ds \tag{B.14}$$

$$E_{77}=\int_s\left(A_{66}\sin^2\theta+A_{55}\cos^2\theta\right)ds\,,\ E_{78}=\int_s\left(A_{66}r\sin\theta+A_{55}q\cos\theta\right)ds$$

$$,\qquad E_{88}=\int_s\left(A_{66}r^2+A_{55}q^2\right)ds \tag{B.15}$$

where $$\left(A_{ij}, B_{ij}, D_{ij}\right) = \int_n \overline{Q}_{ij}^{*}\left(1, n, n^2\right) dn \tag{B.16}$$

The coefficients in Eq. (6.51)

$$m_0 = \int_s I_0 ds\,,\ m_c = \int_s I_1 \cos\theta ds\,,\ m_r = \int_s I_1 r ds\,,\ m_p = \int_s I_0\left(r^2 + q^2\right) ds\,,\ m_q = \int_s I_1 q ds \tag{B.17}$$

$$m_s = \int_s I_1 \sin\theta ds\,,\ m_{\varpi} = \int_s I_0 \varpi ds\,,\ m_2 = \int_s I_2 ds\,,\quad m_{c2} = \int_s I_2 \cos^2\theta ds\,,\ m_{s2} = \int_s I_2 \sin^2\theta ds \tag{B.18}$$

$$m_{q2} = \int_s I_2 q^2 ds\,,\ m_{y2} = \int_s I_0 y^2 ds\,,\ m_{z2} = \int_s I_0 z^2 ds\,,\ m_{\varpi 2} = \int_s I_0 \varpi^2 ds\,,\ m_{cs} = \int_s I_2 \sin\theta\cos\theta ds \tag{B.19}$$

$$m_{qc} = \int_s I_2 q\cos\theta ds\,,\ m_{qs} = \int_s I_2 q\sin\theta ds\,,\ m_{ys} = \int_s I_1 y\sin\theta ds\,,\ m_{zc} = \int_s I_1 z\cos\theta ds \tag{B.20}$$

$$m_{q\varpi} = \int_s I_1 q\varpi ds\,,\ m_{y\varpi} = \int_s I_0 y\varpi ds\,,\ m_{z\varpi} = \int_s I_0 z\varpi ds\,,\ m_{\varpi c} = \int_s I_1 \varpi\cos\theta ds \tag{B.21}$$

$$m_{\varpi s} = \int_s I_1 \varpi\sin\theta ds\,,\ m_{yzcs} = \int_s I_1\left(z\sin\theta - y\cos\theta\right) ds\,,\ m_{y\varpi qs} = \int_s I_1\left(\varpi\sin\theta - qy\right) ds \tag{B.22}$$

$$m_{z\varpi qc} = \int_s I_1\left(qz + \varpi\cos\theta\right) ds \tag{B.23}$$

where $$\left(I_0, I_1, I_2\right) = \int_n \rho\left(1, n, n^2\right) dn \tag{B.24}$$

References

1. J.N. Reddy, *Mechanics of laminated composite plates and shells: theory and analysis* (CRC press, 2004).
2. Y. Ghugal and R. Shimpi, A review of refined shear deformation theories for isotropic and anisotropic laminated beams, *Journal of reinforced plastics and composites*. **20**(3) (2001) 255-272.
3. A.C. Eringen, Nonlocal polar elastic continua, *International journal of engineering science*. **10**(1) (1972) 1-16.
4. W. Koiter, Couple-stresses in the theory of elasticity, I & II, (1969).
5. R.A. Toupin, Elastic materials with couple-stresses, *Archive for Rational Mechanics and Analysis*. **11**(1) (1962) 385-414.
6. R. Mindlin and H. Tiersten, Effects of couple-stresses in linear elasticity, *Archive for Rational Mechanics and analysis*. **11**(1) (1962) 415-448.
7. W. Yang, D. He, and W. Chen, A size-dependent zigzag model for composite laminated micro beams based on a modified couple stress theory, *Composite Structures* (2017).
8. M. Mohammad-Abadi and A. Daneshmehr, Modified couple stress theory applied to dynamic analysis of composite laminated beams by considering different beam theories, *International Journal of Engineering Science*. **87** (2015) 83-102.
9. M. Mohammad-Abadi and A. Daneshmehr, Size dependent buckling analysis of microbeams based on modified couple stress theory with high order theories and general boundary conditions, *International Journal of Engineering Science*. **74** (2014) 1-14.
10. C. Roque, D. Fidalgo, A. Ferreira, and J. Reddy, A study of a microstructure-dependent composite laminated Timoshenko beam using a modified couple stress theory and a meshless method, *Composite Structures*. **96** (2013) 532-537.
11. W. Chen, M. Xu, and L. Li, A model of composite laminated Reddy plate based

on new modified couple stress theory, *Composite Structures*. **94**(7) (2012) 2143-2156.

12. W. Chen, L. Li, and M. Xu, A modified couple stress model for bending analysis of composite laminated beams with first order shear deformation, *Composite Structures*. **93**(11) (2011) 2723-2732.
13. H. Ma, X.-L. Gao, and J. Reddy, A microstructure-dependent Timoshenko beam model based on a modified couple stress theory, *Journal of the Mechanics and Physics of Solids*. **56**(12) (2008) 3379-3391.
14. V.Z. Vlasov, *Thin-walled elastic beams* (Israel Program for Scientific Translations, Jerusalem, 1961).
15. N.R. Bauld and T. Lih-Shyng, A Vlasov theory for fiber-reinforced beams with thin-walled open cross sections, *International Journal of Solids and Structures*. **20**(3) (1984) 277-297.
16. O. Song and L. Librescu, Free Vibration Of Anisotropic Composite Thin-Walled Beams Of Closed Cross-Section Contour, *Journal of Sound and Vibration*. **167**(1) (1993) 129-147.
17. J. Lee and S.-E. Kim, Free vibration of thin-walled composite beams with I-shaped cross-sections, *Composite structures*. **55**(2) (2002) 205-215.
18. J. Lee and S.-E. Kim, Flexural–torsional buckling of thin-walled I-section composites, *Computers & Structures*. **79**(10) (2001) 987-995.
19. T.P. Vo, H.-T. Thai, T.-K. Nguyen, D. Lanc, and A. Karamanli, Flexural analysis of laminated composite and sandwich beams using a four-unknown shear and normal deformation theory, *Composite Structures* (2017).
20. J. Mantari and F. Canales, Finite element formulation of laminated beams with capability to model the thickness expansion, *Composites Part B: Engineering*. **101** (2016) 107-115.
21. T.P. Vo and H.-T. Thai, Vibration and buckling of composite beams using refined shear deformation theory, *International Journal of Mechanical Sciences*. **62**(1) (2012) 67-76.

22. T.P. Vo and H.-T. Thai, Static behavior of composite beams using various refined shear deformation theories, *Composite Structures*. **94**(8) (2012) 2513-2522.
23. P. Vidal and O. Polit, A family of sinus finite elements for the analysis of rectangular laminated beams, *Composite Structures*. **84**(1) (2008) 56-72.
24. M. Murthy, D.R. Mahapatra, K. Badarinarayana, and S. Gopalakrishnan, A refined higher order finite element for asymmetric composite beams, *Composite Structures*. **67**(1) (2005) 27-35.
25. G. Shi and K. Lam, Finite element vibration analysis of composite beams based on higher-order beam theory, *Journal of Sound and Vibration*. **219**(4) (1999) 707-721.
26. S. Marur and T. Kant, Free vibration analysis of fiber reinforced composite beams using higher order theories and finite element modelling, *Journal of Sound and Vibration*. **194**(3) (1996) 337-351.
27. K. Chandrashekhara and K.M. Bangera, Free vibration of composite beams using a refined shear flexible beam element, *Computers & structures*. **43**(4) (1992) 719-727.
28. M. Filippi and E. Carrera, Bending and vibrations analyses of laminated beams by using a zig-zag-layer-wise theory, *Composites Part B: Engineering*. **98** (2016) 269-280.
29. M. Shokrieh and A. Karamnejad, Dynamic response of strain rate dependent Glass/Epoxy composite beams using finite difference method, *Int Scholarly Sci Res Innovation*. **5**(2) (2011) 63-69.
30. K. Numayr, M. Haddad, and A. Ayoub, Investigation of free vibrations of composite beams by using the finite-difference method, *Mechanics of Composite Materials*. **42**(3) (2006) 231-242.
31. M. Filippi, A. Pagani, M. Petrolo, G. Colonna, and E. Carrera, Static and free vibration analysis of laminated beams by refined theory based on Chebyshev polynomials, *Composite Structures*. **132** (2015) 1248-1259.

32. L. Jun, L. Xiaobin, and H. Hongxing, Free vibration analysis of third-order shear deformable composite beams using dynamic stiffness method, *Archive of Applied Mechanics*. **79**(12) (2009) 1083-1098.
33. X. Wang, X. Zhu, and P. Hu, Isogeometric finite element method for buckling analysis of generally laminated composite beams with different boundary conditions, *International Journal of Mechanical Sciences*. **104** (2015) 190-199.
34. M. Lezgy-Nazargah, P. Vidal, and O. Polit, NURBS-based isogeometric analysis of laminated composite beams using refined sinus model, *European Journal of Mechanics-A/Solids*. **53** (2015) 34-47.
35. J. Mantari and F. Canales, A unified quasi-3D HSDT for the bending analysis of laminated beams, *Aerospace Science and Technology*. **54** (2016) 267-275.
36. A.M. Zenkour, Transverse shear and normal deformation theory for bending analysis of laminated and sandwich elastic beams, *Mechanics of Composite Materials and Structures*. **6**(3) (1999) 267-283.
37. M. Mohammadabadi, A. Daneshmehr, and M. Homayounfard, Size-dependent thermal buckling analysis of micro composite laminated beams using modified couple stress theory, *International Journal of Engineering Science*. **92** (2015) 47-62.
38. C. Jin and X. Wang, Accurate free vibration analysis of Euler functionally graded beams by the weak form quadrature element method, *Composite Structures*. **125** (2015) 41-50.
39. S.R. Sahoo, Active Control of Geometrically Nonlinear Vibrations of Laminated Composite Beams Using Piezoelectric Composites by Element-Free Galerkin Method, *International Journal for Computational Methods in Engineering Science and Mechanics* (2019) 1-9.
40. M. Ahmadian, R. Jafari-Talookolaei, and E. Esmailzadeh, Dynamics of a laminated composite beam on Pasternak-viscoelastic foundation subjected to a moving oscillator, *Journal of Vibration and Control*. **14**(6) (2008) 807-830.
41. K. Liew, H. Lim, M. Tan, and X. He, Analysis of laminated composite beams

and plates with piezoelectric patches using the element-free Galerkin method, *Computational Mechanics*. **29**(6) (2002) 486-497.

42. Ö. Özdemir, Application of the differential transform method to the free vibration analysis of functionally graded Timoshenko beams, *Journal of Theoretical and Applied Mechanics*. **54**(4) (2016) 1205--1217.
43. A. Arikoglu and I. Ozkol, Vibration analysis of composite sandwich beams with viscoelastic core by using differential transform method, *Composite Structures*. **92**(12) (2010) 3031-3039.
44. J. Mantari and F. Canales, Free vibration and buckling of laminated beams via hybrid Ritz solution for various penalized boundary conditions, *Composite Structures*. **152** (2016) 306-315.
45. M. Şimşek, Static analysis of a functionally graded beam under a uniformly distributed load by Ritz method, *Int J Eng Appl Sci*. **1**(3) (2009) 1-11.
46. K. Pradhan and S. Chakraverty, Free vibration of Euler and Timoshenko functionally graded beams by Rayleigh–Ritz method, *Composites Part B: Engineering*. **51** (2013) 175-184.
47. M. Aydogdu, Free vibration analysis of angle-ply laminated beams with general boundary conditions, *Journal of reinforced plastics and composites*. **25**(15) (2006) 1571-1583.
48. M. Aydogdu, Buckling analysis of cross-ply laminated beams with general boundary conditions by Ritz method, *Composites Science and Technology*. **66**(10) (2006) 1248-1255.
49. C.H. Thai, A.J.M. Ferreira, and H. Nguyen-Xuan, Isogeometric analysis of size-dependent isotropic and sandwich functionally graded microplates based on modified strain gradient elasticity theory, *Composite Structures*. **192** (2018) 274-288.
50. T.N. Nguyen, T.D. Ngo, and H. Nguyen-Xuan, A novel three-variable shear deformation plate formulation: Theory and Isogeometric implementation, *Computer Methods in Applied Mechanics and Engineering*. **326** (2017) 376-

401.

51. P. Phung-Van, A.J.M. Ferreira, H. Nguyen-Xuan, and M. Abdel Wahab, An isogeometric approach for size-dependent geometrically nonlinear transient analysis of functionally graded nanoplates, *Composites Part B: Engineering*. **118** (2017) 125-134.
52. T.N. Nguyen, C.H. Thai, and H. Nguyen-Xuan, On the general framework of high order shear deformation theories for laminated composite plate structures: A novel unified approach, *International Journal of Mechanical Sciences*. **110** (2016) 242-255.
53. G.R. Liu, K.Y. Dai, and T.T. Nguyen, A Smoothed Finite Element Method for Mechanics Problems, *Computational Mechanics*. **39**(6) (2007) 859-877.
54. T. Nguyen-Thoi, T. Bui-Xuan, P. Phung-Van, H. Nguyen-Xuan, and P. Ngo-Thanh, Static, free vibration and buckling analyses of stiffened plates by CS-FEM-DSG3 using triangular elements, *Computers & Structures*. **125** (2013) 100-113.
55. T. Nguyen-Thoi, P. Phung-Van, S. Nguyen-Hoang, and Q. Lieu-Xuan, A coupled alpha-FEM for dynamic analyses of 2D fluid–solid interaction problems, *Journal of Computational and Applied Mathematics*. **271** (2014) 130-149.
56. N.D. Duc, K. Seung-Eock, and D.Q. Chan, Thermal buckling analysis of FGM sandwich truncated conical shells reinforced by FGM stiffeners resting on elastic foundations using FSDT, *Journal of Thermal Stresses*. **41**(3) (2018) 331-365.
57. N.D. Duc, K. Seung-Eock, T.Q. Quan, D.D. Long, and V.M. Anh, Nonlinear dynamic response and vibration of nanocomposite multilayer organic solar cell, *Composite Structures*. **184** (2018) 1137-1144.
58. N.D. Duc, K. Seung-Eock, N.D. Tuan, P. Tran, and N.D. Khoa, New approach to study nonlinear dynamic response and vibration of sandwich composite cylindrical panels with auxetic honeycomb core layer, *Aerospace Science and*

Technology. **70** (2017) 396-404.

59. N.D. Duc and H.V. Tung, Mechanical and thermal postbuckling of higher order shear deformable functionally graded plates on elastic foundations, *Composite Structures*. **93**(11) (2011) 2874-2881.
60. T.I. Thinh and L.K. Ngoc, Static behavior and vibration control of piezoelectric cantilever composite plates and comparison with experiments, *Computational Materials Science*. **49**(4, Supplement) (2010) S276-S280.
61. T.I. Thinh and T.H. Quoc, Finite element modeling and experimental study on bending and vibration of laminated stiffened glass fiber/polyester composite plates, *Computational Materials Science*. **49**(4, Supplement) (2010) S383-S389.
62. H.V. Tung, Thermal and thermomechanical postbuckling of FGM sandwich plates resting on elastic foundations with tangential edge constraints and temperature dependent properties, *Composite Structures*. **131** (2015) 1028-1039.
63. H. Van Tung, Nonlinear axisymmetric response of FGM shallow spherical shells with tangential edge constraints and resting on elastic foundations, *Composite Structures*. **149** (2016) 231-238.
64. D.K. Nguyen, Large displacement behaviour of tapered cantilever Euler–Bernoulli beams made of functionally graded material, *Applied Mathematics and Computation*. **237** (2014) 340-355.
65. D.K. Nguyen, Large displacement response of tapered cantilever beams made of axially functionally graded material, *Composites Part B: Engineering*. **55** (2013) 298-305.
66. R.P. Shimpi and Y.M. Ghugal, A new layerwise trigonometric shear deformation theory for two-layered cross-ply beams, *Composites Science and Technology*. **61**(9) (2001) 1271-1283.
67. R. Shimpi and Y. Ghugal, A layerwise trigonometric shear deformation theory for two layered cross-ply laminated beams, *Journal of reinforced plastics and*

composites. **18**(16) (1999) 1516-1543.

68. K.P. Soldatos and P. Watson, A general theory for the accurate stress analysis of homogeneous and laminated composite beams, *International journal of Solids and Structures*. **34**(22) (1997) 2857-2885.
69. A. Khdeir and J. Reddy, An exact solution for the bending of thin and thick cross-ply laminated beams, *Composite Structures*. **37**(2) (1997) 195-203.
70. U. Icardi, A three-dimensional zig-zag theory for analysis of thick laminated beams, *Composite structures*. **52**(1) (2001) 123-135.
71. U. Icardi, Higher-order zig-zag model for analysis of thick composite beams with inclusion of transverse normal stress and sublaminates approximations, *Composites Part B: Engineering*. **32**(4) (2001) 343-354.
72. U. Icardi, Applications of zig-zag theories to sandwich beams, *Mechanics of Advanced Materials and Structures*. **10**(1) (2003) 77-97.
73. E. Carrera and G. Giunta, Refined beam theories based on a unified formulation, *International Journal of Applied Mechanics*. **2**(01) (2010) 117-143.
74. A. Catapano, G. Giunta, S. Belouettar, and E. Carrera, Static analysis of laminated beams via a unified formulation, *Composite structures*. **94**(1) (2011) 75-83.
75. J. Bernoulli, Curvatura laminae elasticae, *Acta eruditorum*. **1694**(13) 262-276.
76. S.P. Timoshenko, LXVI. On the correction for shear of the differential equation for transverse vibrations of prismatic bars, *The London, Edinburgh, and Dublin Philosophical Magazine and Journal of Science*. **41**(245) (1921) 744-746.
77. S.P. Timoshenko, X. On the transverse vibrations of bars of uniform cross-section, *The London, Edinburgh, and Dublin Philosophical Magazine and Journal of Science*. **43**(253) (1922) 125-131.
78. K. Chandrashekhara, K. Krishnamurthy, and S. Roy, Free vibration of composite beams including rotary inertia and shear deformation, *Composite*

Structures. **14**(4) (1990) 269-279.

79. M. Levinson, A new rectangular beam theory, *Journal of Sound and vibration*. **74**(1) (1981) 81-87.
80. A. Krishna Murty, Toward a consistent beam theory, *AIAA journal*. **22**(6) (1984) 811-816.
81. J.N. Reddy, A simple higher-order theory for laminated composite plates, *Journal of applied mechanics*. **51**(4) (1984) 745-752.
82. Y. Ghugal and R. Shimpi, A trigonometric shear deformation theory for flexure and free vibration of isotropic thick beams, *Structural Engineering Convention, SEC-2000, IIT Bombay, India*. (2000).
83. H. Matsunaga, Vibration and buckling of multilayered composite beams according to higher order deformation theories, *Journal of Sound and Vibration*. **246**(1) (2001) 47-62.
84. W. Chen, C. Lv, and Z. Bian, Free vibration analysis of generally laminated beams via state-space-based differential quadrature, *Composite Structures*. **63**(3) (2004) 417-425.
85. J. Li, Q. Huo, X. Li, X. Kong, and W. Wu, Vibration analyses of laminated composite beams using refined higher-order shear deformation theory, *International Journal of Mechanics and Materials in Design*. **10**(1) (2014) 43-52.
86. B.M. Shinde and A.S. Sayyad, A Quasi-3D Polynomial Shear and Normal Deformation Theory for Laminated Composite, Sandwich, and Functionally Graded Beams, *Mechanics of Advanced Composite Structures*. **4**(2) (2017) 139-152.
87. T.P. Vo, H.-T. Thai, T.-K. Nguyen, F. Inam, and J. Lee, A quasi-3D theory for vibration and buckling of functionally graded sandwich beams, *Composite Structures*. **119** (2015) 1-12.
88. Z. Kaczkowski, Plates-statistical calculations, *Warsaw: Arkady* (1968).
89. V. Panc, *Theories of elastic plates* (Springer Science & Business Media, 1975).

90. E. Reissner, On transverse bending of plates, including the effect of transverse shear deformation, *International Journal of Solids and Structures*. **11**(5) (1975) 569-573.
91. M. Levinson, An accurate, simple theory of the statics and dynamics of elastic plates, *Mechanics Research Communications*. **7**(6) (1980) 343-350.
92. M. Murthy, An improved transverse shear deformation theory for laminated antisotropic plates, (1981).
93. H. Nguyen-Xuan, C.H. Thai, and T. Nguyen-Thoi, Isogeometric finite element analysis of composite sandwich plates using a higher order shear deformation theory, *Composites Part B: Engineering*. **55** (2013) 558-574.
94. H. Arya, R. Shimpi, and N. Naik, A zigzag model for laminated composite beams, *Composite structures*. **56**(1) (2002) 21-24.
95. K. Soldatos, A transverse shear deformation theory for homogeneous monoclinic plates, *Acta Mechanica*. **94**(3-4) (1992) 195-220.
96. M. Karama, K. Afaq, and S. Mistou, Mechanical behaviour of laminated composite beam by the new multi-layered laminated composite structures model with transverse shear stress continuity, *International Journal of Solids and Structures*. **40**(6) (2003) 1525-1546.
97. C.H. Thai, S. Kulasegaram, L.V. Tran, and H. Nguyen-Xuan, Generalized shear deformation theory for functionally graded isotropic and sandwich plates based on isogeometric approach, *Computers & Structures*. **141** (2014) 94-112.
98. T.-K. Nguyen, T.T.-P. Nguyen, T.P. Vo, and H.-T. Thai, Vibration and buckling analysis of functionally graded sandwich beams by a new higher-order shear deformation theory, *Composites Part B: Engineering*. **76** (2015) 273-285.
99. T.-K. Nguyen and B.-D. Nguyen, A new higher-order shear deformation theory for static, buckling and free vibration analysis of functionally graded sandwich beams, *Journal of Sandwich Structures & Materials*. **17**(6) (2015) 613-631.
100. M. Aydogdu, Vibration analysis of cross-ply laminated beams with general

boundary conditions by Ritz method, *International Journal of Mechanical Sciences*. **47**(11) (2005) 1740-1755.

101. A. Khdeir and J. Reddy, Free vibration of cross-ply laminated beams with arbitrary boundary conditions, *International Journal of Engineering Science*. **32**(12) (1994) 1971-1980.
102. G.M. Cook and A. Tessler, A {3, 2}-order bending theory for laminated composite and sandwich beams, *Composites Part B: Engineering*. **29**(5) (1998) 565-576.
103. A.S. Sayyad and Y.M. Ghugal, Bending, buckling and free vibration of laminated composite and sandwich beams: A critical review of literature, *Composite Structures*. **171** (2017) 486-504.
104. R. Aguiar, F. Moleiro, and C.M. Soares, Assessment of mixed and displacement-based models for static analysis of composite beams of different cross-sections, *Composite Structures*. **94**(2) (2012) 601-616.
105. W. Zhen and C. Wanji, An assessment of several displacement-based theories for the vibration and stability analysis of laminated composite and sandwich beams, *Composite Structures*. **84**(4) (2008) 337-349.
106. P. Subramanian, Dynamic analysis of laminated composite beams using higher order theories and finite elements, *Composite Structures*. **73**(3) (2006) 342-353.
107. M. Karama, B.A. Harb, S. Mistou, and S. Caperaa, Bending, buckling and free vibration of laminated composite with a transverse shear stress continuity model, *Composites Part B: Engineering*. **29**(3) (1998) 223-234.
108. F.-G. Yuan and R.E. Miller, A higher order finite element for laminated beams, *Composite structures*. **14**(2) (1990) 125-150.
109. T. Kant, S. Marur, and G. Rao, Analytical solution to the dynamic analysis of laminated beams using higher order refined theory, *Composite Structures*. **40**(1) (1997) 1-9.
110. A. Khdeir and J. Reddy, Buckling of cross-ply laminated beams with arbitrary

boundary conditions, *Composite Structures*. **1**(37) (1997) 1-3.

111. L. Jun and H. Hongxing, Free vibration analyses of axially loaded laminated composite beams based on higher-order shear deformation theory, *Meccanica*. **46**(6) (2011) 1299-1317.
112. T.-K. Nguyen, T.P. Vo, B.-D. Nguyen, and J. Lee, An analytical solution for buckling and vibration analysis of functionally graded sandwich beams using a quasi-3D shear deformation theory, *Composite Structures*. **156** (2016) 238-252.
113. T.C. Mathew, G. Singh, and G.V. Rao, Thermal buckling of cross-ply composite laminates, *Computers & structures*. **42**(2) (1992) 281-287.
114. J. Lee, Thermally induced buckling of laminated composites by a layerwise theory, *Computers & structures*. **65**(6) (1997) 917-922.
115. T. Kant, S.R. Marur, and G.S. Rao, Analytical solution to the dynamic analysis of laminated beams using higher order refined theory, *Composite Structures*. **40**(1) (1997) 1-9.
116. S. Emam and M. Eltaher, Buckling and postbuckling of composite beams in hygrothermal environments, *Composite Structures*. **152** (2016) 665-675.
117. A. Khdeir and J. Redd, Buckling of cross-ply laminated beams with arbitrary boundary conditions, *Composite Structures*. **37**(1) (1997) 1-3.
118. A. Khdeir, Thermal buckling of cross-ply laminated composite beams, *Acta mechanica*. **149**(1) (2001) 201-213.
119. H. Abramovich, Thermal buckling of cross-ply composite laminates using a first-order shear deformation theory, *Composite structures*. **28**(2) (1994) 201-213.
120. M. Aydogdu, Thermal buckling analysis of cross-ply laminated composite beams with general boundary conditions, *Composites Science and Technology*. **67**(6) (2007) 1096-1104.
121. N. Wattanasakulpong, B.G. Prusty, and D.W. Kelly, Thermal buckling and elastic vibration of third-order shear deformable functionally graded beams,

International Journal of Mechanical Sciences. **53**(9) (2011) 734-743.

122. H. Asadi, M. Bodaghi, M. Shakeri, and M. Aghdam, An analytical approach for nonlinear vibration and thermal stability of shape memory alloy hybrid laminated composite beams, *European Journal of Mechanics-A/Solids*. **42** (2013) 454-468.
123. A. Warminska, E. Manoach, and J. Warminski, Vibrations of a Composite Beam Under Thermal and Mechanical Loadings, *Procedia Engineering*. **144** (2016) 959-966.
124. L. Jun, B. Yuchen, and H. Peng, A dynamic stiffness method for analysis of thermal effect on vibration and buckling of a laminated composite beam, *Archive of Applied Mechanics* (2017) 1-21.
125. A. Vosoughi, P. Malekzadeh, M.R. Banan, and M.R. Banan, Thermal buckling and postbuckling of laminated composite beams with temperature-dependent properties, *International Journal of Non-Linear Mechanics*. **47**(3) (2012) 96-102.
126. F. Canales and J. Mantari, Buckling and free vibration of laminated beams with arbitrary boundary conditions using a refined HSDT, *Composites Part B: Engineering*. **100** (2016) 136-145.
127. D. Shao, S. Hu, Q. Wang, and F. Pang, Free vibration of refined higher-order shear deformation composite laminated beams with general boundary conditions, *Composites Part B: Engineering*. **108** (2017) 75-90.
128. R.B. Abarcar and P.F. Cunniff, The vibration of cantilever beams of fiber reinforced material, *Journal of Composite Materials*. **6**(3) (1972) 504-517.
129. I. Ritchie, H. Rosinger, A. Shillinglaw, and W. Fleury, The dynamic elastic behaviour of a fibre-reinforced composite sheet. I. The precise experimental determination of the principal elastic moduli, *Journal of Physics D: Applied Physics*. **8**(15) (1975) 1733.
130. T.-K. Nguyen, N.-D. Nguyen, T.P. Vo, and H.-T. Thai, Trigonometric-series solution for analysis of laminated composite beams, *Composite Structures*.

160 (2017) 142-151.

131. D.C. Lam, F. Yang, A. Chong, J. Wang, and P. Tong, Experiments and theory in strain gradient elasticity, *Journal of the Mechanics and Physics of Solids*. **51**(8) (2003) 1477-1508.
132. J. Stölken and A. Evans, A microbend test method for measuring the plasticity length scale, *Acta Materialia*. **46**(14) (1998) 5109-5115.
133. N. Fleck, G. Muller, M. Ashby, and J. Hutchinson, Strain gradient plasticity: theory and experiment, *Acta Metallurgica et Materialia*. **42**(2) (1994) 475-487.
134. H.-T. Thai, T.P. Vo, T.-K. Nguyen, and S.-E. Kim, A review of continuum mechanics models for size-dependent analysis of beams and plates, *Composite Structures*. **177**(Supplement C) (2017) 196-219.
135. A.C. Eringen, Linear theory of nonlocal elasticity and dispersion of plane waves, *International Journal of Engineering Science*. **10**(5) (1972) 425-435.
136. A.C. Eringen and D. Edelen, On nonlocal elasticity, *International Journal of Engineering Science*. **10**(3) (1972) 233-248.
137. P. Phung-Van, Q.X. Lieu, H. Nguyen-Xuan, and M.A. Wahab, Size-dependent isogeometric analysis of functionally graded carbon nanotube-reinforced composite nanoplates, *Composite Structures*. **166** (2017) 120-135.
138. P. Phung-Van, A. Ferreira, H. Nguyen-Xuan, and M.A. Wahab, An isogeometric approach for size-dependent geometrically nonlinear transient analysis of functionally graded nanoplates, *Composites Part B: Engineering*. **118** (2017) 125-134.
139. N.-T. Nguyen, N.-I. Kim, and J. Lee, Mixed finite element analysis of nonlocal Euler–Bernoulli nanobeams, *Finite Elements in Analysis and Design*. **106** (2015) 65-72.
140. N.-T. Nguyen, D. Hui, J. Lee, and H. Nguyen-Xuan, An efficient computational approach for size-dependent analysis of functionally graded nanoplates, *Computer Methods in Applied Mechanics and Engineering*. **297** (2015) 191-218.

141. A.C. Eringen, Micropolar fluids with stretch, *International Journal of Engineering Science*. **7**(1) (1969) 115-127.
142. A.C. Eringen, Linear theory of micropolar elasticity, *Journal of Mathematics and Mechanics* (1966) 909-923.
143. A.C. Eringen, Simple microfluids, *International Journal of Engineering Science*. **2**(2) (1964) 205-217.
144. R.D. Mindlin, Second gradient of strain and surface-tension in linear elasticity, *International Journal of Solids and Structures*. **1**(4) (1965) 417-438.
145. F. Yang, A. Chong, D.C. Lam, and P. Tong, Couple stress based strain gradient theory for elasticity, *International Journal of Solids and Structures*. **39**(10) (2002) 2731-2743.
146. C. Wanji, W. Chen, and K. Sze, A model of composite laminated Reddy beam based on a modified couple-stress theory, *Composite Structures*. **94**(8) (2012) 2599-2609.
147. W. Chen and J. Si, A model of composite laminated beam based on the global–local theory and new modified couple-stress theory, *Composite Structures*. **103** (2013) 99-107.
148. M.M. Abadi and A. Daneshmehr, An investigation of modified couple stress theory in buckling analysis of micro composite laminated Euler–Bernoulli and Timoshenko beams, *International Journal of Engineering Science*. **75** (2014) 40-53.
149. W.J. Chen and X.P. Li, Size-dependent free vibration analysis of composite laminated Timoshenko beam based on new modified couple stress theory, *Archive of Applied Mechanics* (2013) 1-14.
150. M. Ghadiri, A. Zajkani, and M.R. Akbarizadeh, Thermal effect on dynamics of thin and thick composite laminated microbeams by modified couple stress theory for different boundary conditions, *Applied Physics A*. **122**(12) (2016) 1023.
151. C.-L. Thanh, P. Phung-Van, C.H. Thai, H. Nguyen-Xuan, and M.A. Wahab,

Isogeometric analysis of functionally graded carbon nanotube reinforced composite nanoplates using modified couple stress theory, *Composite Structures*. **184** (2018) 633-649.

152. N.-D. Nguyen, T.-K. Nguyen, T.-N. Nguyen, and H.-T. Thai, New Ritz-solution shape functions for analysis of thermo-mechanical buckling and vibration of laminated composite beams, *Composite Structures*. **184** (2018) 452-460.
153. M. Şimşek, Non-linear vibration analysis of a functionally graded Timoshenko beam under action of a moving harmonic load, *Composite Structures*. **92**(10) (2010) 2532-2546.
154. M. Fakher and S. Hosseini-Hashemi, Bending and free vibration analysis of nanobeams by differential and integral forms of nonlocal strain gradient with Rayleigh–Ritz method, *Materials Research Express*. **4**(12) (2017) 125025.
155. X.-j. Xu and Z.-c. Deng, Variational principles for buckling and vibration of MWCNTs modeled by strain gradient theory, *Applied Mathematics and Mechanics*. **35**(9) (2014) 1115-1128.
156. S. Ilanko, L. Monterrubio, and Y. Mochida, *The Rayleigh-Ritz method for structural analysis* (John Wiley & Sons, 2015).
157. T.P. Vo, H.-T. Thai, and M. Aydogdu, Free vibration of axially loaded composite beams using a four-unknown shear and normal deformation theory, *Composite Structures* (2017).
158. V. Birman and G.A. Kardomatea, Review of current trends in research and applications of sandwich structures, *Composites Part B: Engineering*. **142** (2018) 221-240.
159. I. Kreja, A literature review on computational models for laminated composite and sandwich panels, *Open Engineering*. **1**(1) (2011) 59-80.
160. T.-T. Nguyen and J. Lee, Flexural-torsional vibration and buckling of thin-walled bi-directional functionally graded beams, *Composites Part B: Engineering*. **154** (2018) 351-362.

161. T.-T. Nguyen and J. Lee, Interactive geometric interpretation and static analysis of thin-walled bi-directional functionally graded beams, *Composite Structures*. **191** (2018) 1-11.
162. M. Vukasović, R. Pavazza, and F. Vlak, An analytic solution for bending of thin-walled laminated composite beams of symmetrical open sections with influence of shear, *The Journal of Strain Analysis for Engineering Design*. **52**(3) (2017) 190-203.
163. T.-T. Nguyen, N.-I. Kim, and J. Lee, Analysis of thin-walled open-section beams with functionally graded materials, *Composite Structures*. **138** (2016) 75-83.
164. H.X. Nguyen, J. Lee, T.P. Vo, and D. Lanc, Vibration and lateral buckling optimisation of thin-walled laminated composite channel-section beams, *Composite Structures*. **143** (2016) 84-92.
165. N.-I. Kim and J. Lee, Exact solutions for stability and free vibration of thin-walled Timoshenko laminated beams under variable forces, *Archive of Applied Mechanics*. **84**(12) (2014).
166. M.T. Piovan, J.M. Ramirez, and R. Sampaio, Dynamics of thin-walled composite beams: Analysis of parametric uncertainties, *Composite Structures*. **105** (2013) 14-28.
167. N.-I. Kim and J. Lee, Improved torsional analysis of laminated box beams, *Meccanica*. **48**(6) (2013) 1369-1386.
168. V. Vlasov, *Thin-walled elastic beams. Israel program for scientific translations, Jerusalem*. 1961, Oldbourne Press, London.
169. A. Gjelsvik, *The theory of thin walled bars* (Krieger Pub Co, 1981).
170. M.D. Pandey, M.Z. Kabir, and A.N. Sherbourne, Flexural-torsional stability of thin-walled composite I-section beams, *Composites Engineering*. **5**(3) (1995) 321-342.
171. S. Rajasekaran and K. Nalinaa, Stability and vibration analysis of non-prismatic thin-walled composite spatial members of generic section,

International Journal of Structural Stability and Dynamics. **5**(04) (2005) 489-520.

172. S.S. Maddur and S.K. Chaturvedi, Laminated composite open profile sections: non-uniform torsion of I-sections, *Composite Structures*. **50**(2) (2000) 159-169.
173. S.S. Maddur and S.K. Chaturvedi, Laminated composite open profile sections: first order shear deformation theory, *Composite Structures*. **45**(2) (1999) 105-114.
174. Z. Qin and L. Librescu, On a shear-deformable theory of anisotropic thin-walled beams: further contribution and validations, *Composite Structures*. **56**(4) (2002) 345-358.
175. J. Lee, Flexural analysis of thin-walled composite beams using shear-deformable beam theory, *Composite Structures*. **70**(2) (2005) 212-222.
176. S.P. Machado and V.H. Cortínez, Non-linear model for stability of thin-walled composite beams with shear deformation, *Thin-Walled Structures*. **43**(10) (2005) 1615-1645.
177. T.P. Vo and J. Lee, Flexural–torsional coupled vibration and buckling of thin-walled open section composite beams using shear-deformable beam theory, *International Journal of Mechanical Sciences*. **51**(9) (2009) 631-641.
178. N.-I. Kim and D.K. Shin, Dynamic stiffness matrix for flexural-torsional, lateral buckling and free vibration analyses of mono-symmetric thin-walled composite beams, *International Journal of Structural Stability and Dynamics*. **9**(03) (2009) 411-436.
179. N.-I. Kim, D.K. Shin, and Y.-S. Park, Dynamic stiffness matrix of thin-walled composite I-beam with symmetric and arbitrary laminations, *Journal of Sound and Vibration*. **318**(1) (2008) 364-388.
180. N.-I. Kim, D.K. Shin, and M.-Y. Kim, Flexural–torsional buckling loads for spatially coupled stability analysis of thin-walled composite columns, *Advances in Engineering Software*. **39**(12) (2008) 949-961.

181. N.-I. Kim, D.K. Shin, and M.-Y. Kim, Improved flexural–torsional stability analysis of thin-walled composite beam and exact stiffness matrix, *International journal of mechanical sciences*. **49**(8) (2007) 950-969.
182. N. Silvestre and D. Camotim, Shear deformable generalized beam theory for the analysis of thin-walled composite members, *Journal of Engineering Mechanics*. **139**(8) (2012) 1010-1024.
183. A. Prokić, D. Lukić, and I. Miličić, Free Vibration Analysis of Cross-Ply Laminated Thin-Walled Beams with Open Cross Sections: Exact Solution, *Journal of Structural Engineering*. **623** (2013).
184. M. Petrolo, M. Nagaraj, I. Kaleel, and E. Carrera, A global-local approach for the elastoplastic analysis of compact and thin-walled structures via refined models, *Computers & Structures*. **206** (2018) 54-65.
185. E. Carrera, I. Kaleel, and M. Petrolo, Elastoplastic analysis of compact and thin-walled structures using classical and refined beam finite element models, *Mechanics of Advanced Materials and Structures* (2017) 1-13.
186. E. Carrera, A. de Miguel, and A. Pagani, Extension of MITC to higher-order beam models and shear locking analysis for compact, thin-walled, and composite structures, *International Journal for Numerical Methods in Engineering*. **112**(13) (2017) 1889-1908.
187. M. Filippi, E. Carrera, and A.M. Regalli, Layerwise analyses of compact and thin-walled beams made of viscoelastic materials, *Journal of Vibration and Acoustics*. **138**(6) (2016) 064501.
188. E. Carrera, M. Filippi, P.K. Mahato, and A. Pagani, Advanced models for free vibration analysis of laminated beams with compact and thin-walled open/closed sections, *Journal of Composite Materials*. **49**(17) (2015) 2085-2101.
189. A.H. Sheikh, A. Asadi, and O.T. Thomsen, Vibration of thin-walled laminated composite beams having open and closed sections, *Composite Structures*. **134** (2015) 209-215.

190. X. Li, Y. Li, and Y. Qin, Free vibration characteristics of a spinning composite thin-walled beam under hygrothermal environment, *International Journal of Mechanical Sciences*. **119** (2016) 253-265.
191. T.-T. Nguyen, P.T. Thang, and J. Lee, Lateral buckling analysis of thin-walled functionally graded open-section beams, *Composite Structures*. **160** (2017) 952-963.
192. T.-T. Nguyen, N.-I. Kim, and J. Lee, Free vibration of thin-walled functionally graded open-section beams, *Composites Part B: Engineering*. **95** (2016) 105-116.
193. D. Lanc, G. Turkalj, T.P. Vo, and J. Brnić, Nonlinear buckling behaviours of thin-walled functionally graded open section beams, *Composite Structures*. **152** (2016) 829-839.
194. N.-I. Kim and J. Lee, Investigation of coupled instability for shear flexible FG sandwich I-beams subjected to variable axial force, *Acta Mechanica*. **229**(1) (2018) 47-70.
195. N.-I. Kim and J. Lee, Coupled vibration characteristics of shear flexible thin-walled functionally graded sandwich I-beams, *Composites Part B: Engineering*. **110** (2017) 229-247.
196. N.-D. Nguyen, T.-K. Nguyen, T.P. Vo, and H.-T. Thai, Ritz-based analytical solutions for bending, buckling and vibration behavior of laminated composite beams, *International Journal of Structural Stability and Dynamics*. **18**(11) (2018) 1850130.
197. N.-D. Nguyen, T.-K. Nguyen, H.-T. Thai, and T.P. Vo, A Ritz type solution with exponential trial functions for laminated composite beams based on the modified couple stress theory, *Composite Structures*. **191** (2018) 154-167.
198. J. Lee, Center of gravity and shear center of thin-walled open-section composite beams, *Composite structures*. **52**(2) (2001) 255-260.
199. T.-K. Nguyen, K. Sab, and G. Bonnet, First-order shear deformation plate models for functionally graded materials, *Composite Structures*. **83**(1) (2008)

25-36.

200. J. Hutchinson, Shear coefficients for Timoshenko beam theory, *Journal of Applied Mechanics*. **68**(1) (2001) 87-92.

201. F. Gruttmann and W. Wagner, Shear correction factors in Timoshenko's beam theory for arbitrary shaped cross-sections, *Computational Mechanics*. **27**(3) (2001) 199-207.

202. E.J. Barbero, R. Lopez-Anido, and J.F. Davalos, On the mechanics of thin-walled laminated composite beams, *Journal of Composite Materials*. **27**(8) (1993) 806-829.

203. J. Lee and S.-h. Lee, Flexural–torsional behavior of thin-walled composite beams, *Thin-Walled Structures*. **42**(9) (2004) 1293-1305.

204. V.H. Cortínez and M.T. Piovan, Stability of composite thin-walled beams with shear deformability, *Computers & structures*. **84**(15-16) (2006) 978-990.

205. N.-D. Nguyen, T.-K. Nguyen, T.P. Vo, T.-N. Nguyen, and S. Lee, Vibration and buckling behaviours of thin-walled composite and functionally graded sandwich I-beams, *Composites Part B: Engineering*. **166** (2019) 414-427.

206. P. Moreno-García, J.V.A. dos Santos, and H. Lopes, A review and study on Ritz method admissible functions with emphasis on buckling and free vibration of isotropic and anisotropic beams and plates, *Archives of Computational Methods in Engineering*. **25**(3) (2018) 785-815.

207. G. Oosterhout, P. Van Der Hoogt, and R. Spiering, Accurate calculation methods for natural frequencies of plates with special attention to the higher modes, *Journal of sound and vibration*. **183**(1) (1995) 33-47.